THE UNIVERSITY OF QUEENSLAND

AUSTRALIA

The Role of Sorting Nexins in Macropinocytosis and *Salmonella* Invasion

Xiaying Qi

BSc

A thesis submitted for the degree of Doctor of Philosophy at

The University of Queensland in 2015

Institute for Molecular Bioscience

Abstract

Salmonella enterica serovar Typhimurium (*S.* Typhimurium) can invade non-phagocytic epithelial cells by injecting virulence factors into the host cell via a type III secretion system (T3SS) to induce macropinocytosis. However, the precise molecular processes that lead to this uptake are currently unknown. In this thesis I show that several sorting nexin (SNX) proteins, i.e. SNX18, SNX20 and SNX21, are involved in *Salmonella* invasion and examined their molecular action during this process.

First I demonstrated that after docking at the plasma membrane *S.* Typhimurium triggers rapid translocation of cytosolic SNX18, a SH3-PX-BAR domain sorting nexin protein, to the bacteria-induced membrane ruffles and to the nascent *Salmonella*-containing vacuole (SCV). SNX18 recruitment required the inositol-phosphatase activity of the *Salmonella* T3SS effector SopB and an intact phosphoinositide-binding site within the PX domain of SNX18, but occurred independently of Rho-GTPases Rac1 and Cdc42 activation. I also demonstrate that SNX18 promotes formation of the SCV from the plasma membrane by acting as a scaffold to recruit Dynamin-2 and N-WASP in a process dependent on the SH3 domain of SNX18. Quantification of bacteria uptake revealed that overexpression of the full-length SNX18 increased the efficiency of bacteria internalization, whereas a decrease was detected in cells overexpressing the phosphoinositide-binding mutant R303Q, the ΔSH3 mutant, and in cells where endogenous levels of SNX18 were knocked-down by shRNA. This study identifies SNX18 as a novel target of SopB and suggests a mechanism where *S.* Typhimurium engages host factors via local manipulation of phosphoinositide composition at the site of invasion to orchestrate the internalization process.

Secondly, I investigated the molecular details of SNX18 recruitment to the plasma membrane during the *Salmonella* invasion process. As we identified a significant cytosolic pool of SNX18 which can translocate to the site of *S.* Typhimurium invasion, we hypothesized that cytosolic SNX18 represents a closed auto-inhibited form where the N-terminal SH3 domain and adjacent low complexity (LC) region fold back onto the C-terminal PX-BAR domains. The cytosolic SNX18 required a conformational change into an open form, exposing the phosphoinositide-binding site

for interaction with membrane. We also show that the bacteria-induced translocation of SNX18 is necessary but not sufficient for transient SNX18 phosphorylation. The LC domain of SNX18 functions in maintenance of the cytosol/membrane equilibrium of the protein and contains a not yet specified kinase binding motif and/or phosphosite(s). Screen for novel SNX18-specific interaction partners identified α-actinin-4 (ACTN4), a potential regulator for macropinocytosis and pathogen invasion as well. Though ACTN4 is recruited to the *Salmonella* induced ruffles, its recruitment is independent from SNX18 recruitment. And Akt translocation and phosphorylation induced by *Salmonella* invasion does not rely on SNX18 or ACTN4. Above all, this chapter provides an insight into the role of SNX18 as a scaffolding protein involved in plasma membrane remodeling and into manipulation of this process by bacterial pathogen.

Finally, I commenced characterization of another SNX subfamily that contains SNX20 and SNX21 as potential regulators of *Salmonella* invasion. The study found that SNX20 and SNX21 localized to early endosomes in mammalian cells and the intact phosphoinositide-binding site in the PX domain is necessary for the localisation. *S.* Typhimurium could also recruit both SNX20 and SNX21 to the newly formed SCVs. However, live cell imaging demonstrated that the association between SNX20 or SNX21 with endosomes or SCVs is very transient. This suggested a role of SNX20 and SNX21 in early time points of endocytic process and pathogen internalization and vacuole maturation.

Declaration by author

This thesis is composed of my original work, and contains no material previously published or written by another person except where due reference has been made in the text. I have clearly stated the contribution by others to jointly-authored works that I have included in my thesis.

I have clearly stated the contribution of others to my thesis as a whole, including statistical assistance, survey design, data analysis, significant technical procedures, professional editorial advice, and any other original research work used or reported in my thesis. The content of my thesis is the result of work I have carried out since the commencement of my research higher degree candidature and does not include a substantial part of work that has been submitted to qualify for the award of any other degree or diploma in any university or other tertiary institution. I have clearly stated which parts of my thesis, if any, have been submitted to qualify for another award.

I acknowledge that an electronic copy of my thesis must be lodged with the University Library and, subject to the policy and procedures of The University of Queensland, the thesis be made available for research and study in accordance with the Copyright Act 1968 unless a period of embargo has been approved by the Dean of the Graduate School.

I acknowledge that copyright of all material contained in my thesis resides with the copyright holder(s) of that material. Where appropriate I have obtained copyright permission from the copyright holder to reproduce material in this thesis.

Publications during candidature

SopB-mediated recruitment of SNX18 facilitates *Salmonella* Typhimurium internalization by the host cell

David Liebl, Xiaying Qi, Yang Zhe, Timothy C. Barnett and Rohan D. Teasdale

Molecular Biology of the Cell. Revision submitted. January, 2015.

Publications included in this thesis

SopB-mediated recruitment of SNX18 facilitates *Salmonella* Typhimurium internalization by the host cell

David Liebl, Xiaying Qi, Yang Zhe, Timothy C. Barnett and Rohan D. Teasdale

Molecular Biology of the Cell. Revision submitted. January, 2015.

Incorporated as Chapter 2.

Contributor	Statement of contribution
Xiaying Qi (Candidate)	Experimental design, data generation and manuscript preparation. Contributed data presented in the following figures of the manuscript: Figure 1, Figure 2, Figure 4, Figure 5, Figure 6, Figure 7, Figure S4, and Figure S5. (36%)
David Liebl	PhD supervisor involved in experimental design, methodology optimisation and preparation of manuscript. Dr Liebl generated the electron microscopy and live cell imaging data. He contributed to the generation of other experimental data which was in part prepared together with X. Qi (candidate). (50%)
Yang Zhe	Experimental design – cell signalling experiments which were performed in conjunction with other authors. (2%)
Timothy C. Barnett	Experimental design – generation of bacterial strains which were then applied by other authors to generate data. (2%)
Rohan D. Teasdale	PhD Supervisor/Academic supervisor involved in project design and preparation of manuscript. (10%)

Contributions by others to the thesis

Rohan Teasdale, David Liebl and Andrea Bugarcic formed the PhD supervisory team that was involved in experimental design and research direction guidance, as well as assisting with the editing and review of this thesis. Dr. Michelle Hill (Diamantina Institute, University of Queensland) provided mass spectrometry service and the filtered data are presented in Chapter 3 and Chapter 4.

Statement of parts of the thesis submitted to qualify for the award of another degree

None

Acknowledgements

Just one week from the commence of my PhD in January 2011, I had to evacuate from the share-house I rented because of the most serious flood since 1974 in Brisbane. That was an unforgettable experience for me as an international student who went aboard for the first time. However, as the Chinese believe that one will boost in business or wealth when involved with water, my PhD life went smoothly from the beginning thanks to the flood. Well, the flood was a little interlude during my PhD. Although sometimes there is still frustration or lack of motivation, I was able to avoid the nightmarish stories others described to me prior to my start. I owe this to the guidance and ongoing support from my immediate research environment, and the understanding and encouragement of my family and friends.

First and foremost I want to thank my supervisor Dr. Rohan Teasdale. I appreciate all his contributions of time, ideas, and funding to make my Ph.D. experience productive and stimulating. I have always been given the freedom to work independently and thinking critically in this research environment. It was undoubtedly a crucial part of my development as a member in the science and technology community. I am also thankful for the guidance and support from my co-supervisors, Dr. David Liebl and Dr. Andrea Bugarcic. David has provided insightful discussions about the projects. He has taught me, both consciously and un-consciously, how good experiment is done and I hope I can be as organized as him and pay attention to details in all aspects. The joy and enthusiasm Andrea has for her research was contagious and motivational for me and she provides an excellent example a successful woman scientist who can balance work and family well. Also I sincerely thank all the members of the Teasdale Group: Dr. Zhe Yang (a nice and helpful person who has been extremely supportive during my experiments and writing, as well as when I am homesick and need some Chinese style conversations and events), Dr. Markus Kerr (an always enthusiastic and energetic person, who is helpful in providing advice in projects, presentation skills and careers many times), Dr Genevieve Kinna (a great lab manager who organise everything in the lab and makes great cakes for us foodies), Jordan Follett and Wei Teo (two hard-working PhD students who share experience and ideas with me and always company me in the lab during weekends), and the numerous past and present staff and students who have come through the lab, for their company throughout these years, greatly expanding my perspective towards science and life. Also to my thesis

committee, Dr. Matt Sweet and Dr. Brett Collins, thanks for their efforts and advice in project progression and in career development. And to Amanda Carozzi, thanks for her patience and continuously support from applying the program and scholarships, all paper works in each PhD milestone, to the final submission of this thesis. Without any of the above help, I will not be able to finish this thesis.

To my friends in Brisbane, especially those I met in University of Queensland Chinese Students and Scholars Association (too many to list here but you know who you are!), I do appreciate all the meetings we had when discussing association business, all the events we organized together, all the parties we had during holidays, as well as all the interesting dialogs we had in group chats. Thanks all for providing support and friendship that I needed and making it like a big family.

To my parents back in China, thank you for supporting my decision of study abroad. Thanks for understanding me when I was too busy to make a call. I knew that I did disappoint them when I was not able to make it home during Chinese New Years. Thanks for taking all the pressures from other families. My hard-working parents have sacrificed their lives for me and provided unconditional love and care and I would not have made it this far without them. I love them so much!

Keywords

macropinocytosis, sorting nexin, *S.* Typhimurium, phosphoinositides

Australian and New Zealand Standard Research Classifications (ANZSRC)

ANZSRC code: 060108, Protein Trafficking, 60%

ANZSRC code: 060109, Proteomics and Intermolecular Interactions (excl. Medical Proteomics), 40%

Fields of Research (FoR) Classification

FoR code: 0601, Biochemistry and Cell Biology, 100%

Table of Contents

List of Figures

List of Tables

List of Abbreviations

Ack	Activated Cdc42-associated kinase
ACTN	Alpha-actinin
ADP	Adenosine diphosphate
AEBSF	4-(2-Aminoethyl) benzenesulfonyl fluoride hydrochloride
AP	Adaptor protein complex
APEX	Enhanced ascorbate peroxidase
ARF	ADP-ribosylation factor
ARK-1	Aurora kinase A
Arp2/3	Actin related protein 2/3
BAR	Bin/Amphiphysin/Rvs domain
BSA	Bovine serum albumin
BTK	Bruton's tyrosine kinase
CAPZA/CAPZB	F-actin capping protein subunits alpha and beta
CART	Cytoskeleton-associated recycling or transport
CCP	Clathrin coated pit
Cdc42	Cell division control protein 42 homolog
CGD	chronic granulomatous disease
CLIC	Clathrin- and caveolin- independent carrier
CME	Clathrin-mediated endocytosis
CtBP1/BARS	C-terminal-binding protein-1/Brefeldin A-ADP-ribosylated substrate
DAPI	4’ 6-diamidino-2-pheylindole
ECL	Enhanced chemi-luminescence
EDTA	Ethylenediaminetetraacetic acid
EE	Early endosome
EEA1	Early endosomal antigen 1
EGF	Epidermal growth factor
EGFR	Epidermal growth factor receptor
EPEC	Enteropathogenic *Escherichia coli*
F-actin	Filamentous actin
FAPPS	Four-phosphate-adaptor-protein
FBS/FCS	Fetal bovine serum/ fetal calf serum

FIP5	Rab11 family interacting protein 5
FYVE	Fab1p/YOTB/Vac1p/EEA1 domain
G-actin	Monomeric actin
GDP	Guanosine diphosphate
GEEC	Glycosyl phosphatidylinositol-anchored protein enriched early endosomal compartments
GEF	Guanine nucleotide exchange factor
GFP	Green fluorescent protein
GLUT4	Glucose transporter 4
GRP1	General receptor for phosphoinositides 1
GTP	Gunaosine triphosphate
HEK	Human embryonic kidney
HEPES	4-(2-hydroxyethyl)-1-piperazineethanesulfonic acid
HGF/SF	Hepatocyte growth factor/ Scatter factor
IF	Immunofluorescence
IgG	Immunoglobulin G
IP	Immunoprecipitation
ITC	Isothermal titration calorimetry
KD	Knock down
kDa	Kilo Dalton
LAMP1	Lysosomal-associated membrane protein 1
LAP	Liposome pelleting assay
LC	Low complexity region
LE	Late endosome
LNT	LAMP1-negative tubule
MDC	Metalloprotease disintegrin
MDCK	Madin-Darby canine kidney
MS	Mass spectrometry
MTOC	Microtubule organizing centre
MVB	Multivesicular bodies
N-WASP	Neuronal-Wiskott-Alldrich syndrome protein
PACS1	Phosphofurin acidic cluster sorting protein 1
PAK1	p21-activated kinase

PBS	Phosphate buffered saline
PCR	Polymerase chain reaction
PDGF	Platelet-derived growth factor
PH	Pleckstrin homology
PI3K	Phosphatidylinositol 3 kinase
PKB/Akt	Protein kinase B
PLCδ1	Phospholipase Cδ1
PLD1	phospholipase D1
PMA	Phorbol myristate acetate
PRD	Proline-rich motif
PSGL-1	P-selection glycoprotein ligand-1
PtdIns	Phosphoinositides
PtdOH	Phosphatidic acid
PtdSer	Phosphatidylserine
PTEN	Phosphatase and tensin homologue on chromosome 10
PVDF	Polyvinylidene difluoride
PX	Phox homology
PXB	PX-associated domain B
Rac1	Ras-related C3 botulinum toxin substrate 1
RACK1	Receptor of activated protein kinase C1
RFP	Red fluorescent protein
RhoG	Ras homology Growth-related
rM-CSF	Recombinant human macrophage colony-stimulating factor
SARA	Smad anchor for receptor activation
SCAMP	Secretory carrier membrane protein 3
SCV	*Salmonella* containing vacuole
SDS-PAGE	Sodium dodecyl sulphate polyacrylamide gel electrophoresis
SH2	Src homology 2
SH3	Src homology 3
SHIP	SH2-containing inositol 5’ -phosphatase
shRNA	Small hairpin RNA
SIF	Salmonella induced filament
SISTs	*Salmonella*-induced SCAMP3 tubules

SLIC-1	Selectin ligand interactor cytosolic-1
SNX	Sorting nexin
Sos	Son of sevenless
SPI	*Salmonella* pathogenicity islands
T3SS	Type III secretion system
TGN	trans-Golgi network
Vps	Vacuolar protein sorting
WGA	Wheat germ agglutinin

1 Introduction

Macropinocytosis is an actin-driven endocytosis process to non-selectively uptake large amount of fluid via massive membrane ruffles. Macropinosomes, the large (≥ 0.5 in diameter) endocytic vacuoles formed by macropinocytosis, share several major features with other endocytic compartments during its biogenesis and maturation. However, how macropinosome formation is regulated is less understood.

This introduction will discuss specifically on macropinocytosis and its regulation, followed by discussions on the aspects related to macropinocytosis, such as phosphoinositide signaling and *Salmonella* infection.

1.1 Macropinocytosis and its regulation

1.1.1 Pathways of endocytosis

Endocytosis has long been recognized as a cellular process to absorb proteins, lipids and signaling molecules from the extracellular environment. It is required in numerous cell activities, including the uptake of nutrients, the regulation of cell-surface receptors, clearance of apoptotic cells, and immune response. In order to accomplish the diverse biological roles, many variants of endocytosis are employed by cells and each pathway has some specific components in its distinct molecular machinery while some molecules participate in more than one pathway (Mayor and Pagano, 2007) . The best understood pathway of endocytosis is clathrin-mediated endocytosis (CME). Clathrin-coated vesicles are formed via receptor-mediated endocytosis and the fission from the plasma membrane mediated by GTPase dynamin (Roth, 2006). The mechanism of CME was considered to be the paradigm for all forms of endocytosis. However it is now known that there are numerous pathways that form clathrin-independent endocytic compartments. Caveolin-dependent caveolae also require dynamin to be excised from the cell surface in endothelial cells, adipocytes, smooth muscle and fibroblasts (Kirkham and Parton, 2005). Large particles can trigger phagocytosis in macrophages (Cox and Greenberg, 2001). Fluid uptake occurs by macropinocytosis in epithelial cells (Swanson and Watts, 1995). Numerous cargoes can be internalized by clathrin- and caveolin- independent carriers

(CLICs), a mechanism that is independent of clathrin, caveolin and dynamin Some others may be delivered into intermediate compartments, such as the caveosome or glycosyl phosphatidylinositol-anchored protein enriched early endosomal compartments (GEEC) first before they form early endosomes.

1.1.2 Macropinosome biogenesis and maturation

Macropinocytosis is an actin-driven endocytic process first described by Warren Lewis in 1931. The most distinguished feature to define macropinocytosis is that the process is not directly initiated by cargo or receptor molecules, but is a result of an overall increase in actin polymerization throughout the cell leading to membrane ruffling.

Membrane ruffling is the first step of macropinocytosis. Some Sheet-like ruffles turn into cup-shaped circular ruffles (macropinocytic cups) and the closure of these cup results in the formation of intracellular macropinosomes (Araki et al., 2000; Swanson and Watts, 1995). Given the essential role of actin polymerization in membrane ruffling, it is unsurprising that actin related proteins and complexes, such as Ras-related C3 botulinum toxin substrate 1 (Rac1), Cell division control protein 42 homolog (Cdc42), Neuronal-Wiskott-Alldrich syndrome protein (N-WASP) and Actin related protein 2/3 (Arp2/3), have been implicated in macropinosome formation (West et al., 2000). As Rho GTPases, Rac1 and Cdc42 can be activated from their GDP- to GTP-bound form. GTP-Rac1 and GTP-Cdc42 can activate p21-activated kinase 1 (PAK1), which is crucial for membrane ruffling and macropinosome formation (Dharmawardhane et al., 2000). PAK1 activates N-WASP (Liberali et al., 2008), leading to the relief of auto-inhibitory conformation of N-WASP (Castellano et al., 1999), which exposes its domain necessary and sufficient to recruit and activate Arp2/3 complex (Millard et al., 2004; Rohatgi et al., 1999). After binding to F-actin, Arp2/3 complex can nucleate G-actin to the uncapped barbed end of actin filaments to form rapidly extending branches. As a result, branched actin network are rapidly formed to induce membrane ruffles and macropinosome formation (Castellano et al., 1999; Liberali et al., 2008; Millard et al., 2004; Rohatgi et al., 1999; West et al., 2000). In the process of macropinocytosis, deactivation of Rac1 is also required for

macropinosome formation (Fujii et al., 2013). PAK1 also phosphorylates the C-terminal-binding protein-1/Brefeldin A-ADP-ribosylated substrate (CtBP1/BARS), leading to the activation of phospholipase D1 (PLD1), which is essential for the fission of macropinosomes from the plasma membrane (Haga et al., 2009; Liberali et al., 2008).

The maturation of macropinosome shares many features in common with the organelles of the endosomal/ lysosomal and phagolysosomal system. Rab5 is rapidly recruited to macropinosomes (Sun et al., 2003) and GTP-Rab5 interacts with vps34-p150, a phosphoinositide 3-kinase (PI3K) (Zerial and McBride, 2001), to produce phosphatidylinositol-3-monophosphate (PtdIns(3)*P*) locally on the membrane of macropinosomes. Consequently, PtdIns(3)*P* binding proteins EEA1 and Rabankyrin-5 are recruited at this stage of maturation (Hamasaki et al., 2004; Schnatwinkel et al., 2004). Then macropinosomes can migrate in a centripetal manner and rapidly lose Rab5 but acquire markers of late endosomes, such as Rab7 (Racoosin and Swanson, 1993). Furthermore, time-lapse video microscopy of macropinosomes revealed an itinerary as macropinosomes acquired early endosomal molecule sorting nexin 5 (SNX5) before exchanging them for Rab7 (Kerr et al., 2006; Lim et al., 2008). Ultimately, fusion of macropinosome with late endosomal and lysosomal compartments requires the PIKfyve on these PtdIns(3)*P* positive macropinosomes, which converts PtdIns(3)*P* to PtdIns(3,5)P2, as over-expression of the catalytically inactive PIKfyve mutant and using a specific inhibitor of PIKfyve catalytic activity YM201636 both lead to a disrupted transition from early endosomes to late endosome/lysosomes (Kerr et al., 2010).

1.1.3 Transient regulation by growth factors

Macropinosome formation level is elevated as a result of a transient response to the stimulation of various growth factors in many cell types (Swanson and Watts, 1995). In mouse macrophages derived from bone marrow, macropinocytosis is up-regulated upon phorbol myristate acetate (PMA) (Swanson, 1989) and recombinant human macrophage colony-stimulating factor (rM-CSF) (Racoosin and Swanson, 1989, 1992). In addition, Platelet-derived growth factor (PDGF) has been shown to trigger

membrane ruffles and macropinocytosis in NIH/3T3 cells (Anton et al., 2003). Epidermal growth factor (EGF) rapidly stimulates fluid uptake in non-polarized A431 and HEK293 cells (Haigler et al., 1979; Kerr et al., 2006), where as Hepatocyte growth factor/ Scatter factor (HGF/SF) is reported to increase dorsal membrane ruffling in polarized MDCK cells (Dowrick et al., 1993).

Upon stimulation, agonists for cell surface signaling receptors activate phosphorylation kinases in several signaling pathways, including PI3K pathway (Araki et al., 1996). The phosphorylation of downstream targets such as Rac1, Cdc42 and N-WASP will lead to robust actin polymerization (Yoshida et al., 2009). Additionally, transiently elevated level of certain phosphoinositides on membranes mediated by PI3K will recruit proteins to these membranes that facilitate actin nucleation (Hoeller et al., 2013).

1.1.4 Constitutive activation of macropinocytosis

Although how constitutive macropinocytosis is maintained has not been characterized, the difference from transiently regulated macropinocytosis may be the constitutive activation of signaling pathways. This suggestion is supported by the fact that overexpression of oncogenes like v/c-Src or K/H-Ras, which are all downstream of growth factors, leads to constitutive macropinocytosis (Amyere et al., 2000; Kasahara et al., 2007; Porat-Shliom et al., 2008). Moreover, high level of macropinocytosis is also observed in cells overexpressing constitutive activated mutants of Rac1 or Cdc42, suggesting that induced actin polymerization can result in constitutive activation as well (Ahram et al., 2000; Castellano et al., 1999; West et al., 2000).

Apart from those factors involved in signaling pathways and actin polymerization, some other proteins have been linked to macropinosome formation including Rabankyrin-5, a co-effector of small GTPase Rab5, and Cadherins. Rabankyrin-5 interacts with Rab5 in a GTP-dependent manner and induces macropinocytosis as a downstream effector Rab5-GTP (Schnatwinkel et al., 2004). Cadherins are observed to be concentrated at the site of membrane ruffles and depletion of Cadherins by siRNA leads to a decrease in macropinocytosis level, implying that Cadherins have an

unexpected role in the closure of cell-autonomous membrane contacts during macropinosome formation (Peter J. B. Sabatini, 2011; Sharma and Henderson, 2007).

Recently in our lab, an image-based screen was developed utilizing systematic over-expression of sorting nexin (SNX) family proteins and the tractability of macropinosomes. This analysis revealed that SNX1, SNX5, SNX9, SNX18 and SNX33 all promote macropinocytosis (Wang et al., 2010). This study is the first systematic functional study of the SNX-PX-BAR family proteins and their impact on macropinocytosis. A further investigation will be necessary to better understand the mechanism of macropinocytosis.

1.2 Phosphoinositide signalling

Phosphoinositides are a family of derivatives of phosphatidylinositol and have been shown to involved in membrane remodelling that is necessary for endocytosis and membrane trafficking (Cullen et al., 2001). Lipid kinases and phosphatase can rapidly phosphorylate or dephosphorylate the inositol ring at the 3, 4 and 5 positions, resulting in the dynamic interconversion between 7 phosphoinositide species. Phosphoinositides function as both signalling molecules and localization cues for PtdIns-binding proteins and have a crucial role in the network of phospholipid messengers and enzymes, which regulates numbers of cellular process. Abnormal phosphoinositide signalling and metabolism has been linked to many human diseases including neuronal system disorders and cancer (Di Paolo and De Camilli, 2006).

1.2.1 Different species

As phosphatidylinositol (PtdIns) can be reversibly phosphorylated at 3, 4 or/and 5 position of the inositol ring, its derivatives include three mono-phosphorylated phosphoinositides (PtdIns(3)*P*, PtdIns(4)*P* and PtdIns(5)*P*), three bi-phosphorylated phosphoinositides (PtdIns(3,4)P_2, PtdIns(3,4)P_2 and PtdIns(4,5)P_2 and one tris-phosphorylated phosphoinositides (PtdIns(3,4,5)P_3). Phosphoinositedes are much less abundant in mammalian cells under basal condition comparing to other acidic

phospholipids (PtdIns constitutes ~8% of all phospholipids). Among all seven phosphoinositides, PtdIns(4)*P* and PtdIns(4,5)P_2 are present in roughly equal amounts, which can be approximately 25-fold of PtdIns(3)*P* and PtdIns(5)*P* and even 500-fold of PtdIns(3,4)P_2, PtdIns(3,5)P_2 and PtdIns(3,4,5)P_3. Phosphoinositides appear to be enriched on membranes of different intracellular organelles as well as plasma membrane, serving as markers for cellular compartments and recognition of these PtdIns is necessary for the sorting and trafficking machinery to distinguish one organelle from another. However, acute phosphoinositides production upon various stimulations has been reported. Phosphoinositide kinases and phosphatases can be activated to shape the phosphoinositide distribution across membrane (Fig 1.1) (Cullen et al., 2001; Lemmon, 2008).

1.2.2Phosphoinositide Binding Module

Proteins associating with the surface of different cellular membranes across the cell are essential for various cellular functions, from protein sorting and trafficking to maintaining cell morphology. The restricted distribution of PtdIns on different membranes provides localization cues for proteins to effectively recognize the specific membrane subdomains via specific PtdIns-binding modules. These modules have narrow or broad specify in recognition of different PtdIns subspecies (Di Paolo and De Camilli, 2006). A full appreciation of how proteins recognize and bind to PtdIns is crucial for understanding the function of PtdIns in signalling and trafficking.

Figure 1.1 – Phosphoinositide in signalling and trafficking. (See next page)
The distribution and interconversion of phosphoinositides across mammalian cellular membranes are shown. Only predominant phosphoinositides are shown for simplicity. Percentages mean the relative level of each phosphoinositide if phosphatidylinositol level is 100% (Lemmon, 2008). The phosphoinositide kinases are shown, as are the lipid phosphatases PTEN (phosphatase and tensin homologue on chromosome 10) and SHIP (SH2-containing inositol 5′-phosphatase). EE, early endosome; LE, late endosome; TGN, trans golgi network; NE, nucleus.

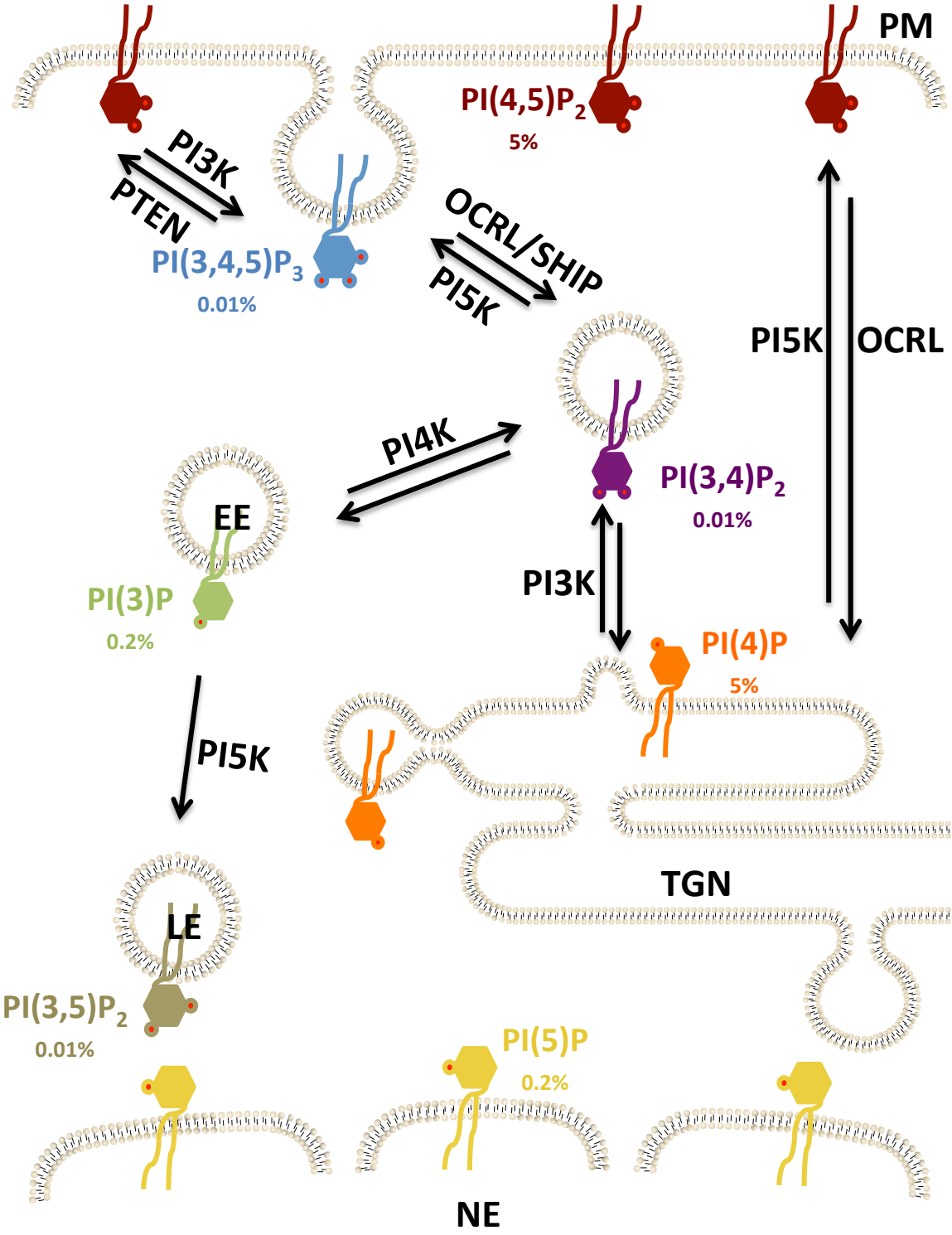

Figure 1.1 - Phosphoinositides in signalling and trafficking
(See legend on previous page)

PX (phox homology) domain

The PX domain family consists of at least 49 mammalian proteins, among which is the sorting nexin (SNX) superfamily, which so far has 34 members. The PX domain has approximately 110 residues in length. Three β-strands and three α-helices are globular folded with a long proline-rich loop between helices α1 and α2 and an electropositive basic pocket that involved in direct binding of phosphoinositides (Seet and Hong, 2006). Though previous consensus reported that PX domain proteins showed a preference for PtdIns(3)*P* among all PtdIns lipids, PtdIns*P*2 and PtdIns*P*3 are also reported to interact with different PX proteins(Ago et al., 2001). The PX domain proteins are involved in the endosomal system from endosome formation to protein sorting and recycling, from membrane trafficking to lysosomal degradation. Furthermore, these proteins have fundamental functions in cell polarity and signalling.

PH (pleckstrin homology) domain

PH domain was identified as a PtdIns-binding domain containing ~100 amino-acid sequence homology that occurs twice in pleckstrin (Harlan et al., 1994). Besides pleckstrin, the PH domain from phospholipase C δ 1 (PLC δ 1) is the most characterized example. PLC δ 1 PH domain binds strongly to PtdIns(4,5)P_2 and even more strongly to its isolated head-group, D-myo-inositol-1,4,5-triphosphate (Ins(1,4,5)P_3) (Lemmon et al., 1995). Another small subclass of PH domain proteins are reported to recognize the lipid second messengers PtdIns(3,4)P_2 and/or PtdIns(3,4,5)*P*3. The specificity and affinity of the PH domains allow them to accurately react to the signal-dependent membrane recruitment, as some key signalling molecules such as BTK, PKB/AKT and GRP1 are all PH domain-containing proteins (Franke et al., 1997; Klarlund et al., 1997; Salim et al., 1996). Thus, mutants in PH domain that abolish phosphoinositides binding can cause severe signalling defects leading to cancer (Carpten et al., 2007), although detailed mechanism remains unclear.

FYVE (Fab1p/YOTB/Vac1p/EEA1) domain

FYVE domain is a ~70 residues zinc binding finger comprising two β-hairpins and a C-terminal α-helix. It has three conserved sequences at the N-terminus (WxxD), the centre (RR/KHHCR), and the C-terminus (RVC) (Kutateladze, 2006). These motifs

forms a binding pocket specifically recognizing PtdIns(3)*P* and target many cytosolic proteins to endosomal membranes. Dimerization of FYVE domain is also necessary to allow efficient binding of FYVE domain proteins to multiple PrdIns(3)*P* containing membrane. Proteins containing FYVE domain have diverse functions at the endosomal membrane. The most characterized one is regulating fusion of endosomal membranes with other organelles in the endocytotic transport and the best example for this is the early endosomal antigen 1 (EEA1) (Dumas et al., 2001; Lawe et al., 2002). Another group of the FYVE domain proteins, such as PIKfyve, act as enzymes at the endosomal membrane (Sbrissa et al., 2002). Moreover, a number of effectors in signal transduction contain the FYVE domain, including Hrs (Hgs) and Smad anchor for receptor activation (SARA) (Miura et al., 2000; Tsukazaki et al., 1998).

1.2.3 Coincidence detection

Phosphoinositide-binding proteins can restrict their localisation to membranes across the cell. However, this phosphoinositide-dependent distribution is also found to require the engagement of other factors to impose a restriction. As there might be hundreds of proteins can recognize to the same type of phosphoinositide and the interaction between proteins and lipids is always weak and dynamic, it might be a common mechanism for phosphoinositide-binding proteins to employ other ligands to enhance their strength of specific membrane binding (Carlton and Cullen, 2005).

Coincidence detection of membrane association proteins and phosphoinositides

Many examples of phosphoinositide binding domain are found alongside other protein interaction domains, such as Src homology 2 (SH2) and Src homology 3 (SH3) domain. Thus, the protein is recruited specifically to membranes that contain the phosphoinositide and the interacting partner, a tyrosine-phosphorylated protein or a motif containing cargo. Alternatively, the phosphoinositide-binding domain itself may bind to a specific membrane-association protein to recruit the protein to certain membranes. This mechanism may explain specific Golgi localization of PH domain-containing protein like FAPPS (four-phosphate-adaptor-protein) that requires both PtdIns(4)*P* and the small monomeric GTPases ADP-ribosylation factor (ARF) as a targeting cue (Godi et al., 2004).

Coincidence detection through binding to multiple lipids

Apart from phosphoinositides binding domains, some proteins may contain another cooperating domain that specifically binds to other lipid, leading to a restriction of the protein to membranes containing both lipids. Additionally, some phosphoinositide-binding domains may have a distinct site to bind to other lipid to achieve specific membrane binding with a high avidity. Examples include PX domain of p47phox which binds to both PtdIns(3,4)P_2 and phosphatidic acid (PtdOH) (Karathanassis et al., 2002) and EEA1-FYVE domain which binds to both PtdIns(3)*P* and phosphatidylserine (PtdSer) (Kutateladze et al., 2004).

Coincidence detection through lipid and curved membrane

Coincidence detection occurs when PH or PX domains are found next to a membrane-binding BAR (Bin/Amphiphysin/Rvs) domain, were they detect phosphoinositides and membrane curvature, respectively. For instance, sorting nexin 1 (SNX1) specifically recognizes highly curved regions of PtdIns(3)*P* containing membrane tubules emanating from endosomes (Carlton et al., 2004). SNX1-PX domain-only cannot efficiently bring it to membrane as it interactss with PtdIns(3)*P* in low affinity in vitro (Cozier et al., 2002), suggesting that SNX1-BAR domain appears to function within its own right and membrane geometry can offer an important cue for protein localization.

1.3 Sorting Nexin Family Proteins

There are 49 known PX domain containing proteins encoded in the human genome, most of which are named sorting nexins (SNXs). The PX domain in all members implicates a commonality in their function of targeting proteins to phosphoinositide-rich membranes. Besides the PX domain, most of SNX family proteins contain one or more additional domains with diverse functions, including membrane remodelling, phosphoinositide kinase activity, phospholipase activity, protein–protein interaction and numerous other functions both known and unknown (Teasdale and Collins, 2012). The PX proteins are classified into subfamilies according to their related structures

(Fig 1.2), and the conserved domain structure within one subfamily provides an important basis for considering both the common and distinct functions of these diverse proteins.

Currently, there are structures of 14 mammalian PX domains available in the Protein Data Bank (PDB). The PX domain has approximately 110 residues in length, composed of three β-strands followed by three α-helices that are folded globularly (Seet and Hong, 2006). Specific features of this domain are a long proline-rich loop between helices α1 and α2, and an electropositive basic pocket that is involved in direct binding of negatively charged phosphate groups of phosphoinositides (Seet and Hong, 2006). Unlike the *Saccharomyces cerevisiae* PX domain molecules that demonstrated an almost absolute PtdIns(3)*P* specificity (Yu and Lemmon, 2001), mammalian PX domains have been reported to have a wide variety of other phosphoinositide specificities (Stahelin et al., 2004; Stahelin et al., 2003; Stahelin et al., 2007). Two distinct basic pockets on the membrane-binding surface are found in the p47(phox) PX domain by X-ray structure study, one preferentially binds PtdIns(3,4)P_2, while the other is able to associate weakly with anionic phospholipids such as phosphatidic acid (PtdOH) or phosphatidylserine. (Karathanassis et al., 2002; Porat-Shliom et al., 2008) The crystal structure of the PX domain from phosphoinositide 3-kinase C2alpha (PI3K-C2alpha) also shows an optimized PtdIns-binding site for PtdIns(4,5)P_2 binding and an important role of the adjacent hydrophobic residues in membrane penetration (Stahelin et al., 2006).

The membrane binding specificity of PX family is not controlled only by the lipid binding PX domain, but also by those additional domains, which drive and enhance membrane attachment through ‘coincidence detection’ (Teasdale and Collins, 2012). This includes those domains that associated independently with membrane, e.g. FERM domains in SNX17, 27, 31, BAR domains in SNX1, 2, 9, 18, etc., and PH domains in PLD1, 2, and those domains that interacts with other membrane-associated proteins, such as SH3 domains in SNX9, 18, 28, 33, p47phox that bind to cargo molecules, and RGS (regulator of G-protein signalling) domains in SNX13, 14, 25 that bind to the trimeric G-protein subunit $G\alpha_s$.

Given the membrane targeting property of PX family proteins, preferentially to

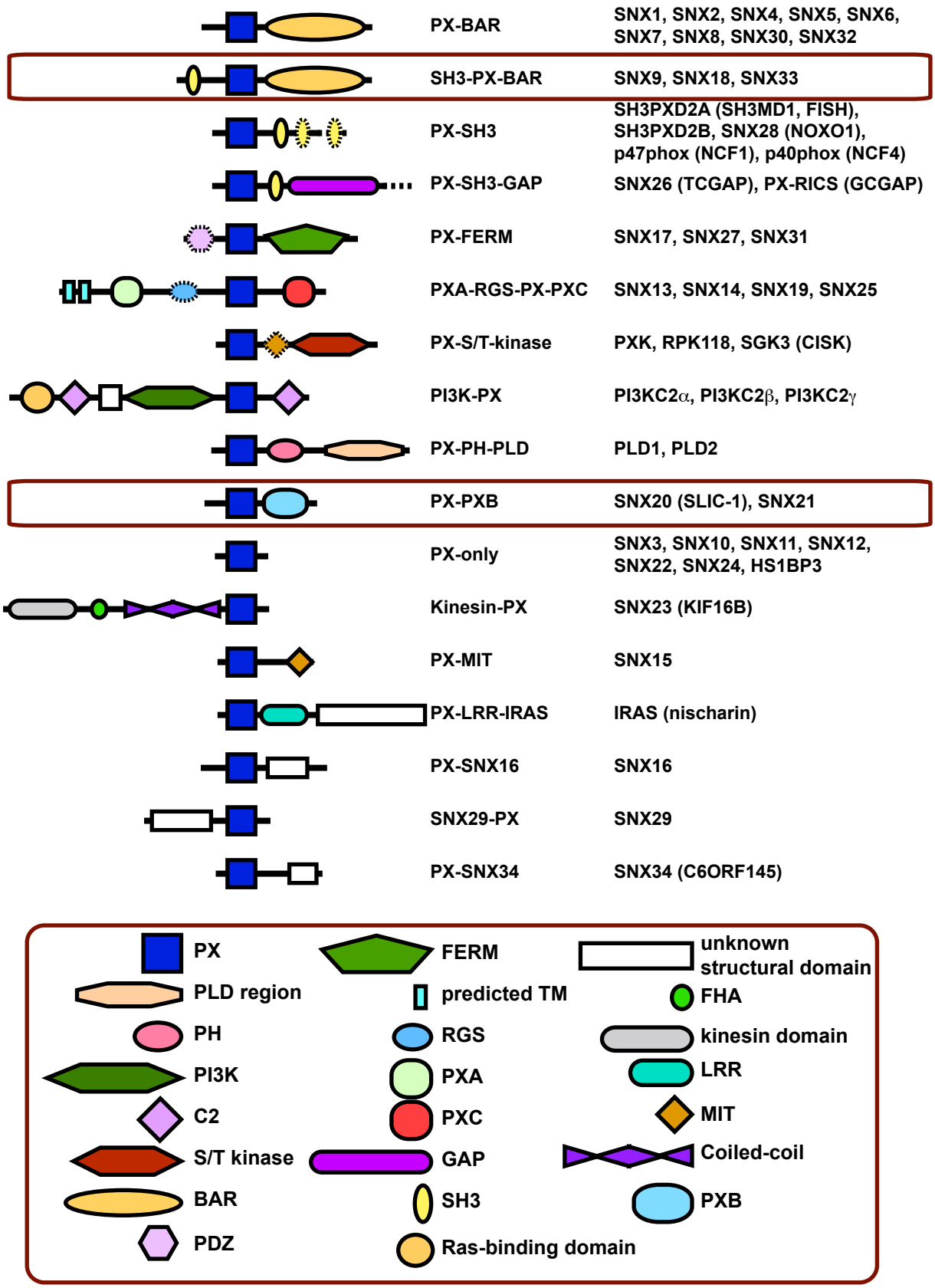

Figure 1.2 - Classification and domain organization of human PX proteins. (See legend on next page)

PtdIns(3)P enriched membranes, it is unsurprising that most members are reported to be involved in the endosomal protein trafficking pathways. For example, one of the best characterized role of the PX proteins is that SNX-BAR proteins, SNX1, 2, 5, and 6 can co-operate with the retromer protein complex in endosome-to TGN cargo recycling pathway (Carlton et al., 2004; Carlton et al., 2005; Rojas et al., 2007). Another subfamily, composed of SNX-FERM proteins SNX17, 27 and 31, is reported to be functioning at a nexus of trafficking pathways critical for transmembrane cargo processing from endosome to cell surface (Ghai et al., 2014; Loo et al., 2014).

As increasing evidence appears to support the essential roles of PX proteins in endocytic system, a few of them are linked to human diseases, such as CGD (chronic granulomatous disease) (Noack et al., 2001), Alzheimer's disease (Danson et al., 2013; Okada et al., 2010; Zhao et al., 2012), inflammatory response (Tabuchi and Kuebler, 2008) and pathogen infection (Braun et al., 2010; Bujny et al., 2008; Utskarpen et al., 2007). However, many questions remain regarding the structural, functional and pathological roles of PX proteins. Therefore, it is imperative to determine how PX proteins contribute to various trafficking pathways and different disease processes.

1.3.1 SNX9 family as Scaffold Proteins

As sorting nexins family proteins are found to link phosphoinositide signalling with endocytic pathways and endosomal membrane trafficking, a sub-family constituted of SNX9, SNX18 and SNX33 (initially annotated as SNX30) are also reported to link PtdIns metabolism, actin assembly and endocytosis. SNX9 family proteins have a

Figure 1.2 - Classification and domain organization of human PX proteins.
(See previous page) (adapted from (Teasdale and Collins, 2012))
Structural classification of PX proteins was based on known domains, and novel conserved domains were identified by secondary-structure prediction and sequence comparison. Note that the diagrams are not to scale. Domains with broken outlines indicate a domain that is only found in some members of the subfamily (PDZ domain in SNX27; MIT domain in RPK118; RGS domain missing in SNX19; TM domains missing in SNX25), or found in variable numbers (SH3 domains of PX-SH3 proteins).

SH3 domain at the N-terminus, followed by a low-complexity (LC) region of variable length, a phosphoinositide-binding PX domain and a membrane-bending BAR domain at C-terminus (Fig 1.3A) (Haberg et al., 2008). However, the structure features, expression and functions of SNX9 are much better studied than the other two members in the protein family. SNX9 has shown to have important functions for the generation of vesicular carriers (Fig 1.3B), so it is of interest to investigate the other two paralogs, SNX18 and SNX33.

SH3 domain is a common protein-protein interaction domain, which, in the case of SNX9 family proteins, binds to various proteins involving in cargo delivering (i.e. metalloprotease disintegrins MDC9 and MDC15 (ADAM9 and ADAM15) and insulin receptor), signalling (i.e. son of sevenless 1 (Sos1) and Sos2 and activated Cdc42-associated kinase 1 (Ack1) and Ack2, trafficking (i.e. Dynamin 1/2, Synaptojanin-1 and ITCH ubiquitin ligase) and cytoskeleton rearrangement (i.e. neuronal Wiskott-Aldrich syndrome protein (N-WASP)) (Haberg et al., 2008; Lundmark and Carlsson, 2002, 2003; Park et al., 2010; Shin et al., 2008; Yarar et al., 2007; Yeow-Fong et al., 2005). SNX9 SH3 domain is also reported to bind to EspF, which is an effector secreted by Enteropathogenic *Escherichia coli* (EPEC) during its invasion (Marches et al., 2006; Weflen et al., 2010).

The LC domains of the three family members have the least similarity and identity in sequences. However, they are reported to contain conserved sequences that bind clathrin and adaptor protein complexes 2 (AP-2) for SNX9 (Lundmark and Carlsson, 2003)or AP-1 for SNX18 (Haberg et al., 2008). All of these partner proteins play a role in clathrin-mediated endocytosis at the plasma membrane, which suggests that SNX9 family proteins play important roles in this process. Moreover, SNX9 binds aldolase to regulate its localization via its LC domain (Rangarajan et al., 2010).

The PX domain of SNX9 and SNX18 associates with a wide variety of phosphoinositides. However, SNX18 has a more specific preference for PtdIns(4,5)P2 than the rather promiscuous SNX9 that also has a high affinity for PtdIns(4,5)P2 (Haberg et al., 2008; Park et al., 2010). This highest preference of the PtdIns(4,5)P2, the lipids enriched in the plasma membrane, rather than other phosphoinositides like

PtdIns(3)*P* also suggests the major function of SNX9 family proteins at the plasma membrane rather than at the endosome.

BAR-domain-containing proteins are known to trigger membrane deformation and invagination, known to be required for the formation of intermediate structures during clathrin-mediated endocytosis. SNX9 family members all contain a BAR domain therefore they can form dimers and oligomers. Whether the BAR domains of SNX9, SNX18 and SNX33 form heterodimers is not clear, as conflicting results have been presented in terms of co-immuno-precipitation and co-localization studies (Haberg et al., 2008; Zhang et al., 2009). It has been shown that SNX9, SNX18 and SNX33 can induce membrane tubules, which requires their PX and BAR domains. (Haberg et al., 2008; Park et al., 2010)

SNX9, SNX18 and SNX33 are defined as scaffold proteins. As they have multiple protein interaction domains so that they can tether other proteins and complexes of a same pathway to the same site. Scaffold proteins are generally involved in important cell processes such as coordinating signalling transduction or nucleation of transport effectors, so that scientists started to investigate the mechanism of SNX9 family proteins in signalling and trafficking as scaffold proteins.

1.3.2 SNX9 in clathrin-mediated endocytosis

SNX9 interacts with proteins involved in CME such as clathrin, AP-2 and N-WASP through its SH3 or LC domain. Studies over the past decade have established a model for the mechanism of SNX9 in CME. As SNX9 is recruited to the clathrin coated pits (CCP) by clathrin and AP-2 (Lundmark and Carlsson, 2002, 2003), it can recognize the highly curved membrane containing enriched PtdIns(4,5)P2 via PtdIns-binding site within PX domain and induce further membrane curvature via the dimerized BAR domain (Yarar et al., 2008). SNX9 may remodel the vesicular neck by recruiting dynamin on to the narrow tubule and stabilizing dynamin oligomer through a few rounds of GTP hydrolysis (Lundmark and Carlsson, 2004; Soulet et al., 2005). Finally, SNX9 recruits and activates N-WASP to the membrane tubules (Shin et al., 2007) as well as Arp2/3 and facilitates actin polymerisation, which assists the release

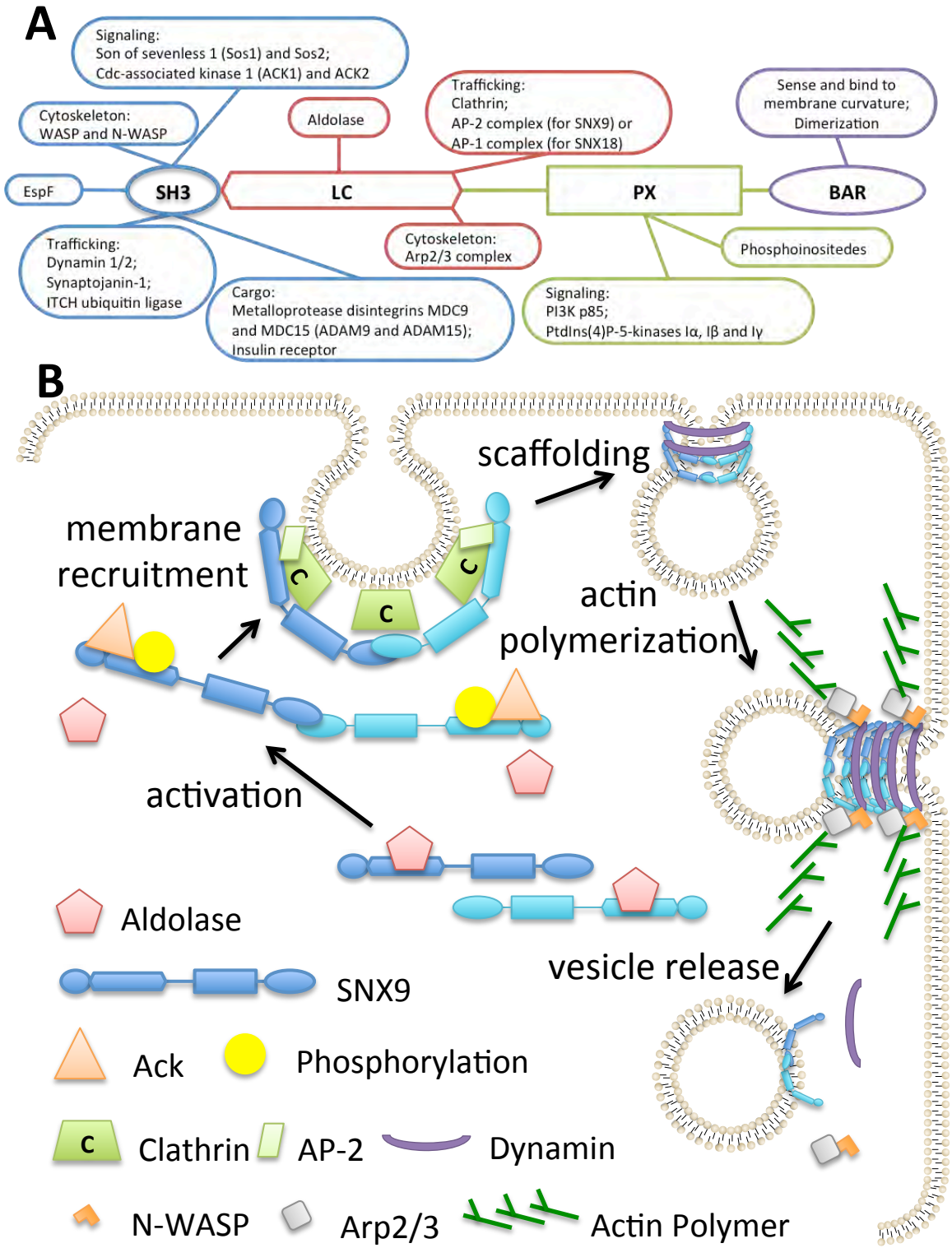

Figure 1.3 - Structure and function of SNX9 family
(See legend on next page)

of the vesicle from the plasma membrane. It is expected that the activity of SNX9 is tightly regulated to maintain a proper level of endocytosis in cells. So far, little is known about the mechanism of its regulation and further investigation is required. SNX9 is reported to bind to Ack and is phosphorylated at tyrosine in SH3 domain (Lin et al., 2002). Dimerization is also required for SNX9 phosphorylation in response to epidermal growth factor signalling (Childress et al., 2006). The Ack phosphorylation makes the SH3 domain unable to bind to proline-rich sequences, which may switch the binding preference of the SNX9 SH3 domain (Worby et al., 2002). It is also possible that the Ack phosphorylation is important to regulate SNX9 in signalling pathways.

The LC domain is also reported to be involved in SNX9 regulation. It possesses binding sites for clathrin and AP-2, which are believed to be the primary determinant for targeting SNX9 to CCP. The LC domain also has a cytosolic binding partner fructose-1,6-bisphosphate aldolase, a metabolic enzyme involving in glycolysis and gluconeogenesis. Aldolase binds with high affinity to a tryptophan-containing acidic sequence in the LC domain that overlaps with the region involved in the interaction of SNX9 with AP-2 (Rangarajan et al., 2010), suggesting that interaction with the abundant enzyme in the cytosol blocks the membrane localization of SNX9 to CCP. Phosphorylation of the LC domain of SNX9 releases aldolase from the native cytosolic complex enabling SNX9 to bind membranes (Lundmark and Carlsson, 2004). As free pool of aldolase can bind to F-actin, tubulin and WASP as well, it therefore appears to provide an essential links for SNX9 to the actin cytoskeleton.

Figure 1.3 – Structure and function of SNX9 family. (See previous page)
(A) SNX9 family proteins share SH3-LC-PX-BAR domain structure. The diagram indicates the major binding partner and function of each domain. (B) SNX9 functions in vesicular release from the plasma membrane during clathrin mediated endocytosis. See text for details.

1.3.3 SNX18 as Paralogs of SNX9

Sharing the similar structure and binding partners, SNX9 and SNX18 have been reported to be redundant in cells. They are both able to localize to and remodel membrane tubules, as the PX-BAR unit can bind to highly curved membranes and induce further curvatures (Haberg et al., 2008). SNX18 is also recruited to CCP together with dynamin and the burst of SNX18 coincides spatio-temporally with a burst of SNX9. Moreover, SNX18 can compensate SNX9 deficiency during CME as over-expression of SNX18 can rescue the reduction of endocytic uptake in SNX9 knockdown cells and vice versa (Park et al., 2010).

However, from an evolutionary point of view, there must be distinct functions of these parologs as mammalian cells have three SNX9 family proteins while *C. elegans* and *Drosophila* only have one homologue. Recent studies starts to reveal the differences between these family members.

All three SNX9 family proteins are expressed in most mouse tissues and in most cell lines from different species, but to a different extent. Specifically, given the result of immuno-fluorescent analysis in Hela cells, all three proteins are present in different localization, suggesting the separate functions of the three family members (Haberg et al., 2008). In contrast, SNX9 is highly expressed in cell lines with quite low expression of SNX18, whereas the opposite is true in other cell lines (Park et al., 2010). This different protein level suggests that SNX9 and SNX18 may have similar role in a same endocytic pathway and the total expression of the protein family needs to be maintained at a suitable level. Moreover, the difference in expression level may also indicate the distinct roles of SNX9 and SNX18 in different tissues and cell lines correlated to the function of the cell.

Different interaction partners between SNX9 and SNX18 involving in different cellular processes are also reported. SNX18 can bind to AP-1 complex via its LC domain and SNX18/AP-1 positive structures in cells co-localize with PACS1, a protein known to involving in retrograde trafficking from endosomes together with AP-1. These data suggest that SNX18 participates in specific carrier formation at endosomes to create membrane curvature and to recruit dynamin for tubular and

vesicular scission (Haberg et al., 2008); however, this conclusion remains controversial as conflicting data are reported (Park et al., 2010). Another example is the interaction between SNX18 and FIP5, a Rab-11-effector protein that is enriched in apical recycling endosomes in polarized epithelial cysts. It is proposed that FIP5 binds to and activates SNX18 at apical recycling endosomes, leading to actin polymerization, membrane bending, vesicle scission and formation of endocytic carriers (Willenborg et al., 2011), although it is a totally different cellular event from SNX9 dependent CME from the plasma membrane. Furthermore, SNX18 is also reported to promote autophagosome formation via direct interaction with LC3, thus SNX18 is required for recruiting Atg16L1 positive recycling endosomes and delivering LC3 positive membranes to autophagosome precursors as a positive regulator of autophagy (Knaevelsrud et al., 2013a; Knaevelsrud et al., 2013b).

Recently in our lab, SNX9, SNX18 and SNX33 are all found to promote macropinosome formation through an image-based screen (Wang et al., 2010). Among the SNX-PX-BAR family proteins, SNX18 exhibits the most significant increases in average macropinosome numbers per 100 transfected cells as compared to control cells. Interestingly, Hela cells, which express low level of SNX18, do not have the activity of macropinocytosis. The speciality of SNX18 indicates the importance of SNX18 in macropinocytosis and it may functions in a distinct manner from SNX9 to regulate the endocytic pathway. Further research is needed to obtain a better understanding of SNX9 family proteins and their different regulation machinery in macropinocytosis.

1.3.4 SNX20 and SNX21 form a novel PX subfamily

SNX20 and SNX21 compose a novel PX domain containing subfamily, which share the PX-associated domain B (PXB) at the C-terminus of the protein (Fig 1.2) (Teasdale and Collins, 2012).

SNX20 and SNX21 are 40% homologous in their protein sequence and share a conserved PXB domain of ~140 residues containing six α-helices downstream of the PX domain on the basis of secondary-structure predictions. Results from the TPRpred

server (http://toolkit.tuebingen.mpg.de/tprpred), which is a toolkit to detect Tetratrico Peptide Repeats (TPRs), Pentatrico Peptide Repeats (PPRs) and SEL1-like repeats from the query sequence and computes the statistical significance for their occurrence, suggest that this region may contain up to three TPRs, α–α-hairpin structures that form helical solenoids (Karpenahalli et al., 2007).

The only study on SNX21 (also known as SNX-L) has been suggested that SNX21 plays a role in liver development, based only on its high expression in human fetal liver tissue, which was decreased in adult tissue (Zeng et al., 2002). SNX21 is also identified as a potential regulator of endo-lysosomal sorting of the activated EGFR as the suppression of SNX21 has a weak effects on EGFR level (Danson et al., 2013), however, no details of how SNX21 function is provided up to date.

Recently, Schaff et al. performed a yeast-two-hybrid screen that identified the SNX20 as a ligand for the cytoplasmic tail of PSGL-1. SNX20 is also called selectin-ligand interacting cytoplasmic 1 (SLIC-1) and overexpression of SNX20 caused a significant redistribution of PSGL-1 from the plasma membrane into endosomes within the leucocyte cells (Schaff et al., 2008). However, the SNX20 knock out mice appeared to be normal and their neutrophils displayed no profound deficiency in PSGL-1 mediated cell adhesion or signalling, which is possibly due to the redundancy of SNX21.

Further studies will be required to determine if SNX20 acts as a sorting molecule that cycles PSGL-1 into endosomes and if SNX21 has a redundant role are correct and whether the SNX20/SNX21 proteins control trafficking of other trans-membrane cargoes.

1.4 Host-Pathogen Interaction During Infection

Numerous of pathogen entry pathways are characterized in non-phagocytic cells, which is essential for a better understanding of infectious diseases and also provides a powerful tool for investigating molecular details in cellular processes. Many pathogens have developed a range of strategies to manipulate specific endocytic

pathways, including macropinocytosis, to invade host cells. Some pathogens like *Salmonella* (Haraga et al., 2008), *Legionella* (Shin and Roy, 2008) and *Shigella* (Schroeder and Hilbi, 2008) can inject bacterial virulence proteins across the host cell's plasma membrane into cytoplasm in order to modulate lipid and protein distribution and activity of macropinocytosis for invasion and survival. Likewise, Mycobacterium can induce macropinocytosis (Garcia-Perez et al., 2008) by secreting factors into the culture media rather than depend on a bacterial secretion system. Another strategy is through direct interaction with cell surface receptors to induce its internalization in to the host cell via macropinocytosis, such as Adenovirus, which can bind to and activate its co-receptor α-v integrin (Meier et al., 2002). Numerous of pathogens manipulate the host cell PtdIns metabolism as well to alter the endocytic processes and to promote invasion and later survival and replication. Pizarro-Cerda and Cossart reviewed that *Yersinia* species and *Listeria* monocytogenes interact with receptors on the host cell surface to trigger the recruitment of PtdIns kinases to the site of invasion, while *Shigella* flexneri and *Salmonella* enterica secretes bacterial effectors as PtdIns kinases into the host cell to directly manipulate the PtdIns at the invasion site. The further maturation of bacteria containing vacuoles is also dependent on the conversion of PtdIns types to trigger (Pizarro-Cerda and Cossart, 2004).

1.4.1 *Salmonella*-induced macropinocytosis and *Salmonella* containing vacuole maturation

Salmonellae are intracellular pathogens responsible for a variety of enteric diseases including typhoid fever, paratyphoid fever and, in the case of *Salmonella* enterica serovar typhimurium (*S.* typhimurium), human gastroenteritis. *Salmonella* utilises macropinocytosis to gain entry into non-phagocytic cells, for example, the epithelial cells on intestinal wall (Francis et al., 1993). Upon docking on the host cell surface, the pathogen delivers a host of bacterial virulence effectors directly into the cytoplasm of host cells via a specialised apparatus called a type III secretion system (T3SS). *Salmonellae* encode two distinct T3SSs within *Salmonella* pathogenicity islands 1 and 2 (SPI1 and SPI2) that function at discrete stages of the infection. SPI1 is active on contact with the host cell surface and serves to translocate virulence proteins across the plasma membrane, leading to the rearrangement of host cell cytoskeleton and

internalisation of the bacteria. SPI2 is active within intracellular organelles during the later stages of infection to manipulate the environment for replication (Haraga et al., 2008).

The effectors involving in invasion are complicated and diverse, but several SPI1 T3SS effectors are identified to be required for efficient invasion of cultured epithelial cells. SopE and SopE2 are potent guanine nucleotide exchange factors (GEFs) for the host Rho GTPases Cdc42, Rac1 and RhoG. The activation of all three GTPases during *Salmonella* infection leads to cytoskeletal reorganization, membrane ruffling and bacterial internalization. SopB, as a phosphoinositide phosphatase, is reported to manipulate PtdIns(4,5)P2 on the host's plasma membrane into PtdIns5P, thus increases other phosphoinositides at the site of *Salmonella* invasion (Terebiznik et al., 2002). The phospholipid conversion by SopB may recruit phosphoinositide-binding proteins, SH3-containing GEF (SGEF) (Patel and Galan, 2006) for example, and then indirectly activate Cdc42 and RhoG. Activation of Rho GTPases then results in the activation of the WASP family members and recruitment of the Arp2/3 complex to sites of *Salmonella* invasion, stimulating actin polymerization and membrane ruffling. The actin-binding effectors SipA and SipC can further modulated the changes in the actin cytoskeleton (Hayward and Koronakis, 1999; Zhou et al., 1999), eventually leading to *Salmonella* uptake via macropinocytosis.

The nascent macropinosome shrinks to form an adherent membrane around one or more bacteria referred as *Salmonella* containing vacuole (SCV) (Fig 1.4). SCVs traffic towards the perinuclear region of the host cell and mature via selective interactions with the endocytic pathway. Intracellular *Salmonellae* can alter the properties of the SCVs to promote the infection process. Whilst SCV appears to share properties with normal endosomes, the maturation process has clearly been modified so that the SCV persists for hours to days. Once the SCV is positioned to the juxtanuclear region adjacent to the microtubule-organising centre (MTOC), which is next to the Golgi apparatus, intracellular bacterial replication begins. This stage is characterised by the formation of SCV tubular structures called Salmonella-induced filaments (SIFs). SIFs are rich in late endocytic markers, such as lysosome-associated membrane proteins (LAMPs). Recent studies highlighted an unexpected level of complexity in the composition and regulation of tubules associated to the SCV. In

addition to SIFs, S. Typhimurium is able to induce SNX tubules, *Salmonella*-induced secretory carrier membrane protein 3 (SCAMP3) tubules (SISTs) and LAMP1-negative tubules (LNTs). SPI-1 and SPI-2 effectors do not operate sequentially and independently of one another as previously thought. Instead, both subsets play key roles in SCV maturation, positioning and replication (Haraga et al., 2008; Malik Kale et al., 2011; Schroeder et al., 2011).

1.4.2 Phosphoinositide signalling and SNX tubular network

A recent HPLC analysis of lipids extracted from *Salmonella*-infected cells revealed significant increase in the relative amounts of PtdIns(4,5)P_2, PtdIns(3,4)P_2 and PtdIns(3,4,5)P_3 as well as moderate increase in PtdIns(3)P comparing to mock infected cells (Bakowski et al., 2010). These phosphoinositides ordinarily serve as anchors to recruit PtdIns-binding proteins in a spatially and temporally dependent manner. For example, the modulation of PtdIns(4,5)P_2 and PtdIns(3,4,5)P_3 on the plasma membrane destabilises the cortical cytoskeleton and promoting bacterial uptake via inducing membrane ruffling and macropinosome formation (Terebiznik et al., 2002). On the other hand, disrupted PtdIns(3,5)P_2 synthesis through perturbation of PIKfive activity led to a remarkable inhibition in the SIF formation, SCV acidification and eventually the replication of *Salmonella* within an intracellular compartment (Kerr et al., 2010). All together, *Salmonella* promotes its internalization into the cell and generate a niche suitable for its replication within the cell through the directly manipulation of the host's phosphoinositide metabolism.

Recently it was revealed that members of SNX family, SNX1 and SNX3, play essential roles in *Salmonella* infection. The formation of early SNX-mediated tubules is dependent on the T3SS-SPI1 effector SopB (Braun et al., 2010; Bujny et al., 2008), as SopB mediates the accumulation of PtdIns3P on the membrane of SCV, which is essential for the recruitment of SNX1 and SNX3.

The SNX1 PX domain binds to PtdIns3P and PtdIns(3,5)P2, targeting SNX1 to early endosomes, whereas its BAR domain enables sensing of membrane curvature and

induces tubulation of endosomal membrane during sorting process (Carlton et al., 2004). Within the first minutes of *Salmonella* infection, SNX1 undergoes a rapid translocation from endosome to the site of *Salmonella* entry. Once enriched on the nascent enlarged SCVs, SNX1 starts to form extensive and highly dynamic tubules. SNX1 is part of the retromer complex and depletion of SNX1 leads to a slower progression of SCVs towards the microtubule-organising centre and a delay of intracellular bacterial proliferation (Bujny et al., 2008). Another sorting nexin, SNX3, also associates with the newly formed SCV and appears on tubular structures at 30 min, peaks at 1h and disappear at 2h after *Salmonella* entry (Braun et al., 2010) This tubular localization requires SNX1 and SNX2, as SNX3 has no BAR domain for tubulation. Depletion of SNX3 blocks the recruitment of Rab7 and LAMP1, and therefore SNX3 plays a role in the control of SCV maturation (Braun et al., 2010).

Recently, a detailed examination of the recruitment of SNXs to the nascent SCV was done by immunofluorescent-labeling of infected cells epitopically expressing SNXs and co-labelled with endogenous SNX1 (Kerr et al., 2012). The study revealed 19 SNXs recruited to the SCV within the first 30mins of infection. Apart from SNX1, 6 SNXs, namely SNX2, SNX4, SNX5, SNX6, SNX7 and SNX8, are found on the SNX1 positive tubular extensions of the SCVs, whilst PLD1, SNX10, SNX11, SNX15, SNX20 and p40phox were restricted to the body of SCV only. Moreover, PLD2, SNX12, SNX16, SNX21, SNX23 and SNX28 were found evenly associated with both the body and the tubules of SCVs. This study suggests the likely diverse functions of SNXs during Salmonella infection and it is of interest to explore the emerging roles of SNXs and how they contribute to the host-pathogen interaction in Salmonella pathogenicity.

Figure 1.4 – *Salmonella*-induced internalization and tubular networks.
(See next page)
Salmonella (orange rod) is internalised into a SCV by manipulating PtdIns and inducing actin-driven macropinocytosis. Early SCV is positive for SNX1 and SNX3. MTOC: microtubule organizing centre; LNTs: LAMP1-negative tubules; SIFs: *Salmonella*-induced filaments; SISTs: *Salmonella*-induced SCAMP3 tubules; SCAMP: secretory carrier membrane protein 3; TGN: trans-Golgi network. See text for details.

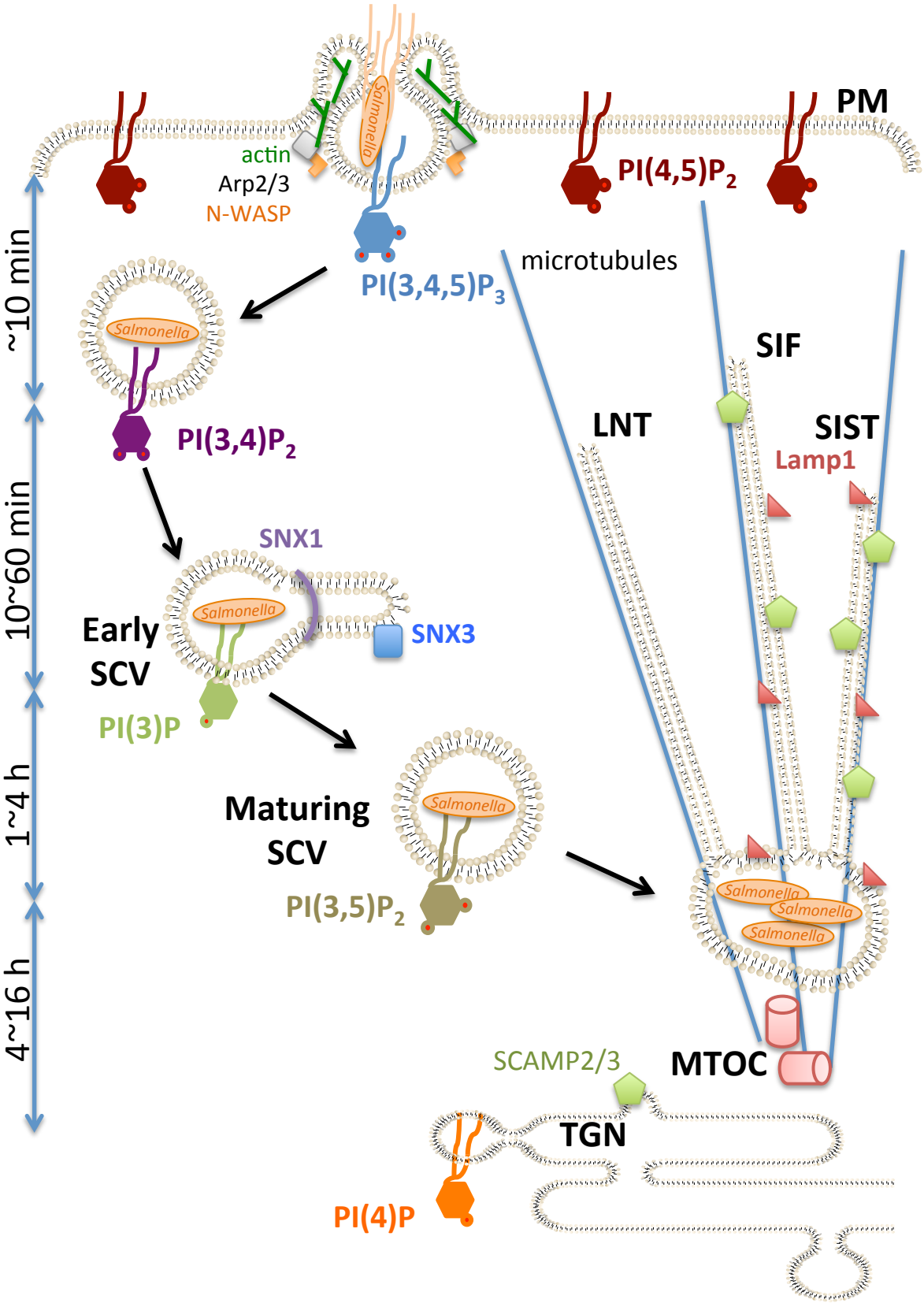

Figure 1.4 - *Salmonella*-induced internalization and tubular networks. (See legend on previous page)

1.5 Conclusion and Perspectives

All together, phosphoinositides, N-WASP and sorting nexins are key components of macropinocytosis. However how these components are collectively organized on specific membrane subdomains during endocytosis and in response to bacterial effectors during pathogen invasion remains elusive.

A great challenge for research on macropinocytosis in non-infected or infected epithelial cells will be to unveil the distinct molecular mechanisms that enable a same set of components to regulate such different processes as clathrin-mediated endocytosis, macropinocytosis and pathogen invasion. On the other hand, different molecules and signalling pathways may also be involved in different strategies to manipulate endocytosis. However, an equally demanding task concerns the elucidation of the principles that arrange all components in a spatio-temporal order, which precisely regulates macropinocytosis. A key to understanding the underlying mechanism is to characterize the localization, activation, mobilization and function of each component. Several factors are described in the past decades, but various gaps in detail between them remains open. Sorting family proteins build links between phosphoinositides signalling, actin polymerization and membrane trafficking. Thus, understanding of the functions of SNXs in diverse endocytic pathways will to be potential material to fill up some gaps.

1.6 Project Aims and Hypothesis

Previous studies revealed SNXs' implication in macropinocytosis, which is relevant towards the immune response, tumour-genesis and pathogen invasion. However the molecular details of how these proteins regulate the process is poorly understood. The main objective of my PhD is to provide further insight, at both molecular and cellular levels, into the molecular components and pathways that regulate macropinocytosis and *Salmonella* invasion. My project can be separated into 3 interrelated aims:

1) **Characteristic of the molecular mechanism of SNX18's recruitment and functions in macropinocytosis and *Salmonella* invasion.** To understand the

function of SNX18, characterization of the impact of each individual domain on different aspects is necessary, including protein localization, mobilization, modification, protein interaction and dimerization/oligomerization. This will require generation of a series of SNX18 truncated or point mutants. Analysis of the expression patterns of these constructs in different cell types and their behaviour in macropinosome formation will be analysed by microscopy imaging. The constructs will be also analysed in cells infected with *Salmonella* to assess how SNX18 is involved in invasion and replication of pathogens that exploit macropinocytosis to invade epithelial cells.

2) **Identification of novel molecules interacting with SNX18.** I will screen for novel interaction partners of SNX18 and test whether and how they are involved in macropinocytic machinery. This involves co-immunoprecipitation/mass spectrometry to screen for SNX18 binding partners. Besides the biochemistry approach, imaging analysis with confocal fluorescence microscopy will also be used to analyse the co-localization and kinetic between SNX18 and the potential associate proteins in cells under different conditions (e.g. using macropinocytosis activators or inhibitors, kinase inhibitors and *Salmonella* infection).

3) **The characterization of SNX-PXB proteins involved in endocytosis and *Salmonella* invasion.** SNX20 and SNX21 will be characterized in terms of their cellular localization, protein interaction ability and the kinetics during *Salmonella* invasion.

The completion of these aims will allow the detailed understanding of the molecular mechanism of SNX18 regulating the macropinocytosis and pathogen internalization, as well as the characterization of its interaction partners within the process. This will extend our understanding of PX domain containing proteins, specifically, their function mechanisms during macropinocytosis and the internalization of some bacterial pathogen exploiting this endocytic machinery.

2 SNX18 facilitates *Salmonella* Typhimurium internalization

2.1 Introduction

Salmonella Typhimurium has been reported to gain entry into non-phagocytic cells by inducing actin-driven macropinocytosis (Haraga et al., 2008). This invasion process includes secretion of Salmonella virulence effectors via type III secretion systems, manipulation phosphoinositides metabolism, rearrangement of actin skeleton and eventually *Salmonella*-containing vacuoles (SCVs) formation. Although the biogenesis of SCV is reported to involve the effector SopB as a phosphoinositides phosphatase (Terebiznik et al., 2002), and cooperating with SopD (Bakowski et al., 2007), to promote membrane fission during the *Salmonella* internalization, the host cell proteins involved in this process is still poorly understood.

Previously, Wang et al. identified SNX18 as a novel regulator of macropinocytosis (Wang et al., 2010). The function and the mechanism of SNX18 is still largely unknown except it is considered to have a redundant role of its parolog SNX9 in endocytosis (Haberg et al., 2008; Park et al., 2010). Previously, SNX1 and SNX3 have been found to modulate the nascent SCV during early stage of *Salmonella* invasion (Braun et al., 2010; Bujny et al., 2008). As a PX-BAR domain containing protein, it is likely that SNX18 functions in response to the phosphoinositides signals and it will be of interest to examine whether SNX18 is also involved in *Salmonella* infection.

In this Chapter, we establish that at early stage of *Salmonella* invasion, SNX18 is recruited to the plasma membrane, which is dependent on its PtdIns-binding PX domain in a SopB dependent manner. We proposed that SNX18 functions as a scaffold by recruiting N-WASP and dynamin at the site of invasion to promote scission of the nascent SCV from plasma membrane, which then facilitates the internalization of bacteria.

The work within this chapter is presented as a manuscript submitted to *Molecular Biology of the Cell (assigned manuscript tracking number: E14-08-1288R)* under the title: "SopB-mediated recruitment of SNX18 facilitates *Salmonella* Typhimurium internalization by the host cell", authored by David Liebl, Xiaying Qi, Yang Zhe, Timothy C. Barnett and Rohan D. Teasdale.

TITLE:

SopB-mediated recruitment of SNX18 facilitates *Salmonella* Typhimurium internalization by the host cell

AUTHORS:

David Liebl[1#], Xiaying Qi[1], Yang Zhe[1], Timothy C. Barnett[2,3] and Rohan D. Teasdale[1,2,*]

AFFILIATIONS:

1. Institute for Molecular Bioscience, The University of Queensland, St Lucia, Queensland, Australia

2. Australian Infectious Diseases Research Centre, The University of Queensland, St Lucia, Queensland, Australia.

3. School of Chemistry and Molecular Biosciences, The University of Queensland, St Lucia, Queensland, Australia.

(*) CORRESPONDING AUTHOR:
Rohan Teasdale, PhD
Institute for Molecular Bioscience
The University of Queensland
St. Lucia, QLD 4072
AUSTRALIA
E-MAIL: R.Teasdale@uq.edu.au
PHONE: 61-7-3346-2056

(#) Current Affiliation
Biology of Cancer and Infection Laboratory
Dept. Bacterial Pathogenesis and Cellular Responses
iRTSV/CEA-Grenoble
38054 GRENOBLE
cedex 09 FRANCE
Phone: +33 (0)4 38 78 35 74
Email: david.liebl@cea.fr

RUNNING TITLE: SNX18 facilitates *S*. Typhimurium internalization

ABSTRACT

To invade epithelial cells, *Salmonella enterica* serovar Typhimurium (S. Typhimurium) induces macropinocytosis through the action of virulence factors delivered across the host cell membrane via a type III secretion system. We show that after docking at the plasma membrane S. Typhimurium triggers rapid translocation of cytosolic SNX18, a SH3-PX-BAR domain sorting nexin protein, to the bacteria-induced membrane ruffles and to the nascent Salmonella-containing vacuole. SNX18 recruitment required the inositol-phosphatase activity of the Salmonella effector SopB and an intact phosphoinositide-binding site within the PX domain of SNX18, but occurred independently of Rho-GTPases Rac1 and Cdc42 activation. SNX18 promotes formation of the SCV from the plasma membrane by acting as a scaffold to recruit Dynamin-2 and N-WASP in a process dependent on the SH3 domain of SNX18. Quantification of bacteria uptake revealed that overexpression of SNX18 increased bacteria internalization, whereas a decrease was detected in cells overexpressing the phosphoinositide-binding mutant R303Q, the ΔSH3 mutant, and in cells where endogenous levels of SNX18 were knocked-down. This study identifies SNX18 as a novel target of SopB and suggests a mechanism where S. Typhimurium engages host factors via local manipulation of phosphoinositide composition at the site of invasion to orchestrate the internalization process.

Highlight Summary

Salmonella facilitates entry into the host cell by recruitment of SNX18 to the site of invasion. Its recruitment requires local changes in phosphoinositide composition generated by bacterial inositol-phosphatase SopB. Once recruited, SNX18 acts as a key molecular component involved in early formation of the Salmonella-containing vacuole.

INTRODUCTION

To gain entry into non-phagocytic epithelial cells, various viral and bacterial human pathogens co-opt the endocytic machinery by modulation of phosphoinositide metabolism (Pizarro-Cerda and Cossart, 2004) or actin cytoskeleton (Haglund and Welch, 2011). One of the most efficient routes for pathogens to enter the host cells is macropinocytosis, a distinct form of endocytosis characteristic for its non-selective and high turnover uptake of extracellular fluid into macropinosomes (Lim *et al.*, 2008; Kerr *et al.*, 2010).

Salmonella are facultative intracellular Gram-negative bacteria, which infect and replicate within both epithelial cells and macrophages. To invade epithelial cells, *Salmonella* induces macropinocytosis at the site of entry (Francis *et al.*, 1993) by translocating a set of effector proteins into the host cell cytoplasm via a type III secretion system (T3SS). Interactions between effectors encoded by *Salmonella* pathogenicity island 1 (SPI1) and their host cell targets result in orchestrated manipulation of phosphoinositide signalling, Rho-GTPase function and actin cytoskeleton remodelling that promotes internalization of the bacteria into a membrane-bound organelle, termed the *Salmonella*-containing vacuole (SCV) (Haraga *et al.*, 2008). Although it has been reported that the biogenesis and release of the nascent SCV from the plasma membrane is mediated by the T3SS virulence factor SopB (Terebiznik *et al.*, 2002), most likely in cooperation with SopD (Bakowski *et al.*, 2007), the host-cell factors involved in this process remain largely unknown.

Salmonella enterica serovar Typhimurium (*S.* Typhimurium) has been used as a model organism to study the role of phosphoinositides in bacteria-mediated manipulation of the host endocytic trafficking pathways (Kerr *et al.*, 2010). The

phosphoinositides are key regulators of the actin cytoskeleton and membrane trafficking and are indispensable for macropinocytosis and maturation of the SCV (Kerr MC, 2012). Specific membrane bound phosphoinositides are essential for recruitment of sorting nexins, a family of Phox homology (PX) domain containing proteins that orchestrate membrane trafficking, cargo sorting and endosomal recycling in coordination with other effectors including RabGTPases (Teasdale and Collins, 2012). Several sorting nexins (SNX), including SNX1, SNX3 and SNX5, have been functionally linked to remodelling of the SCV during early stages of S. Typhimurium infection (Bujny *et al.*, 2008; Shi *et al.*, 2009; Braun *et al.*, 2010) as well as to macropinosome biogenesis in non-infected cells (Bryant *et al.*, 2007; Lim *et al.*, 2008). Our recent screen of SNX-PX-BAR proteins involved in macropinocytosis identified another member of sorting nexin family, SNX18, which significantly increased the fluid phase uptake when overexpressed in epithelial cells (Wang *et al.*, 2010).

The function of SNX18 is still not well understood. Recent studies proposed that SNX18 might function as a paralog of SNX9 that is engaged in endosome formation and scission from the plasma membrane by coupling phosphoinositide recognition to actin assembly (Soulet *et al.*, 2005; Pylypenko *et al.*, 2007; Park *et al.*, 2010). SNX18 and SNX9 share relatively high protein sequence homology, identical SH3-PX-BAR domain modular structure and some binding partners (Haberg *et al.*, 2008; Park *et al.*, 2010). However, variations between the SNX9 and SNX18 expression profile within different cell lines (Park *et al.*, 2010), tissues (Haberg *et al.*, 2008) or embryonic stages (Nakazawa *et al.*, 2011), and differences in their affinity to particular membrane bound phosphoinositides (Haberg *et al.*, 2008; Yarar *et al.*, 2008) suggest that SNX18 and SNX9 may have evolved to perform different functions.

In this study, we investigate the function of SNX18 in *Salmonella*-driven exploitation of macropinocytosis during invasion of epithelial cells. We demonstrate that *S.* Typhimurium recruits SNX18, N-WASP and Dynamin-2 to the site of invasion through the phosphatidylinositol phosphatase activity of the T3SS effector SopB. We propose that modulation of phosphoinositides at the site of *S*. Typhimurium invasion recruits SNX18 as a scaffold to organize the molecular machinery required for formation and scission of the nascent SCV from the cell surface, which increases the efficiency of bacteria internalization.

RESULTS

SNX18 is recruited to the plasma membrane during *S.* Typhimurium invasion

We reported recently (Wang *et al.*, 2010) that SNX18 was the most potent of the three SH3-PX-BAR sorting nexins in increasing the EGF-stimulated macropinocytosis when transiently overexpressed in epithelial cells. Because macropinocytosis is targeted by *S.* Typhimurium, we first aimed to determine the role of SNX18 in *S.* Typhimurium invasion of epithelial cells by assessing the rate of macropinocytosis and efficiency of bacterial internalization in human embryonic kidney epithelial cells (HEK293) overexpressing EGFP-SNX18 and in HEK293 cells where endogenous levels of SNX18 were reduced by inducible shRNA-mediated knockdown. In EGFP-SNX18 transfected cells the SNX18 expression levels were approximately 20-fold higher than endogenous levels (Figure 2.1A), while the endogenous levels of SNX18 in the stable SNX18 shRNA cell line were below detection 6 days post induction of shRNA expression (Figure 2.1B). The efficiency of SNX18 knockdown was assessed by western blotting and the pGIPZ shRNA clone yielding the highest reduction (95%) in SNX18 protein levels was selected to generate pTRIPZ construct for inducible expression.

To analyze the effect of SNX18 expression levels on macropinocytosis, we measured the rate of macropinocytosis in each cell line by dextran uptake assay using fluorescently labelled dextran. Quantification of dextran-positive macropinosomes (integrated fluorescent density) in EGF-treated cells after 10 min of dextran uptake revealed 3-fold increase in cells expressing EGFP-SNX18 in comparison to controls, and a two-fold decrease in SNX18 knockdown cells relative to control knockdown (Figure 2.1C).

Next we investigated whether overexpression or knockdown of SNX18 affects internalization of *S.* Typhimurium. Cells were infected with mRFP-expressing *S.*

Typhimurium (SL-mRFP) and the amount of fully internalized bacteria was determined at 10 min post infection by quantitative fluorescence microscopy. Extracellular bacteria were differentiated from internalised bacteria by immunostaining of non-permeabilized cells with anti-LPS antibody. The amount of internalized bacteria was 32% higher in EGFP-SNX18 expressing cells when compared to EGFP-expressing control cells, while knockdown of SNX18 decreased the amount of intracellular bacteria by 29% relative to controls (Figure 2.1D). Thus, although depletion of SNX18 did not completely abolish macropinocytosis or bacteria internalization, modulation of SNX18 levels resulted in significant impact on both macropinocytosis and *S*. Typhimurium internalization. The observed increase in the levels of S.Typhimurium invasion in EGFP-SNX18 expressing cells was not due to increased passive uptake of bacteria from the media due to these cells having higher levels of macropinocytosis. Active invasion was determined by the monitoring the difference between the invasion of wildtype S.Typhimurium and that of invA mutant S.Typhimurium which are non-invasive but can be internalized passively when membrane ruffling/macropinocytosis is induced (Steele-Mortimer *et al.*, 2002). We observed a 21.5% increase in active invasion for wild-type S. Typhimurium in cells overexpressing SNX18, compared to the 27.8% increase in total invasion levels.

We next examined the subcellular localization and kinetics of EGFP-SNX18 in live HEK293 epithelial cells and RAW264.7 macrophages. Both of these cell types were selected as they undergo constitutive macropinocytosis with the majority of cells having numerous filopodia and also peripheral membrane regions exhibiting “ruffling”. This enables monitoring the capacity of S. Typhimurium to elevate the local recruitment of proteins like SNX18, within the modified plasma membrane regions. During transient expression in non-infected cells, EGFP-SNX18 localization varied with protein

expression levels, where high levels led to formation of elongated, thickened and often branched membrane tubules described previously in cells transfected with myc-tagged PX-BAR construct of SNX18 (Haberg *et al.*, 2008) (Figure 2.S1). Therefore, for further analysis we isolated cells expressing moderate levels of exogenous SNX18, where EGFP-SNX18 localized to the cytosol but a fraction was readily associated with endosomes and with short, endosome-derived tubules usually concentrated at the base of the cell where EGFP-SNX18 co-localized with fluorescent lipophilic vital stain FM4-64 (Figure 2.S2). Upon infection with *S*. Typhimurium, we observed a dramatic relocation of EGFP-SNX18 from the cytosol to the plasma membrane within 10 min post infection. A similar extent of SNX18 relocation was detected in RAW264.7 macrophages (Figure 2.2A) and in other human epithelial lines, including HeLa, MCF-7 and A431 (not shown), suggesting that *Salmonella*-mediated engagement of SNX18 is utilised in multiple cell types including those that do not undergo constitutive macropinocytosis like HeLa cells.

To investigate the dynamics of SNX18 recruitment to the plasma membrane during *S*. Typhimurium internalization, we performed live imaging of EGFP-SNX18-expressing HEK293 cells within the first 10 min of infection. Following docking of bacteria to the plasma membrane at the site of invasion, we observed a rapid burst of SNX18 recruitment within membrane ruffles when compared with non-infected cells, where a transient increase of SNX18 was detected only on the nascent macropinosomes. (Figure 2.2B and movie1). To examine the kinetics of SNX18 recruitment during early stages of infection, we next measured the amount of EGFP-SNX18 at the plasma membrane and cytosol at various time points post infection by quantitating the fluorescence density profiles of selected regions of interest. As shown in Figure 2.2B, the amount of EGFP-SNX18 at the plasma membrane rapidly increased 1.7-fold within the first minute of infection while the concentration (fluorescence density) of the cytosolic pool of SNX18

within the same cell decreased. In contrast, insignificant changes in fluorescent density of EGFP-SNX18 in both, plasma membrane and cytosol were observed in non-infected cells.

To further examine the bacteria-induced recruitment of SNX18 to the plasma membrane at site of invasion, we infected (or mock-infected) the EGFP-SNX18 expressing cells and analysed localization of this construct by electron microscopy using immunogold labelling on cryosections. In mock-infected cells, the gold-coupled marker of EGFP-SNX18 localized predominantly to the cytosol with only minor fraction (24±4.5%) found in plasma membrane, while in infected cells, the majority (58±5.5%) of the marker associated with the plasma membrane of bacteria-containing membrane ruffles and with the SCV during its closure at the cell periphery. In contrast, fully internalized SCV were devoid of SNX18 (not shown), suggesting that association of SNX18 with the SCV is only transient and occurs during the very early stage of the SCV formation (Figure 2.2C).

To confirm that also endogenous SNX18 is recruited to the plasma membrane the levels of cytosolic and membrane-bound SNX18 during bacteria internalization was then examined by cell fractionation and immunoblotting with anti-SNX18 antibodies. In agreement with the above results, the protein levels of membrane-bound endogenous SNX18 increased within the first 10 min of infection (Figure 2.2D) indicating that the presence of the EGFP-tag on SNX18 is not responsible for the induced recruitment to membranes observed during *S*. Typhimurium invasion in live cells.

Since some reports suggest that SNX9 and SNX18 have some redundant functions in plasma membrane remodelling during endocytosis (Haberg *et al.*, 2008; Park *et al.*, 2010), we also analysed cells expressing EGFP-SNX9, a paralog of SNX18, during *S*. Typhimurium invasion which revealed that the SNX9 recruits to the site of bacteria

internalization at the plasma membrane in a similar manner to that of SNX18 (Figure 2.S3). We also quantified *S*. Typhimurium internalization in cells where both SNX18 and SNX9 were depleted by inducible shRNA-mediated knockdown. Although only partial reduction of SNX9 protein levels was achieved we observed no additional impact on the efficiency of bacterial internalization in cells depleted of both SNX9 and SNX18 in comparison to SNX18 only knockdown cells (Figure 2.S4). Therefore SNX18 represents the major contributor to this phenotype on which we focused our further detailed investigation.

We thus identified SNX18 within two fractions: a mobile, cytosolic fraction and a membrane-bound fraction. Furthermore, we show that this ratio rapidly changes when SNX18 is recruited to the site of bacteria internalization. The kinetics of bacteria-induced SNX18 recruitment and the details of SNX18 localization within bacteria-containing membrane ruffles suggested that SNX18 is likely involved in the actin-driven remodelling of the plasma membrane which promotes formation of the nascent SCV.

SNX18 functions as a scaffold for molecular machinery driving formation and scission of the nascent SCV

The dynamics of SNX18 recruitment to the site of bacteria entry was next determined by live imaging at a higher spatio-temporal resolution. We observed a rapid increase in SNX18 at the site of bacterial docking, followed by recruitment of SNX18 to the edge of extending membrane ruffles that folded back to enclose bacteria, and continuous accumulation of SNX18 was then detected in the membrane of the nascent SCV during its formation and scission from the plasma membrane. The local increase in EGFP-SNX18 fluorescence density was detected within 10-20 sec following bacterial contact with the cell surface and the process of internalization and SCV scission was completed

within 1 min. Subsequently, SNX18 rapidly depleted from the fully internalized SCV (Figure 2.3A and movie2).

Next we addressed the possibility that SNX18 functions in actin-driven membrane reorganization leading to bacterial confinement within closing membrane ruffles and scission of the nascent SCV from the plasma membrane. To visualise actin dynamics during bacteria internalization, the EGFP-SNX18 expressing cells were transfected with LifeAct-Ruby, a fluorescent 17-amino acid peptide which detects filamentous actin (F-actin) structures in live cells (Riedl *et al.*, 2008), and infected with non-fluorescent *S*. Typhimurium in the presence of fluorescently coupled wheat germ agglutinin, which selectively binds to plasma membrane. Live imaging of these cells revealed that upon contact of bacteria with the cell surface, the burst of SNX18 correlates with a burst of actin polymerization during closure of the membrane ruffle around the nascent SCV and during SCV scission from the plasma membrane (within the first min of bacteria internalization). Once the SCV was fully internalized, SNX18 rapidly dissociated from the SCV followed by depolymerisation of the F-actin coat (Figure 2.3B). Recently it has been reported that SNX18 directly interacts with proteins required for endosome scission, Dynamin-2 and N-WASP (Park *et al.*, 2010). Importantly, both of these proteins are also involved in the internalization of *S*. Typhimurium (Unsworth *et al.*, 2004; Veiga *et al.*, 2007). To determine whether *S*. Typhimurium can recruit Dynamin-2 and N-WASP to the site of invasion via SNX18, we analyzed colocalization of SNX18 with Dynamin-2 and N-WASP in cells during bacteria internalization. Substantial colocalization of SNX18 with both Dynamin-2 and N-WASP was found within bacteria-containing membrane ruffles and on the nascent SCV (Figure 2.4A,B). However, a significantly lower degree of colocalization was found in cells that co-expressed Dynamin-2 or N-WASP with SNX18 mutant lacking the N-terminal SH3 domain

(SNX18:ΔSH3). Although the SNX18:ΔSH3 was recruited into *Salmonella*-induced membrane ruffles within 10 min of infection to a similar extent as the full length SNX18, its colocalization with Dynamin-2 and N-WASP was markedly reduced as shown on quantification of the colocalization within bacteria-containing membrane ruffles (Figure 2.4A, B).

Together, these results provide the evidence that *S*. Typhimurium triggers rapid recruitment of cytosolic SNX18 to the site of invasion to function in the actin-driven formation and scission of the nascent SCV from the plasma membrane together with Dynamin-2 and N-WASP. We propose that the SH3 domain is dispensable for SNX18 targeting to the plasma membrane but is required for recruitment of Dynamin-2 and N-WASP to distinct membrane subdomains of membrane ruffles during formation and closure of the nascent SCV.

Mutation of SNX18 impairs *S*. Typhimurium internalization

The above results suggested that the SNX18 can mediate the process of *S*. Typhimurium internalization into host cells by acting as a scaffold for the recruitment of Dynamin-2 and N-WASP via its SH3 domain. However, in cells over-expressing SNX18:ΔSH3, neither internalization of *bacteria* nor membrane ruffling was completely abolished, implying that in parallel to SNX18-mediated pathway, *S*. Typhimurium may utilize an alternative mechanism to enter the cells which also contributes to the overall efficiency of internalization.

Therefore, we next investigated whether transient overexpression of SNX18 mutants lacking the SH3 domain (SNX18ΔSH3) or phosphoinositide binding mutant (SNX18:R303Q) will affect the overall efficiency of bacteria internalization. The design of the phosphoinositide binding mutant was based on a structural study of SNX9 (a

paralog of SNX18), which demonstrated that mutation of the corresponding arginine (Arg286) within α1 loop of phosphoinositide-binding pocket abrogates SNX9 binding to liposomes (Pylypenko *et al.*, 2007). HEK293 cells were transfected with plasmids encoding wild-type or mutant SNX18 and infected with mCherry-expressing S. Typhimurium. The amount of internalized bacteria was determined by using a quantitative immunofluorescence assay. At 10 min post infection, cells overexpressing wild-type SNX18 exhibited a significantly higher number of internalized bacteria when compared with control cells. In contrast, a decrease in bacterial uptake was found in cells transfected with SNX18:ΔSH3 or SNX18:R303Q constructs relative to the control cells (Figure 2.5A). These results demonstrated that the efficiency of bacteria internalization is affected by loss-of-function mutations in SNX18.

To determine whether overexpression of SNX18:ΔSH3 and SNX18:R303Q mutants reduces bacteria internalization by interfering with the SCV formation, we analyzed the kinetics of this process by live cell imaging. As demonstrated above, the SNX18:ΔSH3 exhibited little difference in sub-cellular localization, recruitment to the site of bacterial internalization and transient association with the nascent SCV when compared to the full length SNX18. In contrast, the phosphoinositide-binding mutant SNX18:R303Q remained exclusively cytosolic and exhibited no change during bacterial internalization. Although the internalization of bacteria was not blocked in cells expressing the SNX18 mutants, we observed a distinct delay between docking of the bacteria on the host cell and completion of the internalization process (scission of the SCV from the plasma membrane) in comparison to cells expressing the full-length SNX18 construct (Figure 2.5B and movie3, movie4 and movie5).

Taken together, these data suggest that transient overexpression of SNX18:ΔSH3 or SNX18:R303Q may reduce the overall efficiency of *S*. Typhimurium internalization at

the onset of infection, likely through defects or a delay in the recruitment of proteins involved in formation and/or scission of the nascent SCV. Because the uptake of bacteria in cells overexpressing the SNX18 mutants was only partially reduced, as we observed for the SNX18 knockdown cells, we propose that the SNX18-mediated pathway may represent one of the two independent but complementary invasion mechanisms recently described for *S*. Typhimurium (Hanisch *et al.*, 2011) that are regulated either by SopB or by SopE/SopE2 effectors of SPI1-T3SS. When we compared the *S*. Typhimurium strain ST12023, which express SopB but not SopE, with the SL1344 strain used in our study, which expresses both SopB and SopE, both strains triggered the SNX18 recruitment to the site of bacteria internalization at the plasma membrane. However, the quantification of bacteria internalization revealed that the SopE-deficient strain ST12023 was more susceptible to depletion of SNX18 levels when compared to SL1344 strain (Figure 2.S5). This observed requirement of SNX18 for invasion of *S*. Typhimurium with a reduced capacity to utilise the SopE-dependent process, suggests that SNX18 functions via the SopB-mediated invasion mechanism.

Recruitment of SNX18 is triggered by *Salmonella* PtdIns-phosphatase SopB

Internalization of *S*. Typhimurium is mediated by orchestrated action of several SPI1-T3SS effectors, including SopB, SopD, SopE2, SptP, SipA and SipC that disrupt tight junctions and cell polarity (Boyle *et al.*, 2006), induce actin cytoskeleton remodelling (Cain *et al.*, 2008) and promote SCV formation (Terebiznik *et al.*, 2002; Hernandez *et al.*, 2004; Bakowski *et al.*, 2007). We therefore reasoned that the recruitment of SNX18 to the sites of bacterial invasion may be triggered by one or more of these effectors.

First we analyzed whether SNX18 mobilization in infected cells is dependent on activity of SPI1-T3SS and independent of SPI2-T3SS. The SPI1-T3SS deficient mutant of

S. Typhimurium, Δ*invA*, is non-invasive and its contact with the EGFP-SNX18 expressing cells also failed to induce SNX18 relocation to the site of bacterial attachment at the cell surface. In turn, when cells were infected with the SPI2-T3SS deficient mutant, Δ*ssaR*, a burst of SNX18 was detected at the site of bacteria internalization to the extent similar to cells infected with the wild type bacteria (Figure 2.6A). To examine whether a particular SPI1-T3SS effector is sufficient to trigger SNX18 recruitment, we used transient ectopic expression of myc-tagged constructs of individual SPI1-T3SS effectors in cells with stable expression of EGFP-SNX18. To minimize potential toxicity of effectors on the cell structure and functions, the cells were fixed and analysed early at 4-6 hrs post transfection when constructs were become detectable by indirect immunofluorescence. Our screen revealed that SNX18 retained its cytosolic localization except when coexpressed with SopB, where a substantial fraction of SNX18 accumulated in plasma membrane (Figure 2.6B). Although SNX18 remained cytosolic when co-expressed with the other SPI1 effectors, we did observe extensive membrane ruffles in SopE2-expressing cells and impaired actin cytoskeleton organisation in cells expressing SipA, SipC and SptP, which is consistent with the function of these effectors previously reported in the literature (Pizarro-Cerda and Cossart, 2004; Haglund and Welch, 2011).

To confirm that SopB is essential and sufficient for SNX18 recruitment to the sites of bacterial invasion, we next infected cells with an isogenic *sopB* mutant of *S*. Typhimurium (Δ*sopB* mutant). In comparison to the wild type *S*. Typhimurium, the Δ*sopB* mutant failed to recruit cytosolic SNX18 to the plasma membrane and to the site of bacterial internalization (Figure 2.7A). Moreover, quantification of bacterial internalization revealed that the reduction in numbers of internalized wild type *S*. Typhimurium (SLwt) in SNX18 knockdown cells can be restored by transient

overexpression of myc-tagged SNX18. In contrast, numbers of internalized mutant (SLΔ*sopB*) were not significantly changed in SNX18 knockdown cells relative to control knockdown cells (Figure 2.7B). Together, these results further confirm that SNX18 functions in SopB-mediated internalization pathway of bacteria.

We next aimed to determine whether SNX18 recruitment was dependent on the ability of SopB to modify phosphoinositides. We constructed myc-tagged mutants of SopB that have been shown to abolish the phosphoinositide phosphatase activity of this effector: C460S, R466A and K528A (Drecktrah *et al.*, 2004). In cells co-expressing EGFP-SNX18 with wild type SopB, a substantial amount of SNX18 localized to the plasma membrane, while SopB localized primarily to enlarged endosomal structures most likely induced as a result of PtdIns(3)P accumulation at their membrane (Figure 2.7C). In contrast, all three SopB mutants localized to the plasma membrane and small peripheral endosomal structures, suggesting they still can associate with the plasma membrane but fail to induce accumulation of enlarged PtdIns(3)P-positive endosomes. The coexpression of SopB mutants did not alter the predominantly cytosolic localization of SNX18 and neither wild type myc-SopB nor the myc-tagged sopB mutants colocalized with SNX18. Importantly, the failure of Δ*sopB* mutant bacteria to trigger SNX18 relocation to the membrane ruffles was fully restored when *sopB* was expressed from a plasmid in strain SLΔ*sopB*+pSopB. However, complementation was not achieved with introduction of plasmids encoding the inositolphosphatase-deficient mutant of SopB (C460S) (Figure 2.7D). Furthermore, SopB activates Akt/protein kinase B in epithelial cells infected by S. Typhimurium (Steele-Mortimer *et al.*, 2000) and lack of Akt activation in cells infected with Δ*sopB* mutant was efficiently restored in cells infected with SLΔ*sopB*+pSopB strain (data not shown) what implies that the plasmid-encoded SopB in SLΔ*sopB* was efficiently translocated to infected cells.

Since SopB can also indirectly enhance Rho GTPase activation (Patel and Galan, 2006), we next examined whether SNX18 recruitment to the plasma membrane occurs independently or as a consequence of Cdc42 and/or Rac1 activation. Upon expression of constitutively active (CA) forms of Rac1 or Cdc42 in non-infected cells, Rac1 and Cdc42 localized to the plasma membrane and Rac1 induced formation of extensive membrane ruffles. However, in both cases SNX18 retained its cytosolic localization. Expression of dominant negative (GTPase-defective) forms of Cdc42 and Rac1 did not inhibit SNX18 recruitment to the site of bacterial invasion (Figure 2.S6) and inhibition of Rac1-GTPase activity by specific, cell-permeable and reversible inhibitor NSC23766 did not perturb SNX18 recruitment to the site of bacteria internalization (Figure 2.S7).

Collectively, these results demonstrate that relocation of SNX18 to *Salmonella*-induced membrane ruffles occurs independently of Cdc42 and Rac1 activation and that the PtdIns-phosphatase activity of SopB is necessary and sufficient to drive SNX18 recruitment. However, SNX18 and SopB probably do not directly interact, in agreement with our co-immunoprecipitation experiments detecting no interaction between SNX18 and ectopically expressed SopB (not shown).

SNX18 recruits to membrane subdomains enriched in PtdIns(3,4)P2

Given that the phosphoinositide binding of SNX18 is essential for membrane recruitment, and this recruitment is dependent on the PtdIns-phosphatase activity of SopB, we next investigated whether SNX18 is recruited to the plasma membrane subdomains in response to SopB-mediated manipulation of phosphoinositide composition, since it has been previously reported that SopB is essential for local increase in PtdIns(3,4)P2 and PtdIns(3,4,5)P3 and depletion of PtdIns(4,5)P2 at

Salmonella-induced membrane ruffles (Terebiznik *et al.*, 2002; Mason *et al.*, 2007; Mallo *et al.*, 2008).

To visualize the local enrichment or depletion of particular membrane-bound phosphoinositides at the site of bacterial invasion, we transfected HEK293 cells with EGFP-tagged fusion constructs of (i) FERM domain of Ezrin, (ii) Pleckstrin Homology (PH) domain of Akt (also known as Protein Kinase B) or, (iii) 2xFYVE domain construct of mouse Hrs protein (hepatic growth factor-regulated tyrosine kinase substrate). The FERM-EGFP construct recognizes and binds to PtdIns(4,5)P2 while EGFP-AKT-PH construct has affinity to PtdIns(3,4)P2 and/or PtdIns(3,4,5)P3 and 2xFYVE-EGFP has been used as a highly selective probe of PtdIns(3)P (James *et al.*, 1996; Barret *et al.*, 2000; Pattni *et al.*, 2001). Following infection of these cells with mRFP-expressing bacteria, the FERM-EGFP with exclusive plasma membrane localization became markedly enriched at the cell periphery likely in response to an increase in membrane ruffling triggered by invading bacteria. However, closer inspection of membrane ruffles revealed a substantial local depletion of FERM-EGFP at the sites of bacterial internalization within these membrane subdomains and no association of FERM-EGFP was detected on fully internalized SCV (Figure S8). The EGFP-AKT-PH construct localized preferentially to the plasma membrane and to *Salmonella*-induced ruffles and exhibited substantial increase in fluorescence density around bacteria during the SCV formation but not around fully internalized SCV (Figure S8). In cells expressing the 2xFYVE-EGFP, the construct localized to tubular endosomal structures, exhibited a limited recruitment to the site of bacterial invasion, but associated markedly with fully internalized SCV (Figure S8). These results demonstrate that a transition occurs between accumulation of PtdIns(3,4)P2/PtdIns(3,4,5)P3 and PtdIns(3)P on the

membrane of the SCV during early steps of the organelle biogenesis, which is in agreement with previous reports (Pattni *et al.*, 2001; Mallo *et al.*, 2008).

To determine whether SNX18 recruits simultaneously to the same membrane subdomains as EGFP-AKT-PH construct, we monitored the dynamics of EGFP-AKT-PH and mCherry-SNX18 recruitment in live cells during the *S*. Typhimurium internalization. A substantial amount of EGFP-AKT-PH localized to the plasma membrane prior to infection, yet a distinct increase in EGFP fluorescence intensity was detected at the site of bacterial internalization. Moreover, kinetics of relative increase in fluorescence intensity indicated that Akt-PH and SNX18 recruited simultaneously to bacteria-induced membrane ruffles within the first 30 seconds of bacteria internalization (Figure 2.8A and movie6). Since the EGFP-AKT-PH probe does not distinguish between PtdIns(3,4)P2 and PtdIns(3,4,5)P3, we next aimed to determine whether SNX18 exhibits selective affinity to one of these phosphoinositides. For this, we coexpressed mCherry-SNX18 with EGFP-tagged PH domain of Tandem PH-domain containing protein (TAPP1) or with EGFP-tagged PH domain of Bruton's tyrosine kinase (Btk). The PH domain of TAPP1 possesses specific affinity to PtdIns(3,4)P2 (Dowler *et al.*, 2000), while the PH domain of Btk binds exclusively to PtdIns(3,4,5)P3 (Salim *et al.*, 1996). The SNX18 and TAPP1-PH became simultaneously enriched at the site of bacterial docking and internalization and a substantial increase in colocalization was detected during this process (Figure 2.8B and movie6). In contrast, we detected little increase in Btk-PH at the site of bacterial invasion and colocalization with SNX18 was below detection level (Figure 2.8C and movie6). Moreover, in cells overexpressing SNX18 together with AKT-PH or TAPP1-PH constructs the burst of SNX18 recruitment at the plasma membrane triggered by invading bacteria was notably attenuated in comparison to cells expressing mCherry-SNX18 alone or together with the Btk-PH-EGFP. These data suggest that

SNX18, TAPP1-PH and AKT-PH can compete for binding to PtdIns(3,4)P2 and that SNX18 is recruited to membrane subdomains selectively enriched in PtdIns(3,4)P2.

Since we observed the simultaneous burst of SNX18 and Akt within *Salmonella*-induced membrane ruffles, we were interested whether SNX18 recruitment is dependent on the activation of Akt, which can also be triggered by the inositol phosphatase activity of SopB (Steele-Mortimer *et al.*, 2000). Pre-treatment of cells with Akt-specific inhibitor AKTi1/2 did not markedly perturb recruitment of EGFP-SNX18 to the site of bacteria invasion, while the phosphorylation of Akt elicited by wild type *S*. Typhimurium (but less by Δ*sopB* mutant) at 10 min post infection was completely abolished (Figure 2.S9).

Taken together, these results demonstrate that SNX18 translocates to *Salmonella*-induced membrane invaginations in response to SopB-mediated accumulation of PtdIns(3,4)P2 and that SNX18 recruitment occurs together with Akt but independently of Akt activation.

DISCUSSION

S. Typhimurium orchestrates its internalisation into host cells through the action of multiple SPI1-T3SS effectors, which hijack the host macropinocytosis pathway for bacterial uptake. A critical step in this pathway is the formation and scission of the nascent SCV mediated by dynamin-2 and N-WASP, however the precise mechanism of the recruitment of these proteins to the sites of bacterial invasion has not been described. Here we identify a function for SNX18 in this process and demonstrate that engagement of SNX18 occurs via the action of the *Salmonella* SPI1-T3SS effector SopB. The recruitment of SNX18 to the plasma membrane is induced by the expression of SopB alone and SopB's phosphatidylinositol phosphatase activity is essential for the spatial and temporal recruitment of SNX18 induced during *S*. Typhimurium invasion. Furthermore mutation of the phosphoinositide binding site within the PX domain of SNX18 completely abolished SNX18 recruitment to the plasma membrane. We propose that activated SNX18 binds to phosphoinositides locally modified during *Salmonella* invasion and functions as a membrane scaffold for the recruitment of the molecular components of actin-driven membrane remodelling. This study identified SNX18 as a novel target of *S*. Typhimurium and we propose that in contrast to other sorting nexins that have been previously linked to the SCV maturation, SNX18 is engaged at the onset of bacterial internalization to function in biogenesis of membrane ruffles and macropinocytosis. Hereby *S*. Typhimurium recruits SNX18 and its associated proteins via inositol-phosphatase activity of SopB to locally and transiently upregulate macropinocytosis and thus facilitate invasion of the host cell. Nevertheless, the invasion process is - in parallel - orchestrated and dependent on additional Salmonella effector proteins including SopE/E2 which allows S. Typhimurium to fine-tune the efficiency of invasion into various cell types and/or via multiple endocytic pathways. While SNX18

has recently been shown to promote autophagosome formation (Knaevelsrud *et al.*, 2013), the function of SNX18 in *S*. Typhimurium internalization which we describe in our study will likely be independent of any role in the clearance of intracellular *S*. Typhimurium by autophagy at later stages of infection.

Studies on the mechanism of *Salmonella* internalization have been complicated by an array of strategies these bacteria have developed to invade macrophages and polarized or non-polarized epithelial cells, and to activate or suppress various host cell signalling pathways. Thus blocking of a single pathway often results in insignificant changes in the ability of *Salmonella* to invade cells. So far, only cytochalazin D has been found to completely block *S*. Typhimurium internalization in both epithelial cells and macrophages (Finlay *et al.*, 1991; Forsberg *et al.*, 2003), highlighting the indispensable role of actin cytoskeleton remodelling for bacteria entry. Moreover, two independent but complementary mechanisms of SopE-dependent and SopB-mediated internalization pathways of *S*. Typhimurium have been described (Stender *et al.*, 2000; Hanisch *et al.*, 2011). The first is characterized by the activation of Rac1/Cdc42 followed by activation of WAVE and WASH complex and Arp2/3-mediated actin polymerization, leading to extensive membrane ruffle formation, while the second is mediated by Rho kinase and Myosin II activity and occurs through plasma membrane invaginations without membrane ruffling (Stender *et al.*, 2000; Hanisch *et al.*, 2011). Indeed, we observed that bacteria entered the cell by two morphologically distinct mechanisms, but how these mechanisms differ at the molecular level is difficult to discern because both pathways seems to be utilized when multiple bacteria infect a single cell.

We found that cells overexpressing SNX18 exhibited a considerably increased rate of macropinocytosis, whereas the impact on *S*. Typhimurium internalization was relatively mild. Similarly, in SNX18 knockdown cells, the rate of macropinocytosis was reduced to

a greater extent than internalization of bacteria. We argue that since *S*. Typhimurium infection elevates macropinocytosis via action of SPI1-T3SS effectors, any additional gain from the direct expression of SNX18 might be limited. The fact that we observed only partial reduction in bacterial internalization efficiency in SNX18 knockdown cells may reflect the ability of bacteria to trigger the internalization process via a complementary mechanism which can be independent of SopB and SNX18. It will be interesting to find whether *S*. Typhimurium utilizes multiple pathways simultaneously or possesses an ability to fine-tune the invasion efficiency according to environmental cues. Nevertheless, the reduced invasiveness of SopB-deficient mutant of *S*. Typhimurim strain SL1344 or that of the wild type of SopE-deficient strain ST12023, both reported in the literature (Bakowski *et al.*, 2007; Clark *et al.*, 2011), suggests that the ability of these bacteria to trigger and utilize multiple internalization mechanisms enhances the net invasion efficiency. Thus, although we do not question that *S*. Typhimurium can utilize complementary pathway(s), our study describes the role of SNX18 in SopB-dependent invasion mechanism which significantly facilitates bacterial internalization.

The cells overexpressing the SNX18 mutant ΔSH3 or R303Q exhibited a mild but significant decrease in bacterial invasion yet the mechanism by which they interfere is unclear. The most likely explanation is that upon recruitment to the plasma membrane, the SNX18:ΔSH3 can interact with the endogenous pool of SNX18 resulting in production of a higher amount of SNX18 dimers with a reduced functionality. In contrast, similar pseudo-dimer formation between SNX18:R303Q and endogenous SNX18 would induce partial cytosolic retention of SNX18. Indeed, we did not detect any increase in fluorescence intensity of SNX18:R303Q at the site of bacterial internalization or at any other membrane subdomains. Nevertheless, Sorting nexin 9, 18 and 33 can readily be found as homodimers when isolated from cell lysates. Formation of

heterodimers between SNX9-SNX18 and SNX9-SNX33 *in vitro* has been previously reported (Zhang *et al.*, 2009; Park *et al.*, 2010), but not confirmed by a recent study (van Weering *et al.*, 2012) and ourselves (data not shown), and whether possible heterodimers represent functional units in intact cells *in vivo* still remains to be determined.

Interaction between SNX18 and membrane-bound phosphoinositides is essential for regulation of SNX18 function, yet the phosphoinositide specificity of SNX18 PX domain remains unclear. Filter binding assays and liposome co-sedimentation experiments using a GST fusion of SNX18 PX domain or PX-BAR module identified affinity for PtdIns(3,4)P2, PtdIns(3,5)P2 and PtdIns(4,5)P2 (Haberg *et al.*, 2008; Nakazawa *et al.*, 2011) and similar broad lipid specificity has also been reported for SNX9 (Shin *et al.*, 2008; Yarar *et al.*, 2008). However, the specificity of SNX18 and/or SNX9 for individual phosphoinositides in live cells is unknown. Using live cell imaging, our study provides insight into the recruitment of SNX18 to membrane subdomains enriched in PtdIns(3,4)P2 and highlights the importance of cell context in this assay because the spatio-temporal aspects of recruitment or depletion of phosphoinositide binding proteins is difficult to characterize by biochemical approaches. It is important to note that even transient overexpression of phosphoinositide sensing probes may imbalance the phosphoinositide metabolism by irreversible binding of these probes to particular phosphoinositide subspecies. This, as our results suggest, would also lead to affinity-dependent competition between SNX18 and the probes for binding PtdIns(3,4)P2. Nevertheless, our conclusions were based on comparison of recruitment kinetics between SNX18 and individual PtdIns-probes and the kinetics seemed to be comparable to that of cells expressing SNX18 without the PtdIns-probes.

Identification of SNX18 as a host cell factor involved in SopB-mediated formation of the nascent SCV at the plasma membrane builds upon the previously described role of SopB (formerly SigD) in hydrolysis of PtdIns(4,5)P2 during this process (Terebiznik *et al.*, 2002). Terebiznik et al (2002), demonstrated that the break-down of PtdIns(4,5)P2 in cells expressing SigD/SopB reduced the rigidity of the plasma membrane, suggesting that local PtdIns(4,5)P2 depletion may increase susceptibility of membrane for curvature and fusion (Terebiznik *et al.*, 2002). Therefore besides the phosphoinositide sensing PX domain, the curvature-sensing BAR domain of SNX18 is likely equally important for SNX18 recruitment to membrane invaginations and its (indirect) function in the SCV scission.

It has been reported that SopB may act on several substrates *in vitro* including PtdIns(3,4)P2, PtdIns(3,5)P2, PtdIns(4,5)P2 and PtdIns(3,4,5)P3 (Norris *et al.*, 1998; Marcus *et al.*, 2001). However, a more recent study has shown that concentration of PtdIns(3,4)P2 and PtdIns(3,4,5)P3 in *S.* Typhimurium invasion ruffles actually increases, likely by activation of class II PI3-kinases via PtdIns(5)P as a product of SopB-mediated hydrolysis of PtdIns(4,5)P2 (Mallo *et al.*, 2008). We propose that the transient local increase in PtdIns(3,4)P2 may be the driving cue for recruitment of SNX18, together with other phosphoinositide sensing factors like Akt. Plasma membrane recruitment of Akt is coupled with activation by phosphorylation (Steele-Mortimer *et al.*, 2000; Marcus *et al.*, 2001), but whether SNX18 requires activation for relocation or becomes activated upon plasma membrane recruitment still remains to be determined. A possibility remains open that to trigger SNX18 relocation the sole increase in PtdIns(3,4)P2 is not sufficient and may require an additional stimulus linked directly or indirectly to the activity of SopB.

It has been shown that upon delivery to the host cell the SopB targets SH3-containing GEF and thus can indirectly activate RhoG (Patel and Galan, 2006) that promotes Rac1 activation and membrane ruffling. Although we demonstrate that SopB-mediated recruitment of SNX18 to the plasma membrane occurs independently or upstream of Rac1 activation (Fig 2.S6, 2.S7) together with recruitment of Dynamin-2 and N-WASP, it remains to be determined whether SNX18 or SopB are also involved in activation of the GTPase activity of Dynamin-2 or in N-WASP activation of Arp2/3 machinery.

The study we present extends our understanding of *S*. Typhimurium-driven exploitation of the host molecular machinery that allows it to invade and replicate within epithelial cells. We propose that SNX18 and/or other sorting nexins are also involved in the uptake of other bacterial pathogens. It has also been reported that Enteropathogenic *Escherichia coli* (EPEC) secreted protein F (EspF) can directly interact with the SH3 domain of SNX9 and N-WASP to promote EPEC invasion via N-WASP/Arp2/3–mediated actin nucleation (Marches *et al.*, 2006; Alto *et al.*, 2007). However, EPEC induces a local increase of PtdIns(3,4,5)P3 at the site of attachment indirectly via recruitment of phosphatidylinositol 3-kinase in a translocated intimin receptor (Tir)-dependent manner (Sason *et al.*, 2009). Therefore, it is possible that EPEC may recruit SNX9 by an indirect mechanism similar to that of SopB-mediated recruitment of SNX18. In relation to this, the close *Salmonella* relative *Shigella flexneri* utilizes a SopB homologue (IpgD) for activation of PI3K/Akt-survival pathway. IpgD possesses a similar activity *in vitro* and its intact inositol 5'-phosphatase-homology motif is essential for Akt activation (Marcus *et al.*, 2001). However, whether *Shigella* or other bacterial pathogens have developed a similar strategy to exploit the endocytic machinery of the host cell by recruitment of scaffolding proteins from SH3-PX-BAR sorting nexin family remains to be verified.

MATERIALS and METHODS

Antibodies and reagents

The following primary antibodies were used: Rabbit polyclonal anti-SNX18 IgG (AbCam, ab99035); mouse monoclonal anti-myc (Cell Signalling Technology, 2272); Rabbit polyclonal anti-β-Tubulin (LI-COR Biosciences, 926-42211); mouse monoclonal anti-α-tubulin Clone DM 1A (Sigma Aldrich, T9026), anti-α1 Na+/K+ ATPase antibody (ab7671, Abcam), mouse monoclonal anti-LPS (Abcam, ab 8274); Mouse anti-Phospho-Tyrosine antibody, clone 4G10 (Millipore, 05-1050); mouse monoclonal anti-HA (Covance); Rabbit monoclonal anti-Akt (pan) C67E7 (Cell Signalling, 4691) and anti-phospho-Akt (Ser473) D9E (Cell Signalling, 4060). Goat anti-mouse coupled to Alexa fluor 405, 546 or 647 (Invitrogen) were used as secondary antibodies for immunofluorescence. The IRDye800CW goat anti-mouse IgG; IRDye800CW donkey anti-rabbit IgG; IRDye680LT goat anti-rabbit IgG and IRDye680LT donkey anti-mouse IgG were purchased from LI-COR Biosciences. Phalloidin-Alexa Fluor 635, fixable analog of lipophilic membrane stain FM 4-64FX and Wheat germ agglutinin (WGA) coupled to Alexa fluor 647 were from Invitrogen (A34054, F34653 and W324666). Selective inhibitor of Rac1-GEF interaction NSC 23766 was purchased from Tocris Bioscience and the Akt1/2 kinase inhibitor from Sigma Aldrich.

Plasmids and constructs

The Dynamin-2 encoding construct pCBDYN2-HA was obtained from Dr. S.L. Schmid (Scripps Research Institute, La Jolla, CA). The 2xFYVE-EGFP construct was generated as described by Pattni et al. (Pattni *et al.*, 2001) and provided by F. Meunier (University of Queensland, Australia). The construct expressing EGFP-tagged PH domain of Akt was a gift from Prof. C. Mitchell (Monash University, Australia) and the PH domain of TAPP1

(aa 95–400) for generation of EGFP-TAPP1-PH was a gift from Dr. S. Dowler (MRC, University of Dundee, Dundee, UK). The following expression vectors have been described previously: The pEGFP-C1-N-WASP(Lommel *et al.*, 2001), the pcDNA3 expression vectors encoding constitutively active Rac1 or Cdc42 and dominant negative Rac1 or Cdc42 (Wang *et al.*, 2005), the pEGFP-FERM (Marion *et al.*, 2011), the pEGFP-SNX18 and pEGFP-SNX18:ΔSH3 (Wang *et al.*, 2010), the Btk-PH-GFP (Varnai *et al.*, 1999). The LifeAct-Ruby construct was a gift Roland Wedlich-Söldner, Max Planck Institute of Biochemistry, Germany).

The pEGFP-SNX18:R303Q was generated by site-directed mutagenesis from the full length pEGFP-SNX18. Cloning of N-terminal-myc-tagged *S*. Typhimurium effectors was performed by ligation-independent cloning (LIC) (Aslanidis and de Jong, 1990) into the plasmid pcDNA3.1-nMyc-LIC, constructed as follows: A DNA cassette encoding a Myc tag, LIC sequences, chloramphenicol acetyl transferase (*cat*) and *ccdB* was constructed by PCR using primers N-Myc-catccdB-NheI-S and catccdB-ApaI-A and Reading Frame Cassette A template DNA from the Gateway Vector Conversion System (Life Technologies); The resulting PCR product was digested with NheI-ApaI and ligated into NheI-ApaI-digested pcDNA3.1(+). The resulting plasmid, pcDNA3.1-nMyc-LIC, was maintained in *E. coli ccdB* Survival™2 T1^{R} cells (Life Technologies). For LIC reactions, pcDNA3.1-nMyc-LIC was digested with EcoRV and treated with T4 DNA polymerase in the presence of dCTP to generate linearised vector with single-stranded DNA overhangs. The genes encoding individual *S*. Typhimurium effectors were amplified by PCR using primers which incorporated 5' and 3' LIC sequences and *S*. Typhimurium SL1344 template DNA. Each PCR product was treated with T4 DNA polymerase in the presence of dGTP to generate single-stranded overhangs. The polymerase-treated vector and effector DNA fragments were combined on ice and transformed into chemically-

competent *E. coli* DH5α. Vectors encoding Myc-tagged phosphatase inactive SopB mutants SopB:C460S, R466A and K528A were constructed by PCR amplification using pcDNA3.1 (+) vector encoding Myc-tagged SopB (wild type) as a template. All mutants were constructed using the QuikChange XL-site directed mutagenesis kit (Stratagene) according to manufacturer's instructions, and sequences were confirmed by direct DNA sequencing at AGRF (Australian Genome Research Facility). All primers used in this study are listed in Table 2.1.

Cell culture, transfections and generation of SNX18 knockdown

Human epithelial HEK293 cells (CRL-1573) and mouse macrophages RAW264.7 (TIB-71) were grown in complete DMEM medium (Life technologies) supplemented with 10% FCS. Cells were transfected using Lipofectamine 2000 (Invitrogen). For stable expression, transfected cells were selected with 400 μg/ml Geneticin (G418), and cell lines were generated by limit dilution. To generate the shRNA-mediated knockdown of SNX18, the pGIPZ-shRNAmir clones (V2LHS_184681, V2LHS_37858, V2LMM_58706) complementary to human SNX18 and pTRIPZ vector were obtained from Thermo Scientific. HEK293 cells were transfected with pGIPZ constructs using Lipofectamine 2000 (Invitrogen) and non-silencing shRNA was transfected as a control. Cells were split 24 h post transfection and selected in 1 μg/ml puromycin for 3 or more days before SNX18 protein levels were tested by western blot. After validation of the most efficient knockdown, the shRNA clone V2LHS_184681 was subcloned into XhoI-MluI-digested pTRIPZ for inducible expression of shRNA. The pTRIPZ-SNX9-SNX18 double knockdown was generated by subcloning shRNA sequence from validated clone V2LHS9297 (SNX9) into HpaI-XhoI-digested pTRIPZ-SNX18 construct. Cells were then transfected as above, selected with 1 μg/mL puromycin for 7 days to generate stable cell

lines and the shRNA expression was induced with 1 µg/mL Doxycycline for 7 days. Non-induced cells were used as a control knockdown.

Bacteria strains and infections

Wild type *Salmonella enterica* serovar Typhimurium strain SL1344 expressing pBR-mRFP.1 (Birmingham *et al.*, 2006) or pFPV25.1-GFP (Knodler *et al.*, 2005) were used in this study. S. Typhimurium strain ST12023 (NCTC12023) expressing pFPV-mCherry has been described earlier (Rajashekar *et al.*, 2008) and was kindly provided by Prof. M. Hensel (University of Osnabrueck). The isogenic Δ*sopB* mutant has been described earlier (Steele-Mortimer *et al.*, 2000) and provided by Dr. N. Brown (Department of Microbiology and Immunology; University of Melbourne; Australia). The *S.* Typhimurium SL1344 mutants Δ*invA* (SPI1-T3SS deficient) and Δ*ssaR* (SPI2-T3SS deficient) were provided by Prof. R. Strugnell (University of Melbourne, Australia) (Kupz *et al.*, 2012). Where non-fluorescent bacteria were utilized, the mouse monoclonal anti-LPS antibody (Abcam) was used for immunofluorescent detection. To prepare invasive (SPI1-T3SS activated) bacteria, the overnight culture was subcultured 1:60 in LB medium and grown for another 4 hrs to reach late log phase. Bacteria were washed three-times in Hanks buffered salt solution (HBSS) and diluted in serum-free DMEM medium (for immunofluorescence) or in CO2-independent imaging medium (Invitrogen) for live imaging.

For complementation of SopB in *S*. Typhimurium Δ*sopB* mutant bacteria, the coding sequence of the wild type *sopB* and that of the C460S mutant of *sopB* were amplified by PCR using pcDNA3.1 (+) vector encoding Myc-tagged SopB (wild type) or Myc-tagged C460S mutant of SopB as templates. Corresponding primers used for the PCR are listed in Table 2.1. The PCR products were digested with EcoRI and XhoI and subcloned into

pWSK29 vector (GenBank: AF016889.1). The sequence verified plasmids were transformed into electrocompetent *S*. Typhimurium Δ*sopB* mutant bacteria by electroporation using Bio Rad Gene Pulser II Electroporation System and positive clones of complemented *S*. Typhimurium were selected using kanamycin.

Electron microscopy

The HEK293 cells expressing EGFP-SNX18 were infected (or mock infected) with *S*. Typhimurim (SL1344) for 10 min, fixed with 4% formaldehyde and 0.1% glutaraldehyde in 0.1 M phosphate buffer and embedded in 10% gelatine (Sigma). Solidified gelatine blocks were infiltrated with 2.3 M sucrose, mounted on aluminium pins and frozen in liquid nitrogen. Ultrathin sections were cut on Leica EM UC6 cryotome, collected on a drop of sucrose–methylcellulose and transferred on carbon-coated CuPd EM grids with formvar film. EGFP-SNX18 was detected on sections by rabbit anti-GFP antibody (Molecular Probes) followed by protein A coupled with 10 nm gold (CMC Utrecht). Grids were contrasted, embedded in mixture of uranyl acetate–methylcellulose and analyzed with JEOL 1011 electron microscope operating at 80 kV. Micrographs were acquired by microscope-mounted CCD camera and ImageJ software (version 1.46a) was used for contrast adjustment and cropping of the final images. Manual quantification of gold marker localization was performed on micrographs by scoring each gold particle in a set of images for localization in plasma membrane or in cytosol.

Subcellular Fractionation and western blotting

HEK293 cells expressing EGFP-tagged SNX18 were serum starved overnight before bacterial infection at MOI=100 or mock infection. At 10 min post infection, cells were

washed twice with ice-cold PBS and harvested for subcellular fractionation using a modification of the protocol described by Piper et al., 1991 (Piper *et al.*, 1991). Briefly, cells were resuspended in HES buffer (20 mM HEPES, pH 7.4, 0.25 mM sucrose, 1mM EDTA, 10 mM sodium pyrophosphate, 30 mM sodium vanadate, 0.5 mM AEBSF and protease inhibitor cocktail), homogenized and centrifuged at 17,200 g for 20 min to generate crude plasma membrane (PM) fraction and a fraction containing cytosol and microsomes. The cytosol fraction was then purified by microsome sedimentation at 180,000 g for 60 min. Crude PM fractions were washed once and resuspended in HES buffer, and then layered onto 1.12 M sucrose cushion, containing 20 mM HEPES, pH 7.4, 1.12 M sucrose and 1 mM EDTA, followed by centrifugation at 100,000 g for 1 hr to yield a white interface, which contains the purified PM fraction. The white interface was mixed with HES buffer, and centrifuged at 125,000 g for 30 min to pellet the purified PM fraction. For protein electrophoresis, 30 μg of total protein of whole cell lysate or cytosol fractions or 15 μg of total protein of the plasma membrane fractions were loaded on to 8% SDS-PAGE gel and transferred onto a PVDF membrane (Immobilon-FL, Millipore) according to manufacturer's instructions. Western immunoblots were performed with anti-SNX18, anti-α-Tubulin and anti-Na+/K+ ATPase primary antibodies in Odyssey blocker, followed by IRdye800 anti-rabbit secondary antibody, and membranes were scanned using Odyssey Infrared Imaging System (LI-COR Biosciences) according to manufacturer's instructions. The integrated intensity of each band of interest was measured by Odyssey software.

AKT inhibitor treatment and *S*. Typhimurium infection

Overnight serum-starved HEK293 cells were pre-treated with 10 μM AKTi1/2 (Sigma-Aldrich) for 30 min before infection with *S*. Typhimurium (wild type or Δ*sopB*). At 10

min post infection, cells were washed with ice-cold PBS and harvested in lysis buffer (50 mM HEPES (pH 7.4), 1% Triton x-100, 150 mM sodium chloride, 1mM EDTA, 10 mM sodium pyrophosphate, 30 mM sodium vanadate, 0.5 mM AEBSF and protease inhibitor cocktails). Cell lysates were cleared by centrifugation at 16,000 g for 10 min and protein concentrations were quantified by BCA protein assay. Equal amounts of cell lysates were subjected to SDS-PAGE and immunoblotting, staining with anti-phospho Ser^{473} Akt, anti-Akt or anti-Tubulin antibodies, followed by IRdye800 anti-rabbit or IRdye680 anti-mouse secondary antibodies. Fluorescence intensities were detected using the LI-COR Biosciences Odyssey Infrared Imaging system.

Immunofluorescence

For immunofluorescence, cells were grown on poly-L-lysine (PLL)-coated glass coverslips, fixed with 4% formaldehyde in 250mM HEPES and permeabilized with Triton X-100 (0.25% in PBS) before incubation with antibodies. Where non-fluorescent bacteria were used, cell permeabilization was required prior to bacteria immunodetection with anti-LPS antibody. For detection of extracellular and/or incompletely internalized mRFP-expressing bacteria, cells were incubated with the anti-LPS antibody prior to cell permeabilization. Cells on coverslips were incubated with primary antibodies in 0.25% BSA in PBS for 1 hr, followed by wash in PBS and 1 hr incubation with secondary antibodies with or without DAPI and fluorescent Phalloidin (all in 0.25% BSA in PBS). After washing in PBS, coverslips were rinsed in water and mounted on glass slides using Dako Fluorescent Mounting Medium. Fluorescent images were acquired using confocal microscope Zeiss LSM 710 with Plan-Apochromatic 63x/1.4 Oil DIC objective, operated by ZEN2000 acquisition software, or using fluorescence microscope Olympus DP-71 with Plan-Apochromatic 10x/0.40 and

20x/0.75 objective, equipped with 12Mp Colour Camera and images acquired using DP Capture and DP Manager software.

Live cell imaging

Cells were grown on glass bottom chamber slides (Lab-Tek, Thermo Scientific), and the culture medium was replaced with CO2-independent medium (Invitrogen) prior to imaging. To examine the interaction between bacteria and the host cells from the onset of infection, invasive (SPI1-T3SS-induced) bacteria were pre-diluted in CO_2-independent medium and added directly to the chamber slide "on stage" during time-lapse imaging. The confocal z-stacks or time-lapse of single confocal sections were acquired typically during the first 10 min of infection at a frequency of 6 sec between frames and at the maximal resolution of 70 nm of pixel size. A Zeiss LSM 710 FCS inverted confocal microscope operated by ZEN2009 acquisition software and equipped with a temperature controlled incubation chamber and Plan-Apochromat 63x/1.4 Oil DIC objective was used for imaging.

Image processing and image analysis

ImageJ software (version 1.46a) was used for fluorescent channels splitting or merging, image area cropping, orthogonal or maximum z-stack projections, time stamper insertions, montage of selected frames, RGB line profiling and brightness and contrast adjustment of raw acquisition images where required. To analyze the kinetics of protein recruitment or depletion, the increase or decrease of EGFP and mCherry fluorescence intensity was assessed by stack-measurement of integrated fluorescence density of selected ROI (all identical size) after the RGB image was split in separate 8-bit fluorescent channels. Absolute values were normalized to frame 1 for both channels to

demonstrate the fold of fluorescence increase/decrease over time of the sequence. Corresponding ROIs in non-infected cell (on the same movie) were selected as a control for fluorescence fluctuations and bleaching. The colocalization between SNX18 and phosphoinositide binding probes has been analyzed by colocalization highlighter plugin in (ImageJ) and the total colocalization area in each time point of the movie was quantified by particle analysis. Colocalization between SNX18 and Dynamin-2 or N-WASP within bacteria-containing membrane ruffles was quantified by colocalization threshold plugin in ImageJ. From 10 to 20 cells or regions of interest (ROI) per each sample were analyzed. To demonstrate an increase or decrease of colocalization relative to controls, statistics were calculated from values that represent the percentage of voxels which have both channel 1 and channel 2 intensities above threshold, expressed as a percentage of the total number of pixels in the image.

Image-based quantification of macropinocytosis and bacterial uptake

The rate of macropinocytosis was assessed by fluorescent-dextran uptake assay. Briefly, cells were grown on PLL-coated coverslips and starved O/N in FCS-free DMEM medium before adding 100 ug/ml of anionic, fixable Dextran (MW 10000) conjugated to Alexa fluor 647 with 10 ng/ml of EGF. After 10 min of dextran uptake, cells were fixed with 4% formaldehyde in 250 mM HEPES and mounted on coverslips for imaging using fluorescent mounting medium (Dako). As described above for the bacterial uptake assay, stable SNX18 knockdown cells (RFP-positive) and SNX18 overexpressing cells (EGFP-positive) were grown as above and infected with EGFP or RFP-expressing *S*. Typhimurium respectively, at an MOI=50. At 10 min post infection, cells were washed, fixed and mounted for imaging as described above. Macropinosomes and intracellular bacteria were quantified using ImageJ software for image analysis as described

previously (Wang *et al.*, 2010). Briefly, RGB images were split to 8-bit channels (EGFP and RFP), subjected to segmentation by thresholding, cell mask subtraction by image calculator (to exclude extracellular dextran aggregates or non-internalized bacteria) and particle analysis function was then used to measure counts, integrated density and area of spots. Original images were acquired under the same conditions for all samples, batch processing was performed using ImageJ Macro and about 2000-2500 cells were quantified for statistical evaluation.

ACKNOWLEDGMENTS

Fluorescent microscopy was carried out at the Australian Cancer Research Foundation (ACRF)/ Institute for Molecular Bioscience (IMB) Dynamic Imaging Facility for Cancer Biology. Electron microscopy was carried out at the The Centre for Microscopy and Microanalysis (the Queensland Node of the Australian Microscopy and Microanalysis Research Facility). Services and RNAi constructs were provided by the IMB Facility for Life Science Automation (LISA). We thank to Jennifer Stow for providing Akt-PH, Rac1 and Cdc42 constructs used in this study, Brett Collins for help with design of SNX18 mutants and Seetha Karunaratne for help with constructs cloning. We also thank Sabrina Marion (Cochin Institute, University Paris Descartes) for providing FERM-EGFP construct and Jack Wang (University of Queensland) for his contribution to initiate this project.

ABBREVIATIONS LIST

Sorting nexin 18 (SNX18); *Salmonella enterica* serovar *Typhimurium (S. Typhimurium); S*. Typhimurium expressing mRFP (SL-mRFP); *Salmonella*-containing vacuole (SCV); *Salmonella* pathogenicity island 1 - type three secretion system (SPI1-T3SS); Phosphatidylinositol (PtdIns); Neuronal Wiscott-Aldrich syndrome protein (N-WASP); Multiplicity of infection (MOI); Pleckstrin homology domain (PH domain);

REFFERENCES

Alto, N.M., Weflen, A.W., Rardin, M.J., Yarar, D., Lazar, C.S., Tonikian, R., Koller, A., Taylor, S.S., Boone, C., Sidhu, S.S., Schmid, S.L., Hecht, G.A., and Dixon, J.E. (2007). The type III effector EspF coordinates membrane trafficking by the spatiotemporal activation of two eukaryotic signaling pathways. The Journal of cell biology *178*, 1265-1278.

Aslanidis, C., and de Jong, P.J. (1990). Ligation-independent cloning of PCR products (LIC-PCR). Nucleic Acids Res *18*, 6069-6074.

Bakowski, M.A., Cirulis, J.T., Brown, N.F., Finlay, B.B., and Brumell, J.H. (2007). SopD acts cooperatively with SopB during Salmonella enterica serovar Typhimurium invasion. Cellular microbiology *9*, 2839-2855.

Barret, C., Roy, C., Montcourrier, P., Mangeat, P., and Niggli, V. (2000). Mutagenesis of the phosphatidylinositol 4,5-bisphosphate (PIP(2)) binding site in the NH(2)-terminal domain of ezrin correlates with its altered cellular distribution. The Journal of cell biology *151*, 1067-1080.

Birmingham, C.L., Smith, A.C., Bakowski, M.A., Yoshimori, T., and Brumell, J.H. (2006). Autophagy controls Salmonella infection in response to damage to the Salmonella-containing vacuole. J Biol Chem *281*, 11374-11383.

Boyle, E.C., Brown, N.F., and Finlay, B.B. (2006). Salmonella enterica serovar Typhimurium effectors SopB, SopE, SopE2 and SipA disrupt tight junction structure and function. Cellular microbiology *8*, 1946-1957.

Braun, V., Wong, A., Landekic, M., Hong, W.J., Grinstein, S., and Brumell, J.H. (2010). Sorting nexin 3 (SNX3) is a component of a tubular endosomal network induced by Salmonella and involved in maturation of the Salmonella-containing vacuole. Cellular microbiology *12*, 1352-1367.

Bryant, D.M., Kerr, M.C., Hammond, L.A., Joseph, S.R., Mostov, K.E., Teasdale, R.D., and Stow, J.L. (2007). EGF induces macropinocytosis and SNX1-modulated recycling of E-cadherin. J Cell Sci *120*, 1818-1828.

Bujny, M.V., Ewels, P.A., Humphrey, S., Attar, N., Jepson, M.A., and Cullen, P.J. (2008). Sorting nexin-1 defines an early phase of Salmonella-containing vacuole-remodeling during Salmonella infection. J Cell Sci *121*, 2027-2036.

Cain, R.J., Hayward, R.D., and Koronakis, V. (2008). Deciphering interplay between Salmonella invasion effectors. PLoS Pathog *4*, e1000037.

Clark, L., Perrett, C.A., Malt, L., Harward, C., Humphrey, S., Jepson, K.A., Martinez-Argudo, I., Carney, L.J., La Ragione, R.M., Humphrey, T.J., and Jepson, M.A. (2011). Differences in Salmonella enterica serovar Typhimurium strain invasiveness are associated with heterogeneity in SPI-1 gene expression. Microbiology *157*, 2072-2083.

Dowler, S., Currie, R.A., Campbell, D.G., Deak, M., Kular, G., Downes, C.P., and Alessi, D.R. (2000). Identification of pleckstrin-homology-domain-containing proteins with novel phosphoinositide-binding specificities. Biochem J *351*, 19-31.

Drecktrah, D., Knodler, L.A., and Steele-Mortimer, O. (2004). Modulation and utilization of host cell phosphoinositides by Salmonella spp. Infect Immun *72*, 4331-4335.

Finlay, B.B., Ruschkowski, S., and Dedhar, S. (1991). Cytoskeletal Rearrangements Accompanying Salmonella Entry into Epithelial-Cells. Journal of Cell Science *99*, 283-&.

Forsberg, M., Blomgran, R., Lerm, M., Sarndahl, E., Sebti, S.M., Hamilton, A., Stendahl, O., and Zheng, L. (2003). Differential effects of invasion by and phagocytosis of Salmonella typhimurium on apoptosis in human macrophages: potential role of Rho-GTPases and Akt. J Leukoc Biol *74*, 620-629.

Francis, C.L., Ryan, T.A., Jones, B.D., Smith, S.J., and Falkow, S. (1993). Ruffles induced by Salmonella and other stimuli direct macropinocytosis of bacteria. Nature *364*, 639-642.

Haberg, K., Lundmark, R., and Carlsson, S.R. (2008). SNX18 is an SNX9 paralog that acts as a membrane tubulator in AP-1-positive endosomal trafficking. J Cell Sci *121*, 1495-1505.

Haglund, C.M., and Welch, M.D. (2011). Pathogens and polymers: microbe-host interactions illuminate the cytoskeleton. The Journal of cell biology *195*, 7-17.

Hanisch, J., Kolm, R., Wozniczka, M., Bumann, D., Rottner, K., and Stradal, T.E. (2011). Activation of a RhoA/myosin II-dependent but Arp2/3 complex-independent pathway facilitates Salmonella invasion. Cell Host Microbe *9*, 273-285.

Haraga, A., Ohlson, M.B., and Miller, S.I. (2008). Salmonellae interplay with host cells. Nat Rev Microbiol *6*, 53-66.

Hernandez, L.D., Hueffer, K., Wenk, M.R., and Galan, J.E. (2004). Salmonella modulates vesicular traffic by altering phosphoinositide metabolism. Science *304*, 1805-1807.

James, S.R., Downes, C.P., Gigg, R., Grove, S.J., Holmes, A.B., and Alessi, D.R. (1996). Specific binding of the Akt-1 protein kinase to phosphatidylinositol 3,4,5-trisphosphate without subsequent activation. Biochem J *315 (Pt 3)*, 709-713.

Kerr MC, C.N., Karunaratne S, Teasdale RD. (2012). The Phosphoinositides: Key Regulators of Salmonella Containing Vacuole (SCV) Trafficking and Identity. In: Salmonella - Distribution, Adaptation, Control Measures and Molecular Technologies, ed. G.J. Annous BA: InTech, 251-264.

Kerr, M.C., Wang, J.T., Castro, N.A., Hamilton, N.A., Town, L., Brown, D.L., Meunier, F.A., Brown, N.F., Stow, J.L., and Teasdale, R.D. (2010). Inhibition of the PtdIns(5) kinase PIKfyve disrupts intracellular replication of Salmonella. EMBO J *29*, 1331-1347.

Knaevelsrud, H., Soreng, K., Raiborg, C., Haberg, K., Rasmuson, F., Brech, A., Liestol, K., Rusten, T.E., Stenmark, H., Neufeld, T.P., Carlsson, S.R., and Simonsen, A. (2013). Membrane remodeling by the PX-BAR protein SNX18 promotes autophagosome formation. The Journal of cell biology *202*, 331-349.

Knodler, L.A., Bestor, A., Ma, C., Hansen-Wester, I., Hensel, M., Vallance, B.A., and Steele-Mortimer, O. (2005). Cloning vectors and fluorescent proteins can significantly inhibit Salmonella enterica virulence in both epithelial cells and macrophages: implications for bacterial pathogenesis studies. Infect Immun *73*, 7027-7031.

Kupz, A., Guarda, G., Gebhardt, T., Sander, L.E., Short, K.R., Diavatopoulos, D.A., Wijburg, O.L., Cao, H., Waithman, J.C., Chen, W., Fernandez-Ruiz, D., Whitney, P.G., Heath, W.R., Curtiss, R., 3rd, Tschopp, J., Strugnell, R.A., and Bedoui, S. (2012). NLRC4 inflammasomes in dendritic cells regulate noncognate effector function by memory CD8(+) T cells. Nat Immunol *13*, 162-169.

Lim, J.P., Wang, J.T., Kerr, M.C., Teasdale, R.D., and Gleeson, P.A. (2008). A role for SNX5 in the regulation of macropinocytosis. BMC Cell Biol *9*, 58.

Lommel, S., Benesch, S., Rottner, K., Franz, T., Wehland, J., and Kuhn, R. (2001). Actin pedestal formation by enteropathogenic Escherichia coli and intracellular motility of Shigella flexneri are abolished in N-WASP-defective cells. EMBO Rep *2*, 850-857.

Mallo, G.V., Espina, M., Smith, A.C., Terebiznik, M.R., Aleman, A., Finlay, B.B., Rameh, L.E., Grinstein, S., and Brumell, J.H. (2008). SopB promotes phosphatidylinositol 3-phosphate formation on Salmonella vacuoles by recruiting Rab5 and Vps34. The Journal of cell biology *182*, 741-752.

Marches, O., Batchelor, M., Shaw, R.K., Patel, A., Cummings, N., Nagai, T., Sasakawa, C., Carlsson, S.R., Lundmark, R., Cougoule, C., Caron, E., Knutton, S., Connerton, I., and Frankel, G. (2006). EspF of enteropathogenic Escherichia coli binds sorting nexin 9. J Bacteriol *188*, 3110-3115.

Marcus, S.L., Wenk, M.R., Steele-Mortimer, O., and Finlay, B.B. (2001). A synaptojanin-homologous region of Salmonella typhimurium SigD is essential for inositol phosphatase activity and Akt activation. FEBS Lett *494*, 201-207.

Marion, S., Hoffmann, E., Holzer, D., Le Clainche, C., Martin, M., Sachse, M., Ganeva, I., Mangeat, P., and Griffiths, G. (2011). Ezrin promotes actin assembly at the phagosome membrane and regulates phago-lysosomal fusion. Traffic *12*, 421-437.

Mason, D., Mallo, G.V., Terebiznik, M.R., Payrastre, B., Finlay, B.B., Brumell, J.H., Rameh, L., and Grinstein, S. (2007). Alteration of epithelial structure and function associated with PtdIns(4,5)P2 degradation by a bacterial phosphatase. J Gen Physiol *129*, 267-283.

Nakazawa, S., Gotoh, N., Matsumoto, H., Murayama, C., Suzuki, T., and Yamamoto, T. (2011). Expression of sorting nexin 18 (SNX18) is dynamically regulated in developing spinal motor neurons. J Histochem Cytochem *59*, 202-213.

Norris, F.A., Wilson, M.P., Wallis, T.S., Galyov, E.E., and Majerus, P.W. (1998). SopB, a protein required for virulence of Salmonella dublin, is an inositol phosphate phosphatase. Proc Natl Acad Sci U S A *95*, 14057-14059.

Park, J., Kim, Y., Lee, S., Park, J.J., Park, Z.Y., Sun, W., Kim, H., and Chang, S. (2010). SNX18 shares a redundant role with SNX9 and modulates endocytic trafficking at the plasma membrane. J Cell Sci *123*, 1742-1750.

Patel, J.C., and Galan, J.E. (2006). Differential activation and function of Rho GTPases during Salmonella-host cell interactions. The Journal of cell biology *175*, 453-463.

Pattni, K., Jepson, M., Stenmark, H., and Banting, G. (2001). A PtdIns(3)P-specific probe cycles on and off host cell membranes during Salmonella invasion of mammalian cells. Curr Biol *11*, 1636-1642.

Piper, R.C., Hess, L.J., and James, D.E. (1991). Differential sorting of two glucose transporters expressed in insulin-sensitive cells. Am J Physiol *260*, C570-580.

Pizarro-Cerda, J., and Cossart, P. (2004). Subversion of phosphoinositide metabolism by intracellular bacterial pathogens. Nat Cell Biol *6*, 1026-1033.

Pylypenko, O., Lundmark, R., Rasmuson, E., Carlsson, S.R., and Rak, A. (2007). The PX-BAR membrane-remodeling unit of sorting nexin 9. EMBO J *26*, 4788-4800.

Rajashekar, R., Liebl, D., Seitz, A., and Hensel, M. (2008). Dynamic remodeling of the endosomal system during formation of Salmonella-induced filaments by intracellular Salmonella enterica. Traffic *9*, 2100-2116.

Riedl, J., Crevenna, A.H., Kessenbrock, K., Yu, J.H., Neukirchen, D., Bista, M., Bradke, F., Jenne, D., Holak, T.A., Werb, Z., Sixt, M., and Wedlich-Soldner, R. (2008). Lifeact: a versatile marker to visualize F-actin. Nat Methods *5*, 605-607.

Salim, K., Bottomley, M.J., Querfurth, E., Zvelebil, M.J., Gout, I., Scaife, R., Margolis, R.L., Gigg, R., Smith, C.I., Driscoll, P.C., Waterfield, M.D., and Panayotou, G. (1996). Distinct specificity in the recognition of phosphoinositides by the pleckstrin homology domains of dynamin and Bruton's tyrosine kinase. EMBO J *15*, 6241-6250.

Sason, H., Milgrom, M., Weiss, A.M., Melamed-Book, N., Balla, T., Grinstein, S., Backert, S., Rosenshine, I., and Aroeti, B. (2009). Enteropathogenic Escherichia coli subverts phosphatidylinositol 4,5-bisphosphate and phosphatidylinositol 3,4,5-trisphosphate upon epithelial cell infection. Mol Biol Cell *20*, 544-555.

Shi, L., Chowdhury, S.M., Smallwood, H.S., Yoon, H., Mottaz-Brewer, H.M., Norbeck, A.D., McDermott, J.E., Clauss, T.R., Heffron, F., Smith, R.D., and Adkins, J.N. (2009). Proteomic investigation of the time course responses of RAW 264.7 macrophages to infection with Salmonella enterica. Infect Immun *77*, 3227-3233.

Shin, N., Ahn, N., Chang-Ileto, B., Park, J., Takei, K., Ahn, S.G., Kim, S.A., Di Paolo, G., and Chang, S. (2008). SNX9 regulates tubular invagination of the plasma membrane through interaction with actin cytoskeleton and dynamin 2. J Cell Sci *121*, 1252-1263.

Soulet, F., Yarar, D., Leonard, M., and Schmid, S.L. (2005). SNX9 regulates dynamin assembly and is required for efficient clathrin-mediated endocytosis. Mol Biol Cell *16*, 2058-2067.

Steele-Mortimer, O., Brumell, J.H., Knodler, L.A., Meresse, S., Lopez, A., and Finlay, B.B. (2002). The invasion-associated type III secretion system of Salmonella enterica serovar Typhimurium is necessary for intracellular proliferation and vacuole biogenesis in epithelial cells. Cellular microbiology *4*, 43-54.

Steele-Mortimer, O., Knodler, L.A., Marcus, S.L., Scheid, M.P., Goh, B., Pfeifer, C.G., Duronio, V., and Finlay, B.B. (2000). Activation of Akt/protein kinase B in epithelial cells by the Salmonella typhimurium effector sigD. J Biol Chem *275*, 37718-37724.

Stender, S., Friebel, A., Linder, S., Rohde, M., Mirold, S., and Hardt, W.D. (2000). Identification of SopE2 from Salmonella typhimurium, a conserved guanine nucleotide exchange factor for Cdc42 of the host cell. Mol Microbiol *36*, 1206-1221.

Teasdale, R.D., and Collins, B.M. (2012). Insights into the PX (phox-homology) domain and SNX (sorting nexin) protein families: structures, functions and roles in disease. Biochem J *441*, 39-59.

Terebiznik, M.R., Vieira, O.V., Marcus, S.L., Slade, A., Yip, C.M., Trimble, W.S., Meyer, T., Finlay, B.B., and Grinstein, S. (2002). Elimination of host cell PtdIns(4,5)P(2) by bacterial SigD promotes membrane fission during invasion by Salmonella. Nat Cell Biol *4*, 766-773.

Unsworth, K.E., Way, M., McNiven, M., Machesky, L., and Holden, D.W. (2004). Analysis of the mechanisms of Salmonella-induced actin assembly during invasion of host cells and intracellular replication. Cellular microbiology *6*, 1041-1055.

van Weering, J.R., Sessions, R.B., Traer, C.J., Kloer, D.P., Bhatia, V.K., Stamou, D., Carlsson, S.R., Hurley, J.H., and Cullen, P.J. (2012). Molecular basis for SNX-BAR-mediated assembly of distinct endosomal sorting tubules. EMBO J *31*, 4466-4480.

Varnai, P., Rother, K.I., and Balla, T. (1999). Phosphatidylinositol 3-kinase-dependent membrane association of the Bruton's tyrosine kinase pleckstrin homology domain visualized in single living cells. J Biol Chem *274*, 10983-10989.

Veiga, E., Guttman, J.A., Bonazzi, M., Boucrot, E., Toledo-Arana, A., Lin, A.E., Enninga, J., Pizarro-Cerda, J., Finlay, B.B., Kirchhausen, T., and Cossart, P. (2007). Invasive and adherent bacterial pathogens co-Opt host clathrin for infection. Cell Host Microbe *2*, 340-351.

Wang, B., Wylie, F.G., Teasdale, R.D., and Stow, J.L. (2005). Polarized trafficking of E-cadherin is regulated by Rac1 and Cdc42 in Madin-Darby canine kidney cells. Am J Physiol Cell Physiol *288*, C1411-1419.

Wang, J.T., Kerr, M.C., Karunaratne, S., Jeanes, A., Yap, A.S., and Teasdale, R.D. (2010). The SNX-PX-BAR family in macropinocytosis: the regulation of macropinosome formation by SNX-PX-BAR proteins. PLoS One *5*, e13763.

Yarar, D., Surka, M.C., Leonard, M.C., and Schmid, S.L. (2008). SNX9 activities are regulated by multiple phosphoinositides through both PX and BAR domains. Traffic *9*, 133-146.

Zhang, J., Zhang, X., Guo, Y., Xu, L., and Pei, D. (2009). Sorting nexin 33 induces mammalian cell micronucleated phenotype and actin polymerization by interacting with Wiskott-Aldrich syndrome protein. J Biol Chem *284*, 21659-21669.

FIGURE LEGENDS

Figure 2.1. SNX18 functions in macropinocytosis and *S.* Typhimurium internalization. (A) Protein levels of endogenous SNX18 (75kDa) and EGFP-SNX18 (95kDa) in non-transfected HEK293 cells and in cells overexpressing EGFP or EGFP-SNX18 were detected by western blot using anti-SNX18 antibody. (B) Protein levels of endogenous SNX18 in cells 6 days post induction of shRNA-mediated knockdown and in control (non-induced) cells. α-Tubulin was used as a loading control. (C) The rate of macropinocytosis in cells overexpressing SNX18 (left) and in SNX18 knockdown cells (right) assessed by fluorescent dextran uptake assay in EGF-treated HEK293 cells. Numbers of dextran-positive macropinosomes per cell were counted by image analysis. The average values in control cells were normalized to one to demonstrate the fold change in EGFP-SNX18 expressing cells and SNX18 knockdown cells. Between 250-300 cells per sample were analyzed. Bars indicate the mean + standard deviation between 3 experiments. ***$p<0.001$, *$p<0.05$, t-test. (D) Efficiency of bacteria internalization in cells overexpressing SNX18 (left) and in SNX18 knockdown cells (right). The amounts of intracellular bacteria per cell were quantified at 10 min post infection using image analysis with exclusion of extracellular bacteria (labelled by anti-LPS antibody). The average values in control cells were normalized to one to demonstrate the fold change in EGFP-SNX18 expressing cells and SNX18 knockdown cells. Bars indicate the mean + standard deviation between 3 experiments, * $p<0.05$, ** $p<0.01$, t-test.

Figure 2.2. Cytosolic SNX18 is recruited to the site of bacterial invasion at the plasma membrane. (A) Within 10 min of infection, the cytosolic fraction of EGFP-SNX18 translocates to the plasma membrane in both, epithelial cells (HEK293) and macrophages (RAW264.7). Shown is a z-stack of confocal sections through live cells

expressing EGFP-SNX18 pre-infection and 10 min post-infection with SL-mRFP. Bars = 10 μm. (B) Kinetic measurements of SNX18 relocation to the plasma membrane. Upper panel:Series of confocal images from a time-lapse acquisition of HEK293 cells expressing EGFP-SNX18 during 10 min of infection with SL-mRFP (initial docking site of bacteria indicated by an arrow); Lower panel: Quantification of fluorescence (relative integrated density) within selected ROI at plasma membrane and in cytosol of infected (left) and adjacent non-infected control cell (right). Absolute values of integrated density at T = 0 min post infection were normalized to 1 to demonstrate fold-increase/decrease in following time points

(C) Electron micrographs of frozen-hydrated sections through HEK293 cells with stable expression of EGFP-SNX18 fixed 10 min post infection (or mock-infection). The EGFP-SNX18 was detected by anti-GFP antibody followed by 10 nm Protein A-Gold. The marker of SNX18 localizes primarily to the cytosol (cyt) in mock infected cells, while upon infection the SNX18 associates mainly with the plasma membrane (PM) and the membrane of the nascent SCV. Bacteria indicated by asterisk. Bar = 1 μm. Quantification of gold markers associated with plasma membrane in mock-infected cells and cells 10 min p.i. as a percentage of total gold markers per each image analysed. N=10, p=0.002 (t-test). (D) Endogenous SNX18 is also recruited to the plasma membrane during bacteria internalization: Whole cell lysate (WCL), plasma membrane (PM) and cytosolic (CYT) fractions from cells harvested at 10 min post infection (10 mpi) or mock-treatment (as a control). Endogenous SNX18 was detected on Western blot by anti-SNX18 antibody, PM fraction control Na+/K+ ATPase by anti-α1 Na+/K+ ATPase antibody and cytosol fraction control Tubulin by anti-α-Tubulin antibody. .

Figure 2.3. The recruitment of SNX18 to the site of SCV formation correlates with a burst of actin polymerization and membrane scission: (A) Series of confocal sections from a time-lapse of EGFP-SNX18-expressing cells infected with SL-mRFP. SNX18 relocates from cytosol to *Salmonella*-induced membrane ruffles at the site of bacterial attachment with a transient accumulation of SNX18 during the SCV scission from the plasma membrane (arrowheads). Bar = 2 μm. The diagram illustrates SNX18 (green dots) localization during bacterial internalization and at the early stage of the SCV formation. (B) Series of confocal sections from a time-lapse of HEK293 cells coexpressing EGFP-SNX18 with LifeAct-Ruby and infected with SL-mRFP in the presence of wheat germ agglutinin coupled with Alexa fluor 647 (WGA-647). The burst of SNX18 and LifeAct-Ruby probe during bacteria internalization and SCV scission (indicated by arrowheads) and their depletion after the SCV detachment from the plasma membrane. Entering bacteria are visible in DIC. The panel on right shows enlarged details from the left panel. Bars = 10 μm (left panel) or 2 μm (right panel)

Figure 2.4. SNX18 functions as a scaffold for N-WASP and Dynamin-2 recruitment to the site of SCV formation. Colocalization between SNX18 and Dynamin-2 (A) or SNX18 and N-WASP (B) within *Salmonella*-containing membrane ruffles is significantly reduced in cells expressing EGFP-SNX18 construct lacking the SH3 domain. Cells coexpreassing EGFP- or Myc-tagged SNX18 with HA-tagged Dynamin2 (A) or EGFP-N-WASP (B) fixed 10 min post infection (p. i.) and immunolabelled with anti-myc or anti-HA antibody followed by Alexa fluor 546. Bacteria were detected by anti-LPS antibody followed by Alexa fluor 405 secondary antibody and DNA was stained with DAPI. The fluorescent images are pseudocolored as indicated. Bars = 5 μm. Colocalization of indicated proteins in bacteria-containing membrane ruffles was quantified in 10-12

ROIs from different cells for each sample. The ROIs were limited to bacteria-containing membrane ruffles (enlarged inserts) cropped to identical square size (12 X 12 um). Colocalization is presented as a percentage of voxels which have both channel 1 and channel 2 intensities above threshold, expressed as a percentage of the total number of pixels in the image (including zero-zero pixels); t-test, $p<0.05$; Between 10-20 ROI per sample were analysed and bars indicate the mean + standard errors within typical experiment.

Figure 2.5. SNX18 requires the SH3 domain and an intact PtdIns-binding site to facilitate the uptake of the bacteria. (A) Quantification of bacteria internalization in cells overexpressing full length SNX18, SNX18 lacking the SH3 domain (SNX18:ΔSH3) or phosphoinositide binding mutant SNX18:R303Q in comparison to control cells (expressing EGFP only). Cells were fixed at 10 min post infection with SL-mRFP and intracellular bacteria were quantified by image analysis with exclusion of extracellular bacteria (immunolabelled with anti-LPS antibody). The average values in control cells were normalized to one to demonstrate the fold change in cells overexpressing SNX18 or the SNX18 mutants. * $p<0.05$. Bars indicate the mean + standard deviation between 3 experiments. Below: Examples of immunofluorescence images used for quantification. Bars = 10μm. (B) Live imaging of HEK293 cells overexpressing EGFP-tagged SNX18, SNX18:ΔSH3 or SNX18:R303Q constructs and infected with SL-mRFP. Note the delay between bacteria first contact with the cell (arrows) and complete internalization (arrowheads) in cells expressing both SNX18 mutants and no sign of SNX18:R303Q recruitment to the site of bacteria invasion. Series of confocal sections from representative time-lapse are shown. Schematic diagrams of each construct are shown below. Bars = 2 μm.

Figure 2.6. Activity of SPI1-T3SS effector SopB is necessary and sufficient for SNX18 recruitment to the plasma membrane. (A) SNX18 recruitment to the site of bacterial internalization is markedly perturbed in cells infected with the SPI1-T3SS inactive mutant Δ*invA* (left) while in cells infected with the SPI2-T3SS inactive mutant Δ*ssaR* (right) the burst of SNX18 at the site of bacterial internalization is comparable to that of induced by the wild type bacteria. Bacteria were detected by indirect immunofluorescence using anti-LPS antibody followed by secondary antibody coupled to Alexa fluor 546. Bars = 5 μm. (B) Cells with stable expression of EGFP-SNX18 and transient (6 hrs) ectopic expression of myc-tagged SPI1-T3SS effectors with reported function in *S*. Typhimurium internalization. After fixation, the effectors were detected by anti-myc antibody followed by secondary antibody coupled to Alexa fluor 546 (red), DNA was labelled with DAPI (blue) and F-actin was labelled by Phalloidin Alexa fluor 647 (pseudocolored in white); Only expression of SopB resulted in depletion of cytosolic SNX18 and accumulation of SNX18 in the plasma membrane. Bars = 5 μm.

Figure 2.7. The SNX18-mediated invasion pathway of *S*. Typhimurium relies on inositol-phosphatase activity of SopB (A) *S*. Typhimurium mutant Δ*sopB* failed to trigger SNX18 recruitment to the site of invasion. EGFP-SNX18 expressing cells infected with wild type (left) or Δ*sopB* bacteria (right). Cells were fixed 10 min post infection (p. i.) and bacteria were labelled with anti-LPS antibody followed by secondary antibody coupled to Alexa fluor 546 (red). The detail of *Salmonella*-containing ruffle (1) and the projection of confocal z-stack (xz) is shown together with the fluorescence intensity line profile (RGB) across the cell. Bars = 5 μm. (B) Quantification of the bacterial

internalization (wild type and Δ*sopB*) in control knockdown cells, SNX18 knockdown cells and SNX18 knockdown cells transfected with myc-SNX18. Extracellular bacteria were detected by anti-LPS antibody followed by secondary antibody coupled with Alexa fluor 405 and myc-SNX18 was detected by anti-myc antibody followed by secondary antibody coupled with Alexa fluor 647. Numbers of internalized bacteria (mRFP-positive and LPS-negative) were counted by image analysis and average numbers per cell are shown. Bars indicate the mean + standard deviation between 3 experiments. (C) Localization of EGFP-SNX18 after ectopic expression of SopB or PtdIns-phosphatase defective mutants of SopB in non-infected cells. The wild type SopB localizes to endosomes and enlarged vacuoles (arrowheads) and induces SNX18 accumulation at the plasma membrane (arrows) whereas SopB with point mutation within the inositol polyphosphate 4-phosphatase homology (IPPH) motif 2 (C460S or R466A) or within the synaptojanin homology domain (K528A) localizes to the plasma membrane (arrowheads) and peripheral vesicles without visible changes to SNX18 localization. Cells were fixed 6 hrs post transfection, labelled with DAPI and myc-tagged SopB was detected by anti-myc antibody followed by secondary antibody coupled to Alexa fluor 546 (red). Bars = 5 μm. (D) The failure of Δ*sopB* mutant bacteria to trigger SNX18 recruitment during internalization can be rescued by complementation using the full length SopB but not the inositol phosphatase deficient SopB:C460S. The HEK293 cells expressing EGFP-SNX18 were infected with the Δ*sopB* mutant bacteria transformed with pWSK29 plasmid encoding *sopB* or *sopB*:C460S. Immunofluorescence detection of bacteria and the RGB profiles were performed as in (A), Bars = 5 μm.

Figure 2.8. SNX18 is recruited to PtdIns(3,4)P2-enriched membrane subdomains. Correlation between recruitment kinetics of SNX18 and that of Akt-PH (A), TAPP1-PH

(B) and Btk-PH (C) during bacteria internalization; Panels show series of still images from time-lapse movie of cells co-transfected with mCherry-SNX18 and Akt-PH-EGFP (A), TAPP1-EGFP (B) and Btk-PH-EGFP (C) and infected with non-fluorescent bacteria (indicated by arrows in DIC channel); Simultaneous recruitment of SNX18 and Akt-PH or TAPP1 to the site of bacterial internalization is indicated by arrowheads; Below: Correlation of transient increase in fluorescent density between mCherry and EGFP (left) were analyzed from sequence of 21 images (values at T=0 were normalized to 1 to show a relative increase/decrease over time); Time profile of total colocalization area between mCherry and EGFP signal (right); Bars = 5 μm. Shown are results from a typical live imaging experiment.

SUPPORTING FIGURES AND MOVIES

Figure 2.S1. Subcellular localization of EGFP-SNX18 during transient expression in HEK293 cells. At moderate levels of expression, EGFP-SNX18 localizes to the cytosol, endosomes, endosome-derived tubules and nascent macropinosomes (1), while high levels of expression induce formation of extensive network of thickened, elongated, SNX18-positive membrane tubules often derived from (or continuous with) the plasma membrane (2). Confocal sections of cells fixed 12 hrs post transfection. Bars = 5 μm

Figure 2.S2. SNX18 is enriched on plasma membrane-derived tubules during endosome scission from the plasma membrane. Clone selection was used to generate a cell line of HEK293 cells with stable expression of EGFP-SNX18. Confocal sections of live cell after 2 min incubation with 1μM lipophilic fluorescent dye FM4-64 (red), Left: A z-stack shows SNX18 in the cytosol and in association with plasma membrane-derived tubules enriched at the bottom of the cells (shown in detail 1); Right: The xz-projection and the fluorescent intensity line profile below indicates accumulation of EGFP-SNX18 around plasma membrane invaginations.

Figure 2.S3. SNX9 recruits together with SNX18 to *Salmonella*-containing membrane ruffles but into distinct subdomains. Similar to SNX18, SNX9 recruits to membrane ruffles during bacterial internalization. Immunoflourescence images of HEK293 cells expressing EGFP-SNX18 (left) or EGFP-SNX9 (right) 10 min post infection with wild type *S*. Typhimurium. Bacteria were detected by anti-LPS antibody followed by Alexa fluor 405 coupled secondary antibody. RGB line profile across the *Salmonella*-containing membrane ruffle. Bars = 10 μm.

Figure 2.S4. SNX9 depletion by shRNA-mediated knockdown does not affect bacterial internalization. Quantification of bacterial internalization in inducible shRNA-mediated knockdown of SNX18 and SNX18-SNX9 double knockdown cells. Average numbers of internalized bacteria per cell are shown in comparison to control knockdown cells. * p =0.0108, ** p = 0.0011. Right: Endogenous levels of SNX18 and SNX9 in control knockdown, SNX18 knockdown and SNX18-SNX9 double knockdown cells evaluated by western blot using anti-SNX18 and anti-SNX9 antibody (β-Tubulin was used as a loading control). Bars indicate the mean + standard deviation between 3 experiments

Figure 2.S5. **The SopE-deficient strain of *S.* Typhimurium (ST12023) is more susceptible to depletion of SNX18**. Confocal images of cells expressing EGFP-SNX18 (or EGFP only) fixed at 10 min post infection with *S*. Typhimurium strain SL1344 expressing mRFP (left) or strain ST 12023 expressing mCherry (right). Extracellular bacteria were detected by anti-LPS antibody followed by secondary antibody coupled with Alexa fluor 405. Both strains induced a burst of SNX18 at the site of bacterial internalization and no increase in fluorescence was detected within membrane ruffles of EGFP-expressing cells. Below: Quantification of bacterial internalization in SNX18 knockdown cells and in cells overexpressing SNX18 in comparison to controls. The ST12023 strain of *S*. Typhimurium deficient for SopE is more susceptible to both SNX18 depletion and overexpression in comparison to SL1344 strain. Bars indicate the mean + standard deviation between 3 experiments

Figure 2.S6. SopB-mediated recruitment of SNX18 to the plasma membrane is independent on activation of Rho-GTPases. Left panel: In non-infected cells

expressing constitutively active (CA) forms of Rac1 or Cdc42, the Rac1 and Cdc42 localize to the plasma membrane, while SNX18 maintains the cytosolic localization. Note that expression of constitutively-active Rac1 induces formation of extensive membrane ruffles in non-infected cells without recruiting SNX18 (arrowheads). Right panel: Expression of dominant negative (DN) forms of Cdc42 or Rac1 (GTPase-defective) does not inhibit SNX18 recruitment during bacterial internalization. Cells were fixed 10 min p.i. and bacteria were labelled by anti-LPS antibody (Alexa fluor 405) on permeabilized cells. Note that expression of Cdc42:DN (but not of Rac1:DN) abolished bacteria internalization into the cell without perturbing *Salmonella*-induced SNX18 recruitment to the plasma membrane (arrows). Bars = 5 μm.Insets=GFP-Channel.

Figure 2.S7. Inhibition of Rac1 GTPase does not perturb SNX18 recruitment to the site of bacteria invasion. HEK293 cells with stable expression of EGFP-SNX18 treated with 10 μM or 100 μM Rac1-specific inhibitor NSC23766 for 60 min pre-infection and then during 10 min of infection. Cells were fixed and labelled with phalloidin-TRITC and anti-LPS antibody (Alexa fluor 405). Representative confocal sections are shown as merged RGB (top panels) and green channel (EGFP-SNX18) is shown separately in a grey scale (lower panels). Bars = 5 μm.

Figure 2.S8. Recruitment of phosphoinositide binding probes to the site of bacteria invasion. The PtdIns(4,5)P2-binding FERM domain exhibits exclusive plasma membrane localization (1) but depletion from the site of bacteria internalization (2) and does not accumulate on the SCV (3). The PH domain of Akt with affinity to PtdIns(3,4)P2 and PtdIns(3,4,5)P3 localizes to the plasma membrane (1) but a distinct increase can be detected on the nascent SCV at the site of bacteria internalization (2) but not on fully

internalized SCV (3). PtdIns(3)P-sensing 2xFYVE domain localizes to intracellular tubular vesicles (1), shows limited recruitment to the site of *S*. Typhimurium invasion (2) but discernable accumulation on fully internalized SCV (3). Cells were infected 12 hrs post transfection and fixed 10 min post infection with mRFP-expressing bacteria (wild type); confocal sections from representative images are shown (arrowheads indicate the SCV positive for SNX18); Bars = 5 μm

Figure 2.S9. SopB-mediated recruitment of SNX18 is not dependent on Akt activation and signalling. Top: Cells expressing EGFP-SNX18 pre-treated with Akt inhibitor AKTi1/2 are shown pre- and post-infection with *S*. Typhimurium. A series of time-lapse images from a single confocal section from live cells are shown. Bottom: The Akt inhibitor AKTi1/2 can completely reduce the SopB-mediated activation of Akt. Protein levels of total and phosphorylated Akt in cells infected with wild type (wt) or Δ*sopB* bacteria (or mock-infected controls) were analyzed by Western blot using anti-Akt and phospho-Akt-specific antibody. Bars = 5 μm.

movie1: SNX18 (EGFP) translocates from cytosol to the plasma membrane during *S*. Typhimurium (mRFP) invasion. Zoom: Transient SNX18 recruitment to the nascent SCV in infected cell (1) and to the nascent macropinosomes in non-infected cell (2). HEK293 cells with stable expression of EGFP-SNX18, 1-5 min post infection. (0.1 min between frames, 7 fps).

movie2: SNX18 (EGFP) recruits to the edge of *Salmonella*-induced membrane ruffles and accumulates on the nascent SCV during its scission from the plasma membrane.

HEK293 cells with stable expression of EGFP-SNX18, 1-5 min post infection. (0.1 min between frames, 7 fps).

movie3: SNX18 (EGFP) recruits to the site of *S*. Typhimurium (mRFP) attachment at the plasma membrane and accumulates during bacteria internalization into the nascent SCV. HEK293 cells, 16 hrs post transfection, 1-5 min post infection. (0.1 min between frames, 7 fps).

movie4: SNX18:ΔSH3 (EGFP) recruits to the site of *S*. Typhimurium (RFP) attachment at the plasma membrane and accumulates during bacteria internalization into the nascent SCV. HEK293 cells, 16 hrs post transfection, 1-5 min post infection. (0.3 min between frames, 7 fps).

movie5: SNX18:R303Q (EGFP) remains cytosolic during *S*. Typhimurium (RFP) attachment to the plasma membrane and prolonged internalization into the nascent SCV. HEK293 cells, 16 hrs post transfection, 1-5 min post infection. (0.1 min between frames, 7 fps).

movie6: Transient burst of SNX18 (mCherry) at the site of *S*. Typhimurium internalization occurs simultaneously with the Akt-PH and TAPP1-PH (EGFP), whereas no increase in Btk-PH (EGFP) signal was detected. HEK293 cells, 8 hrs post co-transfection, 1-5 min post infection. (0.2 min between frames, 7 fps).

Table 2.1. Primers used in this study.

Primer	Sequence*
N-Myc-catccdB-NheI fwd	5'-GCATGCTAGCCACC**ATGGAGCAGAAGCTGATAAGTGAGGAGGATATC**AGGCA CCCCAGGCTTTACACTTTATGCTTC-3'
catccdB-ApaI rev	5'-GCATGGGCCCGACATGAAGGTTAGGGATATCGACCTGCAGACTGGCTGTGTATA AG-3'
sipA fwd	5'-TGATAAGTGAGGAGGATCTGGTTACAAGTGTAAGGACTCAGC-3'
sipA rev	5'-ATGATGGTTAGGGATCTTAACGCTGCATGTGCAAGCCATC-3'
sipC fwd	5'-TGATAAGTGAGGAGGATCTGTTAATTAGTAATGTGGGAATAAATC-3'
sipC rev	5'-ATGATGGTTAGGGATCTTAAGCGCGAATATTGCCTGCGAT-3'
sopB fwd	5'-TGATAAGTGAGGAGGATCTGCAAATACAGAGCTTCTATCACTC-3'
sopB rev	5'-ATGATGGTTAGGGATCTCAAGATGTGATTAATGAAGAAATGCCTTTTACTG-3'
sopD fwd	5'-TGATAAGTGAGGAGGATCTGCCAGTCACTTTAAGCTTCGGTAATCATC-3'
sopD rev	5'-ATGATGGTTAGGGATCTTATGTCAGTAATATATTACGACTGCACCCATC-3'
sopE2 fwd	5'-TGATAAGTGAGGAGGATCTGACTAACATAACACTATCCACCCAGCAC-3'
sopE2 rev	5'-ATGATGGTTAGGGATCTCAGGAGGCATTCTGAAGATACTTATTC-3'
sptP fwd	5'-TGATAAGTGAGGAGGATCTGCTAAAGTATGAGGAGAGAAAATTGAATAATTTA ACGTTG-3'
sptP rev	5'-ATGATGGTTAGGGATCTCAGCTTGCCGTCGTCATAAG-3'
SopB:C460S fwd	5'-GGTACCCGCCTGGAATAGTAAAAGCGGCAAAG-3'
SopB:C460S rev	5'-CTTTGCCGCTTTTACTATTCCAGGCGGGTACC-3'
SopB:R466A fwd	5'-CCTGGAATTGTAAAAGCGGCAAAGATGCTACAGGGATGATGG-3'
SopB:R466A rev	5'-CCATCATCCCTGTAGCATCTTTGCCGCTTTTACAATTCCAGG-3'
SopB:K528A fwd	5'-GGGCGGGAAACAAAGTAATGGCAAATTTATCGCCAGAGGTGC-3'
SopB:K528A rev	5'-GCACCTCTGGCGATAAATTTGCCATTACTTTGTTTCCCGCCC-3'
SNX18:R303Q fwd	5'-CCAGGTGCCCGTGCACAGGCAATATAAGCACTTCGATTGG-3'
SNX18:R303Q rev	5'-CCAATCGAAGTGCTTATATTGCCTGTGCACGGGCACCTGGG-3'
sopB/sopB:C460S fwd	5'-GCATGAATTCTATTCAGGAATATTAAAAACGCTATGCAAATACAGAGCTTCTATCACTC-3'
sopB/sopB:C460S rev	5'-GCATCTCGAGTACCTCAAGACTCAAGATGTGATTAATGAAGAAATGCCTTTTACTG-3'

fwd, forward; rev, reverse

* Sequences added to the 5' end of primers to allow LIC are underlined. The sequence encoding the Myc tag is in bold font.

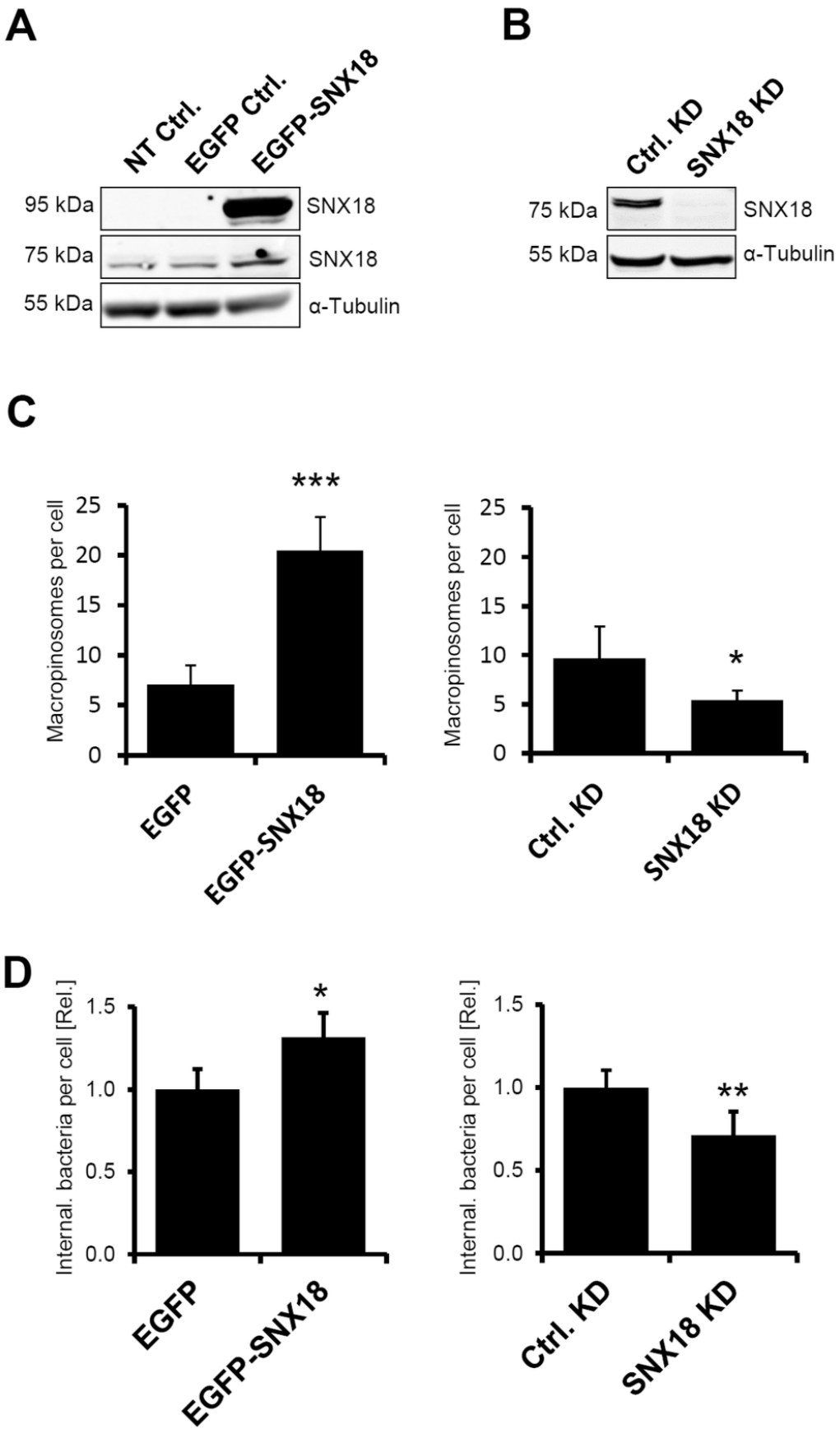
A
NT Ctrl.
EGFP Ctrl.
EGFP-SNX18
95 kDa
SNX18
75 kDa
SNX18
55 kDa
α-Tubulin
B
Ctrl. KD
SNX18 KD
75 kDa
SNX18
55 kDa
α-Tubulin
C
Macropinosomes per cell
25
20
15
10
5
0
***
EGFP
EGFP-SNX18
Macropinosomes per cell
25
20
15
10
5
0
*
Ctrl. KD
SNX18 KD
D
Internal. bacteria per cell [Rel.]
1.5
1.0
0.5
0.0
*
EGFP
EGFP-SNX18
Internal. bacteria per cell [Rel.]
1.5
1.0
0.5
0.0
**
Ctrl. KD
SNX18 KD

Figure 2.1

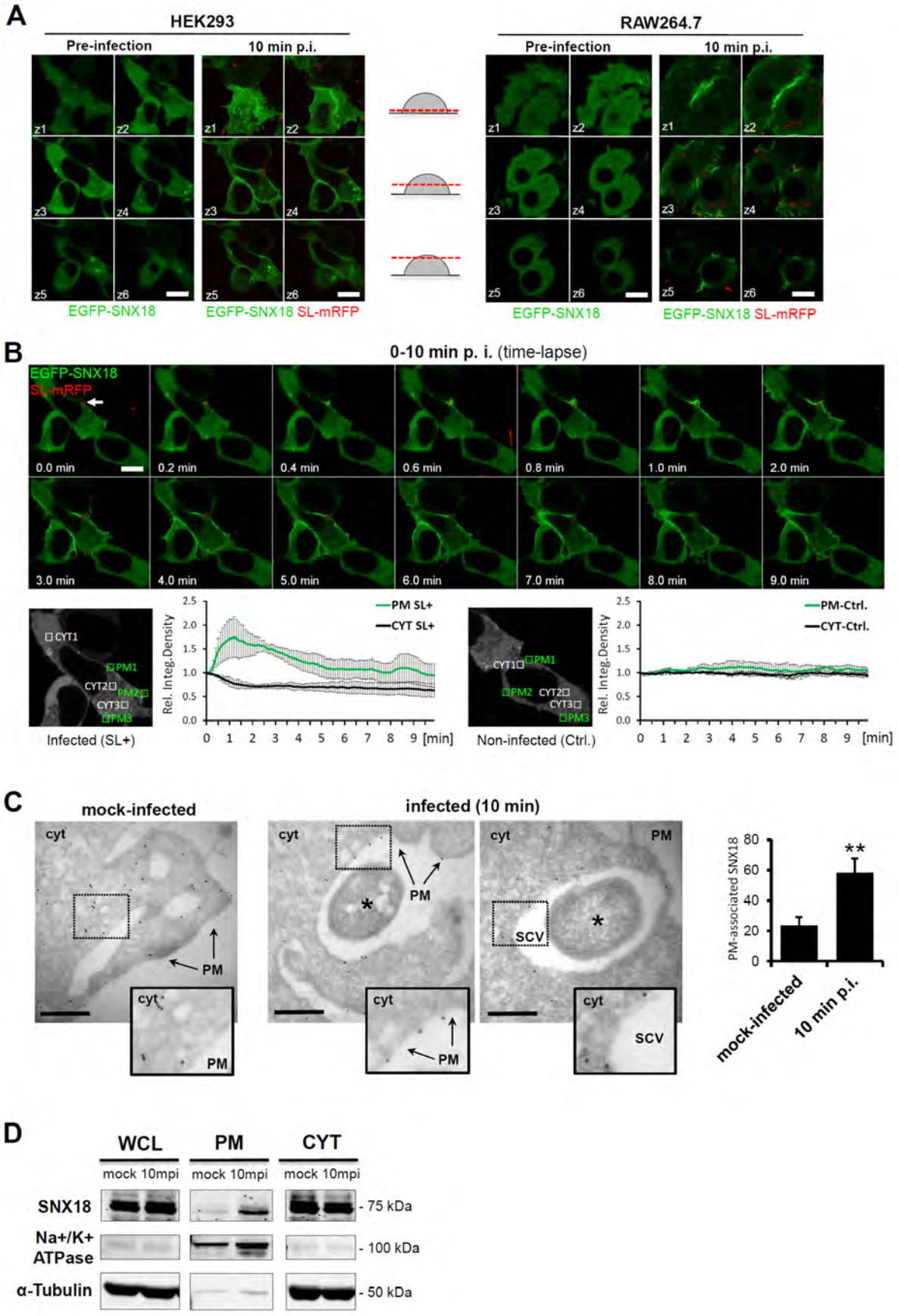
A
HEK293
Pre-infection
10 min p.i.
RAW264.7
Pre-infection
10 min p.i.
z1
z2
z3
z4
z5
z6
EGFP-SNX18
EGFP-SNX18 SL-mRFP
EGFP-SNX18
EGFP-SNX18 SL-mRFP
B
0-10 min p. i. (time-lapse)
EGFP-SNX18
SL-mRFP
0.0 min
0.2 min
0.4 min
0.6 min
0.8 min
1.0 min
2.0 min
3.0 min
4.0 min
5.0 min
6.0 min
7.0 min
8.0 min
9.0 min
CYT1
PM1
CYT2
PM2
CYT3
PM3
Infected (SL+)
Rel. Integ.Density
PM SL+
CYT SL+
[min]
Non-infected (Ctrl.)
PM-Ctrl.
CYT-Ctrl.
C
mock-infected
infected (10 min)
cyt
PM
SCV
PM-associated SNX18
mock-infected
10 min p.i.
D
WCL
PM
CYT
mock 10mpi
SNX18
Na+/K+ ATPase
α-Tubulin
- 75 kDa
- 100 kDa
- 50 kDa

Figure 2.2

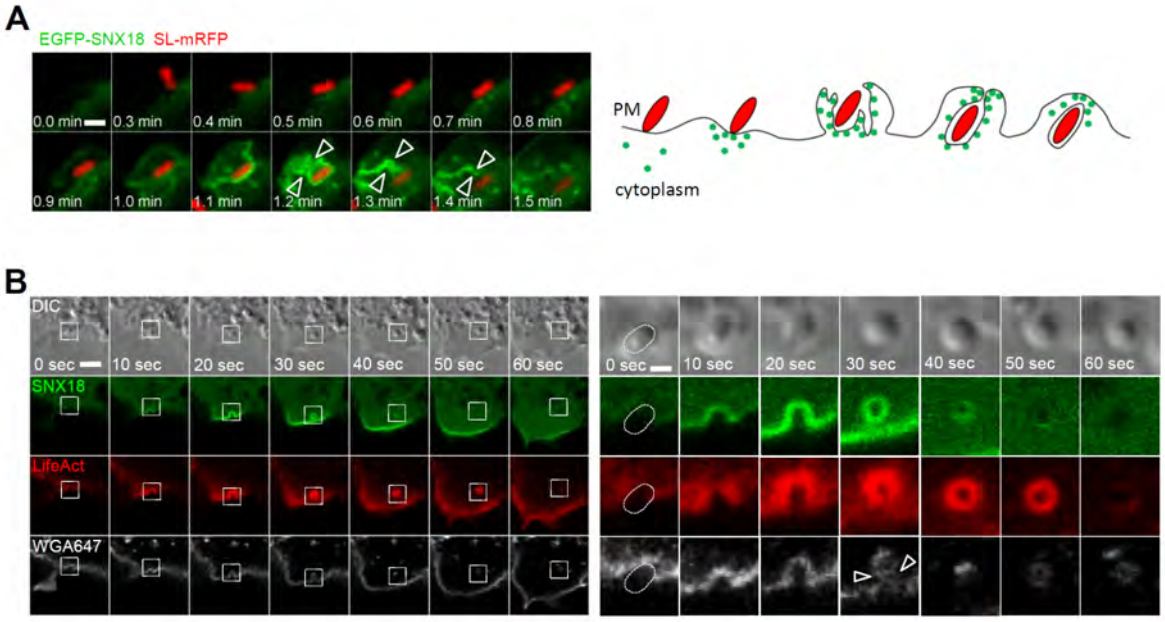
A
EGFP-SNX18 SL-mRFP
0.0 min
0.3 min
0.4 min
0.5 min
0.6 min
0.7 min
0.8 min
0.9 min
1.0 min
1.1 min
1.2 min
1.3 min
1.4 min
1.5 min
PM
cytoplasm
B
DIC
0 sec
10 sec
20 sec
30 sec
40 sec
50 sec
60 sec
SNX18
LifeAct
WGA647

Figure 2.3

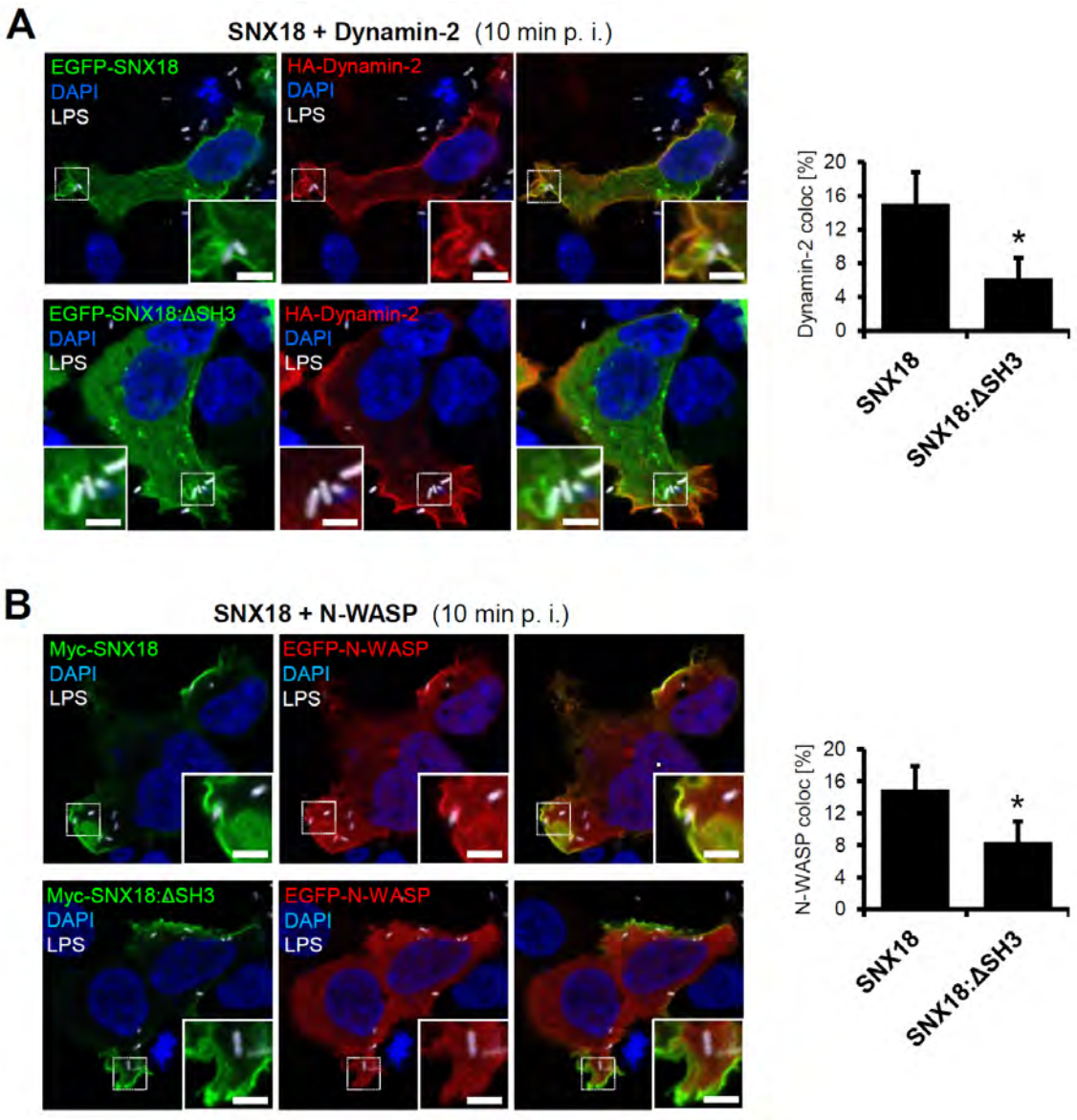
A
SNX18 + Dynamin-2 (10 min p. i.)
EGFP-SNX18
DAPI
LPS
HA-Dynamin-2
DAPI
LPS
EGFP-SNX18:ΔSH3
DAPI
LPS
HA-Dynamin-2
DAPI
LPS
Dynamin-2 coloc [%]
20
16
12
8
4
0
*
SNX18
SNX18:ΔSH3
B
SNX18 + N-WASP (10 min p. i.)
Myc-SNX18
DAPI
LPS
EGFP-N-WASP
DAPI
LPS
Myc-SNX18:ΔSH3
DAPI
LPS
EGFP-N-WASP
DAPI
LPS
N-WASP coloc [%]
20
16
12
8
4
0
*
SNX18
SNX18:ΔSH3

Figure 2.4

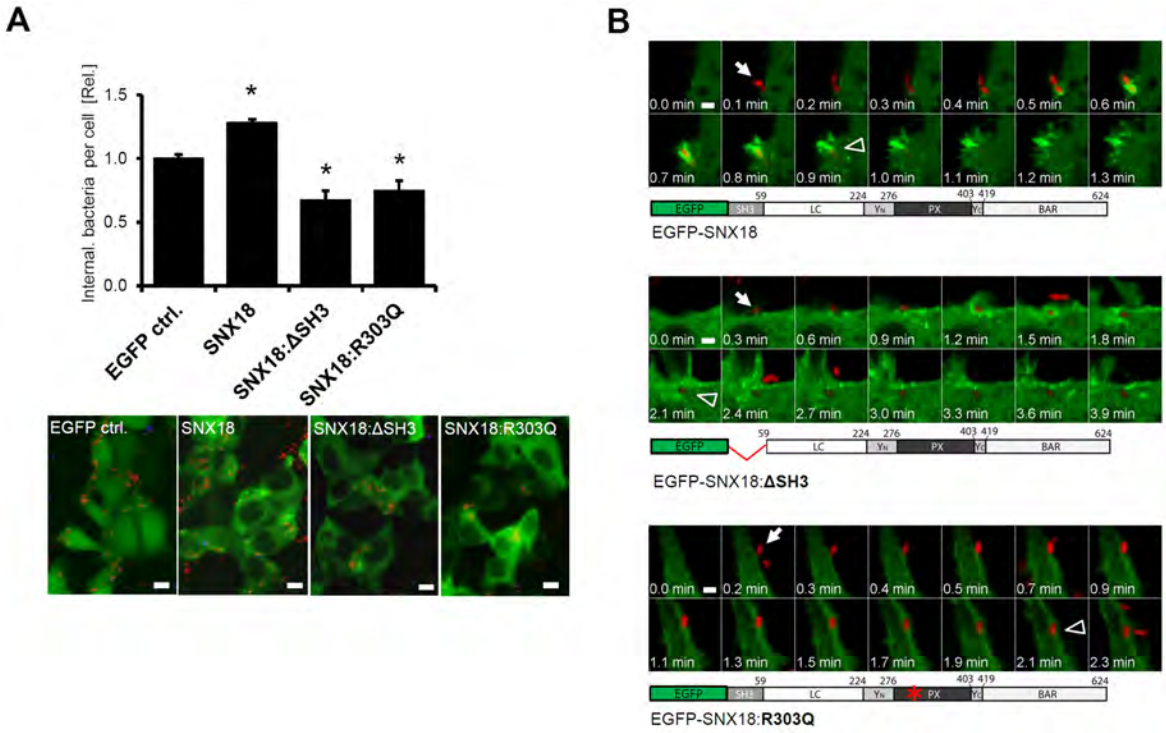
A
Internal. bacteria per cell [Rel.]
1.5
1.0
0.5
0.0
*
*
*
EGFP ctrl.
SNX18
SNX18:ΔSH3
SNX18:R303Q
EGFP ctrl.
SNX18
SNX18:ΔSH3
SNX18:R303Q
B
0.0 min
0.1 min
0.2 min
0.3 min
0.4 min
0.5 min
0.6 min
0.7 min
0.8 min
0.9 min
1.0 min
1.1 min
1.2 min
1.3 min
59
224
276
403
419
624
EGFP
SH3
LC
Yn
PX
Yc
BAR
EGFP-SNX18
0.0 min
0.3 min
0.6 min
0.9 min
1.2 min
1.5 min
1.8 min
2.1 min
2.4 min
2.7 min
3.0 min
3.3 min
3.6 min
3.9 min
EGFP-SNX18:ΔSH3
0.0 min
0.2 min
0.3 min
0.4 min
0.5 min
0.7 min
0.9 min
1.1 min
1.3 min
1.5 min
1.7 min
1.9 min
2.1 min
2.3 min
EGFP-SNX18:R303Q

Figure 2.5

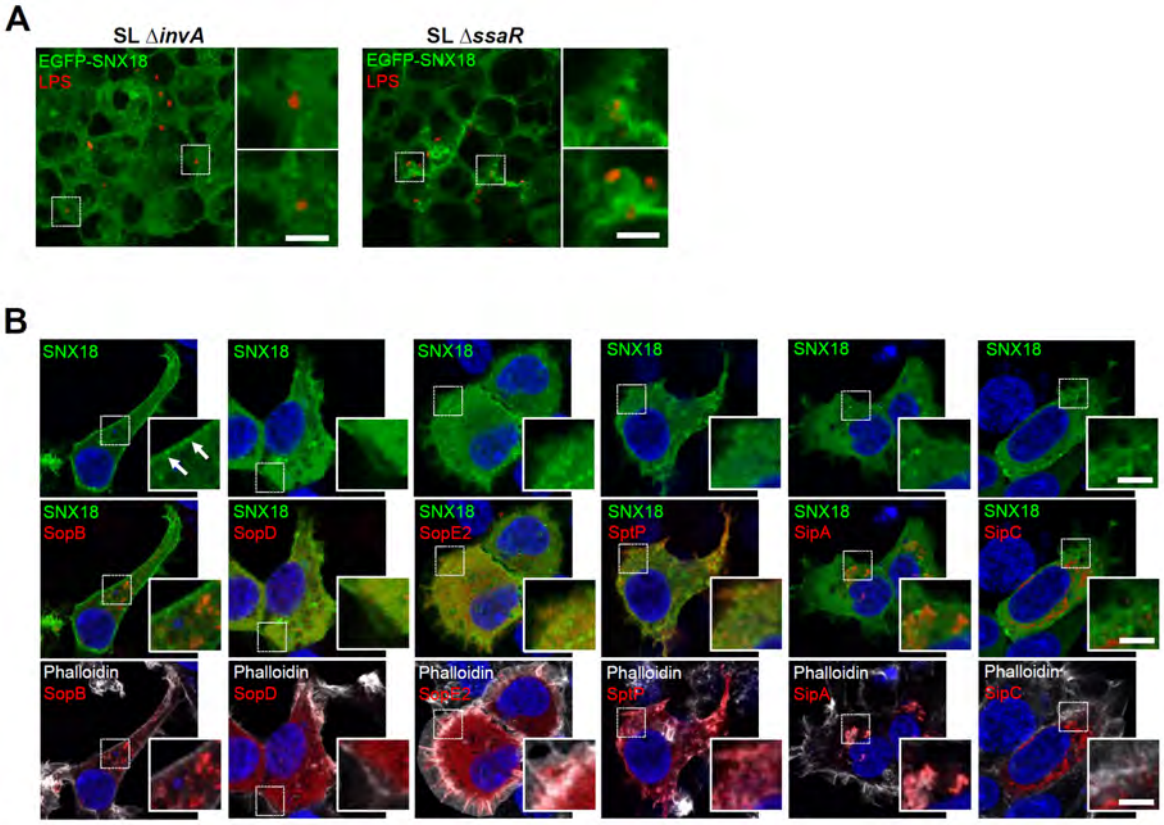
A
SL ΔinvA
SL ΔssaR
EGFP-SNX18
LPS
EGFP-SNX18
LPS
B
SNX18
SNX18
SNX18
SNX18
SNX18
SNX18
SNX18
SopB
SNX18
SopD
SNX18
SopE2
SNX18
SptP
SNX18
SipA
SNX18
SipC
Phalloidin
SopB
Phalloidin
SopD
Phalloidin
SopE2
Phalloidin
SptP
Phalloidin
SipA
Phalloidin
SipC

Figure 2.6

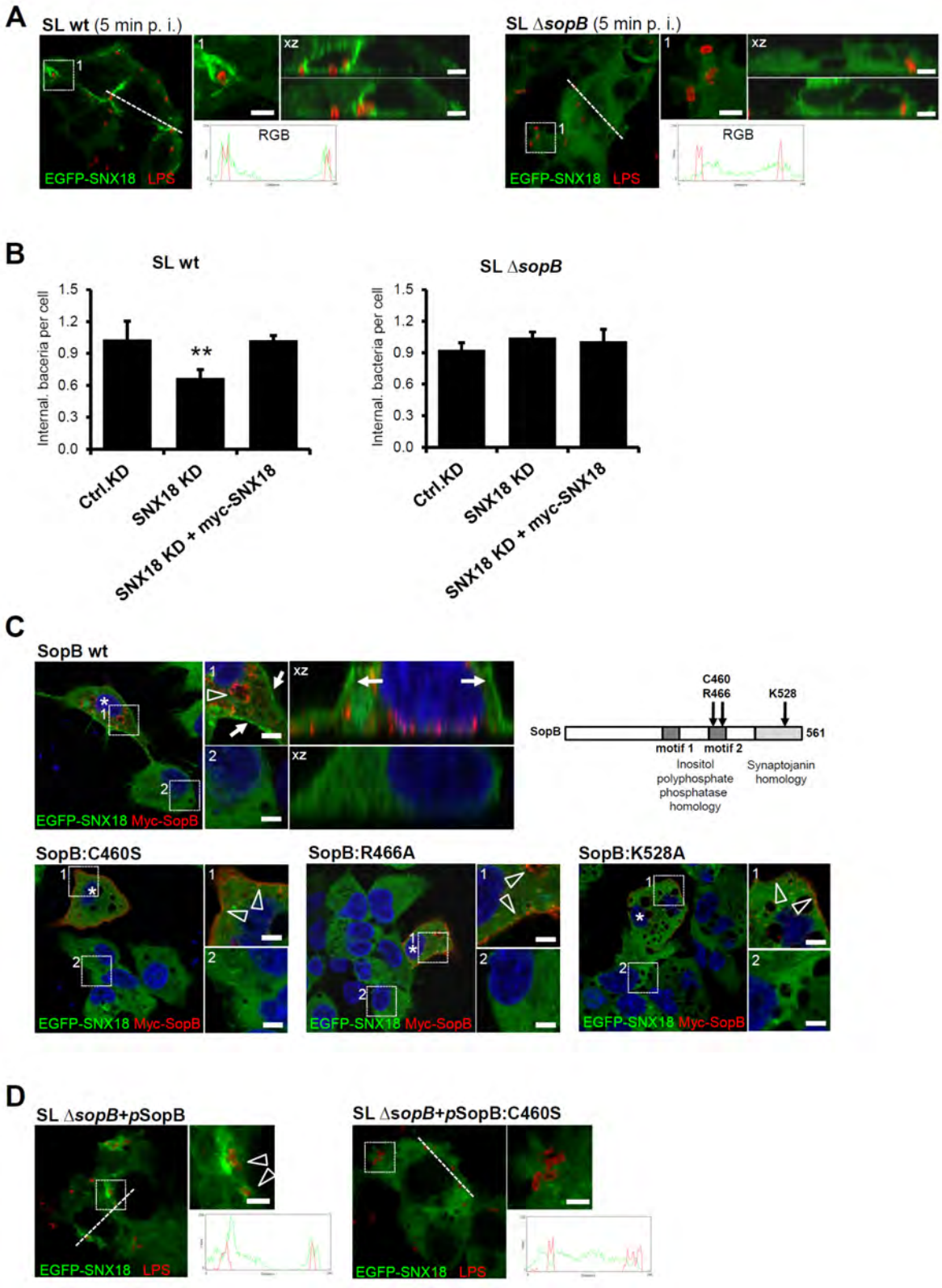
A
SL wt (5 min p. i.)
SL ΔsopB (5 min p. i.)
EGFP-SNX18 LPS
RGB
xz
B
SL wt
SL ΔsopB
Internal. bacteria per cell
1.5
1.2
0.9
0.6
0.3
0.0
**
Ctrl.KD
SNX18 KD
SNX18 KD + myc-SNX18
C
SopB wt
EGFP-SNX18 Myc-SopB
C460
R466
K528
SopB
561
motif 1
motif 2
Inositol polyphosphate phosphatase homology
Synaptojanin homology
SopB:C460S
SopB:R466A
SopB:K528A
D
SL ΔsopB+pSopB
SL ΔsopB+pSopB:C460S

Figure 2.7

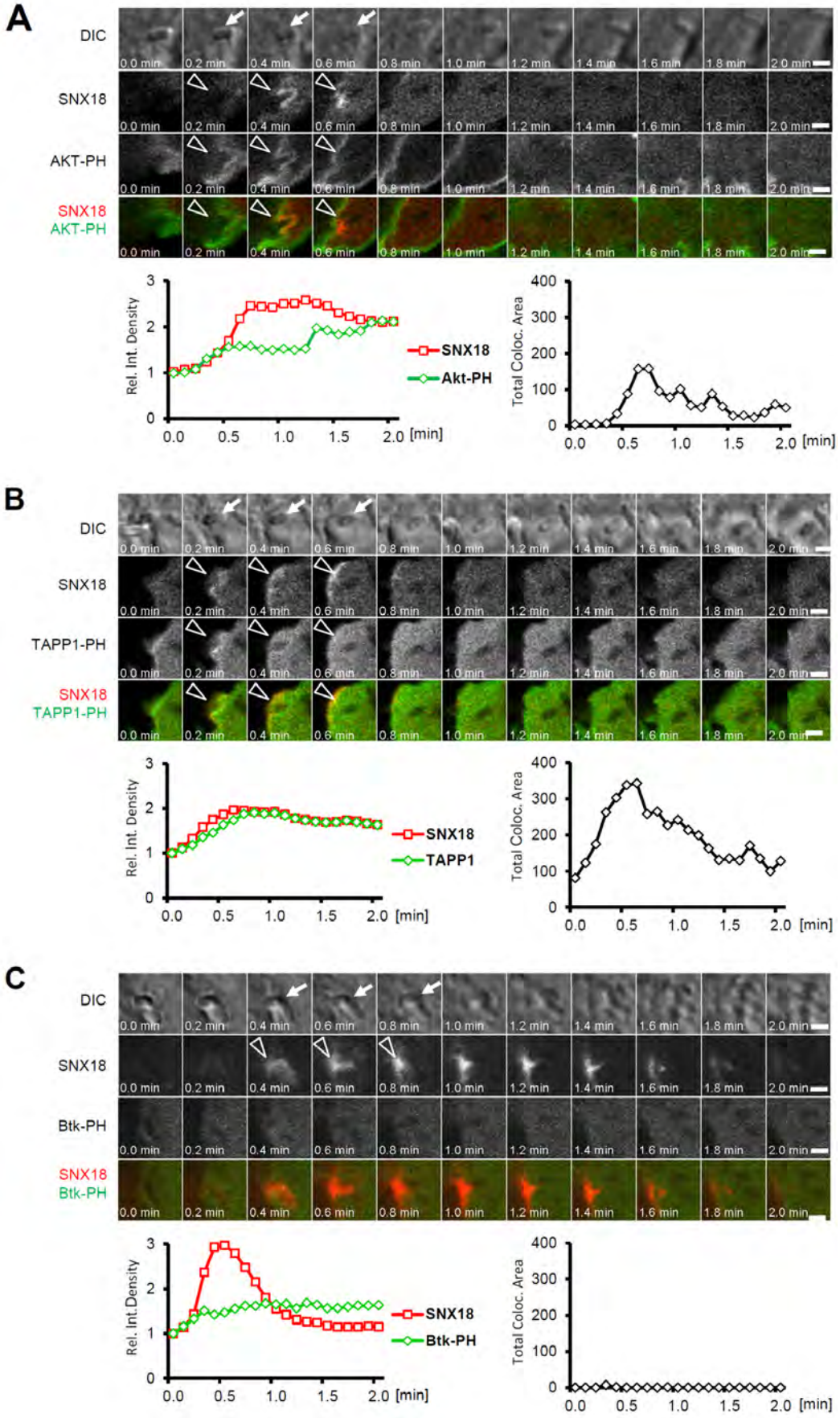
A
DIC
SNX18
AKT-PH
SNX18
AKT-PH
0.0 min
0.2 min
0.4 min
0.6 min
0.8 min
1.0 min
1.2 min
1.4 min
1.6 min
1.8 min
2.0 min
Rel. Int. Density
SNX18
Akt-PH
[min]
Total Coloc. Area
[min]
B
DIC
SNX18
TAPP1-PH
SNX18
TAPP1-PH
Rel. Int. Density
SNX18
TAPP1
[min]
Total Coloc. Area
[min]
C
DIC
SNX18
Btk-PH
SNX18
Btk-PH
Rel. Int.Density
SNX18
Btk-PH
[min]
Total Coloc. Area
[min]

Figure 2.8

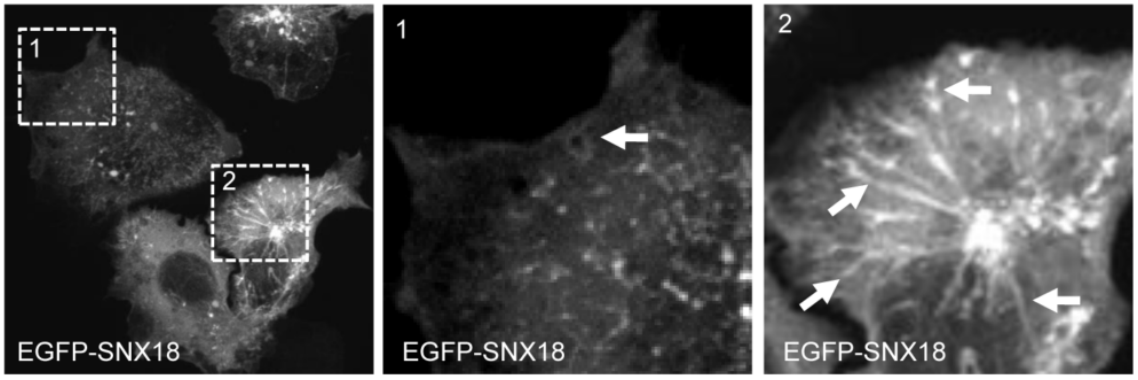

Figure S2.1

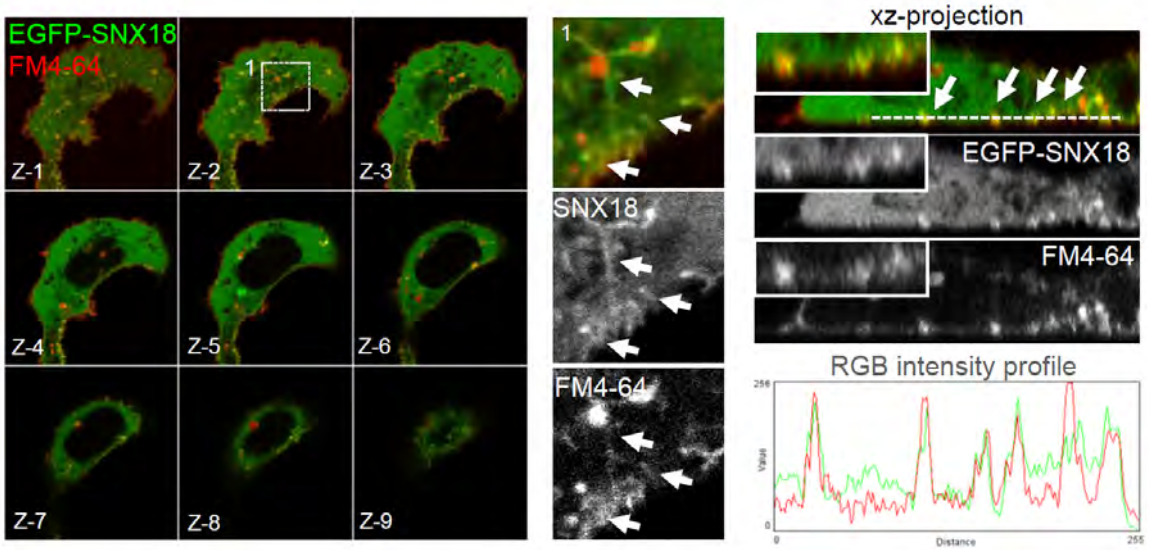
EGFP-SNX18
FM4-64
1
Z-1
Z-2
Z-3
Z-4
Z-5
Z-6
Z-7
Z-8
Z-9
1
SNX18
FM4-64
xz-projection
EGFP-SNX18
FM4-64
RGB intensity profile
256
Value
0
0
Distance
255

Figure S2.2

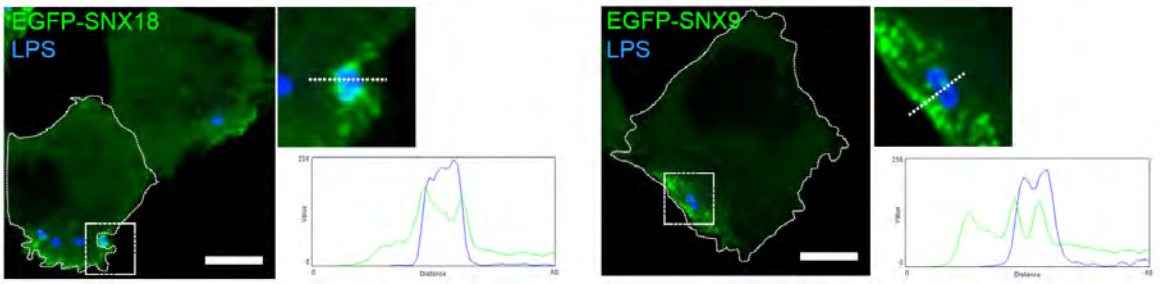

Figure S2.3

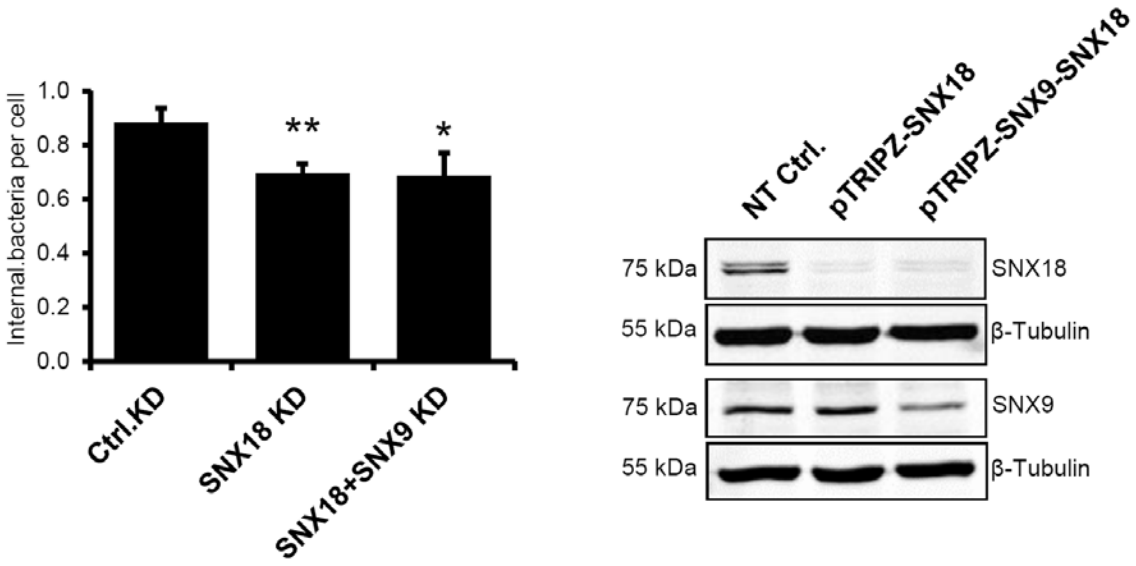
Internal.bacteria per cell
1.0
0.8
0.6
0.4
0.2
0.0
**
*
Ctrl.KD
SNX18 KD
SNX18+SNX9 KD
NT Ctrl.
pTRIPZ-SNX18
pTRIPZ-SNX9-SNX18
75 kDa
SNX18
55 kDa
β-Tubulin
75 kDa
SNX9
55 kDa
β-Tubulin

Figure S2.4

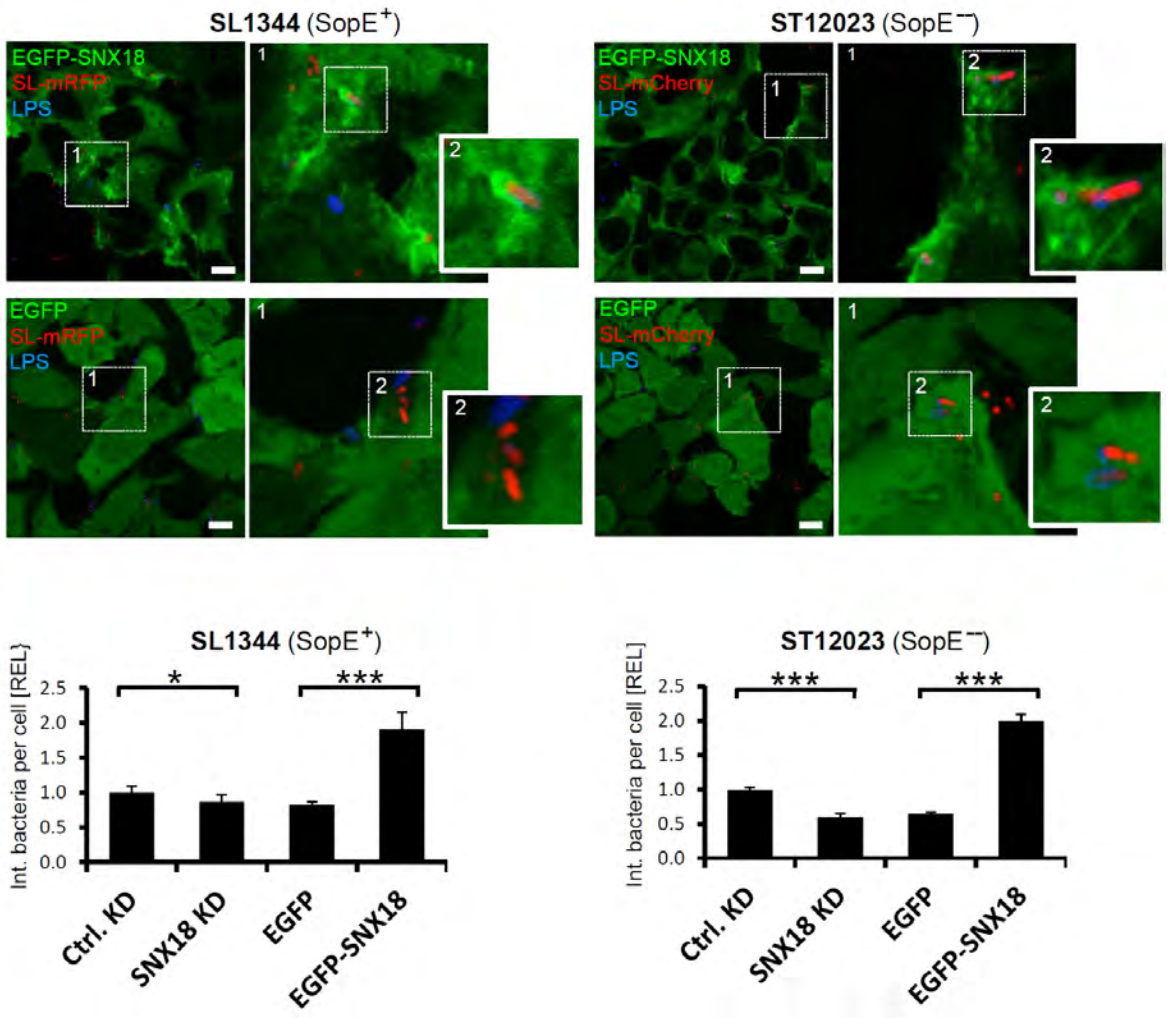
SL1344 (SopE+)
ST12023 (SopE−)
EGFP-SNX18
SL-mRFP
SL-mCherry
LPS
EGFP
1
2
SL1344 (SopE+)
ST12023 (SopE−)
Int. bacteria per cell [REL]
0.0
0.5
1.0
1.5
2.0
2.5
*
***
Ctrl. KD
SNX18 KD
EGFP
EGFP-SNX18

Figure S2.5

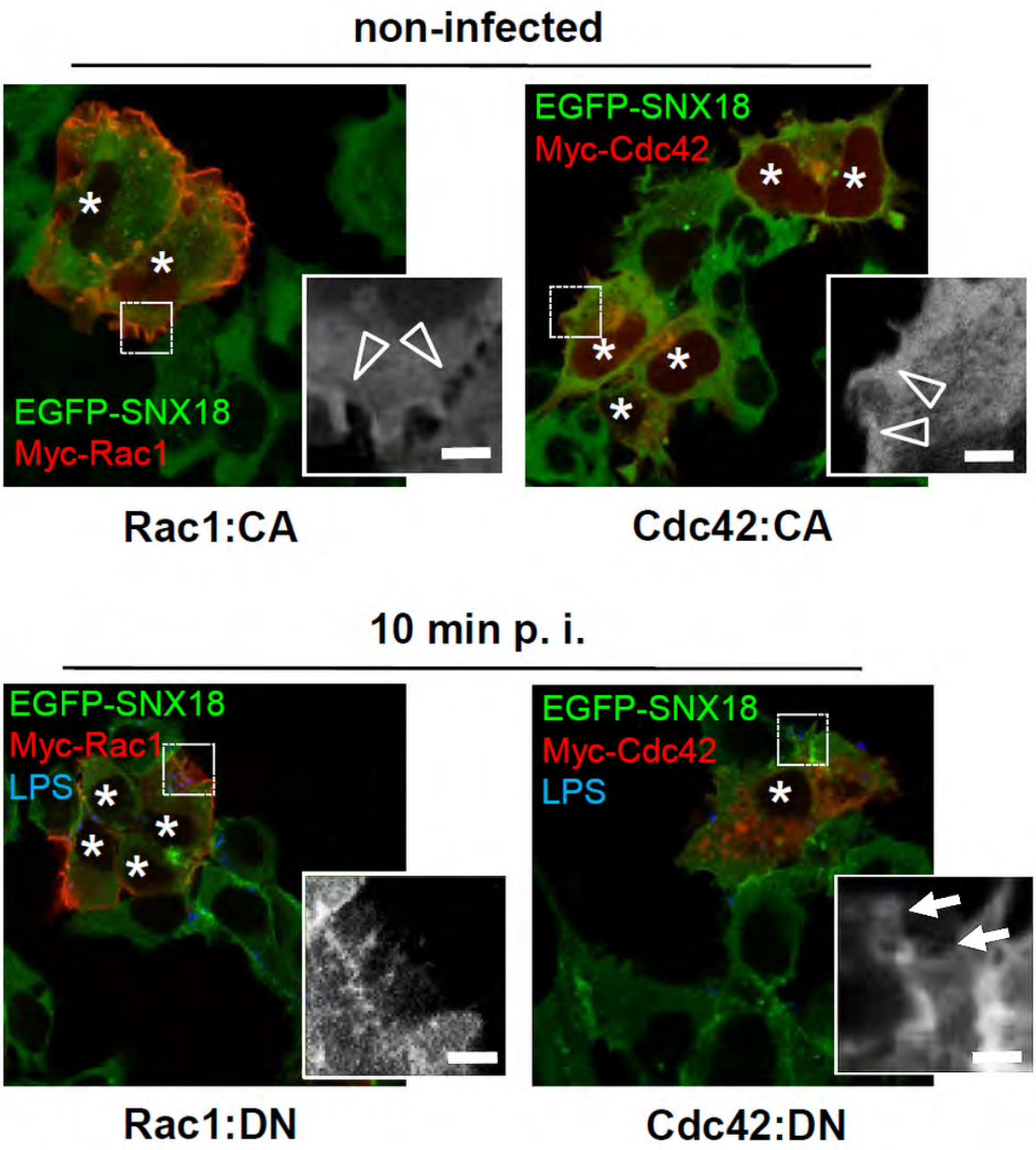
non-infected
EGFP-SNX18
Myc-Rac1
EGFP-SNX18
Myc-Cdc42
Rac1:CA
Cdc42:CA
10 min p. i.
EGFP-SNX18
Myc-Rac1
LPS
EGFP-SNX18
Myc-Cdc42
LPS
Rac1:DN
Cdc42:DN

Figure S2.6

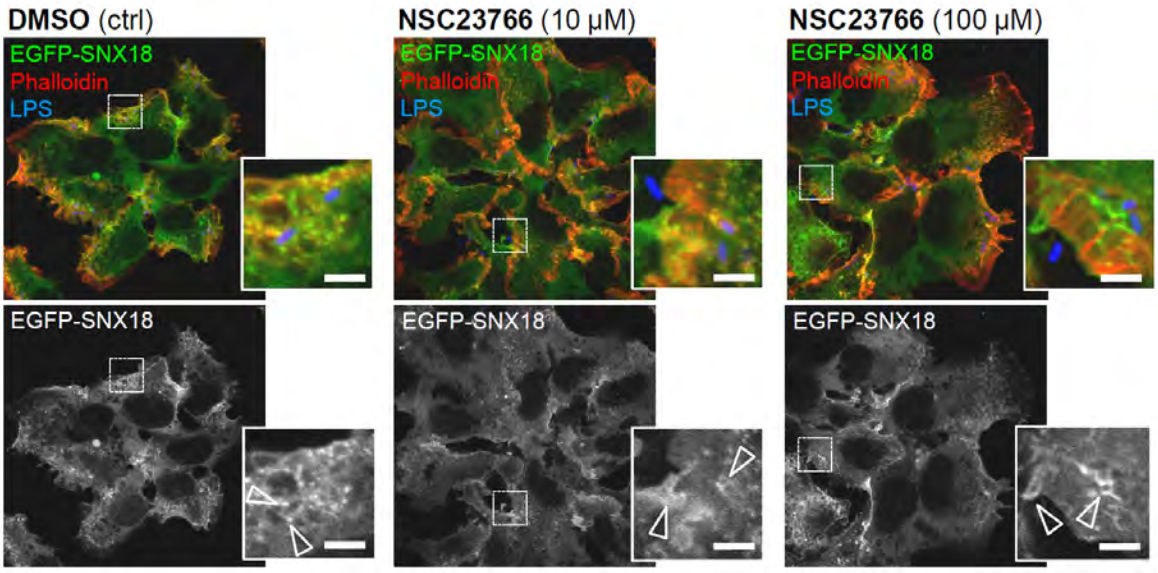
DMSO (ctrl)
NSC23766 (10 μM)
NSC23766 (100 μM)
EGFP-SNX18
Phalloidin
LPS
EGFP-SNX18
EGFP-SNX18
Phalloidin
LPS
EGFP-SNX18
EGFP-SNX18
Phalloidin
LPS
EGFP-SNX18

Figure S2.7

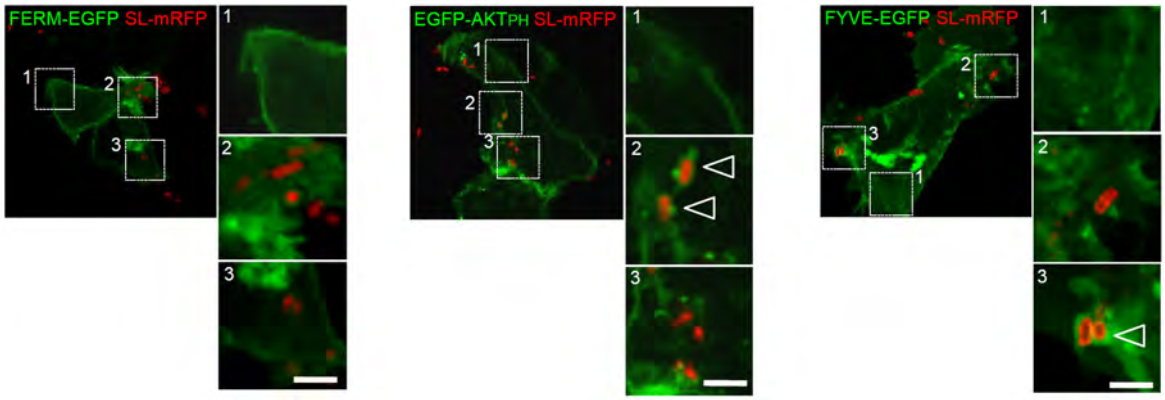

Figure S2.8

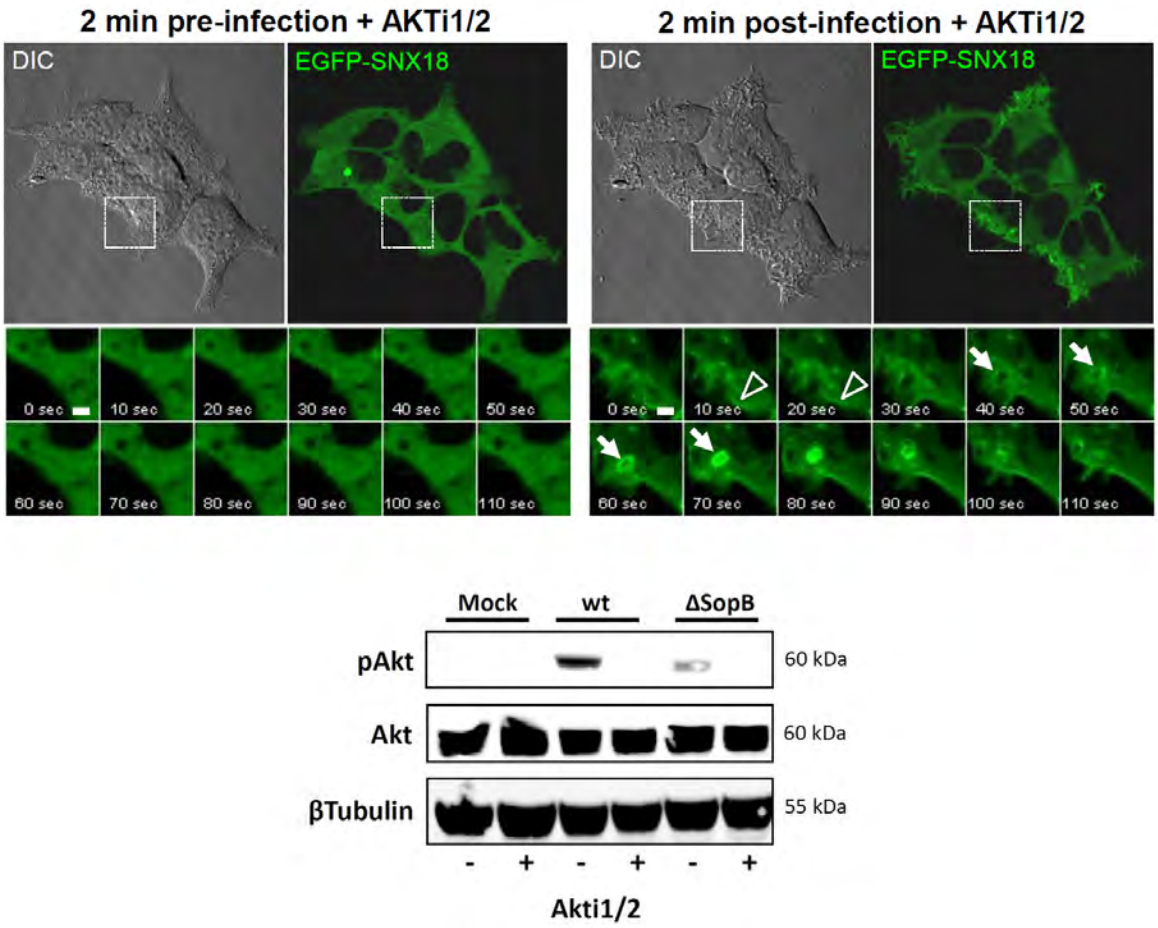
2 min pre-infection + AKTi1/2
2 min post-infection + AKTi1/2
DIC
EGFP-SNX18
DIC
EGFP-SNX18
0 sec
10 sec
20 sec
30 sec
40 sec
50 sec
60 sec
70 sec
80 sec
90 sec
100 sec
110 sec
0 sec
10 sec
20 sec
30 sec
40 sec
50 sec
60 sec
70 sec
80 sec
90 sec
100 sec
110 sec
Mock
wt
ΔSopB
pAkt
60 kDa
Akt
60 kDa
βTubulin
55 kDa
- + - + - +
Akti1/2

Figure S2.9

3 Molecular regulation of SNX18 during macropinocytosis

3.1 Introduction

SNX18 was reported to be a functional redundant paralogue of SNX9. They share the same protein structure and can compensate each other in clathrin-mediated endocytosis (Haberg et al., 2008; Park et al., 2010). However, the level of redundancy between SNX18 and SNX9 at the cellular and biochemical level remains unclear.

Several previous studies have proposed a molecular model for the mechanism of how SNX9 functions in clathrin-dependent endocytosis (Lundmark and Carlsson, 2009). SNX9 is recruited to the clathrin-coated pits (CCP) by interacting with clathrin and AP-2 through SNX9 LC region (Lundmark and Carlsson, 2002, 2003). SNX9 can also recognize the PtdIns(4,5)P2 enriched membrane via PtdIns-binding site within PX domain and induces further membrane curvature via the dimerized BAR domain (Yarar et al., 2008). Although SNX18 was also reported to have a role in clathrin-mediated endocytosis (CME) (Park et al., 2010), it appears to play a more crucial role in macropinocytosis (Wang et al., 2010). Hence, it is important to determine the regulation mechanism of SNX18 during macropinocytosis in order to define similarities and differences between SNX9 and SNX18 at a molecular level.

SNX9 is tightly regulated to maintain an appropriate level of endocytosis within individual cell types. Firstly, SNX9 is reported to bind to a kinase - Ack (Activated Cdc42-associated kinase), which leads to tyrosine phosphorylation of SNX9 within the SH3 domain (Lin et al., 2002). Dimerization is also required for SNX9 phosphorylation in response to epidermal growth factor signalling (Childress et al., 2006). The phosphorylation may switch the protein binding preference for SNX9, which makes it important to place SNX9 in signalling pathways. Secondly, the LC domain has also reported to be involved in SNX9 regulation, via binding to clathrin

and AP-2 on the CCP or the cytosolic protein aldolase (Rangarajan et al., 2010). Phosphorylation of the LC domain may allow SNX9 to release aldolase from the native cytosolic complex and render SNX9 for membrane binding (Lundmark and Carlsson, 2004). Thirdly, protein structure studies suggested that compaction and intra-molecular interactions of the SNX9 SH3-LC region with the PX-BAR unit are likely to occur, and may contribute to the auto-inhibition of SNX9 (Wang et al., 2008; Worby and Dixon, 2002).

Currently it is not known if similar molecular interactions contribute to SNX18 role in the regulated endocytosis pathway, namely macropinocytosis. Within this chapter I will examine if the mechanisms associated with the regulation and recruitment of SNX9 can apply to SNX18. This should determine if we can adapt the same molecular mechanism already described for SNX9 or it requires a different working model for SNX18 to be established.

3.2 Material and Methods

Plasmids

pEGFP-SNX18 and pEGFP-SNX18:ΔSH3 was described before (Wang JT et al., 2010) . pEGFP-SNX18:R303Q was described in Chapter 2.

pEGFP-SNX18:ΔSH3-LC or pEGFP-SNX18:ΔSH3-LC-R303Q was made by PCR amplification of the SNX18 coding sequence encoding the 190-615 amino acids using a 5' primer: CGCGGTACC GAC CTG TCT CTG GGC TCC and a 3' primer: CGCTCTAGA TTA GAC GCT GTC GTA TTT GTG from pEGFP-SNX18 or pEGFP-SNX18:R303Q and sub-cloned into KpnI/XbaI restriction sites of pEGFP-C1 vector.

pEGFP-SNX18:ΔLC or pEGFP-SNX18:ΔLC-R303Q was made by PCR amplification of the SNX18 coding sequence encoding the 1-70 amino acids using a 5' primer: CGCGGATCC GCG CTG CGC GCC CGG GCG CTC and a 3' primer: CGCGGTACC GCC GTC GGC CGG AGG GCC AGG and sub-cloned into BglII/KpnI restriction sites of pEGFP-SNX18: ΔSH3-LC or pEGFP-SNX18:ΔSH3-LC-R303Q construct.

SNX18:GFPint or SNX18:GFPint-R303Q was made by amplification of the SNX18 coding sequence encoding the 1-215 amino acids using a 5' primer: CGCGCTAGC ATG GCG CTG CGC GCC CGG GCG and a 3' primer: CGCACCGGT AC CGT GGC CGA GCT CTT GGC TCC and inserted into NheI/AgeI sites of pEGFP-SNX18: ΔSH3-LC or pEGFP-SNX18:ΔSH3-LC-R303Q construct.

pEGFP-SNX18:Y167F, pEGFP-SNX18:Y256F, pEGFP-SNX18:Y265F, was made from pEGFP-SNX18 using QuikChange® II XL Site-Directed Mutagenesis Kit (Stratagene) with a pair of primers respectively.

Y167F: 5' - GCG CTG GGC AGC GGC GCG TtC CCG GAC CTC GAC GGC, 3' - GCC GTC GAG GTC CGG GaA CGC GCC GCT GCC CAG CGC;

Y256F: 5' - GC GTG GTG CTG GGT CCC TtC GGC CCC GAG TGG C, 3' - G CCA CTC GGG GCC GaA GGG ACC CAG CAC CAC GC;

Y265F: 5’ - GG CAG GAG AAC CCC TtC CCC TTC CAG TGC ACC ATC GAC GAC CC, 3’ - GG GTC GTC GAT GGT GCA CTG GAA GGG GaA GGG GTT CTC CTG CC.

pEGFP-SNX18:FL-ΔY was generated as follows. Initially, a synthetic gene encoding the 1-215 amino acids of SNX18 with tyrosine mutations (Y to F) at Y9, Y55, Y78, Y119, Y132, Y135, Y167 and Y184 positions was purchased from Genscript. The sequence with NheI and AgeI restriction sites is as follow:
GCTAGC ATG GCG CTG CGC GCC CGG GCG CTC TtC GAC TTT AAG TCC GAG AAC CCC GGT GAG ATC TCC CTG CGG GAG CAC GAG GTG CTG AGC CTG TGC AGC GAG CAG GAC ATC GAG GGC TGG CTC GAA GGG ATC AAC AGC CGC GGC GAC CGC GGC CTC TTC CCG GCC TCC TtC GTG CAG GTG ATC CGT GCG CCG GAG CCT GGC CCT CCG GCC GAC GGC GGC CCG GGA GCT CCG GCC CGC TtC GCC AAC GTG CCG CCC GGC GGC TTC GAG CCT TTG CCC GCC GCG CCA CCC GCC GCC TTC CCG CCG CTG CTG CAG CCG CAG GCG TCA CCC GGT TCC TTC CAG CCG CCG GGC GCC GGC TTT CCC TtC GGC GGG GGC GCC CTG CAG CCG TCG CCC CAG CAG CTG TtC GGT GGA TtC CAG GCC AGC CTG GGC AGC GAC GAT GAC TGG GAC GAC GAG TGG GAC GAC AGC TCC ACG GTG GCC GAT GAG CCA GGC GCG CTG GGC AGC GGC GCG TtC CCG GAC CTC GAC GGC TCG TCG TCG GCG GGC GGC GGT GCG GCC GGC CGC TtC CGC CTG TCC ACC CGC TCG GAC CTG TCT CTG GGC TCC CGC GGC GTC TCG GCG CCC CCG GCG CAC CAA GCG TCT GGA GCC AAG AGC TCG GCC ACG GTACCGGT
The mutated fragment from pcDNA3 plasmid was digested and sub-cloned into the NheI/AgeI restriction sites of pEGFP-SNX18: ΔSH3-LC construct.

pEGFP-CAPZA was made by amplification of CAPZA (RIKEN clone FANTOM3:I920091F12) using a 5’ primer: CGCGGATCC GCC GAC TTT GAG GAT CGG GT and a 3’ primer: CGCCTCGAG TTA AGC ATT CTG CAT TTC TTT and sub-cloned into KpnI/XbaI restriction sites of pEGFP-C1 vector.

pEGFP-CAPZB was made by amplification of CAPZB (RIKEN clone FANTOM3:I920049F02) using a 5’ primer: CGCGTCGAC AGC GAT CAG CAG

CTG GAC TG and a 3' primer: CGCGGGCCC TCA ACA CTG CTG CTT TCT CTT C and sub-cloned into SalI/ApaI restriction sites of pEGFP-C1 vector.

pEGFP-ACTN4 was made by amplification of ACTN4 (RIKEN clone FANTOM3:I0C0003G06) using a 5' primer: CGCGTCGAC GTG GAC TAC CAC GCA GCG AA and a 3' primer: CGCGGGCCC TCA CAG GTC GCT CTC CCC AT and sub-cloned into SalI/ApaI restriction sites of pEGFP-C1 vector.

pEGFP-Cbl was made by amplification of (RIKEN clone Cbl FANTOM3:E430004P21) using a 5' primer: CGCGTCGAC GCC GGC AAC GTG AAG AAG AG and a 3' primer: CGCGGGCCC CTA GGT GGC TAC GTG AGC AG and sub-cloned into SalI/ApaI restriction sites of pEGFP-C1 vector.

Antibodies

The following primary antibodies were used in this chapter: Rabbit polyclonal antibodies to SNX18 (AbCam, ab99035), β-tubulin (LI-COR Biosciences, 926-42211) and GFP (Life Technology, A-6455); mouse monoclonal antibodies to phospho-Tyrosine, clone 4G10 (Millipore, 05-1050), α-tubulin Clone DM 1A (Sigma Aldrich), and myc (Cell Signalling Technology, 2272); goat polyclonal α-actinin-4 (N-17) (sc-49333, Santa Cruz Biotechnology); rabbit monoclonal antibodies to Akt (pan) C67E7 (4691) and phospho-Akt (Ser473) D9E (4060) (Cell Signaling Technology).

Alexa Fluor 546 or 647 conjugated goat anti-mouse and Alexa Fluor 488 conjugated donkey anti-goat antibodies for immunofluorescence microscopy were from Life Technologies. Alexa Fluor 647 conjugated phalloidin (A34054) or wheat germ agglutinin (WGA) (W324666) were also from Life Technologies. IRDye® 800CW goat anti-mouse IgG, IRDye® 800CW donkey anti-rabbit IgG, IRDye® 680LT goat anti- rabbit IgG and IRDye® 680LT donkey anti-mouse IgG secondary antibodies for immunblotting were purchased from LI-COR® Biosciences.

Cell culture, transfection and generation of stable cell lines

Human epithelial HEK293 cells (CRL-1573) and human epithelial A431 (CRL-1555) were maintained in complete Dulbecco's modified Eagle's medium (DMEM) (Life

Technologies) supplemented with 10% (v/v) foetal bovine serum (FBS) and 2 mM L-glutamine. Cells were incubated in humidified air/atmosphere (5% CO_2) at 37°C. Cells were transfected with Lipofectamine 2000 as per manufacturer's instructions (Life Technologies). 0.8 µg of DNA and 2 µL of Lipofectamine 2000 were used per well of a 24 well plate. To generate the shRNA-mediated knockdown of SNX18 or ACTN4, the pGIPZ-shRNAmir clone (V2LHS_184681) complementary to human SNX18 and pGIPZ-shRNAmir clones (V3LHS_399576, V3LHS_399575, V3LHS_399577, V3LHS_399579, V3LHS_399578, V3LHS_41018) complementary to human ACTN4 were obtained from Thermo Scientific. HEK293 cells were transfected with pGIPZ constructs using Lipofectamine 2000 (Invitrogen) and non-silencing shRNA was transfected as a control. Cells were split 24 h post transfection and selected in 1 µg/ml puromycin for 7 or more days before protein levels were tested by western blot.

Cell lysis and immunoprecipitation

HEK293 cells on 10 cm dishes were transfected using Lipofectamine 2000 (Life Technologies). 16 hours post transfection the cells were washed twice with cold PBS and lysed inTK lysis buffer containing 50mM hydroxyethyl piperazineethanesulfonic acid (HEPES), 150mM NaCl, 10mM $Na_4P_2O_7$, 30mM NaF, 2mM Na_3VO_4, 10mM ethylenediaminetetraacetic acid (EDTA), 0.5% NP-40, 0.5mM 4-benzenesulfonyl fluoride hydrochloride (AEBSF), protease inhibitor cocktail. Lysates were centrifuged at 13 300 rpm for 10 minutes at 4°C, and the resulting supernatant was subjected to BCA assay to determine protein concentrations as per manufacturer's instructions, by using a microplate reader (PowerWave XS, Bio-Tek) at 560nm wavelength.

To perform immunoprecipitation, equivalent amounts of protein samples were pre-cleared with 30 µl protein G conjugated agarose beads (50% slurry in PBS) for 1 hour at 4°C. The cleared supernatants were then either subjected to GFP immunoprecipitation with GFP-nanoTrap beads (AIBN, The University of Queensland) for 1hr at 4°C, or Myc immunoprecipitation by using mouse monoclonal anti-myc antibody coupling with Protein G conjugated agarose beads overnight. The beads were then washed three times with lysis buffer, before bound proteins eluted by boiling the beads for 5 minutes in SDS-PAGE protein loading buffer.

SDS-PAGE and Western Blotting

Equal amounts of cell lysates or immunoprecipitation samples resuspended in SDS-PAGE protein loading buffer were resolved on SDS-PAGE gels and transferred onto a PVDF membrane (Immobilon-FL, Millipore) using a semi-dry transfer apparatus (Bio-Rad) according to manufacturer's instructions. After blocking in diluted Odyssey blocker (1:1 ratio in PBS) at room temperature for 1 hour, membranes primary antibodies in diluted Odyssey blocker with 0.1% Tween-20 for overnight at 4°C. Membranes were washed in PBST three times for 5 minutes each wash, followed by the incubation of membranes with IRDye® secondary antibodies for 1 hour at room temperature. Fluorescence intensities were detected by LI-COR Odyssey Infrared Imaging System (LI-COR Biosciences) (Bugarcic et al., 2011). For the detection of less sensitive signals, enhanced chemiluminescence (ECL) detection kit (Super Signal ECL substrate, Thermo Scientific) was used, as previously described (Choy et al., 2004). Calculated relative molecular weight of each protein is indicated on the gels.

Assay for monitoring *Salmonella*-induced SNX18 phosphorylation

HEK293 cells transfected with indicated GFP tagged SNX18 constructs were serum starved for 16 h before infection with *Salmonella* (as described in Chapter 2). Cells were incubated with *Salmonella* at MOI=100 for the time as indicated. Cells were lysed and samples were prepared as GFP-nanoTrap immunoprecipitation previously described. Protein samples were then analysed by SDS-PAGE and Western Blotting. Membranes were scanned and fluorescence intensities were detected by Odyssey imaging system according to manufacturer's instructions. The integrated intensity of each band of interest was measured by Odyssey software.

Indirect immunofluorescence, *Salmonella* infection, image-based quantification of macropinocytosis (Dextran uptake) and live cell imaging were described as in Chapter 2.

3.3 Results

3.3.1 Model for SNX18 recruitment

I identified two pools of SNX18 in epithelial cells, cytosolic and membrane-bound, and suggested that membrane relocation is linked with functional activation of SNX18 (Chapter 2). To understand how the equilibrium of the two pools is regulated, I examined the subcellular localization of truncated SNX18 mutants (Fig 3.1). While depletion of SH3 domain (SNX18:ΔSH3) had little impact on SNX18 localization prior to *Salmonella* infection and it can translocate to the plasma membrane upon *Salmonella* invasion (Chapter 2), the depletion of LC domain (SNX18:ΔLC) or both SH3 and LC domains (SNX18: ΔSH3-LC) resulted in increased levels of SNX18 at the plasma membrane even in the absence of any stimulation (Fig 3.2A). Therefore, the presence of the LC domain is required for maintaining SNX18 in the cytosol.

Furthermore, membrane-recruitment of SNX18 is disrupted when a single mutation within SNX18 PtdIns-binding pocket (SNX18:R303Q) is introduced (Chapter 2). I propose that SNX18 employs an auto-inhibitory mechanism to block the PtdIns-binding pocket that prevents its recruitment to the plasma membrane. One of the common auto-inhibitory mechanisms is the closed-and-opened regulation of the protein confirmation. In the case of SNX18, I postulated that the protein is maintained in a closed form where the SH3-LC domains are folded back onto PX-BAR domains to shelter the PtdIns-binding pocket. The LC domain would therefore represent one of the domains that enables maintenance of the SNX18 closed form. During *Salmonella*-induced macropinocytosis, SNX18 could undergo a conformational change into an opened form, exposing the PtdIns-binding pocket so that SNX18 can be directed to the plasma membrane by recognizing the specific PtdIns(3,4)P_2 at the membrane invagination.

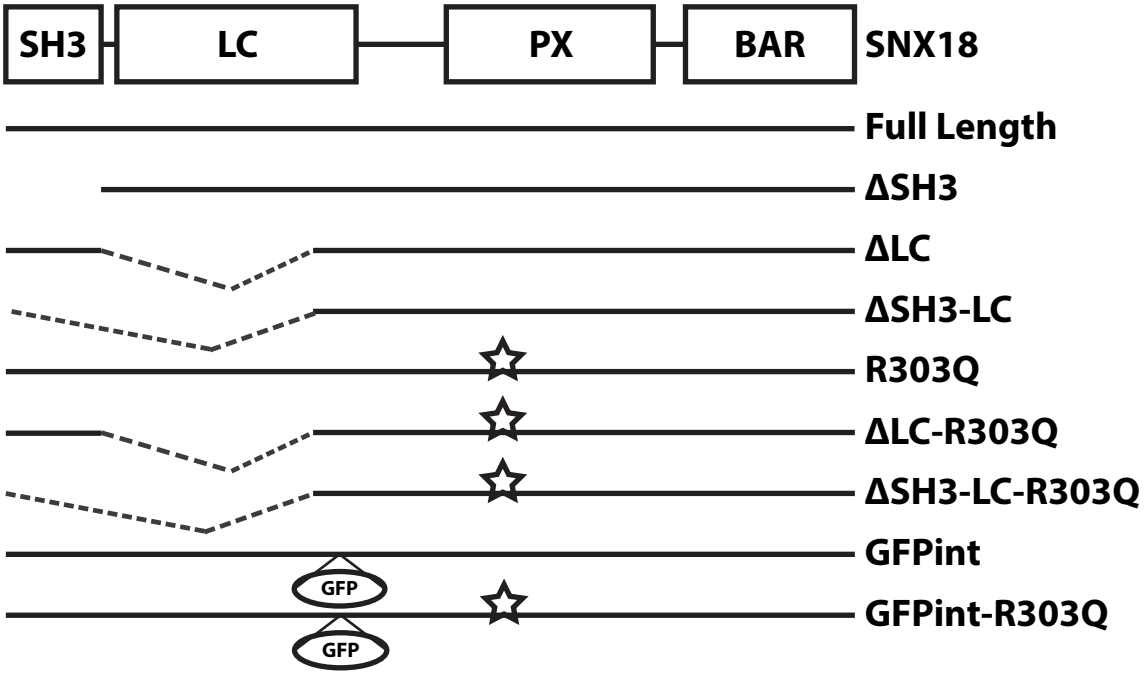

Figure 3.1 - SNX18 mutants diagram.

SNX18 mutants used in this chapter, showing domain truncation (dashed lines) and point mutations (star).

Figure 3.2 - SNX18 mutants have impact on equilibrium between cytosolic and membrane-bound pools of SNX18. (See next page)

(A) EGFP-SNX18:ΔLC or EGFP-SNX18:ΔSH3-LC was transiently expressed in HEK293 cells and 24 hours post transfection GFP positive cells were imaged live using confocal microscopy. A section near the basal surface of the cell monolayer (left panel) and a section in the middle (right panel) are shown for each construct. (B) SNX18:GFPint or SNX18: GFPint-R303Q was transiently expressed in HEK293 cells. 24 hours after transfection, cells were fixed in 4% PFA. The subcellular localization of each construct is shown in one XY view section together with a projection of Z-stack (XZ orthogonal view). Scale bars = 5 μm.

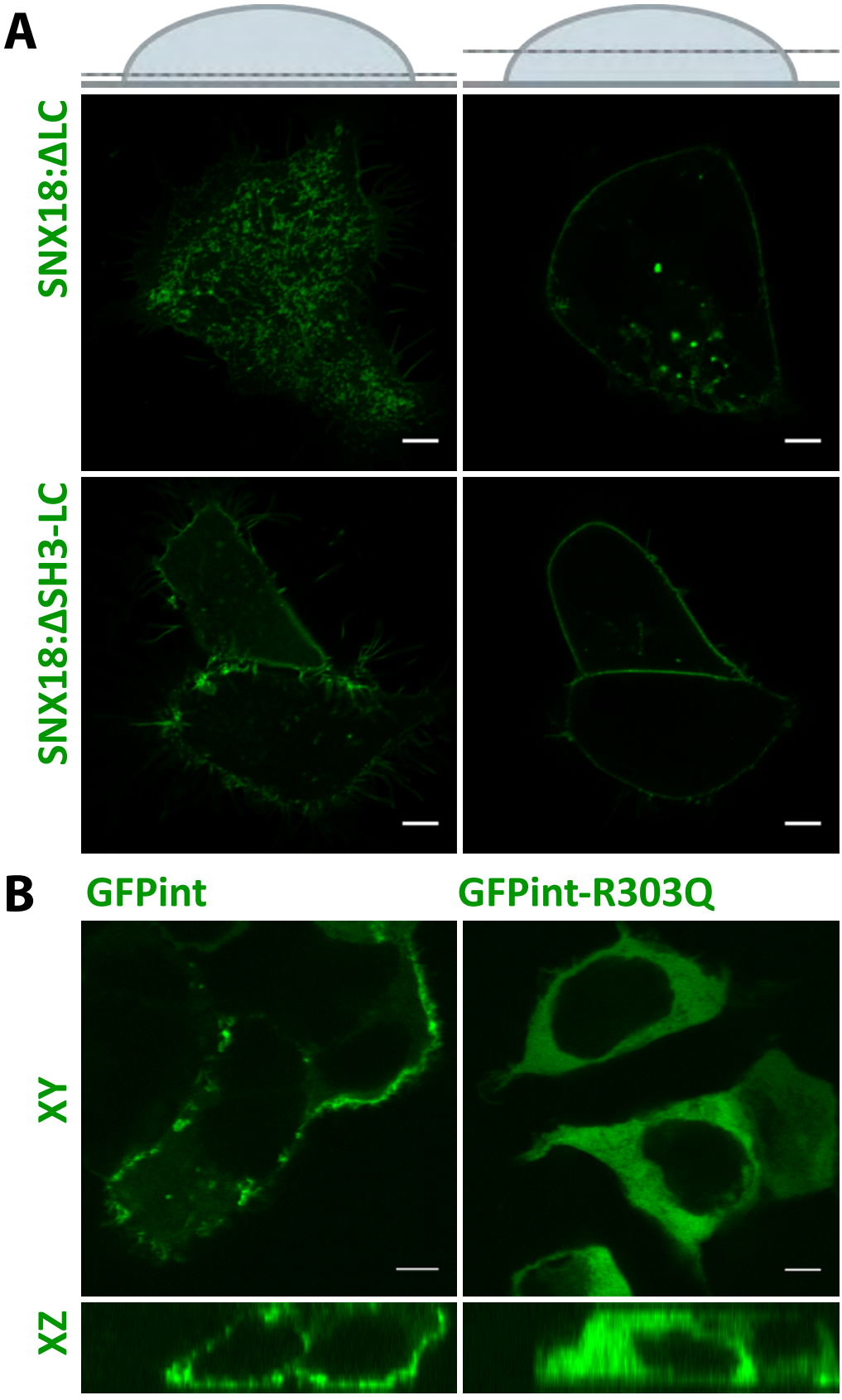

Figure 3.2 - SNX18 mutants have impact on equilibrium between cytosolic and membrane-bound pools of SNX18. (See legend on previous page)

To investigate this model, I generated a SNX18 construct with GFP inserted between LC and PX domain (SNX18:GFPint) and proposed that this GFP insertion will interfere with SNX18 folding and keep it in a constitutively open form. When SNX18:GFPint was expressed in cells, it showed predominantly membrane localization, especially enriched in certain subdomains on the plasma membrane and membrane tubules (Fig 3.2 B). Mutation of the PtdIns-binding site within this protein (SNX18:GFPint-R303Q) was sufficient to inhibit its recruitment to the plasma membrane (Fig 3.2 B), indicating that the disruption of PtdIns-binding is sufficient to keep SNX18 in the cytosol regardless of its protein structure.

To further analyse whether the SNX18:GFPint protein represents an open form rather than a closed form, fluorescently labelled dextran uptake assay was used to examine if the macropinocytosis levels in cells transiently overexpressing SNX18-GFPint was elevated. The rate of macropinocytosis of each cell line was quantified by numbers of dextran-positive macropinosomes in GFP-positive cells after 10 min of dextran uptake (Wang et al., 2010). Cells expressing SNX18-GFPint, in comparison to GFP only control cells, had a 2-fold increase in macropinocytosis rates. However, this increase was lower than that 3-fold increase observed when EGFP-SNX18 is expressed (Fig 3.3). Therefore, while SNX18:GFPint protein encodes all of the intact SNX18 domains and can function as an up-regulator of macropinocytosis, whether it does this an open confirmation that represents an active form of SNX18 needs further investigation.

3.3.2 Regulation of SNX18 activity

The membrane recruitment of SNX9 is regulated by phosphorylation. SNX9 recruitment to plasma membrane occurs when its LC domain is phosphorylated during stimulation, which subsequently results in the release of aldolase, a molecule which prevents SNX9 recruitment to the plasma membrane (Lundmark and Carlsson, 2004; Rangarajan et al., 2010). To examine whether the regulation of SNX18 recruitment adopts the similar mechanism, the phosphorylation of SNX18 was tested. GFP-SNX18 was immunoprecipiated from transient transfected HEK293 cells using

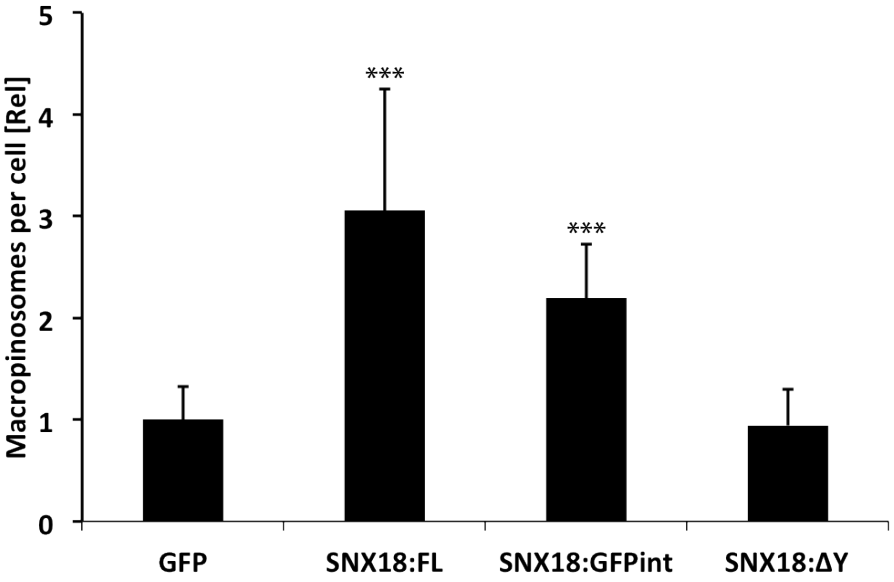

Figure 3.3 - Macropinocytosis is upregulated in SNX18 overexpressing cells.

The rate of macropinocytosis in cells overexpressing SNX18:FL, SNX18:GFPint or SNX18:ΔY were assessed by fluorescent dextran uptake assay in HEK293 cells. Number of dextran-positive macropinosomes per cell was counted using ImageJ image analysis software. The average values in control cells were normalized to one to demon strate the fold change in EGFP-SNX18 expressing cells. Between 370-550 cells per sample were analysed with an average of 3.31 +/- 1.08 macropinosomes observed in GFP expressing cells. Bars indicate the mean + standard deviation between 3 technical repeats in one experiment. *** $p<0.001$, t-test.

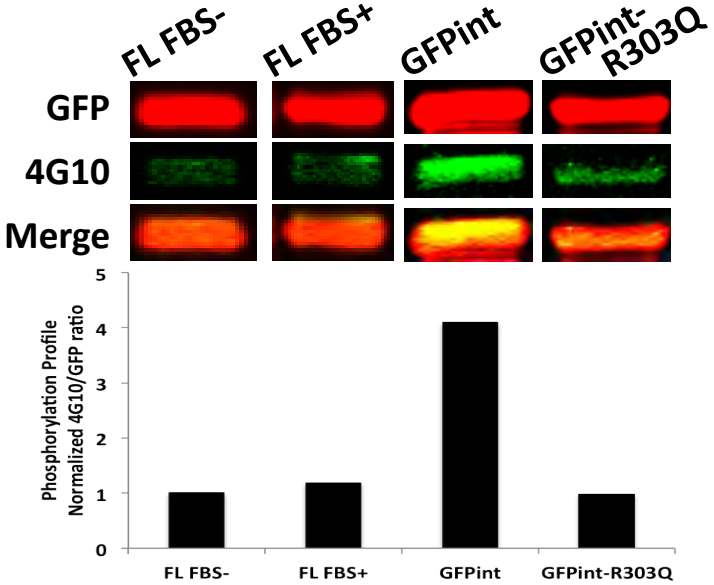

Figure 3.4 - SNX18 is phosphorylated. (See legend on next page)

GFP-nanoTrap beads, and tyrosine phosphorylation on SNX18 was detected by phospho-tyrosine antibody (4G10). I observed a low proportion of SNX18 could be phosphorylated at tyrosine residues under basal, serum-starved condition, which increased when serum was added (Fig 3.4). The highest level of tyrosine phosphorylation was observed in the cells transfected with the plasma membrane-bound SNX18:GFPint, while phosphorylation was almost undetectable in the cells transfected with the cytosol localized mutant SNX18 GFPint-R303Q where the PtdIns binding pocket was mutated (Fig 3.4).

As SNX18 is recruited to the *Salmonella* induced membrane ruffles (Chapter 2), the phosphorylation levels of SNX18 during *Salmonella* infection were also examined. HEK293 cells transiently overexpressing wild-type full-length SNX18 (GFP-SNX18:FL) were serum-starved overnight prior to *Salmonella* infection. The GFP-SNX18 was immunoprecipitated using GFP-nanoTrap beads and the amount of phosphorylated SNX18 was detected by western blotting using anti-phospho-tyrosine antibody. The level of tyrosine phosphorylation on SNX18 had a 6-fold increase at 5 min post *Salmonella* infection when compared to mock-infected cells (Fig 3.5A). By 10 min post infection, the phosphorylation level decreased to approximately 2-fold increase over mock-infected cells.

Figure 3.4 - SNX18 is phosphorylated. (See previous page)
Phosphorylation profile of SNX18:FL, SNX18:GFPint and SNX18:GFPint-R303Q in non-infected cells. EGFP-SNX18 mutants were transiently expressed in HEK293 cells. 24 hours post transfection, cells were cultured in medium supplemented with or without fetal bovine serum (FBS) overnight. Cells were lysed and SNX18 proteins were immuno-precipitated using GFP-nanoTrap. Tyrosine phosphorylated SNX18 was detected by anti-phosphotyrosine antibody 4G10 (green) and total SNX18 was detected by anti-GFP antibody (red). The intensity of 4G10 bands and GFP bands on the western blot were measured by Odyssey software. Quantitative analysis showed the ratios of 4G10 to GFP intensities from this blot that was normalized to the sample from cells expressing GFP-SNX18:FL in FBS- condition (FL FBS-).

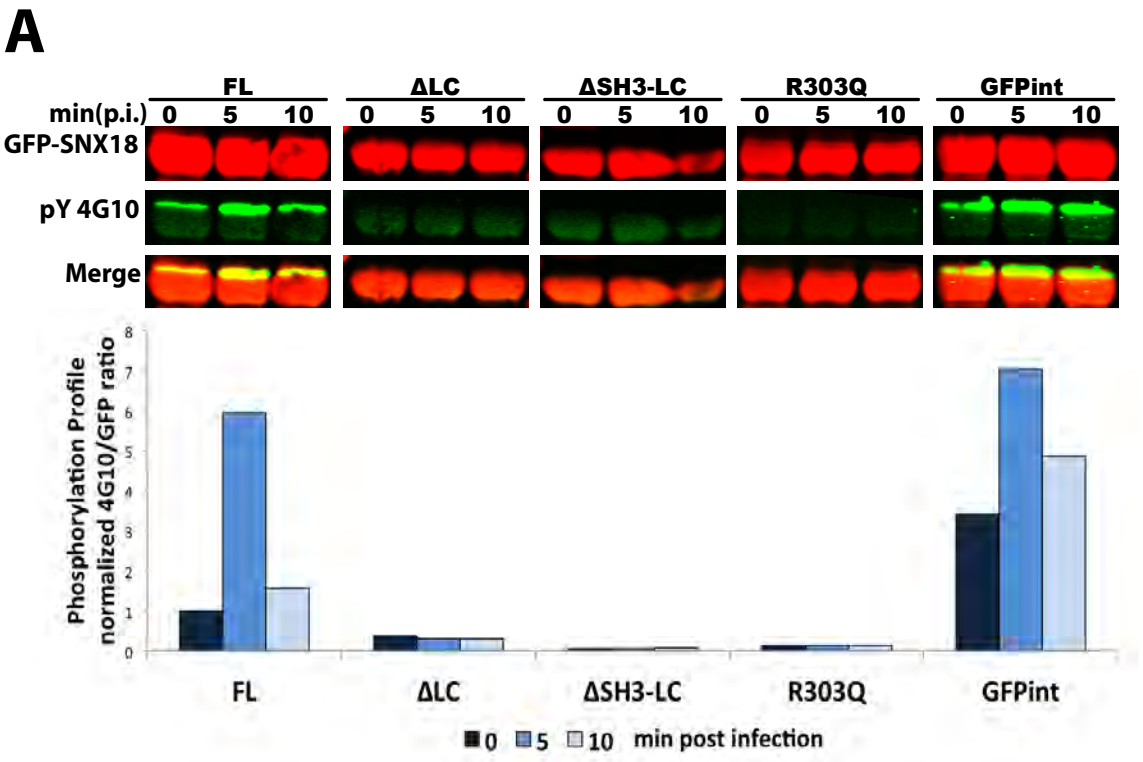

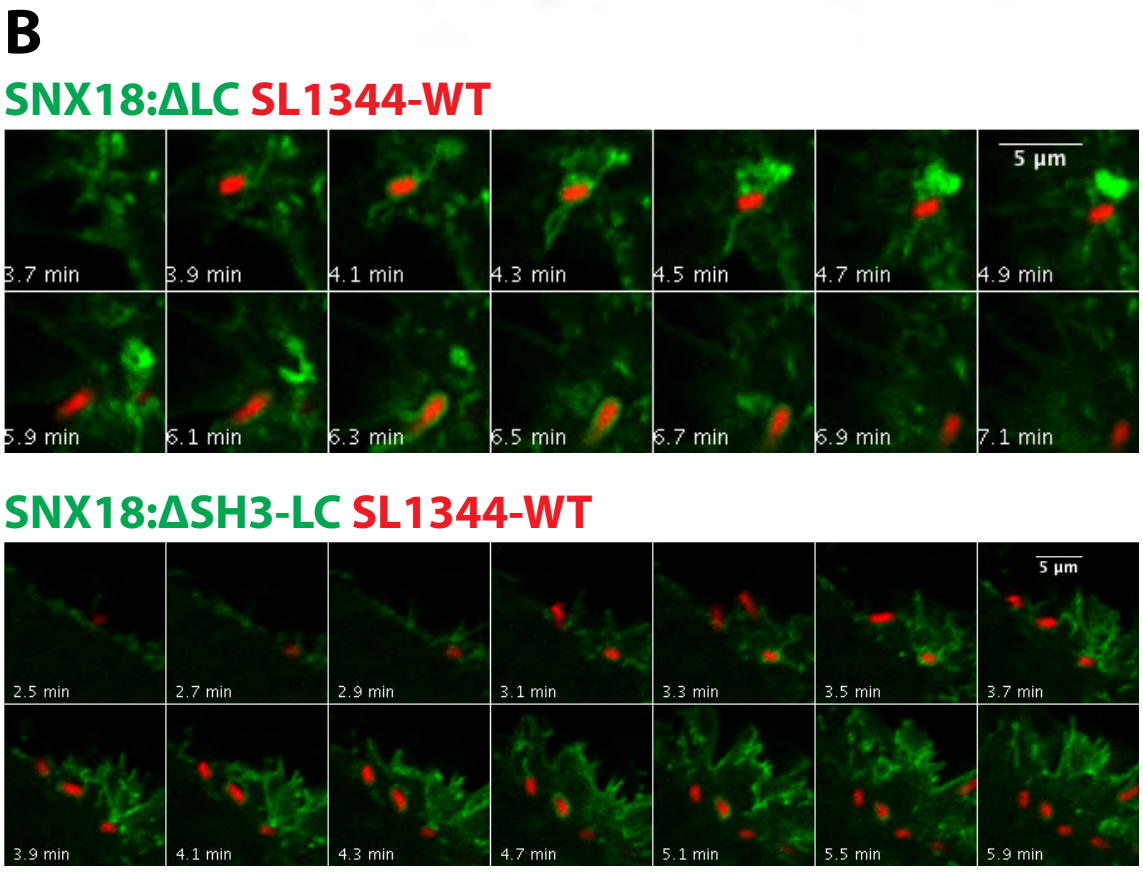

Figure 3.5 - Intact LC region and PI-binding site of SNX18 are necessary for tyrosine phosphorylation. (See legend on next page)

To determine which of the SNX18 domains could be phosphorylated, the phosphorylation profiles of truncated SNX18 mutants and PtdIns-binding mutant were also tested. Western immunoblotting experiments showed that SNX18:ΔLC and SNX18:ΔSH3-LC were not phosphorylated in either mock or *Salmonella* infected cells, suggesting that deletion of LC domain or both SH3 and LC domain prevented *Salmonella*-induced SNX18 phosphorylation (Fig 3.5A). Interestingly, in live cell imaging movies, both GFP-SNX18:ΔLC and GFP-SNX18:ΔSH3-LC localized to the plasma membrane prior to infection and their local recruitment to plasma membrane subdomains of SCV was still increased during *Salmonella* internalization (Fig 3.5B). Therefore, SNX18:ΔLC and SNX18:ΔSH3-LC both showed plasma membrane localization without any phosphorylation detected, which suggests that the membrane recruitment is not sufficient for the triggering of SNX18 phosphorylation.

Figure 3.5 - Intact LC region and PI-binding site of SNX18 are necessary for tyrosine phosphorylation. (See previous page)

(A) Phosphorylation profile of SNX18:FL, SNX18:ΔSH3, SNX18:ΔLC, SNX18:ΔSH3-LC and SNX18:GFPint during *Salmonella* invasion. EGFP-SNX18 mutants were transiently expressed in HEK293 cells. 24 hours post transfection cells were lysed at 5min or 10min after infection with wild type *Salmonella* SL1344. Cells treated with infection medium without *Salmonella* for 10min were used as mock infected controls. SNX18 proteins were immunoprecipitated using GFP-nanoTrap. Tyrosine phosphorylated SNX18 was detected by anti-phosphotyrosine antibody 4G10 (green) and total SNX18 was detected by anti-GFP antibody (red). The intensity of 4G10 bands and GFP bands on the western blot were measured by Odyssey software. Quantitative analysis of this representative blot from two biological repeats showed the ratio of 4G10 to GFP at each time point that was normalized to the mock infected cells expressing GFP-SNX18:FL. (B) A series of confocal sections from a time-lapse of EGFP-SNX18 mutants expressing cells (green) infected with wild type *Salmonella* SL1344 expressing pBR-mRFP.1 (SL1344-WT, red). Montage of movie 8 and movie 10. SNX18 mutants SNX18:ΔLC and SNX18:ΔSH3-LC were relocated from the cytosol to *Salmonella*-induced membrane ruffles at the site of bacterial attachment with a transient accumulation of SNX18 during the SCV scission from the plasma membrane. Scale bars = 5μm.

This conclusion is further supported by the expression of two SNX18 mutants which I showed have either a constitutive plasma membrane (SNX18:GFPint) or cytosolic (GFP-SNX18:R303Q) localisation. The plasma membrane-bound SNX18:GFPint appears to have high basal level of tyrosine phosphorylation in mock-infected cells while *Salmonella* infection leads to a further 2-fold increase in phosphorylation, which decreased to the level similar to the mock-infection by 10 min post-infection (Fig 3.5A). On the other hand, GFP-SNX18:R303Q mutant, which remained in the cytosol during *Salmonella* invasion (Chapter 2, Fig 2.5) does not appear to be phosphorylated (Fig 3.5A), indicating that SNX18 localisation at the plasma membrane is required for its phosphorylation. Thus, I conclude that the recruitment of SNX18 to the plasma membrane is necessary but not sufficient for its phosphorylation. In other words, the tyrosine phosphorylation takes place subsequently to the recruitment, which may lead to the functional activation of SNX18.

Studies on SNX9 phosphorylation (Lundmark and Carlsson, 2004) and several online phosphosites prediction databases (PhosphositePlus (http://www.phosphosite.org), NetPhos 2.0 Server (http://www.cbs.dtu.dk/services/NetPhos/), and Human Protein Reference Database (http://www.hprd.org)), predict two phosphosites (tyrosine 256 or tyrosine 265) within the York domain, which links the LC and PX domains, and one

Figure 3.6 - SNX18 single tyrosine point mutation is not sufficient to block phosphorylation and membrane translocation during *Salmonella* invasion.
(See next page)
(A) Phosphorylation profile of SNX18 single tyrosine point mutations, Y256F, Y265F and Y167F, during *Salmonella* invasion. HEK293 cells transiently expressing EGFP-SNX18 tyrosine mutants were used and the phosphorylation profiles were generated from the representative experiment as described in Fig 3.5. (B) A series of confocal sections from a time-lapse of EGFP-SNX18 tyrosine mutants expressing cells (green) infected with wild type *Salmonella* SL1344 expressing pBR-mRFP.1 (SL1344-WT, red). Montage of movie 12, movie 14 and movie 16. Scale bars = 5 μm.

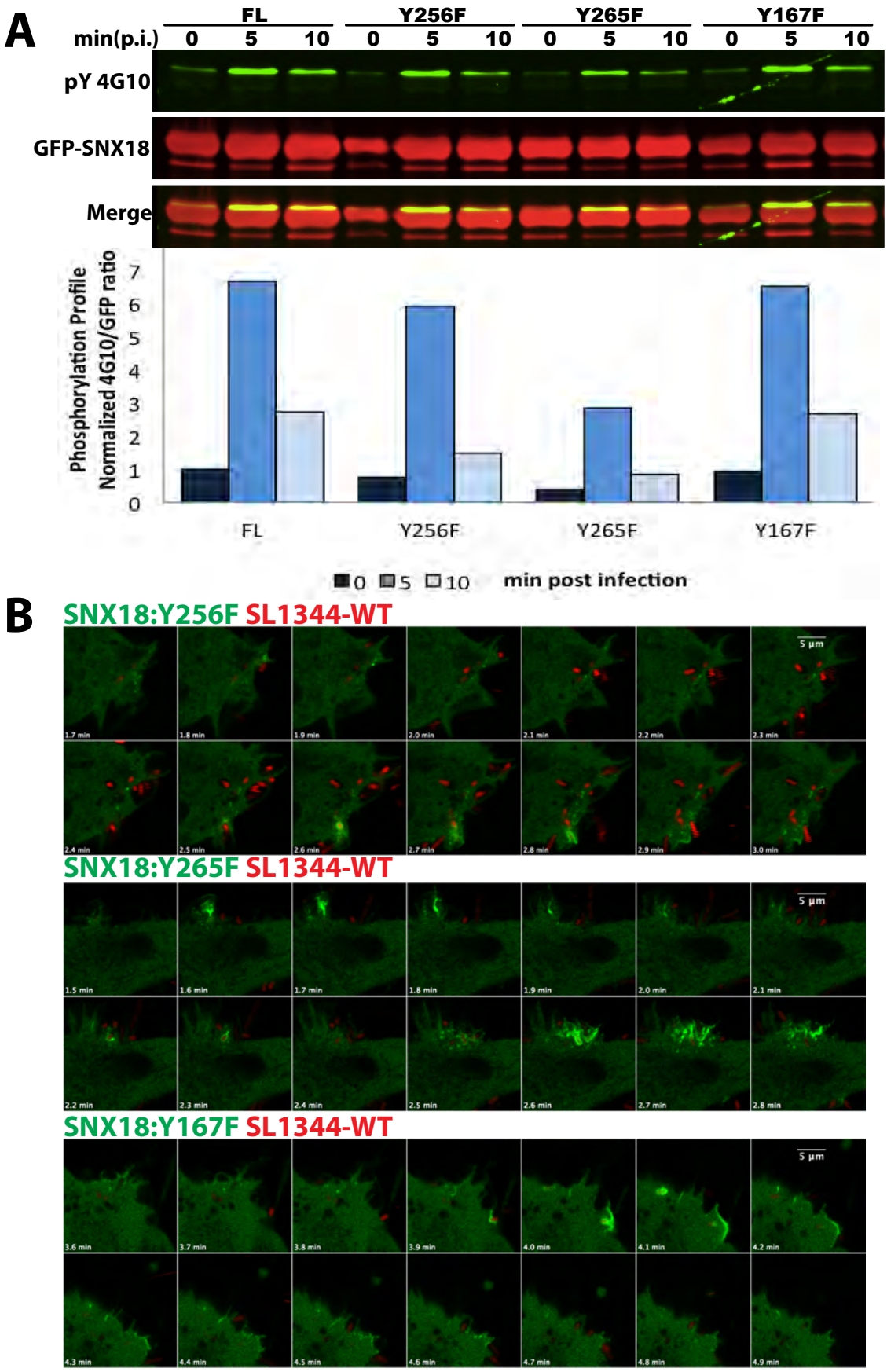

Figure 3.6 - SNX18 single tyrosine point mutation is not sufficient to block phosphorylation and membrane translocation during Salmonella invasion. (See legend on previous page)

phosphosite (tyrosine 167) within LC domain as potential phosphosites on SNX18. Single point mutations on these residues were made by substitution of tyrosine to phenylalanine (Y167F, Y256F and Y265F) by site-directed mutagenesis. The phosphorylation profiles of these mutants during *Salmonella* invasion were examined and compared to wild type SNX18. As shown in the quantification of the western immunoblotting experiments, total tyrosine phosphorylation level on SNX18:Y256F mutant had a slight decrease whereas phosphorylation on SNX18:Y265F mutant showed a 50% decrease compared to the wild type SNX18 (Fig 3.6A). However, *Salmonella* infection still enabled the 6-fold increase in tyrosine phosphorylation, which peaked at 5 minutes post infection (Fig 3.6A). The decreased, rather than complete absence, phosphorylation on the single mutants suggests that there are multiple tyrosine residues within SNX18 that can be phosphorylated during *Salmonella* invasion. Moreover, the SNX18 recruitment to the plasma membrane at the site of invasion was still observed in cells expressing the phosphosite mutant (Fig 3.6B).

To address the possibility of multiple tyrosine being phoshorylated, I generated another mutant SNX18 (SNX18:FL-ΔY) in which all the potential phosphosites, including Y9, Y55 within the SH3 domain and Y78, Y119, Y132, Y135, Y167, Y184 in the LC region were mutated to phenylalanine. The phosphorylation profile of this mutant showed no phosphorylation upon *Salmonella* invasion (Fig 3.7A). To determine whether the phosphorylation of SNX18 is required for SNX18 recruitment, the live cell imaging was performed. Despite no phosphorylation detected, SNX18:FL-ΔY still translocated to the site of *Salmonella* invasion transiently, with kinetics similar to the recruitment of the wild type SNX18 (Fig 3.7B). Combined, all the data from phosphosite mutations show that the recruitment of SNX18 to the membrane at the site of *Salmonella* invasion is not dependent on the phosphorylation of SNX18.

To test whether the membrane recruited SNX18:FL-ΔY is still functional, imaging based dextran uptake assay was used to examine the macropinocytosis level in EGFP-SNX18:FL-ΔY expressing cells (Fig 3.3). The macropinosome numbers per cell in the SNX18:FL-ΔY overexpressing cell had no significant difference from GFP only control cells, suggesting that SNX18:FL-ΔY can not up-regulate macropinosome

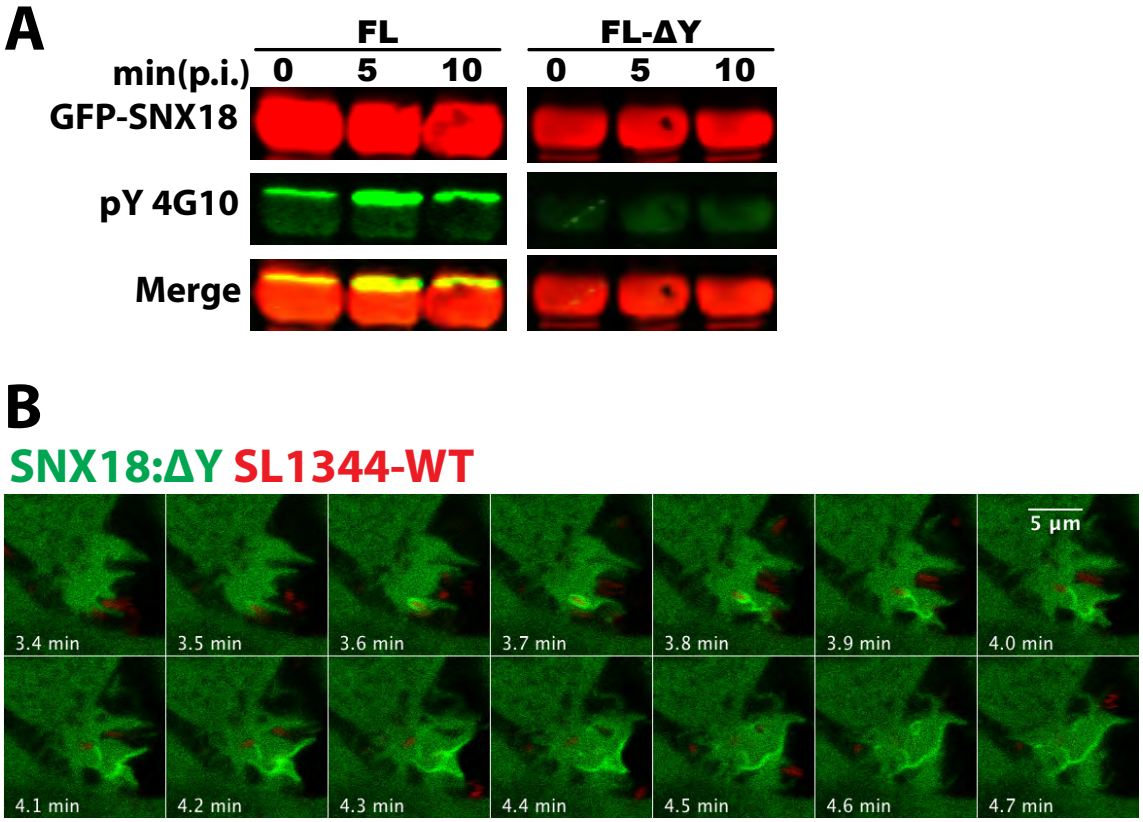

Figure 3.7 - Phosphorylation of SNX18 is not required for its membrane translocation during *Salmonella* invasion.

(A) Phosphorylation profile of SNX18 multiple tyrosine point mutation mutant (EGFP-SNX18:ΔY) during *Salmonella* invasion. HEK293 cells transiently expressing EGFP-SNX18 tyrosine mutants were used and the phosphorylation profile were generated as previously described. (B) A series of confocal sections from a time-lapse of EGFP-SNX18:ΔY-expressing cells infected with SL1344-WT. Montage of movie 18. Scale bars = 5 µm.

formation as wild type SNX18 does. In other words, phosphorylation on SNX18 is required for its further molecular process after membrane recruitment during macropinocytosis.

3.3.3 Identification of SNX18 interaction partners

3.3.3.1 Co-immunoprecipitation and Mass Spectrometry

To identify proteins that interact with SNX18, co-immunoprecipitation coupled with mass spectrometry approach was used, in collaboration with Dr. Michelle Hill (Diamantina Institute, University of Queensland). Initially, I optimized co-immunoprecipitation conditions under which SNX18 efficiently co-immunoprecipitated with Dynamin-2 and N-WASP, two of the known binding partners for SNX9 and SNX18 (data not shown) (Badour et al., 2007; Haberg et al., 2008; Lundmark and Carlsson, 2003; Park et al., 2010; Shin et al., 2007).

Upon optimization of the co-immunoprecipitation conditions, HEK293 cells transiently transfected with myc-tagged SNX18 were used for the screening of SNX18 binding partners, whereas untransfected cells were used as a negative control. After immunoprecipitation of SNX18 by mouse monoclonal anti-myc antibody, immunoprecipitated samples were subjected to SDS-PAGE, followed by in-gel digestion and mass spectrometry. Only those proteins identified in >2 independent peptides precipitated from SNX18 transfected cells and absent from the controls were considered as *bona fide* SNX18 binding proteins (Table. 1). Among those hits were F-actin capping protein subunits alpha and beta (CAPZA and CAPZB) and alpha-actinin-4 (ACTN4). CAPZA and CAPZB are components of WASH complex, involved in vesicle trafficking and cytoskeleton rearrangement (Derivery et al., 2009). ACTN4, expressed in non-muscle cells, is also an actin binding protein and an important component of the actin crosslinking functional modules that organize the cytoskeleton (Sjoblom et al., 2008). However, dynamin or NWASP, known SNX18 binding partners, were not identified as positive co-precipitated proteins from these experiments.

Table 3.1 - Positive hits from myc-SNX18 co-immumoprecipitation and mass spectrometry

# Spectra	# Unique Peps	% Coverage	Accession Number	Protein Name
4	4	20%	P52907	**F-actin-capping protein subunit alpha-1**
6	3	3%	O43707	**Alpha-actinin-4**
4	3	11%	P47756	**F-actin-capping protein subunit beta**
3	3	11%	Q96C19	EF-hand domain-containing protein D2
2	2	0%	P49327	Fatty acid synthase
3	2	2%	Q6WCQ1	Myosin phosphatase Rho-interacting protein
2	2	2%	P06241	Tyrosine-protein kinase Fyn
2	2	8%	Q9NYL9	Tropomodulin-3
9	2	4%	Q15056	Eukaryotic translation initiation factor 4H
2	1	2%	Q9ULV4	Coronin-1C
2	1	11%	P62158	Calmodulin
2	1	9%	P62277	40S ribosomal protein S13
2	1	7%	P25398	40S ribosomal protein S12

Table 3.2 - Positive hits from SNX18:GFPint and SNX18:GFPint-R303Q co-immumoprecipitation and mass spectrometry

SNX18:GFPint # spectra % Cov	SNX18:GFPint-R303Q # spectra % Cov	Accession Number	Protein Name
3	7	P30048	Thioredoxin-dependent peroxide reductase, mitochondrial
19.10%	32.40%		
6	6	P63244	**Guanine nucleotide-binding protein subunit beta-2-like 1**
24.90%	22.00%		
7	5	P62241	40S ribosomal protein S8
30.70%	22.50%		
4	3	O14965	**Aurora kinase A**
13.10%	7.90%		
4	9	Q99714	3-hydroxyacyl-CoA dehydrogenase type-2
18.70%	31.40%		
4	4	O94868	**FCH and double SH3 domains protein 2**
7.70%	5.50%		
1	6	P47756	**F-actin-capping protein subunit beta**
5.00%	18.70%		
4	0	P35573	Glycogen debranching enzyme
3.10%	0.00%		
3	4	P23526	Adenosylhomocysteinase
7.80%	9.90%		
1	3	P48643	T-complex protein 1 subunit epsilon
1.80%	5.30%		
3	0	Q07021	Complement component 1 Q subcomponent-binding protein, mitochondrial
9.50%	0.00%		
2	1	Q15181	Inorganic pyrophosphataseInorganic pyrophosphatase 2, mitochondrial
10.70%	3.10%		
5	3	P46782	40S ribosomal protein S5
17.60%	13.70%		
1	3	P21266	Glutathione S-transferase Mu 3Glutathione S-transferase Mu 2Glutathione S-transferase Mu 5
5.30%	12.00%		
1	2	P60981	Destrin
6.60%	11.50%		
1	2	Q8NBS9	Thioredoxin domain-containing protein 5
2.00%	6.70%		
3	0	Q00325	Phosphate carrier protein, mitochondrial
7.40%	0.00%		
2	3	P41240	**Tyrosine-protein kinase CSK**
6.20%	8.60%		
1	2	P26641	Elongation factor 1-gamma
2.20%	4.50%		
1	2	P29692	Elongation factor 1-delta
8.50%	12.80%		
3	5	Q07020	60S ribosomal protein L18
13.80%	13.80%		
4	3	P50914	60S ribosomal protein L14
10.60%	10.60%		
2	3	P18621	60S ribosomal protein L17
16.30%	16.30%		
1	2	Q9Y266	Nuclear migration protein nudC
3.30%	5.70%		
0	2	P62937	Peptidyl-prolyl cis-trans isomerase A

0.00%	13.90%		
1	2	P46777	60S ribosomal protein L5
3.30%	5.30%		
2	2	Q2TAA2	Isoamyl acetate-hydrolyzing esterase 1 homolog
11.60%	11.60%		
0	2	Q9BV57	1,2-dihydroxy-3-keto-5-methylthiopentene dioxygenase
0.00%	11.70%		
2	0	P55084	Trifunctional enzyme subunit beta, mitochondrial
4.20%	0.00%		
0	2	P40429	60S ribosomal protein L13a
0.00%	6.40%		
1	2	P49207	60S ribosomal protein L34
5.90%	13.60%		
2	2	P62826	GTP-binding nuclear protein Ran
11.10%	11.10%		
0	2	P62424	60S ribosomal protein L7a
0.00%	7.10%		
1	2	P49368	T-complex protein 1 subunit gamma
2.00%	4.20%		
1	2	P30042	ES1 protein homolog, mitochondrial
9.30%	9.30%		
1	2	Q13642	Four and a half LIM domains protein 1
3.70%	3.70%		
0	2	Q96AB3	Isochorismatase domain-containing protein 2, mitochondrial
0.00%	7.30%		
2	0	P46783	40S ribosomal protein S10
5.40%	0.00%		
0	2	O95619	YEATS domain-containing protein 4
0.00%	6.60%		
1	2	P83731	60S ribosomal protein L24
5.00%	5.00%		
1	2	P21108	Ribose-phosphate pyrophosphokinase 3
5.30%	5.30%		
5	3	Q15056	Eukaryotic translation initiation factor 4H
4.40%	4.40%		
1	2	P61353	60S ribosomal protein L27
6.60%	6.60%		
0	2	Q86U90	YrdC domain-containing protein, mitochondrial
0.00%	5.00%		
1	4	Q8TF72	Protein Shroom3
0.40%	0.40%		
0	3	Q6N021	Methylcytosine dioxygenase TET2
0.00%	0.30%		
1	2	Q9HD42	Charged multivesicular body protein 1a
4.00%	4.00%		
2	0	P35609	**Alpha-actinin**
0.70%	0.00%		
0	2	P46781	40S ribosomal protein S9
0.00%	4.10%		

One of the limitations of performing wild type SNX18 co-immunoprecipitation is that it may enrich for the interactions that occur in the cytoplasm. In an attempt to identify the interactions that occur when SNX18 is at the plasma membrane, cells overexpressing the membrane-bound SNX18:GFPint were examined. The cytosolic version of SNX18:GFPint-R303Q was included for the comparison while cells expressing GFP only was used as a negative control (Table. 2). Same selection criteria were applied for protein identifications by mass spectrometry (MS). Positive hits included trafficking related proteins, like Receptor of activated protein kinase C1 (RACK1), and kinases, like Aurora Kinase A (ARK-1) and Tyrosine protein kinase CSK. Notably, ARK-1 is involved in mitosis (Marumoto et al., 2003), and SNX9 family proteins have been shown to have a role in mitosis (Ma and Chircop, 2012). Moreover, the CAPZB and actinin were again identified. Comparing the number of peptides identified by MS from SNX18-GFPint and SNX18-GFPint-R303Q immuno-precipitated samples, CAPZB preferred to bind to SNX18 in the cytosol, whereas ACTN4 preferred to bind SNX18 on the plasma membrane, suggesting that they have different roles and may bind to SNX18 at distinct stages. Unfortunately, there was no known SNX18 binding partners identified as positive from these experiments either.

3.3.3.2 Validation of SNX18 interaction partners

To validate the interaction of these candidates with SNX18, I examined SNX18 binding to several actin related proteins, as well as Cbl, a ubiquitin ligase which has been reported as a SNX18 binding partner in a published proteomic study (Selbach and Mann, 2006). Mouse cDNAs of selected candidates (CAPZA, CAPZB, ACTN4, Cbl) from Fantom3 database were subcloned into pEGFP-C1 vector. Firstly, a co-immunoprecipitation was performed in the cells co-expressing GFP constructs and myc tagged SNX18. GFP-N-WASP, a known binding partner for SNX18 (Park et al., 2010), was used as the positive control. Proteins were immunoprecipitated by anti-myc monoclonal antibody and detected by immunoblotting with a polyclonal anti-GFP antibody. SNX18 precipitated with CAPZA, CAPZB and ACTN4 to a higher extent as N-WASP, whereas less Cbl was detected from SNX18 immunoprecipitated samples (Fig 3.8A). A reversed immunoprecipitation using GFP-nanoTrap to pull down GFP-tagged proteins together with myc-SNX18 was also performed to confirm

these co-precipitations. Overall, the data validates the interactions of SNX18 with those potentially positive hits from the mass spectrometry.

I then examined the subcellular distribution of these binding partners and tested whether they co-localize with SNX18 in cells. GFP tagged F-actin capping proteins, including CAPZA, CAPZB, were transiently transfected into HEK293 cells. Immunofluorescence microscopy showed GFP tagged CAPZA, CAPZB were expressed mostly in the cytosol, but also showed peripheral punctate structures near membrane ruffles. These punctate structures were positive for SNX18 (Fig 3.8B, top panels). Similarly to CAPZA and CAPZB, GFP-Cbl was predominantly distributed throughout the cytoplasm but showed some degree of co-localization with SNX18 on peripheral membrane structures (Fig 3.8B, bottom left panel). In contrast, ACTN4 predominantly localized on the plasma membrane and was clearly enriched on membrane ruffles and lamellipodia, particularly at the invaginations of the plasma membrane that is the site of SNX18 subcellular localisation (Fig 3.8B, bottom right). This observation is consistent with SNX18 and ACTN4 interacting with each other, suggesting that they function together on the membrane ruffles during macropinocytosis.

Figure 3.8 - Co-immunoprecipitation and co-localization of SNX18 interacting proteins. (See next page)

(A). Myc tagged SNX18 was transiently expressed in HEK293T cells with different GFP tagged candidate proteins CAPZA1, CAPZB2, ACTN4 and Cbl, and tested for interaction by immunoprecipitation using anti-myc antibody. GFP-NWASP was using as a positive control for interaction. (B) Co-localization of SNX18 and interacting candidates. mCherry-SNX18 was transiently expressed in HEK293T cells together with GFP tagged CAPZA, CAPZB, Cbl and ACTN4 respectively. 24 hours post transfection, cells were fixed in 4% PFA/PBS and images were captured by confocal microscope. Scale bars = 5 μm.

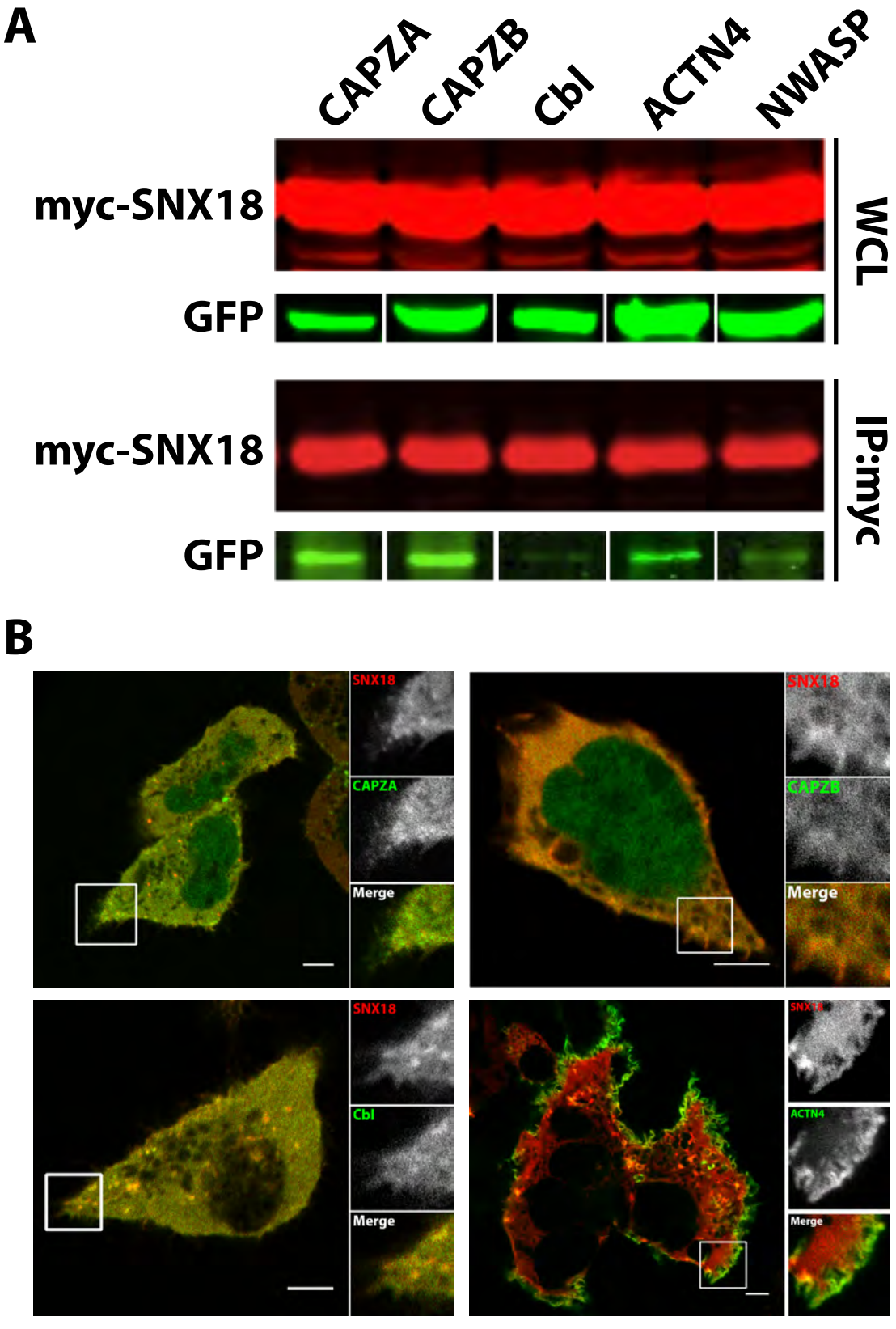

Figure 3.8 - Co-immunoprecipitation and co-localisation of SNX18 interacting proteins. (See legend on previous page)

3.3.3.3 SNX18 and ACTN4 are recruited to the plasma membrane independently

ACTN4 belongs to actinin family which has 4 closely related proteins, ACTN1 and ACTN4 are widely expressed in non-muscle cells, whereas ACTN2 and ACTN3 are highly expressed in muscle cells. They share the N terminal F-actin binding domain (ABD), spectrin repeats (S or SR), and a C-terminal calmodulin (CaM)-like domain (Sjoblom et al., 2008), binding to integrin (Kelly and Taylor, 2005; Otey et al., 1990), catenin (Nieset et al., 1997) or vinculin (Bois et al., 2005; McGregor et al., 1994). ACTN4, and not ACTN1, has been reported to be involved in macropinocytosis (Araki et al., 2000). ACTN4 is also involved in PI3K-induced actin rearrangement (Fraley et al., 2005) and tight junction formation (Nakatsuji et al., 2008). Given that the membrane localization of ACTN4, determining if SNX18 functions together with ACTN4 during macropinocytosis was examined.

To determine if membrane recruitment of SNX18 depends on ACTN4 or vice versa, stable SNX18 or ACTN4 knock down (KD) cell lines were generated using small hairpin RNA (shRNA) approach. HEK293 cells were transfected with pGIPZ-shRNAmir plasmids targeting ACTN4 or SNX18, selected using puromycin and knock-down efficiency was determined using western immunoblotting. This approach led to ~ 75% decrease in ACTN4 protein level and ~ 95% reduction of SNX18 level (Fig 3.9A). Transfection of myc-SNX18 into ACTN4 KD cells resulted in similar levels of *Salmonella*-induced SNX18 translocation to the plasma membrane as compared to the control cells expressing a non-silencing shRNAmir (Fig 3.9B). In the SNX18 KD cells, endogenous ACTN4 was still enriched on the membrane ruffles at the site of *Salmonella* entry to the levels similar to that observed in the control knockdown cells (Fig 3.9B). Based on these observations, I conclude that the recruitment of SNX18 is not dependent on the recruitment of ACTN4 and vice versa.

We previously identified the recruitment of SNX18 to the plasma membrane is triggered by *Salmonella* PtdIns-phosphatase SopB (Chapter 2). Whether or not ACTN4's plasma membrane recruitment during *Salmonella* invasion depends on SopB is unknown. To investigate if SopB is essential and sufficient for ACTN4 recruitment to the sites of bacterial invasion, HEK293 cells overexpressing GFP

tagged ACTN4 were infected with wild type *Salmonella* SL1344 strain or isogenic *sopB* mutant strain of *S.* Typhimurium (Δ*sopB* mutant). Interestingly, while the recruitment of SNX18 to the membrane upon *Salmonella* infection relies on the presence of SopB, both wild type *S.* Typhimurium and the Δ*sopB* mutant are able to recruit cytosolic ACTN4 to the membrane ruffles at the site of bacterial internalization (Fig 3.10), suggesting that ACTN4 functions in a SopB-independent pathway of bacteria internalization. Taken together, the ACTN4 may function together with SNX18 on the membrane after both are recruited to the same site independently.

3.3.3.4 Akt translocation and phosphorylation is not dependent on SNX18 and ACTN4

Akt1, also know as protein kinase B or PKB, has been linked to *Salmonella* invasion and replication (Kuijl et al., 2007; Steele-Mortimer et al., 2000). As an interaction partner of SNX18, ACTN4 was reported to be essential for Akt translocation to the plasma membrane and Akt activation (Ding et al., 2006), which indicates possible involvement of SNX18 in the Akt signaling pathway.

Akt has a PH domain with binding affinities to the PtdIns(3,4)P2 and PtdIns(3,4,5)P3 on the membrane of the cells. Live cell imaging showed that GFP tagged Akt-PH domain was recruited to the plasma membrane during *Salmonella* invasion and was on the same regions of the plasma membrane during the period in which SNX18 was recruited. To test whether Akt activation is required for SNX18 recruitment, we blocked the Akt activity by treating the cells with the Akt1/2 kinase inhibitor (Sigma Aldrich) before infecting the cells with wild type *Salmonella*. However, the down regulation of Akt activity did not affect SNX18 recruitment to the membrane and SCV. Thus, SNX18 is recruited to the membrane in an Akt-independent manner (Chapter 2).

Whether SNX18, and its binding partner ACTN4, act upstream of Akt translocation and activation or in a parallel pathway still remains unclear. Immunofluorescent

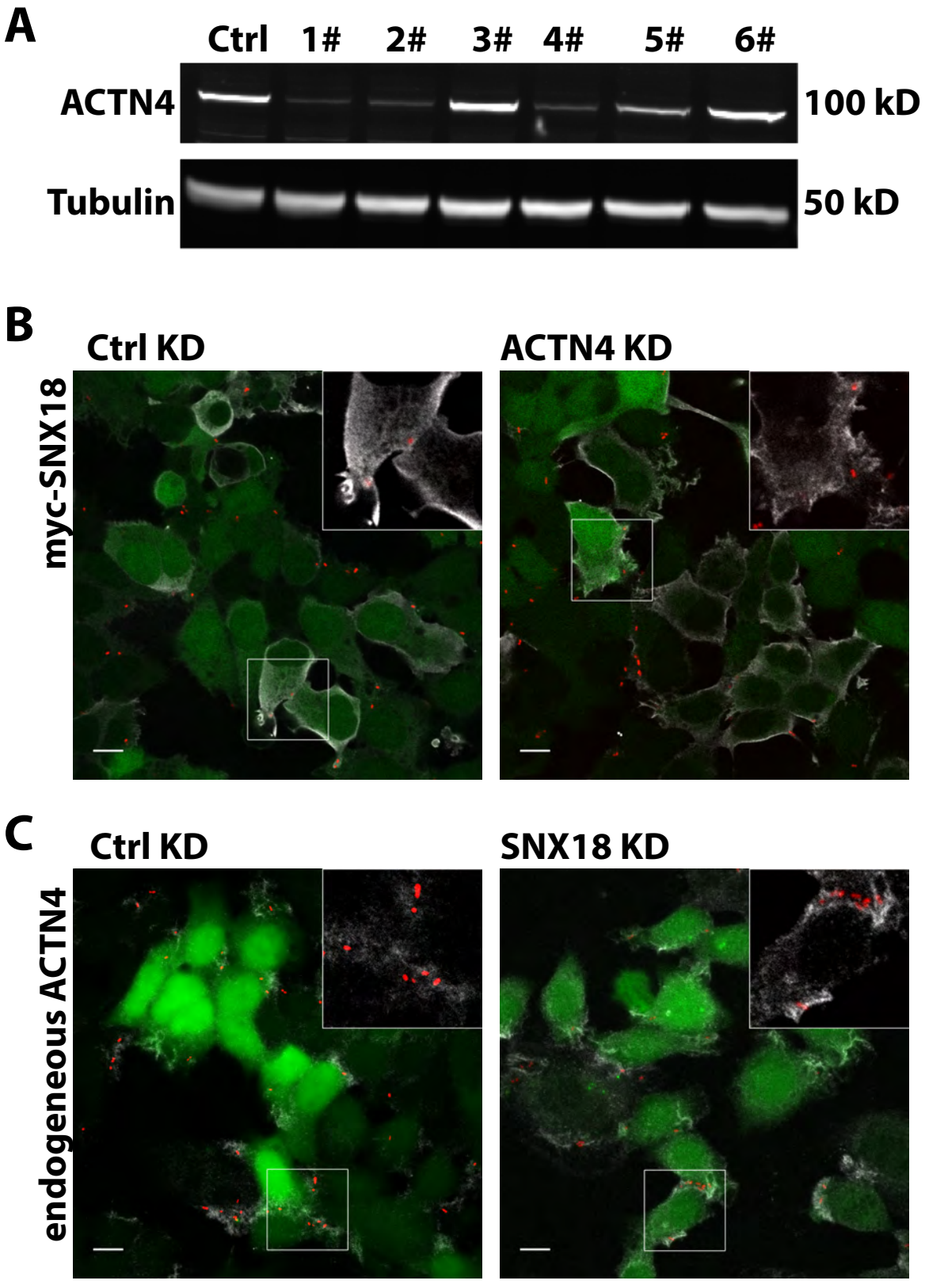

Figure 3.9 - SNX18 and ACTN4 can be recruited to the plasma membrane independently of each other. (See legend on next page)

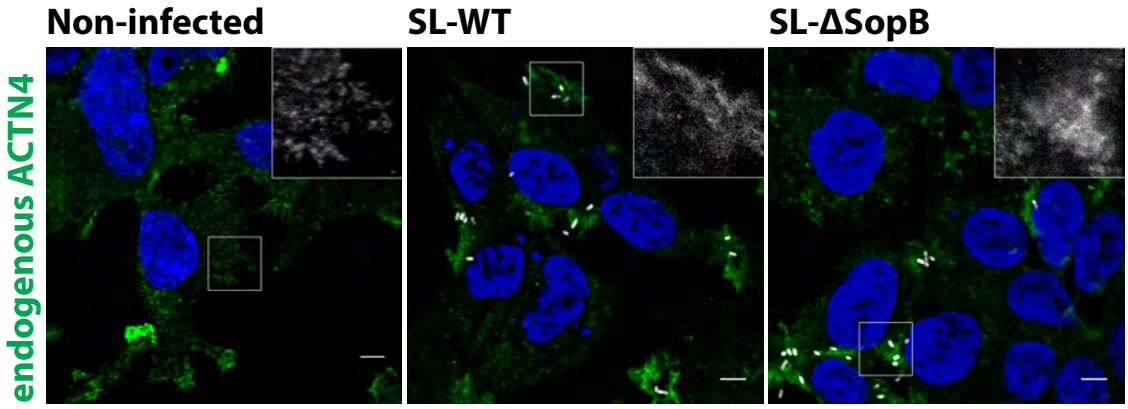

Figure 3.10 - ACTN4 is recruited to *Salmonella* induced membrane ruffles in a SopB independent manner.

HEK293 cells were infected with RFP wild type *Salmonella* or ΔsopB mutant (SL-ΔSopB, grey) for 10min at 37 °C. Cells were then fixed in 4% PFA/PBS for 15 min at room temperature. The cells were permeablised with Triton X-100, and labeled with anti-ACTN4 antibody and anti-goat Alex Flour 488 (green). The nucleus was labeled by DAPI (blue). The images were captured using confocal microscope. Scale bars = 5 µm.

Figure 3.9 - SNX18 and ACTN4 can be recruited to the plasma membrane independently of each other. (See previous page)

(A) Protein levels of endogenous ACTN4 in HEK293 cells 7 days post transfection with shRNA and in control knockdown cells were detected by western blot using anti-ACTN4 antibody. α-Tubulin was used as a loading control. (B) myc-SNX18 was transiently expressed in control knockdown and ACTN4 stable knockdown cells (GFP positive cells; green). 24 hours post transfection, cells were fixed in 4% PFA/PBS for 15 min at room temperature after infection by RFP-Salmonella (red) for 10 min at 37 °C. The cells were permeablised with Triton-X100, and labeled with anti-myc antibody and anti-mouse Alexa Fluor 647 (gray). (C) Control and SNX18 stable knockdown cells (GFP positive; green) were infected with RFP-Salmonella (red). Cells were fixed in 4% PFA at 10min post infection and immunolabeled with anti-ACTN4 antibody and anti-mouse Alexa Fluor 647 (grey). The maximum Z-projection images were taken under the confocal microscope. Scale bars = 10 µm.

images of control knockdown cells demonstrated that no phosphorylation at Akt Ser^{473} was detected in starved cells, whereas phosphorylated Akt was enriched on plasma membrane when the cells were treated with EGF or infected by wild type *Salmonella* for 10 minutes (Fig 3.11A). The *Salmonella* induced Akt phosphorylation was dependent on the present of *Salmonella* effector SopB (Fig 3.11A). However, there is no significant difference of Akt phosphorylation observed by immunofluorescence images when either SNX18 or ACTN4 was depleted compared to control cells. Consistent with this, western immunoblotting showed that the depletion of either SNX18 or ACTN4 did not influence the Akt phosphorylation levels upon various stimuli (Fig 3.11B). These results were inconsistent with a previous report that ACTN4 knockdown leads to the reduced EGF-stimualted Akt phosphorylation (Ding et al., 2006). One explanation could be that partial loss of SNX18 or ACTN4 protein level is not efficient enough to impact on the cell signaling responses upon stimulation.

Figure 3.11 - Akt translocation and phosphorylation is not impacted by ACTN4 or SNX18 depletion from the cells. (See next page)

(A) A431 control knockdown cells and ACTN4 or SNX18 knockdown cells (GFP positive; green) were untreated or treated with EGF, wild type *Salmonella* (SL-WT, grey) or Δ*sopB* mutant (SL-ΔSopB, grey) for 10min after 16 hrs starvation. Cells were then fixed in 4% PFA/PBS for 15 min at room temperature. The cells were permeablised with Triton X-100, and labeled with anti-phospho-Akt (S473) antibody and anti-rabbit Alex Flour 647 (red). The nucleus was labeled by DAPI (blue). The images of the phospho-Akt (S473) were shown in grey scale to the right of each merged image. The images of maximum Z-projection were captured using confocal microscopy. One experiment with two technical repeats of each condition was performed and representative images are shown. Scale bars = 10 μm. (B) Whole cell lysate of control knockdown cells and ACTN4 or SNX18 knockdown cells were collected after untreated or treated with EGF, wild type *Salmonella* (SL-WT) or Δ*sopB* mutant (SL-ΔSopB)for 10min after 16 hrs starvation. 30μg of total protein from each lysate were separated on 8% SDS-PAGE gel, proteins transferred onto PVDF membrane and the blots incubated with anti-phospho-Akt (S473), anti-total Akt, anti-SNX18, anti-ACTN4 and anti-α-tubulin antibodies.

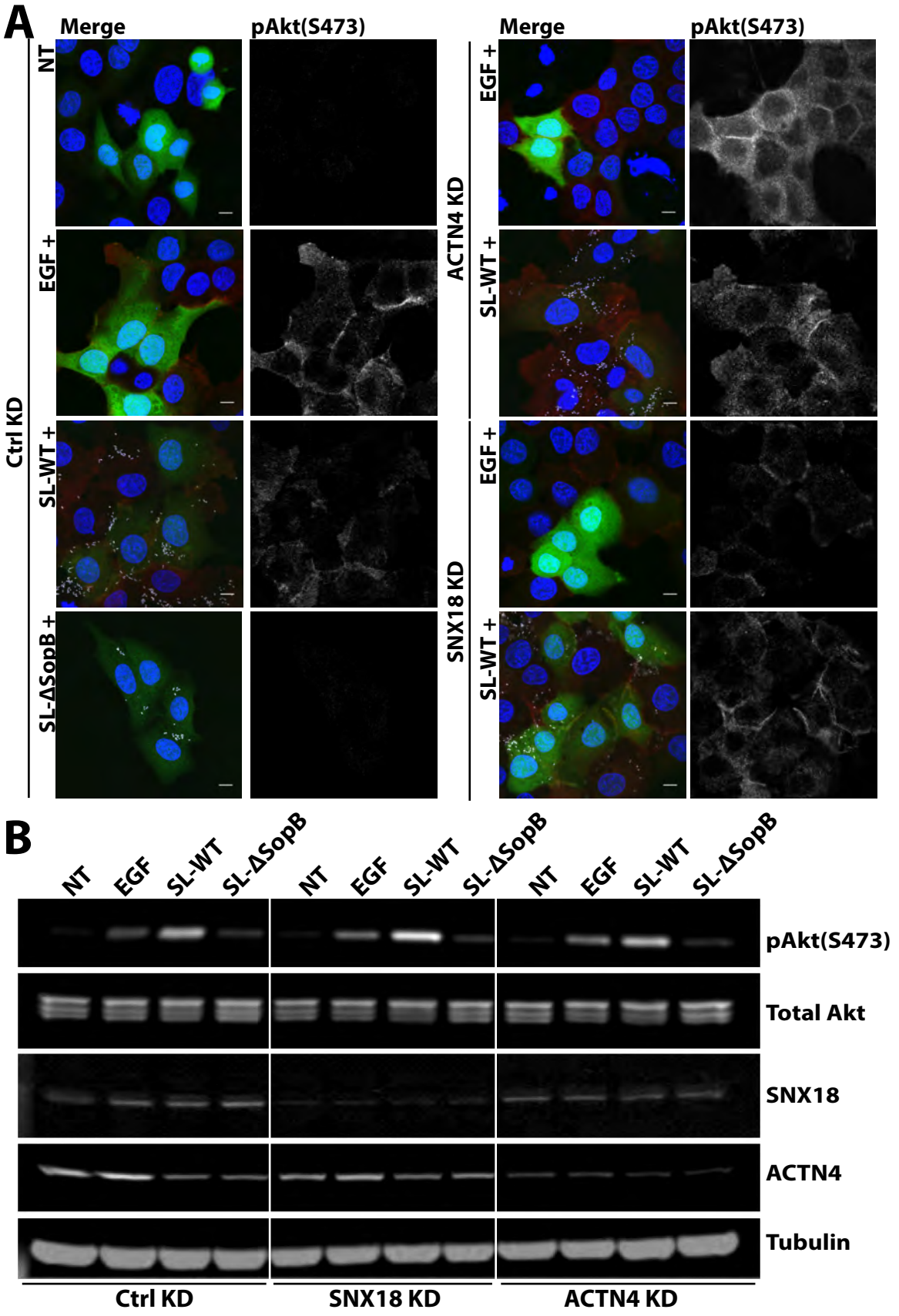

Figure 3.11 - Akt translocation and phosphorylation is not impacted by ACTN4 or SNX18 depletion from the cells. (See legend on previous page)

3.4 Conclusions and Discussion

In this study, I have provided a new insight into the SNX18-driven regulation and molecular mechanism of macropinocytosis. I have generated evidence that SNX18 is regulated via an open-and-closed conformational change based on auto-inhibitory mechanism that controls its recruitment to the plasma membrane at the site of macropinosome formation. Further, I show that tyrosine phosphorylation within SH3-LC SNX18 domains may control its activation. Taken together with published studies, I propose that SNX18 may act as a scaffold protein, where membrane-localised SNX18 is involved in actin remodelling and ruffle formation by interacting with N-WASP (Park et al., 2010) and the novel binding partner ACTN4. While I show that the tyrosine phosphorylation does not seem to be involved in SNX18 membrane recruitment, it may control its activation and/or binding to interacting proteins once SNX18 is already engaged with the membrane. As SNX18 also recruits dynamin at the plasma membrane, this interaction will also complete membrane fission and release the macropinosome into the cytosol (Park et al., 2010). Overall, SNX18 is emerging as a central player in the coordination of the macropinosome formation at the plasma membrane.

Wishart et al. (Wishart et al., 2001) proposed that the localisation of PX domain containing proteins can be controlled by an inter- or intra- molecular interaction between the SH3 domain and proline-rich motifs (PxxP) within the PX domain. This intriguing possibility is further supported by an *in vitro* study where the SH3 domain of *Drosophila* orthologue of SNX9, DSH3PX1, was shown to interact with the PxxP motif present in its PX domain (Worby et al., 2001). Furthermore, a recent structural study of SNX9 revealed that the full length SNX9 and truncated SNX9-PX-BAR proteins had a similar solution scattering profile, suggesting that the SH3 domain and LC region fold back onto PX-BAR domains in solution (Wang et al., 2008). Based on this evidence, I proposed that proteins like SNX18 which contain both a SH3 domain and PX domain can adopt an auto-inhibitory mechanism to regulate the PtdIns binding capabilities of the PX domain which will in turn control its recruitment to membranes. Consistent with this hypothesis, I showed that by altering SNX18's domain architecture I was able to regulate the membrane recruitment of SNX18. While depletion of the SH3 domain of SNX18 did not increase its membrane

recruitment to the plasma membrane, the depletion of the LC domain did, suggesting that the LC region but not SH3 is essential for maintaining SNX18 in an auto-inhibited status and the auto-inhibition of SNX18 may not rely on the interaction between the SH3 domain and PX domain. The spacing of the domains within SNX18 was modulated by the insertion of GFP between LC and PX domain (SNX18:GFPint) which was predicted to perturb the folding of SH3-LC domain back onto the PX-BAR domains. This constitutive open form of SNX18 results in constitutive localization of SNX18 to the plasma membrane. Evaluation of the "activation" status of SNX18:GFPint was examined by overexpression the SNX18:GFPint in cells to monitor the increase in macropinocytosis rates. Expression of this SNX18 mutant did result in an increase in the level of macropinocytosis, but this was lower than that observed when SNX18:FL was expressed. I still consider the open form of SNX18 as an "activated" confirmation and one explanation for the lower increase in the level of macropinocytosis is that the continuously open form of SNX18 disrupts the equilibrium of the exchange of SNX18 between the membrane and the cytosol. This, in turn, may disrupt the normal protein trafficking in the cells under the resting conditions, thus preventing elevated rates of macropinocytosis.

An alternative mechanism of regulating the membrane/cytosol ratio of SNX18 would be existence of a cytosol localised binding partner to maintain SNX18 in its inactive form in the cytosol. For example, SNX9 is reported to be assembled as a "resting complex" in the cytosol by interacting with the glycolytic enzyme fructose-1,6-bisphosphate aldolase via its LC region, thus blocking the exposure of PX-BAR domains (Lundmark and Carlsson, 2004). Aldolase is released from SNX9 by an activation step involving SNX9 phosphorylation within the LC region (Lundmark and Carlsson, 2004; Rangarajan et al., 2010). SNX18 shares similar domain structures and properties with SNX9, suggesting that cytosolic interacting partners for SNX18 could also inhibit SNX18 activity and that reversible post-translation modifications, such as phosphorylation, could control either a conformational change of SNX18 or cause the release of an inhibitory protein which enables transition between its open and closed states. I have shown here that SNX18 can be phosphorylated in cells undergoing constitutive macropinocytosis and that the levels of phosphorylation are elevated when macropinocytosis is induced during *Salmonella* invasion. However, single point mutations on tyrosine residues led to decreased phosphorylation without any decrease

on the levels of SNX18 membrane recruitment, indicating multiple phosphosites can be modified during this process. The phosphorylation of membrane-bound SNX18:ΔLC and SNX18:ΔSH3-LC mutants were not detected under any condition, neither was the SNX18:ΔY mutant with all tyrosine residues removed within the SH3-LC domains, suggesting that SNX18 LC domain is critical for the modulation of SNX18 functions, as it contain either the putative phosphosite(s) or/and the kinase(s) recognition motif(s).

Taken all the localisation and phosphorylation profile of all SNX18 mutants, I also conclude that membrane recruitment of SNX18 is necessary but not sufficient for phosphorylation. Although SNX18:ΔLC, SNX18:ΔSH3-LC and SNX18:ΔY have similar dynamics of recruitment to the plasma membrane and ruffles as wild type SNX18, they are not phosphorylated under any condition. On the other hand, the membrane bound SNX18:GFPint possesses high level of constitutive tyrosine phosphorylation under basal conditions, indicating that the tyrosine phosphorylation of SNX18 occurs subsequently to the membrane recruitment. Consistent with this, the cytosol-localised SNX18 mutants, SNX18:R303Q and SNX18:GFPint:R303Q, were not detected to be phosphorylated. Furthermore, cells overexpressing SNX18:ΔY display no further increase in the level of macropinosome formation, when compared with wild type SNX18, suggesting that it may have deficiencies in the later stage process of macropinocytosis namely membrane fission and closure to form internalized vacuoles. For example, previous studies showed that DSH3PX1 phosphorylation diminishes the interaction of its SH3 domain with WASP, while enabling DSH3PX1 to associate with Dock, the *Drosophila* orthologue of Nck (Worby et al., 2002). Similarly to DSH3PX1, phosphorylation of SNX18 while recruited to the membrane can enable SNX18 to switch different binding partners in order to facilitate the next step in macropinosome formation: from actin remodelling, membrane ruffling to membrane fission and closure.

Using unbiased proteomics I identified several novel SNX18 interacting partners, including ACTN4, CAPZA, CAPZB, RACK1, ARK-1 and CSK. Although the immunoprecipitation conditions were optimised on the type and concentration of detergents, the incubation time and washing times, none of previously known SNX18 binding partners, i.e. dynamin, N-WASP or AP-1/2, were identified under the chosen

conditions that displayed the highest levels of co-precipitated protein as detected by Western Blot. As SNX18 is involved in the macropinosome formation that is both spatially and temporally regulated, the interactions between SNX18 and its partners could be transient and not readily maintained during the process of co-immunoprecipitation and proteins I identified could have higher affinity for SNX18 binding than other previously identified interacting proteins. Alternatively, dynamin, N-WASP or AP-1/2 interact with SNX18 only while it is in its transient active state. The top candidates, including CAPZA, CAPZB, Cbl and ACTN4, were validated by co-immunoprecipitation from whole cell lysates; and their co-localisation was performed by immunofluorescence microscopy.

Interestingly, when GFP-ACTN4 was overexpressed by transient transfection, I observed it predominately localised to the plasma membrane and membrane ruffles, which is consistent with the previously described functions for ACTN4. These include functions as an actin cross-linking protein in non-muscle cells, and contributes to several actin related cellular processes, including EGFR recycling (Yan et al., 2005), GLUT4 trafficking (Talior-Volodarsky et al., 2008), the formation of functional tight junctions (Nakatsuji et al., 2008), as well as formation of circular ruffling and macropinocytosis in mouse macrophages (Araki et al., 2000). Therefore, the interaction between SNX18 and ACTN4 suggests a potential role for this novel SNX18 binding partner in the formation of macropinosomes at the plasma membrane through a local actin-mediated process. Interestingly, depletion of ACTN4 by shRNA did not affect the recruitment of SNX18 to the membrane ruffles during induced macropinocytosis and vice versa, suggesting that the membrane localisation of both SNX18 and ACTN4 is independent of each other. I would propose that SNX18 and ACTN4 associate with each other on the membrane, rather than in the cytosol, to generate a stable protein complex or scaffold. Thus, the translocation of SNX18 from the cytosol to the membrane ruffles enables the SNX18 and ACTN4 interaction occurring on the membrane despite their sequential recruitment to the membranes. Although the functions of ACTN4 and SNX18 are still emerging, they appear to mainly function within the endocytic pathways including trafficking the cargos from the plasma membrane into endosomes and also recycling from endosomes to the plasma membrane. ACTN4 was identified in a CART (cytoskeleton-associated recycling or transport) complex composed of hrs/actinin-4/BERP/myosin V, which is

necessary for efficient TfR recycling, but not for EGFR degradation (Yan et al., 2005). A recent study has also shown that SNX18, via its binding to FIP5 (Rab11 family interacting proteins), participates in the formation and /or scission of endocytic transport carriers from recycling endosomes to the plasma membrane during apical lumen morphogenesis (Willenborg et al., 2011). The interaction between SNX18 and ACTN4 would therefore provide novel molecular mechanism for the actin-dependent rapid recycling of constitutively recycled plasma membrane receptors. Furthermore, ACTN4 is also revealed to play a role in pathogen infections (Bandyopadhyay et al., 2014; Sharma et al., 2014). This suggests a potential role of ACTN4 together with SNX18 in the *Salmonella* infection. Consistent with this, ACTN4 is enriched on the *Salmonella* induced membrane ruffle, but unlike SNX18, the recruitment is independent of SopB, a *Salmonella* effector, indicating that ACTN4 and SNX18's localisation on the membrane is not regulated in the same manner in the context of pathogen cell invasion.

In summary, my current working model of SNX18 is that the resting pool of SNX18 remains in the cytosol where it adopts an auto-inhibitory confirmation via the fold-back mechanism where SH3-LC are in direct contact with PX-BAR domains. This closed protein structure shields the PtdIns-binding site within the PX domain preventing its capacity to be accessed for membrane recruitment. During macropinocytosis, both constitutively or transiently induced by growth factors or pathogens, SNX18 undergoes a conformational change from the closed form to an open form, which allows the PtdIns-binding site in the PX domain to interact with PtdIns(3,4)P_2 on the membrane ruffles. It is unclear if this conformational switch is continuously occurring or is regulated by some as yet undefined molecular or cell signalling process. The BAR domain of SNX18 can sense membrane curvatures and is responsible for the SNX18 homodimerization at the membrane. SNX18 is then phosphorylated while associated with the membrane at its multiple phosphorylation sites in SH3 and LC domains. The membrane bound SNX18 can act as a scaffold by interacting with ACTN4, N-WASP and dynamin (Park et al., 2010) to further drive actin remodelling and macropinosome closure. Although the full picture of the molecular mechanism during the macropinosome formation is not yet complete, it is clear that SNX18 and its binding partners play a key role in protein scaffolding, actin

remodelling, membrane ruffling and membrane scission to drive an important cellular process, macropinocytosis.

3.5 List of Supplementary Movies

Movie7: SNX18:ΔLC (EGFP) is enriched at the site of *S.* Typhimurium (mRFP) invasion on the plasma membrane and accumulates during bacteria internalization into the nascent SCV. HEK293 cells, 16 hrs post transfection, 0-10 min post infection. (0.1 min between frames, 7 fps). Bar=5 μm.

Movie8: A zoom in of Movie7, from which the montage of movie in Figure 3.5 is made. Bar=2 μm.

Movie9: SNX18:ΔSH3-LC (EGFP) is enriched at the site of *S.* Typhimurium (mRFP) invasion on the plasma membrane and accumulates during bacteria internalization into the nascent SCV. HEK293 cells, 16 hrs post transfection, 0-10 min post infection. (0.1 min between frames, 7 fps). Bar=5 μm.

Movie10: A zoom in of Movie9, from which the montage of movie in Figure 3.5 is made. Bar=2 μm.

Movie11: SNX18:Y256F (EGFP) recruits to the site of *S.* Typhimurium (mRFP) attachment at the plasma membrane and accumulates during bacteria internalization into the nascent SCV. HEK293 cells, 16 hrs post transfection, 0-5 min post infection. (0.1 min between frames, 7 fps). Bar=5 μm.

Movie12: A zoom in of Movie11, from which the montage of movie in Figure 3.6 is made. Bar=2 μm.

Movie13: SNX18:Y265F (EGFP) recruits to the site of *S.* Typhimurium (mRFP) attachment at the plasma membrane and accumulates during bacteria internalization

into the nascent SCV. HEK293 cells, 16 hrs post transfection, 0-5 min post infection. (0.1 min between frames, 7 fps). Bar=5 μm.

Movie14: A zoom in of Movie13, from which the montage of movie in Figure 3.6 is made. Bar=2 μm.

Movie15: SNX18:Y167F (EGFP) recruits to the site of *S.* Typhimurium (mRFP) attachment at the plasma membrane and accumulates during bacteria internalization into the nascent SCV. HEK293 cells, 16 hrs post transfection, 0-5 min post infection. (0.1 min between frames, 7 fps). Bar=5 μm.

Movie16: A zoom in of Movie15, from which the montage of movie in Figure 3.6 is made. Bar=2 μm.

Movie17: SNX18:ΔY (EGFP) recruits to the site of *S.* Typhimurium (mRFP) attachment at the plasma membrane and accumulates during bacteria internalization into the nascent SCV. HEK293 cells, 16 hrs post transfection, 0-10 min post infection. (0.1 min between frames, 7 fps). Bar=5 μm.

Movie18: A zoom in of Movie17, from which the montage of movie in Figure 3.7 is made. Bar=2 μm.

4 Characterising SNX20/21 in mammalian cells

4.1 Introduction

Phox-homology domain (PX domain) is responsible for binding to phosphoinositide(s) (PtdIns) to attach proteins to the cellular membrane (Ago et al., 2001). Although several PX proteins, most of which are classified as sorting nexins (SNXs), have been revealed as important regulators in membrane trafficking, cell signalling and organelle motility, there are many others that remain to be characterised in detail. SNX20 and SNX21 compose a novel subfamily of PX domain containing proteins. Besides the PX domain that is responsible for PtdIns-binding, SNX20 and SNX21 share a highly similar region termed the PXB domain at the C-terminus of the proteins (Teasdale and Collins, 2012).

The functions of these two molecules are very poorly understood. SNX21 (also known as SNX-L) has been suggested to play a role in liver development, based only on its high expression in human fetal liver tissue, which was decreased in adult tissue (Zeng et al., 2002). The only SNX20 study (also known as selectin ligand interactor cytosolic-1 (SLIC-1)) reported that SNX20 interacted with the cytoplasmic domain of P-selection glycoprotein ligand-1 (PSGL-1) using a yeast two-hybrid (Y2H) screen. However, they concluded from co-immunoprecipitation and motif mapping that direct interaction occurred between SLIC-1 PX domain and PSGL-1, which is inconsistent with the fact that SNX20 sequences they obtained from the Y2H screen were only partial PX and complete C-terminal domains. Although the co-localization experiment demonstrated SNX20 could drive the distribution of PSGL-1 from plasma membrane to early endosomes, deficiency in the murine homologue of SLIC-1 did not modulate PSGL-1- dependent signalling nor alter neutrophil adhesion through PSGL-1 (Schaff et al., 2008).

In this chapter, I characterized the SNX20 and SNX21 expression levels in different cell lines and observed their association with early endosomes, suggesting SNX20 and SNX21 are likely to be involved in endosomal trafficking. Moreover, both proteins were observed to be recruited to newly formed SCVs when the cells were infected. PSGL-1 was found to partly co-localize with SNX20 or SNX21 on the early endosomes, but the interaction between PSGL-1 and SNXs was not detected by co-immunoprecipitation. A new approach, the APEX (enhanced ascorbate peroxidase) - mediated biotinylation technique followed by mass spectrometry was introduced to assist detection of potential interaction partners of SNX20 and SNX21.

4.2 Materials and Methods

Plasmids

pcDNA-3.1-n-myc-SNX20 was generated by inserting amplified murine SNX20 cDNA using primers BamH1 Fwd CGC GGATCC GCA AGT CCA GAG CAT CCT and Xba Rev CCC TCTAGA TCA GGA CAG ATA CTC CCG into the BamHI/XbaI sites of pcDNA-3.1-n-myc backbone. pcDNA-3.1-n-myc-SNX21 was generated by inserting amplified murine SNX21 cDNA using PCR primers infusion_1 AGAAGACCTG GGATCC GCC TCG CGG CTC CTA CAC CGG and infusion_2 GCCC TCTAGA CTCGAG TTA GTC CAG CAC CTC TTT GAT into the BamHI/XbaI sites of pcDNA-3.1-n-myc backbone.

pEGFP-SNX20 was generated by subcloning SNX20 between BamHI and ApaI sites from pcDNA-3.1-n-myc-SNX20 into the BglII and ApaI sites of pEGFP-C1 vector. pEGFP-SNX21 was described as previously (Kerr et al, 2012).

pcDNA-3.1-n-myc-SNX20-R313Q, pcDNA-3.1-n-myc-SNX21-R331Q, CD8-P-selectin, CD8-PSGL-1 were obtained from Thomas Clairfeuille, Group Collins, IMB, UQ.

V5-APEX was amplified from pcDNA3-Soybean-APEX (IMS) (Rhee et al., 2013) using oligos V5 Fwd NheI (ATG included): CGC GCTAGC ATG GGC AAG CCC ATC CCC AA, and APEX Rev BglII (UAA excluded): CGC AGATCT GGC ATC AGC AAA CCC AAG CT. The V5-APEX was inserted into the pEGFP-C1 vector between NheI and BglII sites to replace the EGFP sequence, which generated the pAPEX-C1 vector.

Murine SNX20 full length was digested from pcDNA3.1-n-myc-SNX20 between BamHI and Apal and inserted into BglII and ApaI sites of pAPEX-C1. Murine SNX21 was amplified from pcDNA3.1-n-myc-SNX21 using oligos BclI_snx21Fwd CCC TGATCA GCC TCG CGG CTC CTA CAC CGG, and Rev380snx21_Inf GCCC TCTAGA CTC GAG TTA GTC CAG CAC CTC TTT GAT digested with BamHI and XhoI, and inserted into BglII and SalI sites of pAPEX-C1.

Antibodies

The following primary antibodies were used: mouse monoclonal anti-Myc tag (9B11) antibody (Cell Signalling Technology, 2272); mouse anti-EEA1 antibody (BD Transduction Laboratories, 610457), mouse anti-human CD107a/LAMP-1 antibody (BD Pharmingen, 555798), mouse monoclonal anti-human CD8a purified clone OKT8 antibody (eBioscience, 14-0086-80), mouse monoclonal V5 tag antibody (Life Technologies, R960-25), Rabbit polyclonal c-Myc antibody (Novus Biologicals, NB600-336), rabbit polyclonal anti-CD8 (Lieu et al., 2007).

Donkey anti-mouse coupled to Alexa Fluor® 488 or 647 and donkey anti-rabbit coupled to Alexa Fluor® 488or 647 (Life Technologies) were used as secondary antibodies for immunofluorescence. The IRDye®800CW donkey anti-rabbit IgG, IRDye®680LT goat anti-mouse IgG and IRDye®800CW Streptavidin were purchased from LI-COR Biosciences. Streptavidin, Alexa Fluor® 488 conjugate were purchased from Life Technologies.

Generation of anti-SNX20 and anti-SNX21 rabbit polyclonal antibodies

Recombinant SNX20 and SNX21 proteins were obtained from Thomas Clairfeuille, Group Collins, IMB, UQ. The immunisation of rabbits was performed by the WEHI Antibody Facility. Briefly, pre-bleed was collected one day prior to the first immunization. Rabbits were subjected to three immunisations by injecting 200μg antigen on Day 0, Day 28 and Day 56. Two test bleeds were obtained on Day 40 and Day 68 while the terminal bleeds were collected on day 75. Two rabbits for each antigen were immunized, R1404 and R1405 for SNX20; and R1406 and R1407 for SNX21.

Cell culture, transfection and generation of stable cell lines

Human epithelial HEK293 cells (CRL-1573), human epithelial HeLa (CCL-2), and mouse fibroblast NIH/3T3 (CRL-165) were maintained in complete Dulbecco's modified Eagle's medium (DMEM) (Life Technologies) supplemented with 10% (v/v) foetal bovine serum (FBS) and 2 mM L-glutamine. Cells were incubated in humidified air/atmosphere (5% CO_2) at 37°C. Cells were transfected with Lipofectamine 2000 as per manufacturer's instructions (Life Technologies). 0.8 μg of DNA and 2 μL of Lipofectamine 2000 was used per well of a 24 well plate. For stable

expression, transfected cells were maintained in complete medium supplemented with G418, Geneticin® (Life Technologies) at concentration of 400 µg/mL for selection or 200 µg/mL for maintenance of stable cell lines.

APEX mediated biotinylation

Cell monolayers were incubated in the complete cell culture media supplement with 500 µM biotin-phenol (custom synthesis, JenaBioScience GmbH) for 30 minutes at 37°C. H_2O_2 was then added to a final concentration of 1 mM for 1 minute at room temperature to initiate biotinylation. To terminate the reaction, the cells were washed three times with a "quencher solution" consisting of 10 mM sodium azide, 10 mM sodium ascorbate, and 5 mM Trolox in Dulbecco's Phosphate Buffered Saline (DPBS, Life Technologies).

For immunofluorescence (IF), the cells are fixed, washed, permeabilised and blocked as described in the indirect immunofluorescence. To detect APEX expression, incubate the cells with anti-V5 (Invitrogen R960-25; 1:1000 dilution) mouse antibodies in blocking buffer for 1 hour at room temperature and with secondary antibody in blocking buffer for another 1 hour at room temperature after 3 times washing in blocking buffer. To detect biotinylated proteins, the cells are incubated with streptavidin-Alexa488 (1:400) in blocking buffer for 1h, washed and mounted onto slides for imaging.

For immunoprecipitation (IP), cells were washed twice with the quencher solution and twice with DPBS to remove excess biotin-phenol. After the final wash, the cells are collected in 500µL of freshly prepared TK lysis buffer on ice. Lysates are clarified by centrifugation at 13,000 rpm for 10 minutes at 4 °C. Protein concentration in the supernatant is measured using the Pierce Protein Assay kit, with bovine serum albumin as the reference standard. Streptavidin-coated magnetic beads (Pierce) were prepared by washing twice with TK lysis buffer. 2 mg of total protein (at 2 mg/mL protein concentration) from each replicate sample was mixed with 50 µL of streptavidin bead slurry. The suspensions were incubated at 4°C overnight with gentle rotation. Streptavidin beads were then washed with 2 × 1 mL TK lysis buffer, once with 1 mL of 2M urea in 10 mM Tris-HCl pH 8.0, and again with 2 × 1 mL TK lysis buffer. Biotinylated proteins were eluted by incubating the beads with 50 µL 2x

Sample Buffer supplemented with 20 mM DTT and 2 mM biotin and heating to 95 °C for 10 minutes. To detect biotynilated proteins, SDS-PAGE and Western blotting was performed as described above using 1:1000 dilution of Streptavidin-IRdye800CW at 4 °C overnight. Blots are then rinsed in PBST for 3 × 5 minutes before imaged with Odyssey imaging system.

Salmonella infection and live cell imaging were described in Chapter 2. Cell lysis, immunoprecipitation, SDS-PAGE and Western blotting were described in Chapter 3.

4.3 Results

4.3.1 Antibody evaluation

To evaluate the rabbit polyclonal antibodies generated against SNX20 and SNX21, western immunoblotting and indirect immunofluorescence microscopy were performed on HeLa cells expressing GFP-SNX20 and GFP-SNX21. For immunofluorescence, the GFP-positive punctate structures in the cells were also immunolabelled with the secondary bleeds for either SNX20 or SNX21 (Fig 4.1A). Western immunoblotting was also performed using the same bleed on murine NIH-3T3 cells expressing myc-SNX20 and myc-SNX21. A 37 kDa protein and 50 kDa protein was detected which corresponded to myc-SNX20 and myc-SNX21 respectively. The pre-bleed control at the same dilution from both rabbits showed no reactivity with expressed fusion proteins in the transfected cells. Moreover, in the non-transfected cells, a weak positive signal was observed when compared to the pre-bleed controls, indicating these antibodies weakly detect endogenous proteins or these cell lines don't express these proteins.

4.3.2 Expression level in different mammalian cell lines

The expression profile of SNX20 or SNX21 proteins is unclear from the current literature. To date, SNX21 has been reported to be highly expressed in infant liver samples, with a decrease in the expression levels observed during the development (Zeng et al., 2002). The high-throughput gene expression profiling data on BioGPS.org provide gene diverse array results from tissues, organs and cell lines of human and mouse origin. Here, SNX20 mRNA levels were reported to be high in lymphatic tissues, including spleen, lymph nodes, bone marrow and osteoclasts. High SNX20 level was also found in T cells, B-cells, dendritic cells, macrophages and RAW_264.7 cell lines. On the other hand, SNX21 was found expressed broadly across different tissues while relatively high expression in mouse tissues such as dorsal root ganglia, skeletal muscle and brown adipose was detected.

Guided by BioGPS.org data, generated rabbit polyclonal antibodies against SNX20 and SNX21 were used for immunoblotting analysis of the expression of the proteins in different mammalian cell lines. The SNX20 appears ubiquitously expressed in most

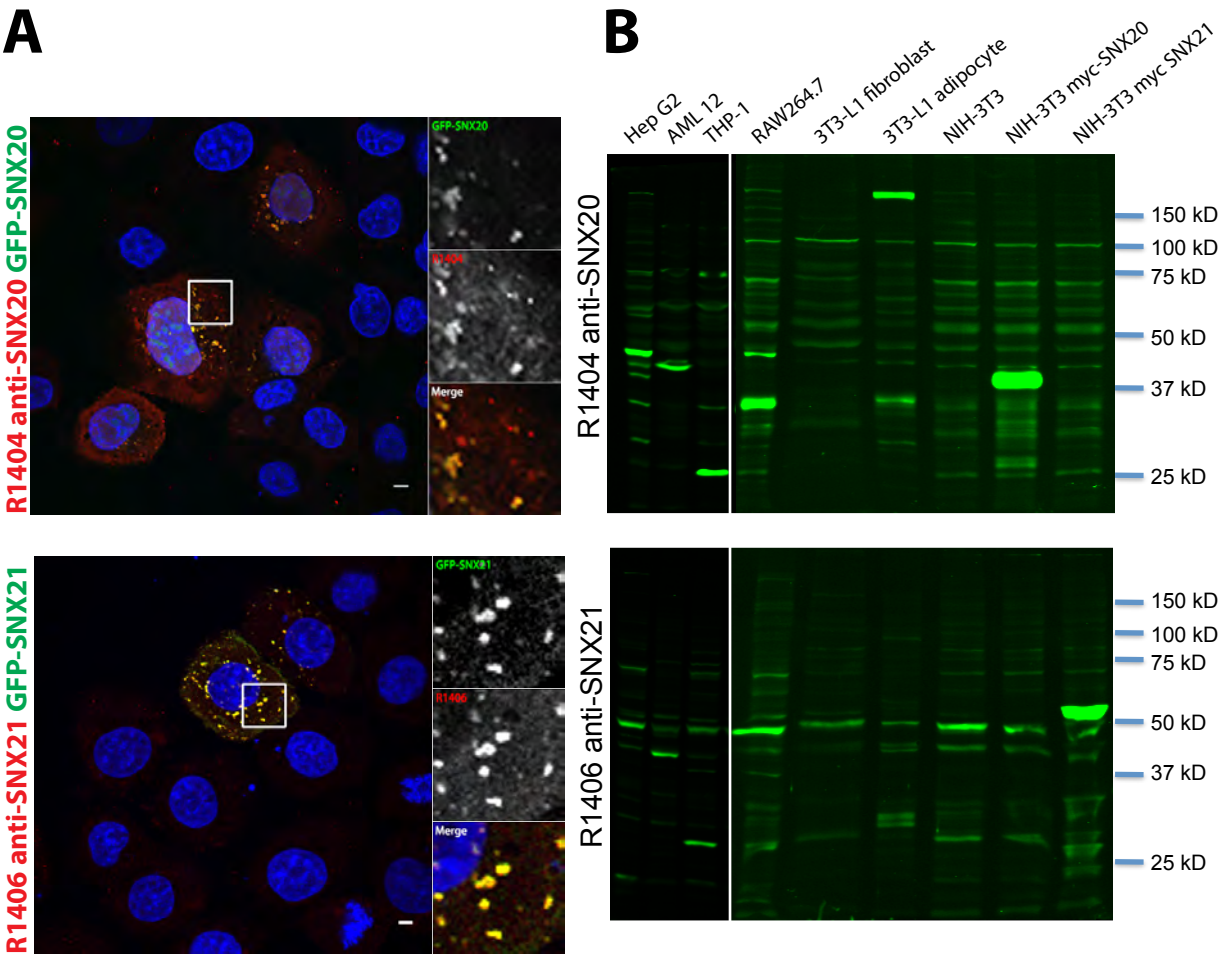

Figure 4.1 - Characterization of SNX20 and SNX21 rabbit polyclonal antibodies.

(A) HeLa cells were transfected with GFP-SNX20 or GFP-SNX21 (Green). 24 hours post transfection, the cells were fixed in 4% PFA/PBS for 15 min at room temperature. The cells were permeablised with Triton X-100, and labeled with R1404 anti SNX20 sera from 2nd bleed (upper images), or labeled with R1406 anti SNX21 sera from 2nd bleed (lower images) and anti-rabbit-Alexa Fluor 647 was used as secondary antibody (red). Scale bars = 5 µm. (B) Whole cell lysate of different cell lines (30 µg each) were separated on 10% SDS-PAGE gels. Western immunoblotting was performed with R1404 anti-SNX20 sera (upper) or R1406 anti-SNX21 sera (lower) from 2nd bleed, respectively, and IRDye800CW anti-rabbit antibody was used at secondary antibody. The images were captured using Odyssey imaging system.

cell lines with varying expression levels. For example, it was relatively highly expressed in RAW 264.7, a macrophage like cell line. Interestingly, SNX20 expression was up regulated in differentiated 3T3-L1 adipocytes as compared to the fibroblast sample (Fig 4.1B). On the other hand, SNX21 also appeared ubiquitously expressed in relatively equal levels across different cell lines (Fig 4.1B).

4.3.3 SNX20 and SNX21 localize to early endosomes

The subcellular localisation of SNX20 and SNX21 is unknown. To determine this, myc-SNX20 and myc-SNX21 were ectopically expressed in HeLa cells. Myc-SNX20 was found to localise to the cytosol, nucleus and intracellular vesicles (Fig 4.2A), while majority of myc-SNX21 localised to endosomal vesicles (Fig 4.2B). To determine the type of endosomes SNX20 and SNX21 are recruited to, co-localisation with EEA1, the early endosome marker, or Lamp1, the late endosome/lysosome marker was performed. Both SNX20 and SNX21 localized on the EEA1 but not Lamp1 positive endosomes (Fig 4.2A and B), indicating that they are enriched on early endosomes. The majority of SNX proteins are recruited to the early endosome through their capacity of their PX domains to bind PtdIns(3)*P*. Based on structural alignments with other PX domains, the conserved arginine residue within the PX domain that is essential for binding to the 3-phosphate of the PtdIns(3)*P* head group was identified and site-directed mutagenesis was performed. The generated myc-SNX20-R113Q mutant and myc-SNX21-R161Q mutant were ectopically expressed in HeLa cells and, as expected, localised to the cytoplasm and no longer associated with early endosomal membrane (Fig 4.2A and B). Taken together, we conclude that the PtdIins(3)P binding ability of the SNX20 and SNX21 PX domain is necessary for their early endosomal membrane localization.

4.3.4 Interaction of SNX20 or SNX21 with PSGL-1

SNX20 was reported to interact with the PSGL-1 cytoplasmic tail (Schaff et al., 2008), however the molecular basis of the interaction remains unclear. Initially, I investigated if SNX20 and SNX21 co-localisation with a CD8 reporter construct encoding the PSGL-1 cytoplasmic domain. HeLa cells transfected with CD8-PSGL1

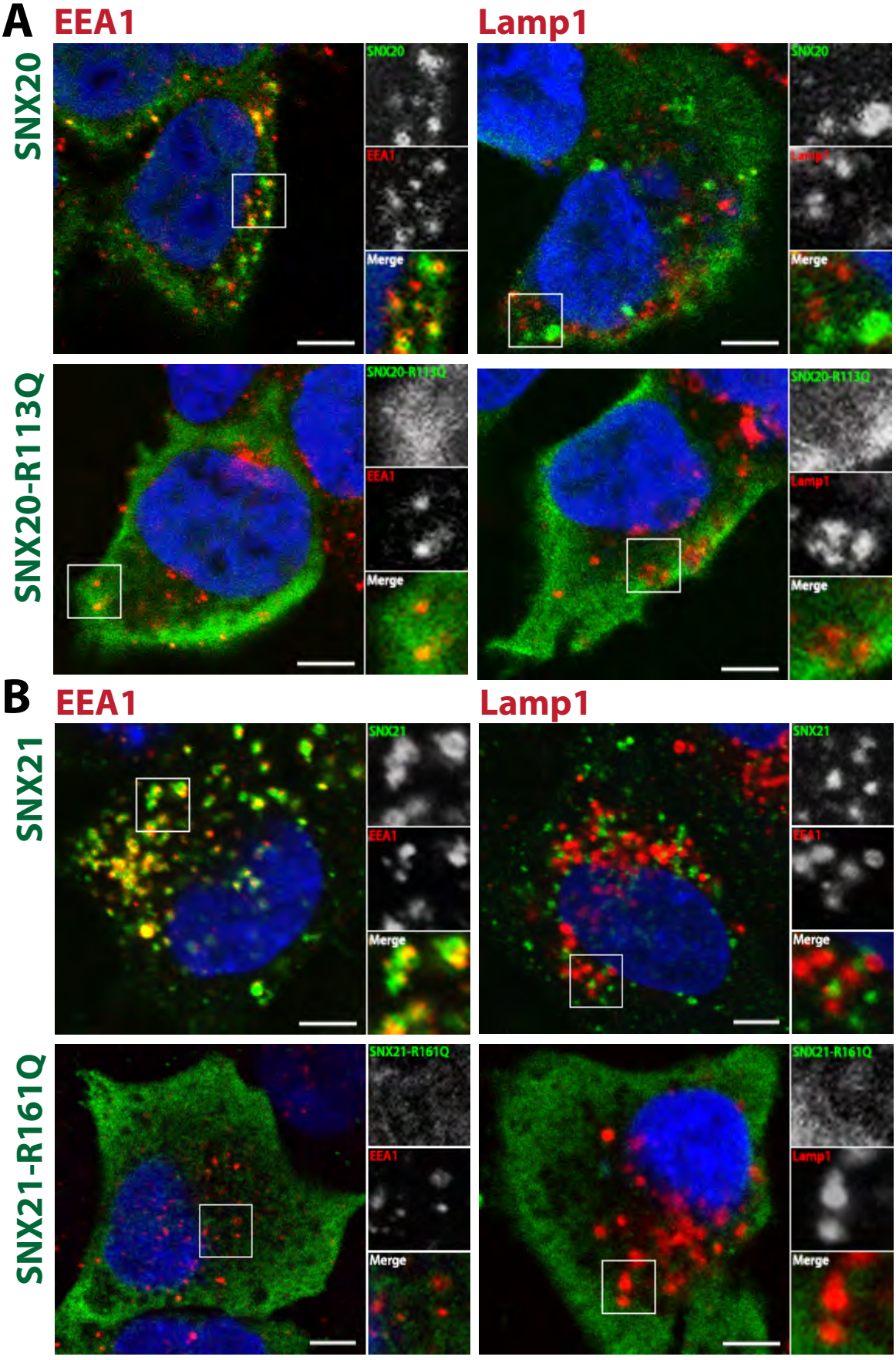

Figure 4.2 - SNX20 and SNX21 localize to early endosomes.
(See legend on next page)

alone or together with GFP-SNX20 or GFP-SNX21 were examined using indirect immunofluorescence and confocal microscopy. CD8-PSGL1 alone was predominantly localized at the plasma membrane (Fig 4.3A), but a proportion of PSGL-1 was located on endosomal structures, which were SNX20 or SNX21 positive (Fig 4.3B). The observation of SNX20/PSGL-1 positive and SNX21/PSGL-1 positive punctate structures suggests CD8-PSGL1 co-localised with SNX-PXB proteins on early endosomes but not the plasma membrane. This partial co-localization indicates a potential direct interaction between PSGL1 and SNX-PXB molecules, which is likely to occur at the early endosomes rather than the plasma membrane.

To further test this hypothesis, CD8-PSGL1 together with myc-SNX20 or myc-SNX21 were overexpressed in HEK293 cells and immunoprecipitated from total cell lysate using an anti-myc antibody. Co-immunoprecipitated proteins were detected by Western blot analysis. Neither SNX20 nor SNX21 was co-immunoprecipitated with CD8-PSGL1 (Fig 4.3C), so previously reported interaction between SNX20 and PSGL1 was not confirmed. Possible explanations for this negative observation may indicate the low affinity of the interaction that can not be maintained during the immunoprecipitation, or that the interaction is relatively transient so that the amount of proteins that can be pulled down is below detection.

Figure 4.2 - SNX20 and SNX21 localize to early endosomes. (See previous page)
HeLa cells were grown on coverslips and transfected with myc-SNX20, myc-SNX20-R113Q (A), or myc-SNX21, myc-SNX21-R161Q (B). 24 hrs post transfection, cells were fixed in 4% PFA/PBS for 15 min at room temperature. The cells were permeabilised with Triton X100, and co-labeled with anti-myc antibody with anti-rabbit Alexa488 (green) and anti-EEA1 antibody or anti-Lamp1 antibody with anti-mouse Alexa647 (red). Scale bars = 5 μm.

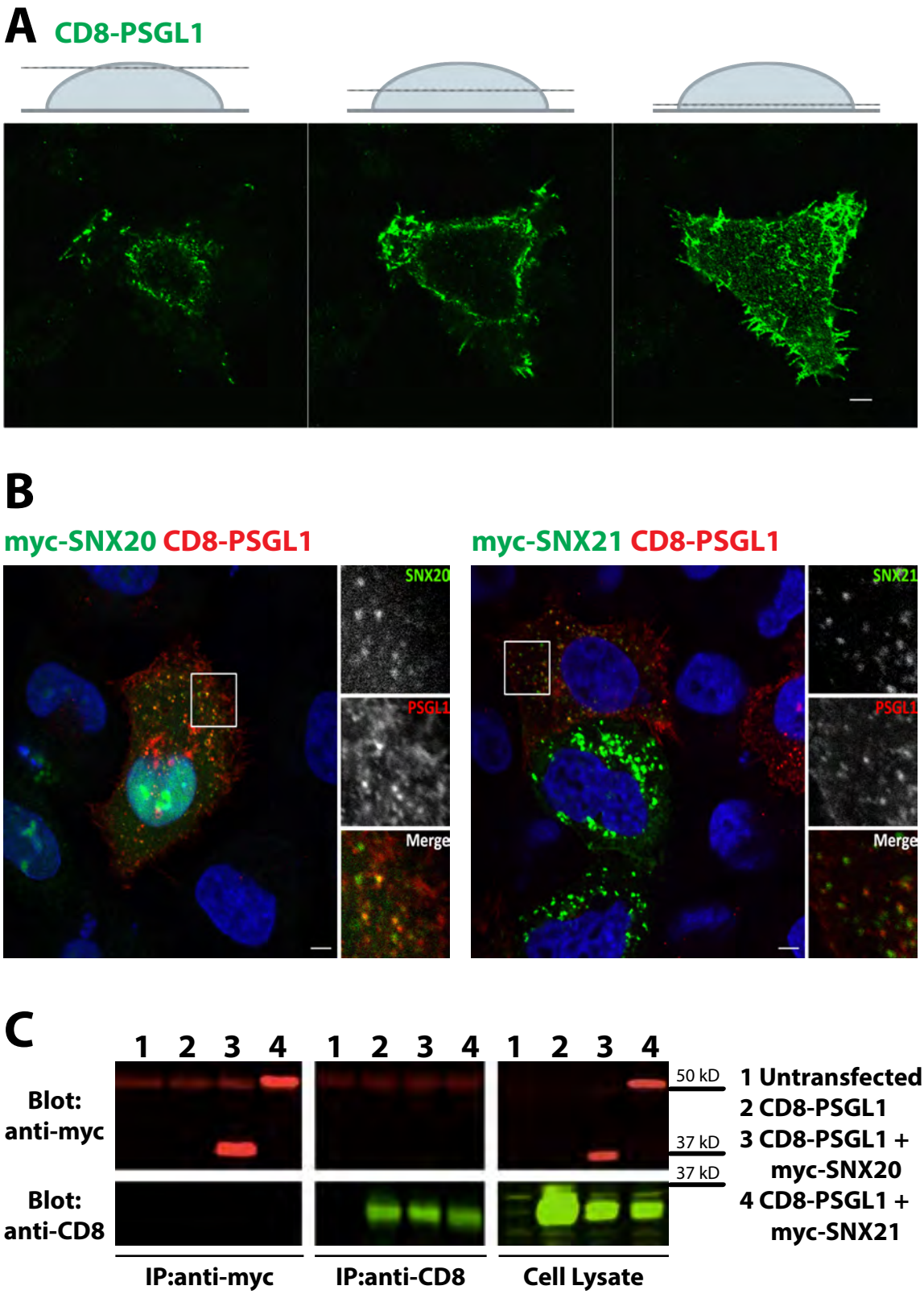

Figure 4.3 - Co-localization and interaction between PSGL1 and SNX20 / SNX21. (See legend on next page)

4.3.5 APEX-mediated biotinylation

HEK293 cells transiently transfected with myc-tagged SNX20 or SNX21 were used for the screening of SNX20 or SNX21 binding partners, whereas untransfected cells were used as a negative control. After immunoprecipitation of SNXs by mouse monoclonal anti-myc antibody, immunoprecipitated samples were subjected to SDS-PAGE, followed by in-gel digestion and mass spectrometry. Only those proteins identified in >2 independent peptides precipitated from SNXs samples and absent from the controls were considered as *bona fide* SNXs binding proteins (Table 4.1). However, only few hits are considered positive for SNX21 and no hits for SNX20. Therefore, I introduced the APEX-mediated biotinylation, as an alternative approach to co-immunoprecipitation to determine the proteins that interact with SNX20 and SNX21. The APEX technique enables the detection of interacting proteins by biotinylating proteins within 20nm range from the enzyme in the intact cells (Rhee et al., 2013). Therefore, this should also include membrane cargo proteins that are difficult to detect in cell lystes using standard co-immunoprecipitation techniques.

Figure 4.3 - Co-localization and interaction between PSGL1 and SNX20/21.
(See previous page)

(A) HeLa cells were grown on coverslips and transfected with CD8-PSGL-1. 24 hrs post transfection, cells were fixed and permeabilised and indirect immunofluorescence performed using antibody with rabbit anti-CD8 antibodies and anti-rabbit Alexa488 (green). Z-stack sections depict highlight of plasma CD8-PSGL-1 membrane localization at steady state. Scale bars = 5 μm. (B) CD8-PSGL1 was co-expressed with myc-SNX20 (left) or myc-SNX21 (right) and their co-localisation determined by indirect immunofluorescence. Scale bars = 5 μm. (C) Co-immunoprecipitation from HeLa cells transiently expressing the indicated construct(s) was performed using anti-myc or anti-CD8 antibodies respectively. Whole cell lysates (30μg) and the immunoprecipitates were resolved on 10% SDS-PAGE and western immunoblotting using anti-myc (red) and anti-CD8 (green) antibodies was performed.

Table 4.1 - Potential interaction partners for SNX20/SNX21 from the anti-myc co-immunoprecipitation and mass spectrometry

Control # spectra # distinct peptide % coverage	myc-SNX20 # spectra # distinct peptide % coverage	myc-SNX21 # spectra # distinct peptide % coverage	Database Accession #	Protein Name
2 1 4.20%	2 1 4.20%	42 12 32.70%	Q969T3	Sorting nexin-21
0 0 0	20 5 12.90%	0 0 0	Q7Z614	Sorting nexin-20
0 0 0	1 1 3.80%	3 3 10%	P12235	ADP/ATP translocase 1
0 0 0	4 2 4%	0 0 0	Q53G59	Kelch-like protein 12
0 0 0	0 0 0	2 2 7.60%	P60174	Triosephosphate isomerase
0 0 0	0 0 0	2 2 5%	Q06830	Peroxiredoxin-1
0 0 0	0 0 0	2 1 1.50%	O43175	D-3-phosphoglycerate dehydrogenase
0 0 0	0 0 0	2 1 3.70%	Q13642	Four and a half LIM domains protein 1
0 0 0	0 0 0	2 1 2.30%	P0CG48	Polyubiquitin-C

Initially, to validate all the reagents and the protocol, the pcDNA3-Soybean-APEX IMS construct was ectopically expressed in HeLa cells. Immunofluorescence microscopy and immunoprecipitatation were performed as described in Methods. The APEX-IMS (mitochondrial intermembrane space localization peptide fused to N-terminus of APEX) had restricted expression in the mitochondria (Fig 4.4A), as described in the literature (Rhee et al., 2013). After the biotin-phenol and H_2O_2 treatment, these mitochondria were also positive for streptavidin staining. Omitting either biotin-phenol or H_2O_2 would prevent the reaction of biotinylation in the APEX-IMS positive structure (Fig 4.4A). Furthermore, the endogenous proteins biotinylated by APEX-IMS for 1 min in HeLa cells were enriched using streptavidin-coated beads (Fig 4.5).

After confirming the technique, I engineered plasmids to express full-length SNX20 and SNX21 proteins fused to APEX. Full-length APEX sequence together with a N-terminal V5 tag from APEX-IMS plasmid were inserted into the pGFP-C1 backbone to replace the GFP fragment. Murine SNX20 and SNX21 full-length cDNAs were then subcloned into the pAPEX-C1 vector. Before performing the proteomic experiment, the pAPEX-C1, pAPEX-C1-SNX20 and pAPEX-C1-SNX21 constructs were validated for APEX-mediated biotinylation using immuno-fluorescence. APEX-

Figure 4.4 - APEX-mediated biotinylation with SNX20/21 fusion constructs.
(See next page)
24 hrs after transfection with pAPEX-IMS (A), pAPEX-C1-SNX20 or pAPEX-C1-SNX21 (B) constructs, cells were first incubated in complete medium with 500μM biotin-phenol for 30 min at 37°C, and then 1mM H_2O_2 was added for 1 min to initiate the biotinylation. In control samples cells were treated with medium lacking one or both reagents as indicated. Cells were washed three times with a "quencher solution" consisting of 10 mM sodium azide, 10 mM sodium ascorbate, and 5 mM Trolox in DPBS and then fixed and permeabilised before co-labeled with Streptavidin-Alexa488 (green) and anti-V5 antibody followed by anti mouse Alexa fluor 647 (red). Confocal microscopy was performed using Zeiss LSM 710 confocal microscope. The experiments were performed at least twice with technical triplicates and the representative images were shown. Scale bars = 10 μm.

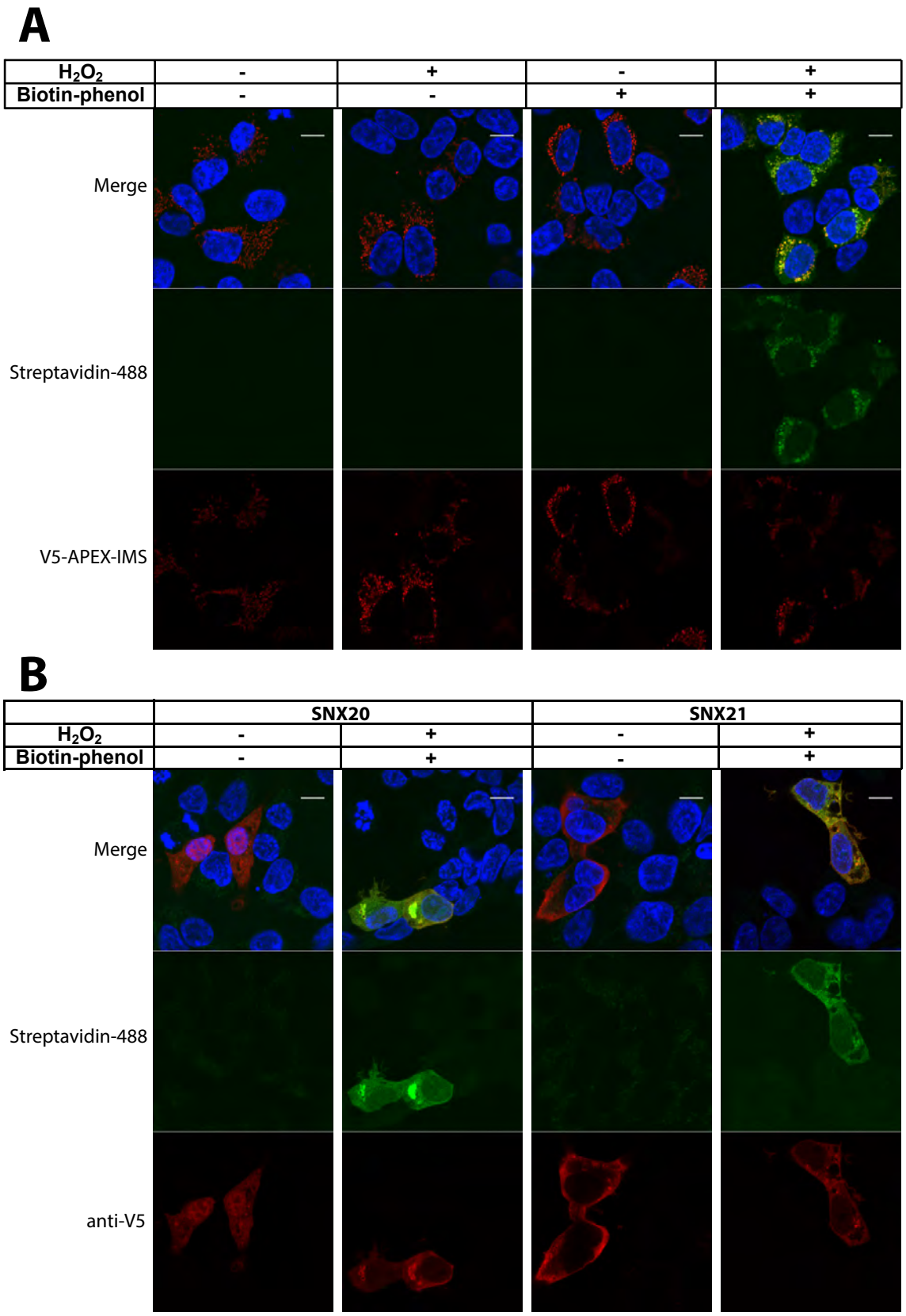

Figure 4.4 - APEX-mediated biotinylation with SNX20/21 fusion constructs. (See legend on previous page)

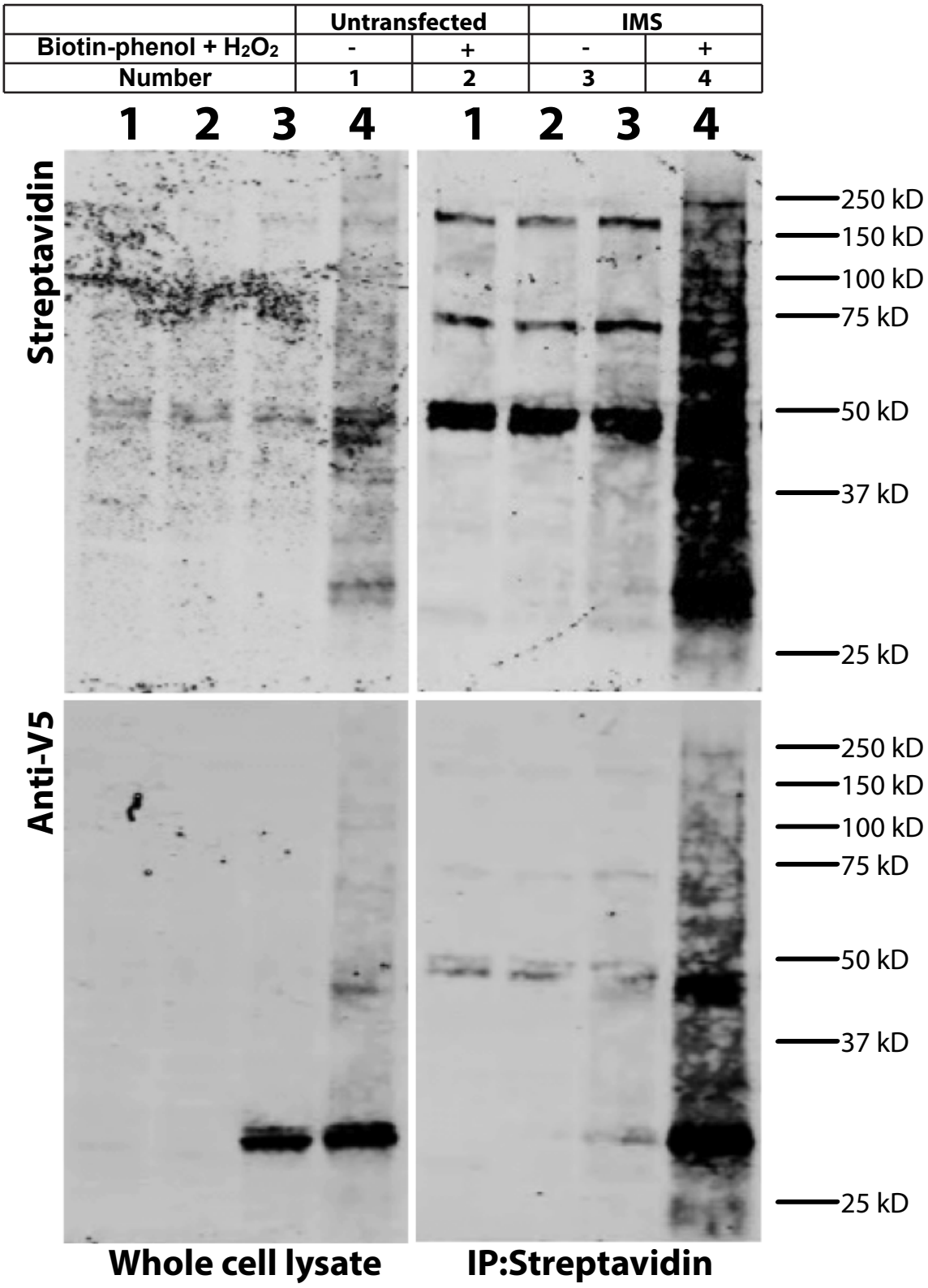

Figure 4.5 - Precipitation of biotinylated proteins from APEX-IMS transfected cells. (See legend on next page)

SNX20 and APEX-SNX21 maintained the endosomal localization in the HeLa cells, while APEX-C1 appeared to be cytosolic. When the APEX-SNX20 or APEX-SNX21 cells were treated with biotin-phenol and H_2O_2, the biotinylated proteins labelled by streptavidin overlapped tightly with the APEX-SNX20 or SNX21 constructs (Fig 4.4B). Clonal HeLa stable cell lines expressing pAPEX-C1, pAPEX-C1-SNX20 and pAPEX-C1-SNX21 were generated. However, as the expression level of the constructs was relatively low in the stable cell lines (Fig 4.6), the specific endogenous biotinylated proteins, including biotinylated SNX20 and SNX21, were not detectable by the mass spectrometry after streptavidin beads enrichment approach. The experimental conditions need to be optimized for further studies.

Figure 4.5 - Precipitation of biotinylated proteins from APEX-IMS transfected cells. (See previous page)

Non-transfected or HEK293 cells transiently expressing APEX-IMS were lysed after biotinylation treatment by incubation with or without biotin-phenol and H_2O_2. To isolate the biotinylated proteins, whole cell lysates were prepared using TK lysis buffer with 1% Triton X-100 before incubation with streptavidin-coated beads overnight at 4°C. Samples were eluted by boiling in 2x sample buffer and separated on 10% SDS-PAGE gels. Western blotting were performed with both streptavidin coupled with IRdye800 and anti-V5 antibody followed with IRDye680LT anti-mouse secondary antibody. The blot images were captured using Odyssey imaging system.

	pAPEX-C1		pAPEX-C1-SNX20		pAPEX-C1-SNX21	
Biotin-phenol + H_2O_2	-	+	-	+	-	+
Number	1	2	3	4	5	6

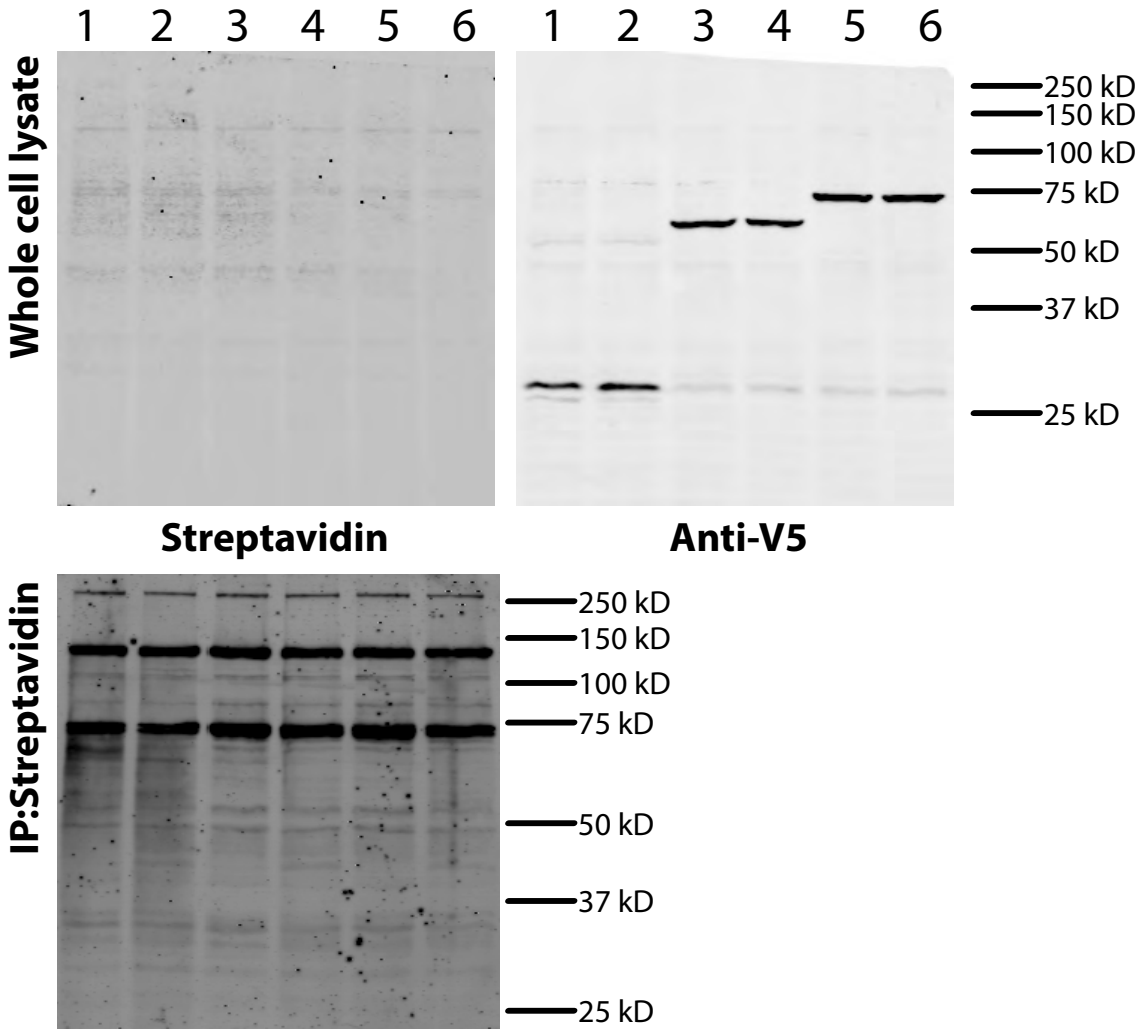

Figure 4.6 - Precipitation of biotinylated proteins from APEX-SNXs transfected cells.

Cells transiently expressing pAPEX-C1, pAPEX-C1-SNX20 or pAPEX-C1-SNX21 were lysed after treatment with or without biotin-phenol and H_2O_2 incubation. The biotinylated proteins were isolated from whole cell lysates using streptavidin-coated beads. Samples were separated on 10% SDS-PAGE gels and the Western blotting was performed with streptavidin-coupled IRdye800 and mouse anti-V5 antibody followed by IRDye680LT anti-mouse secondary antibody. The blot images were captured using Odyssey imaging system.

4.3.6 Recruitment of SNX20 and SNX21 to the newly formed SCV

Salmonella invade the cells via macropinocytosis and engage the endosomal system for their survival and replication (Malik Kale et al., 2011). Given the endosomal localisation of SNX20 and SNX21, whether these proteins are also linked to *Salmonella* infection process is unknown. To investigate the spatial and temporal localisation of SNX20 and SNX21 during *Salmonella* invasion, GFP-SNX20 or GFP-SNX21 expressing HeLa cells were monitored by live cell imaging when they were infected by RFP tagged *Salmonella*. From the time-lapse images, endosomal localised GFP-SNX20 initially accumulated on the membrane around *Salmonella* as the pathogen was being internalized, but the association was transient and SNX20 rapidly disassociated from the membrane within 1 min. (Fig 4.7A) GFP-SNX21 showed similar kinetic to GFP-SNX20 when the cell was infected by *Salmonella* (Fig 4.7B). As the early stage of SCVs are PtdIns(3)*P* positive membrane structure (Pattni et al., 2001), the burst of SNX20 and SNX21 during *Salmonella* invasion process suggests that SNX20 and SNX21 are enriched on endosomal structures due to binding to PtdIns(3)*P*.

Figure 4.7 - SNX20 and SNX21 can be recruited to SCV. (See next page)
Series of confocal sections from a time-lapse of EGFP-SNX20 (A) or EGFP-SNX21 (B) expressing cells (green) infected with mRFP wild-type *Salmonella* (SL1344-WT, red). Montage of movie 20 and movie 22. HEK293 cells were transfected with EGFP-SNX20 or EGFP-SNX21. 24 hours post transfection, cells were imaged live under confocal microscope during the infection of *Salmonella.* Bars = 5 μm. Arrows indicate the sites of *Salmonella* invasion and SNXs recruitment.

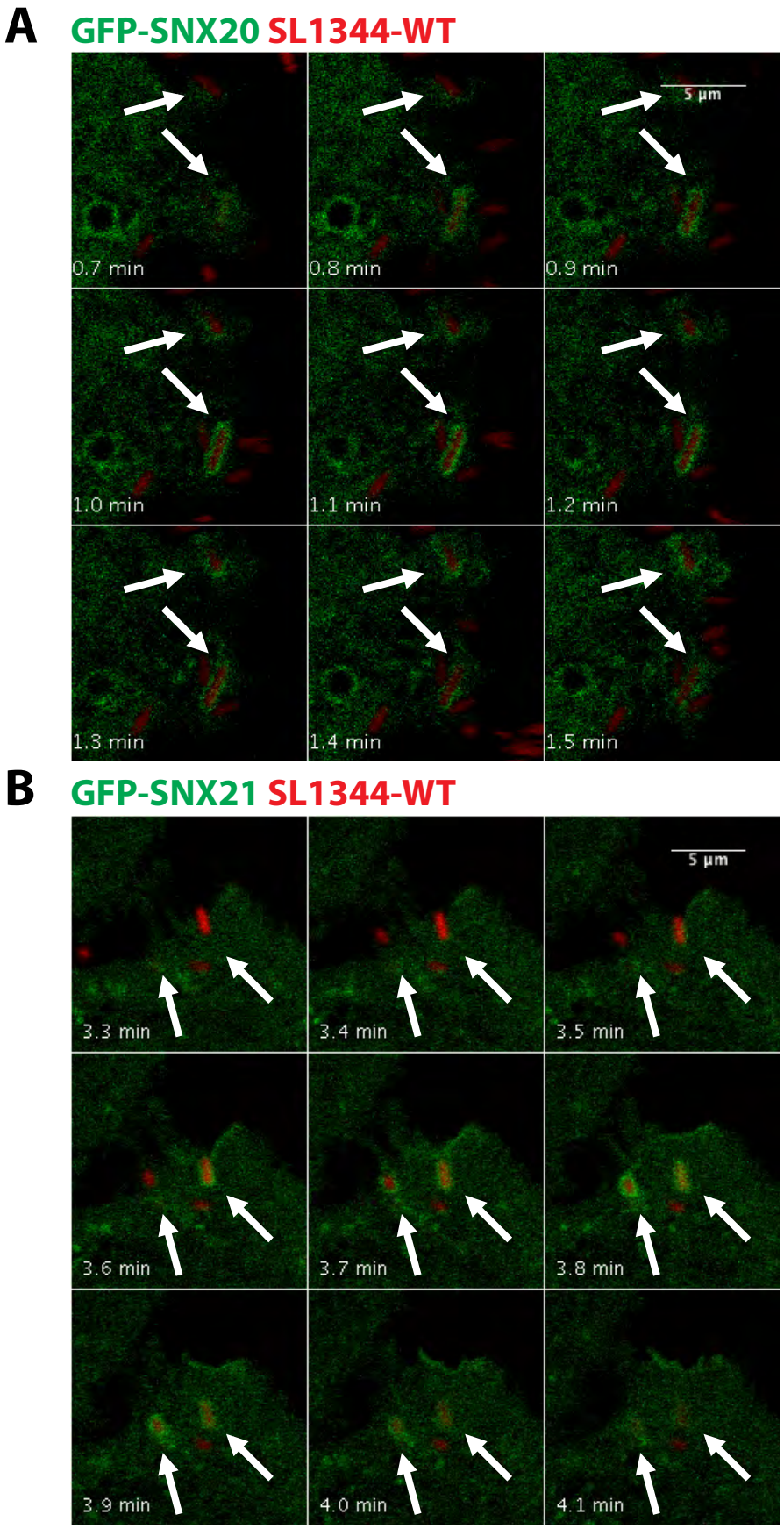

Figure 4.7 - SNX20 and SNX21 can be recruited to SCV.
(See legend on previous page)

4.4 Conclusion and Discussion

The sorting nexin/PX proteins SNX20 and SNX21 are currently poorly characterised with no defined role in endosomally-associated cellular or trafficking processes. In this study, I determined that SNX20 and SNX21 associate with endosomes and, like other sorting nexins, this occurs via the PtdIns-binding ability of their PX domains. Both proteins co-localised with EEA1 on the PtdIns(3)P enriched early endosomes and this membrane recruitment was dependent on the PtdIns(3)P binding site in the PX domain. These observations were supported by *in vitro* isothermal titration calorimetry (ITC) and liposome pelleting assay (LPA) assays that identified that PX domains of SNX20 and SNX21 interacted with PtdIns(3)P (personal communication, Thomas Clairfeuille, Group Collins, IMB, UQ).

The cargo binding capacity of SNX20 and SNX21 remains unclear. Based on a yeast 2-hybrid screen, SNX20 was identified to interact with the PSGL-1 cytoplasmic tail (Schaff et al., 2008). However, my co-immunoprecipitation experiments failed to detect any interaction between SNX20 and PSGL-1 cytoplasmic tail. Furthermore, the *in vitro* pull-down assay using recombinant SNX20 or SNX21 with PSGL-1 tail was not able to detect the interaction (personal communication, Thomas Clairfeuille, Group Collins, IMB, UQ). Even though SNX20 and SNX21 co-localize with PSGL-1 in endosomal structures, it remains unclear if they physically interact. Interestingly, SNX21, but not SNX20, was identified to regulate the endo-lysosomal sorting of the activated EGFR in the SNX-directed loss-of-function screen (Danson et al., 2013), suggesting SNX21 may also be involved in cargo transport within cells.

SNX20 and SNX21 have a unique C-terminal domain termed PXB (PX-associated domain B) (Teasdale and Collins, 2012). The structure of SNX21-PXB domain is composed of three TPR helical repeats and each TPR motif consists of an inner and an outer helix that form a concave structure (personal communication, Thomas Clairfeuille, Group Collins, IMB, UQ), which, in other TPR containing domains, is a common site responsible for protein-protein interactions. To date, there are more than 100 structures of TPR-containing proteins determined, allowing the study of TPR-mediated protein interaction at atomic resolution. However, TPR-containing proteins display great binding variety and no common feature of the TPR interaction partners

has been defined. In addition, the super-helical fold of TPR repeats presents several binding surfaces that can promote the formation of multi-protein complexes (Zeytuni et al, 2012), suggesting that TPR-containing proteins can act as scaffolds and participate in diverse cellular processes. Thus, SNX20 and SNX21, as TPR-containing proteins, have great potential to scaffold other regulators during the early stages of endocytosis and to facilitate transport of ligands or cargos within endosomal trafficking system.

I introduced a new approach here to identify interacting proteins of SNX20 and SNX21. A genetically encoded targetable enzyme APEX (enhanced ascorbate peroxidase) –mediated biotinylation combined with mass spectrometry (MS) offers spatially and temporally resolved proteomic maps of endogenous proteins within living cells (Rhee et al., 2013). This distance-based method can biotinylate the nearby proteins within a small radius (<20 nm) from the protein of interest during a short reaction time (1 min). The biotin-labeled proteins can then be purified and identified by MS. Compared to the traditional co-immunoprecipitation/MS proteomic approach, APEX-mediated biotinylation/MS approach allows the identification of transient protein interactions or the interaction with low binding affinity which may not be able to be maintained during the *in vitro* pull-down. The application of the new technology for SNX20 and SNX21 revealed several issues that needed to be addressed. Firstly, unlike the original application in which APEX-IMS is restricted to be within the mitochondria, both SNX20 and SNX21 were not exclusively localized on the early endosomes. The presence of the APEX fusion proteins within the cytoplasm could result in the detection of abundant false positive cytoplasmic proteins. As a control, I used a cytosolic APEX non-fusion protein here to determine non-specific binding proteins. Secondly, as the transient expression levels of pAPEX-C1-SNX20 and SNX21 differ from cell to cell, stable cell lines were generated. However, the stable expression of APEX-fusion SNX20 and SNX21 was relatively low and therefore only a low amount of biotinylated proteins were available for further analysis. To better utilize the APEX-mediated proteomics approach in characterizing SNX20 and SNX21, the experiment conditions still need to be further optimized. To resolve the low amount of total biotinylated proteins detected, scaling up of the experiment through using larger numbers of stable cells may improve the sensitivity but is not likely to change the specificity issue. Likewise a longer reaction time (more than 1

minute) could be used, allowing more biotinlytion events to occur in the samples. However, as the major purpose of these experiments was to detect interactions on endosomes and the major benefit of this approach is to allow this short snapshot of molecules in the proximity of SNX20 and SNX21 particularly trans-membrane proteins within endosomes. Extension of the reaction time is likely to increase the level of background signal by increasing the detection of the cytoplasmic proteins when these molecules are not associated with endosomes, which could be controlled by comparing to the non-PI(3)P binding PX domain mutants which are not recruited to endosomes. Further modification of the protocol to removal of excess biotin-phenol could be further optimized in order to increase the efficiency of biotinylated proteins binding to the streptavidin-coated beads.

In summary, this study commenced to characterize the properties of the PX-PXB domain containing SNX proteins, SNX20 and SNX21, at molecular and cellular level. Their early endosome localization via PX domain, regulated recruitment to newly formed SCV and their potential protein interaction capability via PXB domain suggest SNX20 and SNX21 will play an important role within the endosome like other sorting nexins.

4.5 List of Supplementary Movies

Movie19: SNX20 (EGFP) recruits to the nascent SCV during *S.* Typhimurium (mRFP) internalization into the HeLa cells. 16 hrs post transfection, 5-10 min post infection. (0.1 min between frames, 7 fps). Bar=5 μm.

Movie20: A zoom in of Movie19, from which the montage of movie in Figure4.7 is made. Bar=2 μm.

Movie21: SNX21 (EGFP) recruits to the nascent SCV during *S.* Typhimurium (mRFP) internalization into the HeLa cells. 16 hrs post transfection, 0-10 min post infection. (0.1 min between frames, 7 fps). Bar=5 μm.

Movie22: A zoom in of Movie21, from which the montage of movie in Figure 4.7 is made. Bar=2 μm.

5 General Discussion

Within this thesis I have enhanced our understanding of several members of the Sorting Nexin/PX-domain protein family at both cellular and molecular level. SNX18 has been defined as a novel regulator of macropinocytosis and *Salmonella* invasion (in Chapter 2) and its own activity appears regulated by an open-closed conformational auto-inhibitory mechanism during these biological processes (in Chapter 3). In addition, the characterizing of SNX-PXB proteins reveals the emerging role of SNX20 and SNX21 in endocytosis and *Salmonella* invasion (in Chapter 4). Though SNX18 and SNX20/21 belong to different subfamilies of PX proteins via the structural classification, they show similar spatial and temporal recruitment during the formation of a Salmonella containing vacuole/macropinosome during *Salmonella* invasion.

5.1 Phosphoinositide-binding specificity of PX domain

The majority of the PX domain containing proteins are reported to be associated with trafficking and signaling process in endosomal systems in mammalian cells. The phosphoinositides binding ability of PX domain drive the proteins to the membranes, defining the cellular localization of the different PX proteins. PtdIns(3)*P* is the most common phosphoinositides bound by PX domain, and most PX proteins were observed to localize on the PtdIns(3)*P* enriched membranes, i.e. early endosome membrane. However, not all PX proteins are localized on PtdIns(3)*P* enriched organelles. One example is SNX18, which translocate from the cytosol to the ruffles at the plasma membrane during macropinocytosis (See Chapter 2). The *in vitro* liposome co-sedimentation assay illustrated that SNX18-PX-BAR has a preference for PtdIns(4,5)P_2 and PtdIns(3,4)P_2 rather than PtdIns(3)*P* (Haberg et al., 2008). Consistent with this, the wild type full length SNX18 are observed to be recruited to the membrane ruffles and newly formed macropinosomes where PtdIns(3,4)P_2 is locally concentrated. Meanwhile, when the structure of SNX18 was disrupted by depletion of LC or/and SH3 domains or insertion of GFP between LC and PX

domains, SNX18 is predominately localized to the plasma membrane where PtdIns(4,5)P_2 normally exists. Both membrane localization of SNX18 rely on the same PtdIns-binding pocket as mutation of the conserved arginine residue that forms part of the phophoinositide binding site prevents recruitment of these proteins to the plasma membrane. However, the *in vivo* control of SNX18 spatial and temporal recruitment clearly depends on other molecular interactions in conjunction with the PtdIns-binding preference of SNX18.

Like other PX domains, SNX20 and SNX21 PX domains are both able to bind to PtdIns(3)*P* in ITC assay. This was supported by the recruitment of both SNX20 and SNX21 to early endosomes in fixed and living cells. In contrast, the liposome precipitation assay data also showed a substantial amount of SNX20 and SNX21 in the pellet fraction of POPC-PE:PtdIns(4,5)P_2, suggesting that the PX domain of SNX20 and SNX21 may not exclusively bind to PtdIns(3)*P*. Live cell imaging demonstrated a transient recruitment of SNX20 and SNX21 with the early endosome and a very transient interaction with the newly forming SCV. The association time of SNX-PXB proteins with endosomes is much shorter than the process of converting PtdIns(3)*P* enriched early endosome to PtdIns(3,5)P_2 enriched late endosome (Huotari and Helenius, 2011), indicating that the disassociation of SNX20 and SNX21 is not simply due to the PtdIns-binding availability. In other word, apart from the PX domain, there are appears to be other factors influencing the membrane localization of SNX-PXB proteins.

These findings are not the first to demonstrate that PX domain can bind to other phosphoinositides than PtdIns(3)P. SNX9 PX domain structure (PDB code 2RAK) is one of the only two PX domain structures that have been solved in complex with PtdIns(3)*P* (Pylypenko et al., 2007). Previous LPA data shows that SNX9 PX-BAR unit has a boarder binding profile to different phosphoinositides (Yarar et al., 2008) and the mutation of the PX domain abolishes its binding to PtdIns(3)*P* but not PtdIns(4,5)P_2. This suggests that the SNX9 PX domain is specific for PtdIns(3)*P*, whereas the binding of PtdIns(4,5)P_2 is mediated primarily by the SNX9 BAR domain (Pylypenko et al., 2007). Given all the evidence that in the presence of other domains, PX domain containing proteins may change the PtdIns-binding preferences which in

turn target them to specific membrane sub-domains. This preference change can occur via different types of coincidence detection, i.e. recognition of cargo, other lipids, membrane-associated proteins or membrane curvature (Carlton and Cullen, 2005). Although a detailed structure of how PX domain and other phosphoinositides are associated is still required, it is clear that the PX domains have specificities for phosphoinositides other than PtdIns(3)P and the PtdIns-binding property can be regulated by associated domains encoded within the PX proteins *in vivo*.

5.2 PX proteins as scaffolds on membranes

Most PX domain containing proteins possess one or more other domains, which have various functions including membrane remodeling, phospholipase activity, phosphoinositide kinase activity, protein-protein interaction and numerous other known or unknown functions (Teasdale and Collins, 2012). Among those known domains, a few of them, i.e. PDZ, SH3, PXB/TPR, FERM and MIT, are considered protein-protein interaction domains which recognize motifs in other proteins and can associate with diverse collections of proteins such as cargos, GTPases, tyrosine phosphorylation kinases and components of the actin cytoskeleton. PX proteins with these domains are defined as scaffold proteins and they share the following features: 1) They have one or more protein interaction motifs/domains; 2) They can target to a specific localization and tether other proteins and complexes to the same site; 3) They can coordinate signaling transduction, nucleation of transport effectors or orchestrate protein arrangement in other important cellular processes. An example is the FERM domain, which is at the C-terminal of PX domain in SNX17, SNX27 and SNX31. The FERM domain is composed of three modules named F1, F2 and F3 and the C-terminal F3 module is capable of binding a Asn-Pro-Xaa-Tyr (NPxY) motif that is common the cytoplasmic domains of transmembrane cargo proteins including, LDLR ((lowdensity lipoprotein receptor), LRP1 (LDLR related protein 1), P-selectin and APP (Teasdale and Collins, 2012). Multiple non-cargo partners like Krit1 (Krev interaction trapped 1) (Czubayko et al., 2006; Stiegler et al., 2014) and Ras GTPase (Ghai et al., 2011) are also found to interact with FERM domain thus these PX-FERM proteins are capable of scaffolding of transmembrane proteins with cell signaling complexes (Teasdale and Collins, 2012).

SH3 and LC domains of SNX9/18/33 family proteins have common protein-protein interaction domains. When SNX9 participates in the CME, it is targeted to the CCP via interacting with clathrin and its adaptor protein AP-2. SNX9 recruits dynamin on to the vesicular neck to form narrow tubule from the plasma membrane (Lundmark and Carlsson, 2004; Soulet et al., 2005). Finally, SNX9 facilitates the rearrangement of cytoskeleton around CCP via interacting with N-WASP to get the vesicle released (Shin et al., 2007). The whole process may also require the signalling transduction by ACK or Sos1/2 via their interaction with SNX9 (Lin et al., 2002; Worby et al., 2002). As SNX18 has been shown to interact with dynamin, N-WASP and AP-1, it logically follows that similar protein recruitment can occur when SNX18 is involved in up-regulating macropinocytosis. Previous worked showed that SNX18 SH3 domain depletion mutant, which is not able to bind dynamin and N-WASP, fails to elevate macropinosome formation (Wang et al., 2010), suggesting that the interaction is necessary for an intact function of SNX18. In Chapter 2 and 3, I identified that SNX18 is recruited to the plasma membrane at the site of macropinocytosis and then recruit N-WASP and dynamin to the membrane. SNX18 can also interact with ACTN4 on the membrane though their membrane recruitment is independent of each other. As SNX18 activity and function during macropinocytosis is precisely regulated by PtdIns-binding ability, protein phosphorylation and protein-protein interactions, its scaffolding property seems to also serve for the regulation of itself, by coordinating phosphokinases, inhibition effectors and dimers to the right position at the right stage in order to regulate its own activation and function. Another SNX subfamily discussed here, composing of SNX20 and SNX21, also has the potential to be scaffolds during endocytosis. Apart from the PtdIns-binding PX domain, SNX20 and SNX21 share a PXB domain in structure, which contains three TPR motifs as protein-protein interaction motifs. Though no specific cargos or binding partners have been identified for SNX20 or SNX21 yet, it will be of great interest to investigate their functional mechanism in endocytic pathways.

5.3 PX proteins in *Salmonella* infection

Salmonella enterica has developed sophisticated systems to manipulate the host cells including during the initial attachment to the cell membrane for invasion and the subsequent intracellular propagation of the bacteria within the lumen of a modified

membrane endosome-like niche. Increasing evidence suggests that during the *Salmonella* infection, the cellular phosphoinositides levels undergo striking changes (Bakowski et al., 2010), mainly as a result of the delivery and direct function of SopB/SigD, a *Salmonella* virulence factors with PtdIns-phosphatase activity (Roppenser et al., 2012). This manipulation on PtdIns-metabolism in turn impacts the localization and function of PtdIns-binding proteins including most of PX proteins (Kerr et al, 2012).

In Chapter 2 and 3, SNX18 was identified as a regulator of *Salmonella* induced macropinocytosis. SNX18 is recruited to the plasma membrane and membrane ruffles at the site of *Salmonella* entry and disassembled after transient association with nascent SCVs. PX-BAR proteins are known to regulate membrane tubulation via dimerization and sensing membrane curvature (Bhatia et al., 2009; Gallop and McMahon, 2005), while SNX18 appears to facilitate the membrane reorganisation at the neck of macropinosomes required to release the macropinosome from the plasma membrane rather than the formation of tubular vesicular carrier from SCVs.. In a previous study, SNX1, a PX protein that normally associates with early endosomes and regulates transport to the trans-Golgi network (TGN), was the first sorting nexin to be reported to undergo a rapid translocation to sites of bacterial entry and SCVs (Bujny et al., 2008). The SNX1-driven formation of extensive long-range tubules is coupled with the contraction of SCVs and the removal of TGN cargos. Critically, suppression of SNX18 decreased the rate of *Salmonella* induced macropinocytosis, resulting in a deficiency in internalization of *Salmonella* (Chapter 2), while suppression of SNX1 perturbs the maturation of SCVs into the cell, resulting in a delay of *Salmonella* replication (Bujny et al., 2008). The PX-only protein SNX3 also plays an important for *Salmonella* infection (Braun et al., 2010). Similarly to SNX1, SNX3 is recruited to SCVs and tubules at early times post invasion, and its depletion leads to impaired SCV maturation. However it was found that SNX3 recruitment occurs after SNX1, and in fact SNX3 depends on SNX1 (and SNX2) for localization to these tubules. SNX20 and SNX21, the SNX-PXB proteins, are also recruited to early SCVs. Live cell imaging showed that both SNX20 and SNX21 translocate to sites of *Salmonella* entry at the plasma membrane and nascent SCVs. The transient accumulation of SNX-PXB proteins is eliminated during the progression of SCVs into

the cell. Recently, Kerr et al (Kerr et al, 2012) employed an ectopic screening strategy to demonstrate that 19 PX proteins are recruited to the SCVs within the first 30 minutes of infection. Though SNX18 was not included in this study, SNX21 was found to associate with the tubules and the body of the SCVs. Interestingly, other SNXs have precise distributions on the membrane of the SCVs body and/or membrane tubules derived from SCVs, indicating that apart from SNX1, SNX3, SNX18 and SNX20/21, other SNXs may also function in different steps of *Salmonella* infection.

As a scaffolding protein, SNX18 recruits other proteins to the site of *Salmonella* entry to facilitate the formation of SCV, including several key actin-regulatory molecules such as N-WASP and ACTN4. As the *Salmonella* induced membrane ruffles and macropinosome formation is an actin-driven process, it is unsurprising that actin and its key regulators are associated with this pathogen internalization activity. The Cdc42 and Rac effector N-WASP are recruited to SPI-1-induced actin-rich membrane ruffles during *Salmonella* invasion and the inhibition of its interaction with F-actin and Arp2/3 complex by expression of N-WASPΔWA reduces the invasion efficiency (Unsworth et al., 2004). In Chapter 2, we showed that the recruitment of N-WASP to the membrane is depended on SNX18 recruitment and SNX18 SH3 domain is required. Therefore, SNX18 could exploit N-WASP for its function on the plasma membrane, via the activation of Cdc42 and Rac, leading to actin polymerization for *Salmonella* induced membrane ruffling.

In addition to the important role in *Salmonella* infection, PX proteins are critical for the uptake and the processing of several other pathogens. SNX1 has been found to be important for the efficient passage of STx (Bujny et al., 2007; Lieu and Gleeson, 2010), the Shiga toxin secreted by *Shigella* dysenteriae to manipulate CME and bypass the degradative pathways (Sandvig et al., 2002). SNX5 has been identified in the macropinocytosis of Ebola virus (Aleksandrowicz et al., 2011), and SNX16 has been implicated in the infection by VSV (vesicular stomatitis virus), via regulating the export of the nucleocapsid from late endosomes to the cytosol for viral replication [128]. Another SH3-PX-BAR protein SNX9 is also reported to involve in EPEC (*Enteropathogenic Escherichia coli*) invasion via its SH3 domain interaction with

EPEC effector EspF (Alto et al., 2007; Marches et al., 2006). It will be interesting to see the likely roles of SNX18 in the other pathogenicity emerge in the near future.

In conclusion, SNX18 and its molecular associations with partners could directly contribute to their capacity to promote *Salmonella* internalization in a distinguishing mechanism from other PX-BAR subgroup. It also provides a clue for SNX18 to involve in other infection event where the pathogens can manipulate actin-driven membrane remolding during their invasion.

6 References

Ago, T., Takeya, R., Hiroaki, H., Kuribayashi, F., Ito, T., Kohda, D., and Sumimoto, H. (2001). The PX domain as a novel phosphoinositide- binding module. Biochemical and biophysical research communications *287*, 733-738.

Ahram, M., Sameni, M., Qiu, R.G., Linebaugh, B., Kirn, D., and Sloane, B.F. (2000). Rac1-induced endocytosis is associated with intracellular proteolysis during migration through a three-dimensional matrix. Experimental cell research *260*, 292-303.

Aleksandrowicz, P., Marzi, A., Biedenkopf, N., Beimforde, N., Becker, S., Hoenen, T., Feldmann, H., and Schnittler, H.J. (2011). Ebola virus enters host cells by macropinocytosis and clathrin-mediated endocytosis. The Journal of infectious diseases *204 Suppl 3*, S957-967.

Alto, N.M., Weflen, A.W., Rardin, M.J., Yarar, D., Lazar, C.S., Tonikian, R., Koller, A., Taylor, S.S., Boone, C., Sidhu, S.S., *et al.* (2007). The type III effector EspF coordinates membrane trafficking by the spatiotemporal activation of two eukaryotic signaling pathways. J Cell Biol *178*, 1265-1278.

Amyere, M., Payrastre, B., Krause, U., Van Der Smissen, P., Veithen, A., and Courtoy, P.J. (2000). Constitutive macropinocytosis in oncogene-transformed fibroblasts depends on sequential permanent activation of phosphoinositide 3-kinase and phospholipase C. Mol Biol Cell *11*, 3453-3467.

Anton, I.M., Saville, S.P., Byrne, M.J., Curcio, C., Ramesh, N., Hartwig, J.H., and Geha, R.S. (2003). WIP participates in actin reorganization and ruffle formation induced by PDGF. J Cell Sci *116*, 2443-2451.

Araki, N., Hatae, T., Yamada, T., and Hirohashi, S. (2000). Actinin-4 is preferentially involved in circular ruffling and macropinocytosis in mouse macrophages: analysis by fluorescence ratio imaging. J Cell Sci *113 (Pt 18)*, 3329-3340.

Araki, N., Johnson, M.T., and Swanson, J.A. (1996). A role for phosphoinositide 3-kinase in the completion of macropinocytosis and phagocytosis by macrophages. J Cell Biol *135*, 1249-1260.

Badour, K., McGavin, M.K., Zhang, J., Freeman, S., Vieira, C., Filipp, D., Julius, M., Mills, G.B., and Siminovitch, K.A. (2007). Interaction of the Wiskott-Aldrich syndrome protein with sorting nexin 9 is required for CD28 endocytosis and cosignaling in T cells. Proc Natl Acad Sci U S A *104*, 1593-1598.

Bakowski, M.A., Braun, V., Lam, G.Y., Yeung, T., Heo, W.D., Meyer, T., Finlay, B.B., Grinstein, S., and Brumell, J.H. (2010). The phosphoinositide phosphatase SopB manipulates membrane surface charge and trafficking of the Salmonella-containing vacuole. Cell host & microbe *7*, 453-462.

Bakowski, M.A., Cirulis, J.T., Brown, N.F., Finlay, B.B., and Brumell, J.H. (2007). SopD acts cooperatively with SopB during Salmonella enterica serovar Typhimurium invasion. Cell Microbiol *9*, 2839-2855.

Bandyopadhyay, C., Valiya-Veettil, M., Dutta, D., Chakraborty, S., and Chandran, B. (2014). CIB1 synergizes with EphrinA2 to regulate Kaposi's sarcoma-associated herpesvirus macropinocytic entry in human microvascular dermal endothelial cells. PLoS pathogens *10*, e1003941.

Bhatia, V.K., Madsen, K.L., Bolinger, P.Y., Kunding, A., Hedegard, P., Gether, U., and Stamou, D. (2009). Amphipathic motifs in BAR domains are essential for membrane curvature sensing. EMBO J *28*, 3303-3314.

Bois, P.R., Borgon, R.A., Vonrhein, C., and Izard, T. (2005). Structural dynamics of alpha-actinin-vinculin interactions. Molecular and cellular biology *25*, 6112-6122.

Braun, V., Wong, A., Landekic, M., Hong, W.J., Grinstein, S., and Brumell, J.H. (2010). Sorting nexin 3 (SNX3) is a component of a tubular endosomal network induced by Salmonella and involved in maturation of the Salmonella-containing vacuole. Cell Microbiol *12*, 1352-1367.

Bujny, M.V., Ewels, P.A., Humphrey, S., Attar, N., Jepson, M.A., and Cullen, P.J. (2008). Sorting nexin-1 defines an early phase of Salmonella-containing vacuole-remodeling during Salmonella infection. J Cell Sci *121*, 2027-2036.

Bujny, M.V., Popoff, V., Johannes, L., and Cullen, P.J. (2007). The retromer component sorting nexin-1 is required for efficient retrograde transport of Shiga toxin from early endosome to the trans Golgi network. J Cell Sci *120*, 2010-2021.

Carlton, J., Bujny, M., Peter, B.J., Oorschot, V.M., Rutherford, A., Mellor, H., Klumperman, J., McMahon, H.T., and Cullen, P.J. (2004). Sorting nexin-1 mediates tubular endosome-to-TGN transport through coincidence sensing of high- curvature membranes and 3-phosphoinositides. Current biology : CB *14*, 1791-1800.

Carlton, J.G., Bujny, M.V., Peter, B.J., Oorschot, V.M., Rutherford, A., Arkell, R.S., Klumperman, J., McMahon, H.T., and Cullen, P.J. (2005). Sorting nexin-2 is associated with tubular elements of the early endosome, but is not essential for retromer-mediated endosome-to-TGN transport. J Cell Sci *118*, 4527-4539.

Carlton, J.G., and Cullen, P.J. (2005). Coincidence detection in phosphoinositide signaling. Trends Cell Biol *15*, 540-547.

Carpten, J.D., Faber, A.L., Horn, C., Donoho, G.P., Briggs, S.L., Robbins, C.M., Hostetter, G., Boguslawski, S., Moses, T.Y., Savage, S.*, et al.* (2007). A transforming mutation in the pleckstrin homology domain of AKT1 in cancer. Nature *448*, 439-444.

Castellano, F., Montcourrier, P., Guillemot, J.C., Gouin, E., Machesky, L., Cossart, P., and Chavrier, P. (1999). Inducible recruitment of Cdc42 or WASP to a cell-surface receptor triggers actin polymerization and filopodium formation. Current biology : CB *9*, 351-360.

Childress, C., Lin, Q., and Yang, W. (2006). Dimerization is required for SH3PX1 tyrosine phosphorylation in response to epidermal growth factor signalling and interaction with ACK2. Biochem J *394*, 693-698.

Cox, D., and Greenberg, S. (2001). Phagocytic signaling strategies: Fc(gamma)receptor-mediated phagocytosis as a model system. Semin Immunol *13*, 339-345.

Cozier, G.E., Carlton, J., McGregor, A.H., Gleeson, P.A., Teasdale, R.D., Mellor, H., and Cullen, P.J. (2002). The phox homology (PX) domain-dependent, 3-phosphoinositide-mediated association of sorting nexin-1 with an early sorting endosomal compartment is required for its ability to regulate epidermal growth factor receptor degradation. The Journal of biological chemistry *277*, 48730-48736.

Cullen, P.J., Cozier, G.E., Banting, G., and Mellor, H. (2001). Modular phosphoinositide-binding domains--their role in signalling and membrane trafficking. Current biology : CB *11*, R882-893.

Czubayko, M., Knauth, P., Schluter, T., Florian, V., and Bohnensack, R. (2006). Sorting nexin 17, a non-self-assembling and a PtdIns(3)P high class affinity protein, interacts with the cerebral cavernous malformation related protein KRIT1. Biochemical and biophysical research communications *345*, 1264-1272.

Danson, C., Brown, E., Hemmings, O.J., McGough, I.J., Yarwood, S., Heesom, K.J., Carlton, J.G., Martin-Serrano, J., May, M.T., Verkade, P*., et al.* (2013). SNX15 links clathrin endocytosis to the PtdIns(3)P early endosome independent of the APPL1 endosome. J Cell Sci.

Derivery, E., Sousa, C., Gautier, J.J., Lombard, B., Loew, D., and Gautreau, A. (2009). The Arp2/3 activator WASH controls the fission of endosomes through a large multiprotein complex. Dev Cell *17*, 712-723.

Dharmawardhane, S., Schurmann, A., Sells, M.A., Chernoff, J., Schmid, S.L., and Bokoch, G.M. (2000). Regulation of macropinocytosis by p21-activated kinase-1. Mol Biol Cell *11*, 3341-3352.

Di Paolo, G., and De Camilli, P. (2006). Phosphoinositides in cell regulation and membrane dynamics. Nature *443*, 651-657.

Ding, Z., Liang, J., Lu, Y., Yu, Q., Songyang, Z., Lin, S.Y., and Mills, G.B. (2006). A retrovirus-based protein complementation assay screen reveals functional AKT1-binding partners. Proc Natl Acad Sci U S A *103*, 15014-15019.

Dowrick, P., Kenworthy, P., McCann, B., and Warn, R. (1993). Circular ruffle formation and closure lead to macropinocytosis in hepatocyte growth factor/scatter factor-treated cells. European journal of cell biology *61*, 44-53.

Dumas, J.J., Merithew, E., Sudharshan, E., Rajamani, D., Hayes, S., Lawe, D., Corvera, S., and Lambright, D.G. (2001). Multivalent endosome targeting by homodimeric EEA1. Molecular cell *8*, 947-958.

Fraley, T.S., Pereira, C.B., Tran, T.C., Singleton, C., and Greenwood, J.A. (2005). Phosphoinositide binding regulates alpha-actinin dynamics: mechanism for modulating cytoskeletal remodeling. J Biol Chem *280*, 15479-15482.

Francis, C.L., Ryan, T.A., Jones, B.D., Smith, S.J., and Falkow, S. (1993). Ruffles induced by Salmonella and other stimuli direct macropinocytosis of bacteria. Nature *364*, 639-642.

Franke, T.F., Kaplan, D.R., Cantley, L.C., and Toker, A. (1997). Direct regulation of the Akt proto-oncogene product by phosphatidylinositol-3,4-bisphosphate. Science *275*, 665-668.

Fujii, M., Kawai, K., Egami, Y., and Araki, N. (2013). Dissecting the roles of Rac1 activation and deactivation in macropinocytosis using microscopic photo-manipulation. Scientific reports *3*, 2385.

Gallop, J.L., and McMahon, H.T. (2005). BAR domains and membrane curvature: bringing your curves to the BAR. Biochemical Society symposium, 223-231.

Garcia-Perez, B.E., Hernandez-Gonzalez, J.C., Garcia-Nieto, S., and Luna-Herrera, J. (2008). Internalization of a non-pathogenic mycobacteria by macropinocytosis in human alveolar epithelial A549 cells. Microbial pathogenesis *45*, 1-6.

Ghai, R., Mobli, M., and Collins, B.M. (2014). Measuring interactions of FERM domain-containing sorting Nexin proteins with endosomal lipids and cargo molecules. Methods Enzymol *534*, 331-349.

Ghai, R., Mobli, M., Norwood, S.J., Bugarcic, A., Teasdale, R.D., King, G.F., and Collins, B.M. (2011). Phox homology band 4.1/ezrin/radixin/moesin-like proteins function as molecular scaffolds that interact with cargo receptors and Ras GTPases. Proc Natl Acad Sci U S A *108*, 7763-7768.

Godi, A., Di Campli, A., Konstantakopoulos, A., Di Tullio, G., Alessi, D.R., Kular, G.S., Daniele, T., Marra, P., Lucocq, J.M., and De Matteis, M.A. (2004). FAPPs control Golgi-to-cell-surface membrane traffic by binding to ARF and PtdIns(4)P. Nature cell biology *6*, 393-404.

Haberg, K., Lundmark, R., and Carlsson, S.R. (2008). SNX18 is an SNX9 paralog that acts as a membrane tubulator in AP-1-positive endosomal trafficking. J Cell Sci *121*, 1495-1505.

Haga, Y., Miwa, N., Jahangeer, S., Okada, T., and Nakamura, S. (2009). CtBP1/BARS is an activator of phospholipase D1 necessary for agonist-induced macropinocytosis. EMBO J *28*, 1197-1207.

Haigler, H.T., McKanna, J.A., and Cohen, S. (1979). Rapid stimulation of pinocytosis in human carcinoma cells A-431 by epidermal growth factor. J Cell Biol *83*, 82-90.

Hamasaki, M., Araki, N., and Hatae, T. (2004). Association of early endosomal autoantigen 1 with macropinocytosis in EGF-stimulated A431 cells. The anatomical record Part A, Discoveries in molecular, cellular, and evolutionary biology *277*, 298-306.

Haraga, A., Ohlson, M.B., and Miller, S.I. (2008). Salmonellae interplay with host cells. Nature reviews Microbiology *6*, 53-66.

Harlan, J.E., Hajduk, P.J., Yoon, H.S., and Fesik, S.W. (1994). Pleckstrin homology domains bind to phosphatidylinositol-4,5-bisphosphate. Nature *371*, 168-170.

Hayward, R.D., and Koronakis, V. (1999). Direct nucleation and bundling of actin by the SipC protein of invasive Salmonella. EMBO J *18*, 4926-4934.

Hoeller, O., Bolourani, P., Clark, J., Stephens, L.R., Hawkins, P.T., Weiner, O.D., Weeks, G., and Kay, R.R. (2013). Two distinct functions for PI3-kinases in macropinocytosis. J Cell Sci *126*, 4296-4307.

Huotari, J., and Helenius, A. (2011). Endosome maturation. EMBO J *30*, 3481-3500.

Karathanassis, D., Stahelin, R.V., Bravo, J., Perisic, O., Pacold, C.M., Cho, W., and Williams, R.L. (2002). Binding of the PX domain of p47(phox) to phosphatidylinositol 3,4-bisphosphate and phosphatidic acid is masked by an intramolecular interaction. EMBO J *21*, 5057-5068.

Karpenahalli, M.R., Lupas, A.N., and Soding, J. (2007). TPRpred: a tool for prediction of TPR-, PPR- and SEL1-like repeats from protein sequences. BMC bioinformatics *8*, 2.

Kasahara, K., Nakayama, Y., Sato, I., Ikeda, K., Hoshino, M., Endo, T., and Yamaguchi, N. (2007). Role of Src-family kinases in formation and trafficking of macropinosomes. Journal of cellular physiology *211*, 220-232.

Kelly, D.F., and Taylor, K.A. (2005). Identification of the beta1-integrin binding site on alpha-actinin by cryoelectron microscopy. J Struct Biol *149*, 290-302.

Kerr, M.C., Lindsay, M.R., Luetterforst, R., Hamilton, N., Simpson, F., Parton, R.G., Gleeson, P.A., and Teasdale, R.D. (2006). Visualisation of macropinosome maturation by the recruitment of sorting nexins. J Cell Sci *119*, 3967-3980.

Kerr, M.C., Wang, J.T., Castro, N.A., Hamilton, N.A., Town, L., Brown, D.L., Meunier, F.A., Brown, N.F., Stow, J.L., and Teasdale, R.D. (2010). Inhibition of the PtdIns(5) kinase PIKfyve disrupts intracellular replication of Salmonella. EMBO J *29*, 1331-1347.

Kerr, M.C., Castro, N.A., Karunaratne, S. and Teasdale, R.D. (2012). The Phosphoinositides: Key Regulators of Salmonella Containing Vacuole (SCV) Trafficking and Identity, Salmonella - Distribution, Adaptation, Control Measures and Molecular Technologies, Dr Bassam Annous (Ed.), ISBN: 978-953-51-0661-6, InTech, DOI: 10.5772/30761.

Kirkham, M., and Parton, R.G. (2005). Clathrin-independent endocytosis: new insights into caveolae and non-caveolar lipid raft carriers. Biochim Biophys Acta *1746*, 349-363.

Klarlund, J.K., Guilherme, A., Holik, J.J., Virbasius, J.V., Chawla, A., and Czech, M.P. (1997). Signaling by phosphoinositide-3,4,5-trisphosphate through proteins containing pleckstrin and Sec7 homology domains. Science *275*, 1927-1930.

Knaevelsrud, H., Carlsson, S.R., and Simonsen, A. (2013a). SNX18 tubulates recycling endosomes for autophagosome biogenesis. Autophagy *9*, 1639-1641.

Knaevelsrud, H., Soreng, K., Raiborg, C., Haberg, K., Rasmuson, F., Brech, A., Liestol, K., Rusten, T.E., Stenmark, H., Neufeld, T.P.*, et al.* (2013b). Membrane remodeling by the PX-BAR protein SNX18 promotes autophagosome formation. J Cell Biol *202*, 331-349.

Kuijl, C., Savage, N.D., Marsman, M., Tuin, A.W., Janssen, L., Egan, D.A., Ketema, M., van den Nieuwendijk, R., van den Eeden, S.J., Geluk, A.*, et al.* (2007). Intracellular bacterial growth is controlled by a kinase network around PKB/AKT1. Nature *450*, 725-730.

Kutateladze, T.G. (2006). Phosphatidylinositol 3-phosphate recognition and membrane docking by the FYVE domain. Biochimica et biophysica acta *1761*, 868-877.

Kutateladze, T.G., Capelluto, D.G., Ferguson, C.G., Cheever, M.L., Kutateladze, A.G., Prestwich, G.D., and Overduin, M. (2004). Multivalent mechanism of membrane insertion by the FYVE domain. The Journal of biological chemistry *279*, 3050-3057.

Lawe, D.C., Chawla, A., Merithew, E., Dumas, J., Carrington, W., Fogarty, K., Lifshitz, L., Tuft, R., Lambright, D., and Corvera, S. (2002). Sequential roles for phosphatidylinositol 3-phosphate and Rab5 in tethering and fusion of early endosomes via their interaction with EEA1. The Journal of biological chemistry *277*, 8611-8617.

Lemmon, M.A. (2008). Membrane recognition by phospholipid-binding domains. Nature reviews Molecular cell biology *9*, 99-111.

Lemmon, M.A., Ferguson, K.M., O'Brien, R., Sigler, P.B., and Schlessinger, J. (1995). Specific and high-affinity binding of inositol phosphates to an isolated pleckstrin homology domain. Proceedings of the National Academy of Sciences of the United States of America *92*, 10472-10476.

Liberali, P., Kakkonen, E., Turacchio, G., Valente, C., Spaar, A., Perinetti, G., Bockmann, R.A., Corda, D., Colanzi, A., Marjomaki, V.*, et al.* (2008). The closure of Pak1-dependent macropinosomes requires the phosphorylation of CtBP1/BARS. EMBO J *27*, 970-981.

Lieu, Z.Z., Derby, M.C., Teasdale, R.D., Hart, C., Gunn, P., and Gleeson, P.A. (2007). The golgin GCC88 is required for efficient retrograde transport of cargo from the early endosomes to the trans-Golgi network. Mol Biol Cell *18*, 4979-4991.

Lieu, Z.Z., and Gleeson, P.A. (2010). Identification of different itineraries and retromer components for endosome-to-Golgi transport of TGN38 and Shiga toxin. European journal of cell biology *89*, 379-393.

Lim, J.P., Wang, J.T., Kerr, M.C., Teasdale, R.D., and Gleeson, P.A. (2008). A role for SNX5 in the regulation of macropinocytosis. BMC Cell Biol *9*, 58.

Lin, Q., Lo, C.G., Cerione, R.A., and Yang, W. (2002). The Cdc42 target ACK2 interacts with sorting nexin 9 (SH3PX1) to regulate epidermal growth factor receptor degradation. J Biol Chem *277*, 10134-10138.

Loo, L.S., Tang, N., Al-Haddawi, M., Dawe, G.S., and Hong, W. (2014). A role for sorting nexin 27 in AMPA receptor trafficking. Nature communications *5*, 3176.

Lundmark, R., and Carlsson, S.R. (2002). The beta-appendages of the four adaptor-protein (AP) complexes: structure and binding properties, and identification of sorting nexin 9 as an accessory protein to AP-2. Biochem J *362*, 597-607.

Lundmark, R., and Carlsson, S.R. (2003). Sorting nexin 9 participates in clathrin-mediated endocytosis through interactions with the core components. J Biol Chem *278*, 46772-46781.

Lundmark, R., and Carlsson, S.R. (2004). Regulated membrane recruitment of dynamin-2 mediated by sorting nexin 9. J Biol Chem *279*, 42694-42702.

Lundmark, R., and Carlsson, S.R. (2009). SNX9 - a prelude to vesicle release. J Cell Sci *122*, 5-11.

Ma, M.P., and Chircop, M. (2012). SNX9, SNX18 and SNX33 are required for progression through and completion of mitosis. J Cell Sci *125*, 4372-4382.

Malik Kale, P., Jolly, C.E., Lathrop, S., Winfree, S., Luterbach, C., and Steele-Mortimer, O. (2011). Salmonella - at home in the host cell. Frontiers in Microbiology *2*.

Marches, O., Batchelor, M., Shaw, R.K., Patel, A., Cummings, N., Nagai, T., Sasakawa, C., Carlsson, S.R., Lundmark, R., Cougoule, C*., et al.* (2006). EspF of enteropathogenic Escherichia coli binds sorting nexin 9. J Bacteriol *188*, 3110-3115.

Marumoto, T., Honda, S., Hara, T., Nitta, M., Hirota, T., Kohmura, E., and Saya, H. (2003). Aurora-A kinase maintains the fidelity of early and late mitotic events in HeLa cells. J Biol Chem *278*, 51786-51795.

Mayor, S., and Pagano, R.E. (2007). Pathways of clathrin-independent endocytosis. Nature reviews Molecular cell biology *8*, 603-612.

McGregor, A., Blanchard, A.D., Rowe, A.J., and Critchley, D.R. (1994). Identification of the vinculin-binding site in the cytoskeletal protein alpha-actinin. Biochem J *301 (Pt 1)*, 225-233.

Meier, O., Boucke, K., Hammer, S.V., Keller, S., Stidwill, R.P., Hemmi, S., and Greber, U.F. (2002). Adenovirus triggers macropinocytosis and endosomal leakage together with its clathrin-mediated uptake. J Cell Biol *158*, 1119-1131.

Millard, T.H., Sharp, S.J., and Machesky, L.M. (2004). Signalling to actin assembly via the WASP (Wiskott-Aldrich syndrome protein)-family proteins and the Arp2/3 complex. Biochem J *380*, 1-17.

Miura, S., Takeshita, T., Asao, H., Kimura, Y., Murata, K., Sasaki, Y., Hanai, J.I., Beppu, H., Tsukazaki, T., Wrana, J.L.*, et al.* (2000). Hgs (Hrs), a FYVE domain protein, is involved in Smad signaling through cooperation with SARA. Molecular and cellular biology *20*, 9346-9355.

Nakatsuji, H., Nishimura, N., Yamamura, R., Kanayama, H.O., and Sasaki, T. (2008). Involvement of actinin-4 in the recruitment of JRAB/MICAL-L2 to cell-cell junctions and the formation of functional tight junctions. Molecular and cellular biology *28*, 3324-3335.

Nieset, J.E., Redfield, A.R., Jin, F., Knudsen, K.A., Johnson, K.R., and Wheelock, M.J. (1997). Characterization of the interactions of alpha-catenin with alpha-actinin and beta-catenin/plakoglobin. J Cell Sci *110 (Pt 8)*, 1013-1022.

Noack, D., Rae, J., Cross, A.R., Ellis, B.A., Newburger, P.E., Curnutte, J.T., and Heyworth, P.G. (2001). Autosomal recessive chronic granulomatous disease caused by defects in NCF-1, the gene encoding the phagocyte p47-phox: mutations not arising in the NCF-1 pseudogenes. Blood *97*, 305-311.

Okada, H., Zhang, W., Peterhoff, C., Hwang, J.C., Nixon, R.A., Ryu, S.H., and Kim, T.W. (2010). Proteomic identification of sorting nexin 6 as a negative regulator of BACE1-mediated APP processing. FASEB journal : official publication of the Federation of American Societies for Experimental Biology *24*, 2783-2794.

Otey, C.A., Pavalko, F.M., and Burridge, K. (1990). An interaction between alpha-actinin and the beta 1 integrin subunit in vitro. J Cell Biol *111*, 721-729.

Park, J., Kim, Y., Lee, S., Park, J.J., Park, Z.Y., Sun, W., Kim, H., and Chang, S. (2010). SNX18 shares a redundant role with SNX9 and modulates endocytic trafficking at the plasma membrane. J Cell Sci *123*, 1742-1750.

Patel, J.C., and Galan, J.E. (2006). Differential activation and function of Rho GTPases during Salmonella-host cell interactions. J Cell Biol *175*, 453-463.

Pattni, K., Jepson, M., Stenmark, H., and Banting, G. (2001). A PtdIns(3)P-specific probe cycles on and off host cell membranes during Salmonella invasion of mammalian cells. Current biology : CB *11*, 1636-1642.

Peter J. B. Sabatini, M.Z., Rosalind V. Silverman-Gavrila and Michelle P. Bendeck (2011). Cadherins at cell-autonomous membrane contacts control macropinocytosis. Journal of Cell Science *124, 2013-2020*.

Pizarro-Cerda, J., and Cossart, P. (2004). Subversion of phosphoinositide metabolism by intracellular bacterial pathogens. Nature cell biology *6*, 1026-1033.

Porat-Shliom, N., Kloog, Y., and Donaldson, J.G. (2008). A unique platform for H-Ras signaling involving clathrin-independent endocytosis. Mol Biol Cell *19*, 765-775.

Pylypenko, O., Lundmark, R., Rasmuson, E., Carlsson, S.R., and Rak, A. (2007). The PX-BAR membrane-remodeling unit of sorting nexin 9. EMBO J *26*, 4788-4800.

Racoosin, E.L., and Swanson, J.A. (1989). Macrophage colony-stimulating factor (rM-CSF) stimulates pinocytosis in bone marrow-derived macrophages. The Journal of experimental medicine *170*, 1635-1648.

Racoosin, E.L., and Swanson, J.A. (1992). M-CSF-induced macropinocytosis increases solute endocytosis but not receptor-mediated endocytosis in mouse macrophages. J Cell Sci *102 (Pt 4)*, 867-880.

Racoosin, E.L., and Swanson, J.A. (1993). Macropinosome maturation and fusion with tubular lysosomes in macrophages. J Cell Biol *121*, 1011-1020.

Rangarajan, E.S., Park, H., Fortin, E., Sygusch, J., and Izard, T. (2010). Mechanism of aldolase control of sorting nexin 9 function in endocytosis. J Biol Chem *285*, 11983-11990.

Rhee, H.W., Zou, P., Udeshi, N.D., Martell, J.D., Mootha, V.K., Carr, S.A., and Ting, A.Y. (2013). Proteomic mapping of mitochondria in living cells via spatially restricted enzymatic tagging. Science *339*, 1328-1331.

Rohatgi, R., Ma, L., Miki, H., Lopez, M., Kirchhausen, T., Takenawa, T., and Kirschner, M.W. (1999). The interaction between N-WASP and the Arp2/3 complex links Cdc42-dependent signals to actin assembly. Cell *97*, 221-231.

Rojas, R., Kametaka, S., Haft, C.R., and Bonifacino, J.S. (2007). Interchangeable but essential functions of SNX1 and SNX2 in the association of retromer with endosomes and the trafficking of mannose 6-phosphate receptors. Molecular and cellular biology *27*, 1112-1124.

Roppenser, B., Grinstein, S., and Brumell, J.H. (2012). Modulation of host phosphoinositide metabolism during Salmonella invasion by the type III secreted effector SopB. Methods in cell biology *108*, 173-186.

Roth, M.G. (2006). Clathrin-mediated endocytosis before fluorescent proteins. Nature reviews Molecular cell biology *7*, 63-68.

Salim, K., Bottomley, M.J., Querfurth, E., Zvelebil, M.J., Gout, I., Scaife, R., Margolis, R.L., Gigg, R., Smith, C.I., Driscoll, P.C.*, et al.* (1996). Distinct specificity in the recognition of phosphoinositides by the pleckstrin homology domains of dynamin and Bruton's tyrosine kinase. The EMBO journal *15*, 6241-6250.

Sandvig, K., Grimmer, S., Lauvrak, S.U., Torgersen, M.L., Skretting, G., van Deurs, B., and Iversen, T.G. (2002). Pathways followed by ricin and Shiga toxin into cells. Histochemistry and cell biology *117*, 131-141.

Sbrissa, D., Ikonomov, O.C., and Shisheva, A. (2002). Phosphatidylinositol 3-phosphate-interacting domains in PIKfyve. Binding specificity and role in PIKfyve. Endomenbrane localization. The Journal of biological chemistry *277*, 6073-6079.

Schaff, U.Y., Shih, H.H., Lorenz, M., Sako, D., Kriz, R., Milarski, K., Bates, B., Tchernychev, B., Shaw, G.D., and Simon, S.I. (2008). SLIC-1/sorting nexin 20: a novel sorting nexin that directs subcellular distribution of PSGL-1. European journal of immunology *38*, 550-564.

Schnatwinkel, C., Christoforidis, S., Lindsay, M.R., Uttenweiler-Joseph, S., Wilm, M., Parton, R.G., and Zerial, M. (2004). The Rab5 effector Rabankyrin-5 regulates and coordinates different endocytic mechanisms. PLoS Biol *2*, E261.

Schroeder, G.N., and Hilbi, H. (2008). Molecular pathogenesis of Shigella spp.: controlling host cell signaling, invasion, and death by type III secretion. Clinical microbiology reviews *21*, 134-156.

Schroeder, N., Mota, L.J., and Meresse, S. (2011). Salmonella-induced tubular networks. Trends in microbiology *19*, 268-277.

Seet, L.F., and Hong, W. (2006). The Phox (PX) domain proteins and membrane traffic. Biochim Biophys Acta *1761*, 878-896.

Selbach, M., and Mann, M. (2006). Protein interaction screening by quantitative immunoprecipitation combined with knockdown (QUICK). Nature methods *3*, 981-983.

Sharma, M., and Henderson, B.R. (2007). IQ-domain GTPase-activating protein 1 regulates beta-catenin at membrane ruffles and its role in macropinocytosis of N-cadherin and adenomatous polyposis coli. J Biol Chem *282*, 8545-8556.

Sharma, S., Mayank, A.K., Nailwal, H., Tripathi, S., Patel, J.R., Bowzard, J.B., Gaur, P., Donis, R.O., Katz, J.M., Cox, N.J.*, et al.* (2014). Influenza A viral nucleoprotein interacts with cytoskeleton scaffolding protein alpha-actinin-4 for viral replication. FEBS J *281*, 2899-2914.

Shin, N., Ahn, N., Chang-Ileto, B., Park, J., Takei, K., Ahn, S.G., Kim, S.A., Di Paolo, G., and Chang, S. (2008). SNX9 regulates tubular invagination of the plasma membrane through interaction with actin cytoskeleton and dynamin 2. J Cell Sci *121*, 1252-1263.

Shin, N., Lee, S., Ahn, N., Kim, S.A., Ahn, S.G., YongPark, Z., and Chang, S. (2007). Sorting nexin 9 interacts with dynamin 1 and N-WASP and coordinates synaptic vesicle endocytosis. J Biol Chem *282*, 28939-28950.

Shin, S., and Roy, C.R. (2008). Host cell processes that influence the intracellular survival of Legionella pneumophila. Cell Microbiol *10*, 1209-1220.

Sjoblom, B., Salmazo, A., and Djinovic-Carugo, K. (2008). Alpha-actinin structure and regulation. Cellular and molecular life sciences : CMLS *65*, 2688-2701.

Soulet, F., Yarar, D., Leonard, M., and Schmid, S.L. (2005). SNX9 regulates dynamin assembly and is required for efficient clathrin-mediated endocytosis. Mol Biol Cell *16*, 2058-2067.

Stahelin, R.V., Ananthanarayanan, B., Blatner, N.R., Singh, S., Bruzik, K.S., Murray, D., and Cho, W. (2004). Mechanism of membrane binding of the phospholipase D1 PX domain. J Biol Chem *279*, 54918-54926.

Stahelin, R.V., Burian, A., Bruzik, K.S., Murray, D., and Cho, W. (2003). Membrane binding mechanisms of the PX domains of NADPH oxidase p40phox and p47phox. J Biol Chem *278*, 14469-14479.

Stahelin, R.V., Karathanassis, D., Bruzik, K.S., Waterfield, M.D., Bravo, J., Williams, R.L., and Cho, W. (2006). Structural and membrane binding analysis of the Phox homology domain of phosphoinositide 3-kinase-C2alpha. J Biol Chem *281*, 39396-39406.

Stahelin, R.V., Karathanassis, D., Murray, D., Williams, R.L., and Cho, W. (2007). Structural and membrane binding analysis of the Phox homology domain of Bem1p: basis of phosphatidylinositol 4-phosphate specificity. J Biol Chem *282*, 25737-25747.

Steele-Mortimer, O., Knodler, L.A., Marcus, S.L., Scheid, M.P., Goh, B., Pfeifer, C.G., Duronio, V., and Finlay, B.B. (2000). Activation of Akt/protein kinase B in epithelial cells by the Salmonella typhimurium effector sigD. J Biol Chem *275*, 37718-37724.

Stiegler, A.L., Zhang, R., Liu, W., and Boggon, T.J. (2014). Structural determinants for binding of sorting nexin 17 (SNX17) to the cytoplasmic adaptor protein Krev interaction trapped 1 (KRIT1). J Biol Chem *289*, 25362-25373.

Sun, P., Yamamoto, H., Suetsugu, S., Miki, H., Takenawa, T., and Endo, T. (2003). Small GTPase Rah/Rab34 is associated with membrane ruffles and macropinosomes and promotes macropinosome formation. J Biol Chem *278*, 4063-4071.

Swanson, J.A. (1989). Phorbol esters stimulate macropinocytosis and solute flow through macrophages. J Cell Sci *94 (Pt 1)*, 135-142.

Swanson, J.A., and Watts, C. (1995). Macropinocytosis. Trends Cell Biol *5*, 424-428.

Tabuchi, A., and Kuebler, W.M. (2008). Endothelium-platelet interactions in inflammatory lung disease. Vascular pharmacology *49*, 141-150.

Talior-Volodarsky, I., Randhawa, V.K., Zaid, H., and Klip, A. (2008). Alpha-actinin-4 is selectively required for insulin-induced GLUT4 translocation. J Biol Chem *283*, 25115-25123.

Teasdale, R.D., and Collins, B.M. (2012). Insights into the PX (phox-homology) domain and SNX (sorting nexin) protein families: structures, functions and roles in disease. Biochem J *441*, 39-59.

Terebiznik, M.R., Vieira, O.V., Marcus, S.L., Slade, A., Yip, C.M., Trimble, W.S., Meyer, T., Finlay, B.B., and Grinstein, S. (2002). Elimination of host cell PtdIns(4,5)P(2) by bacterial SigD promotes membrane fission during invasion by Salmonella. Nature cell biology *4*, 766-773.

Tsukazaki, T., Chiang, T.A., Davison, A.F., Attisano, L., and Wrana, J.L. (1998). SARA, a FYVE domain protein that recruits Smad2 to the TGFbeta receptor. Cell *95*, 779-791.

Unsworth, K.E., Way, M., McNiven, M., Machesky, L., and Holden, D.W. (2004). Analysis of the mechanisms of Salmonella-induced actin assembly during invasion of host cells and intracellular replication. Cell Microbiol *6*, 1041-1055.

Utskarpen, A., Slagsvold, H.H., Dyve, A.B., Skanland, S.S., and Sandvig, K. (2007). SNX1 and SNX2 mediate retrograde transport of Shiga toxin. Biochemical and biophysical research communications *358*, 566-570.

Wang, J.T., Kerr, M.C., Karunaratne, S., Jeanes, A., Yap, A.S., and Teasdale, R.D. (2010). The SNX-PX-BAR family in macropinocytosis: the regulation of macropinosome formation by SNX-PX-BAR proteins. PLoS One *5*, e13763.

Wang, Q., Kaan, H.Y., Hooda, R.N., Goh, S.L., and Sondermann, H. (2008). Structure and plasticity of Endophilin and Sorting Nexin 9. Structure *16*, 1574-1587.

Weflen, A.W., Alto, N.M., Viswanathan, V.K., and Hecht, G. (2010). E. coli secreted protein F promotes EPEC invasion of intestinal epithelial cells via an SNX9-dependent mechanism. Cell Microbiol *12*, 919-929.

West, M.A., Prescott, A.R., Eskelinen, E.L., Ridley, A.J., and Watts, C. (2000). Rac is required for constitutive macropinocytosis by dendritic cells but does not control its downregulation. Current biology : CB *10*, 839-848.

Willenborg, C., Jing, J., Wu, C., Matern, H., Schaack, J., Burden, J., and Prekeris, R. (2011). Interaction between FIP5 and SNX18 regulates epithelial lumen formation. J Cell Biol *195*, 71-86.

Wishart, M.J., Taylor, G.S., and Dixon, J.E. (2001). Phoxy lipids: revealing PX domains as phosphoinositide binding modules. Cell *105*, 817-820.

Worby, C.A., and Dixon, J.E. (2002). Sorting out the cellular functions of sorting nexins. Nature reviews Molecular cell biology *3*, 919-931.

Worby, C.A., Simonson-Leff, N., Clemens, J.C., Huddler, D., Jr., Muda, M., and Dixon, J.E. (2002). Drosophila Ack targets its substrate, the sorting nexin DSH3PX1, to a protein complex involved in axonal guidance. J Biol Chem *277*, 9422-9428.

Worby, C.A., Simonson-Leff, N., Clemens, J.C., Kruger, R.P., Muda, M., and Dixon, J.E. (2001). The sorting nexin, DSH3PX1, connects the axonal guidance receptor, Dscam, to the actin cytoskeleton. J Biol Chem *276*, 41782-41789.

Yan, Q., Sun, W., Kujala, P., Lotfi, Y., Vida, T.A., and Bean, A.J. (2005). CART: an Hrs/actinin-4/BERP/myosin V protein complex required for efficient receptor recycling. Mol Biol Cell *16*, 2470-2482.

Yarar, D., Surka, M.C., Leonard, M.C., and Schmid, S.L. (2008). SNX9 activities are regulated by multiple phosphoinositides through both PX and BAR domains. Traffic *9*, 133-146.

Yarar, D., Waterman-Storer, C.M., and Schmid, S.L. (2007). SNX9 couples actin assembly to phosphoinositide signals and is required for membrane remodeling during endocytosis. Dev Cell *13*, 43-56.

Yeow-Fong, L., Lim, L., and Manser, E. (2005). SNX9 as an adaptor for linking synaptojanin-1 to the Cdc42 effector ACK1. FEBS Lett *579*, 5040-5048.

Yoshida, S., Hoppe, A.D., Araki, N., and Swanson, J.A. (2009). Sequential signaling in plasma-membrane domains during macropinosome formation in macrophages. J Cell Sci *122*, 3250-3261.

Yu, J.W., and Lemmon, M.A. (2001). All phox homology (PX) domains from Saccharomyces cerevisiae specifically recognize phosphatidylinositol 3-phosphate. J Biol Chem *276*, 44179-44184.

Zeng, W., Yuan, W., Wang, Y., Jiao, W., Zhu, Y., Huang, C., Li, D., Li, Y., Zhu, C., Wu, X*., et al.* (2002). Expression of a novel member of sorting nexin gene family, SNX-L, in human liver development. Biochemical and biophysical research communications *299*, 542-548.

Zerial, M., and McBride, H. (2001). Rab proteins as membrane organizers. Nature reviews Molecular cell biology *2*, 107-117.

Zeytuni, Z and Zarivach, R. (2012). The TPR Motif as a Protein Interaction Module - A Discussion of Structure and Function, Protein Interactions, Dr. Jianfeng Cai (Ed.), ISBN: 978-953-51-0244-1, InTech, DOI: 10.5772/37566.

Zhang, J., Zhang, X., Guo, Y., Xu, L., and Pei, D. (2009). Sorting nexin 33 induces mammalian cell micronucleated phenotype and actin polymerization by interacting with Wiskott-Aldrich syndrome protein. J Biol Chem *284*, 21659-21669.

Zhao, Y., Wang, Y., Yang, J., Wang, X., Zhao, Y., Zhang, X., and Zhang, Y.W. (2012). Sorting nexin 12 interacts with BACE1 and regulates BACE1-mediated APP processing. Molecular neurodegeneration *7*, 30.

Zhou, D., Mooseker, M.S., and Galan, J.E. (1999). Role of the S. typhimurium actin-binding protein SipA in bacterial internalization. Science *283*, 2092-2095.